Dissertation zur Erlangung des Doktorgrades
der Fakultät Chemie und Pharmazie der
Ludwig-Maximilians-Universität München

Formulation and Implementation of Accurate and Efficient Low-Scaling Methods for Explicitly Correlated F12 Theory

---

Lars Urban

aus

Achern

2026

Erklärung
Diese Dissertation wurde im Sinne von §7 der Promotionsordnung vom 28. November 2011 von Herrn Prof. Dr. Christian Ochsenfeld betreut.

Eidstattliche Versicherung
Diese Dissertation wurde eigenständig und ohne unerlaubte Hilfe erarbeitet.

München, 18.03.2026 _____

(Lars Urban)

Dissertation eingereicht am	22.01.2026
1. Gutachter:	Prof. Dr. Christian Ochsenfeld
2. Gutachter:	Prof. Dr. Benjamin P. Fingerhut
Mündliche Prüfung am	03.03.2026

Danksagung

An erster Stelle gilt mein Dank Prof. Dr. Christian Ochsenfeld für die Möglichkeit, in seiner Arbeitsgruppe zu forschen und meine Dissertation anzufertigen sowie für das große Maß an Freiheit und Unterstützung, das ich während dieser Zeit genießen durfte. Mein Dank gilt außerdem Prof. Dr. Benjamin Fingerhut für die Erstellung des Zweitgutachtens.

Besonderer Dank gebührt Dr. Henryk Laqua für seine konstante Unterstützung und den stets ergiebigen fachlichen Austausch sowie Dr. Travis Thompson für seine Hilfe und die Grundlagen, die diese Arbeit erst ermöglicht haben. Außerdem möchte ich Yannick Lemke und Dr. Felix Bangerter für die produktive und freundschaftliche Zusammenarbeit danken. Weiterer Dank gilt zudem allen ehemaligen und aktuellen Mitgliedern des Arbeitskreis Ochsenfeld für das freundliche und positive Arbeitsklima und die vielen hilfreichen wissenschaftlichen Diskussionen.

Mein herzlichster Dank gilt meinen Eltern Heidi und Werner sowie meinem Bruder Kai für ihre Unterstützung, Anleitung und Liebe während meiner Doktorarbeit und in meinem gesamten Leben. Schließlich möchte ich allen danken, die mich auf meinem Weg durch Freundschaft und finanzielle Unterstützung begleitet haben.

List of Publications

This cumulative dissertation comprises four articles submitted or published in peer-reviewed journals (**I**–**IV**). Each article is listed below, together with a description of the author's contributions.

I **L. Urban**, T. H. Thompson, and C. Ochsenfeld,
"A scaled explicitly correlated F12 correction to second-order Møller–Plesset perturbation theory",
J. Chem. Phys. **2021**, *154*, 044101,
Contributions by the author: *Parts of the derivation, all of the implementation, all calculations, and writing of the manuscript.*

II **L. Urban**, H. Laqua, and C. Ochsenfeld,
"Highly Efficient and Accurate Computation of Multiple Orbital Spaces Spanning Fock Matrix Elements on Central and Graphics Processing Units for Application in F12 Theory",
J. Chem. Theory Comput. **2022**, *18*, 4218,
Contributions by the author: *Most of the derivation, most of the implementation, all calculations, and writing of the manuscript.*

III **L. Urban**, H. Laqua, T. H. Thompson, and C. Ochsenfeld,
"Efficient Exploitation of Numerical Quadrature with Distance-Dependent Integral Screening in Explicitly Correlated F12 Theory: Linear Scaling Evaluation of the Most Expensive RI-MP2-F12 Term",
J. Chem. Theory Comput. **2024**, *20*, 3706,
Contributions by the author: *Parts of the derivation, most of the implementation, all calculations, and most of the writing of the manuscript.*

IV **L. Urban**, H. Laqua, T. H. Thompson, and C. Ochsenfeld,
"Formulation of an Efficient $\mathcal{O}(M^4)$-Scaling Explicitly Correlated MP2-F12 Correction by Combining Numerical Quadrature with Density Fitting and CABS-RI",
J. Chem. Theory Comput. **2026**, DOI: https://doi.org/10.1021/acs.jctc.5c01874,
Contributions by the author: *Most of the derivation, all of the implementation, all calculations, and writing of the manuscript.*

Abstract

One of the major obstacles in modern quantum chemistry is the need to employ exceedingly large one-electron basis sets in electron correlation methods to obtain reliably accurate results. The family of explicitly correlated wave function methods circumvents this issue by introducing terms that explicitly depend on the interelectronic distance, thereby enforcing the correct electron–electron cusp behavior, albeit at the cost of additional complicated many-electron integrals when evaluated without further approximation.
The main focus of the present work is the efficient, low-scaling evaluation of explicitly correlated approaches, examined here through the explicitly correlated correction to second-order Møller–Plesset perturbation theory (MP2-F12) as a representative example. While these methods are highly effective in reducing the basis set incompleteness error, the cost associated with the corresponding correction often far exceeds that of the underlying correlation method. To overcome these limitations, several techniques and strategies are introduced to significantly reduce computational demand and resolve the main bottlenecks that arise. A particularly straightforward approach is provided by the scaled MP2-F12 ansatz, which introduces a single empirically determined factor that scales the direct-type geminal–geminal terms to closely reproduce the MP2-F12 correction, thereby omitting the most expensive exchange-type contributions. Furthermore, the computation of Fock matrix elements spanning multiple orbital spaces is drastically accelerated by extending techniques originally developed for Hartree–Fock and density functional theory. The direct contributions are evaluated using a modified resolution-of-the-identity Coulomb (RI-J) approach employing the J-engine ansatz for integral construction, while the exchange contributions are treated via three-dimensional numerical quadrature in the form of the seminumerical snLinK method. These approaches reduce the computational cost by more than three orders of magnitude compared to the approximation-free evaluation while maintaining high accuracy, with additional speedups achieved by exploiting the massive parallelism of graphics processing units. The central focus of this work is the efficient decomposition of complicated exchange-type multi-electron integrals, where numerical quadrature plays a key role in improving performance. The complementary auxiliary basis set resolution of the identity (CABS-RI) reduces the most expensive exchange-type integral to a three-electron integral, which is then efficiently decomposed via numerical quadrature. In this context, a highly efficient batch-wise, distance-dependent integral screening exploiting the short-range behavior of F12 operators is introduced, significantly improving performance and enabling near-linear-scaling evaluations while retaining high accuracy. These strategies are extended to all exchange-type contributions in F12 theory, leading to an alternative formulation of integrals better suited for efficient factorization. A novel combination of numerical quadrature with density fitting is presented for the efficient computation of products of four-center two-electron integrals, alongside algorithms covering all exchange-type contributions, including advantageous batching strategies. In general, the formal computational cost with system size M is reduced from $\mathcal{O}(M^5)$ to $\mathcal{O}(M^4)$, with further improvements appearing feasible through the use of localized molecular orbitals combined with advanced integral screening techniques.

Contents

Chapter 1

Introduction

Quantum chemistry ultimately aims to solve the equations of motion for electrons and nuclei, revealing the governing principles and enabling fundamental understanding and reliable prediction of chemical phenomena. The quantum nature of these particles necessitates a description in terms of a wave function Ψ, which completely encodes the information about a system. Solving the Schrödinger equation,[1] the central equation of quantum mechanics, for Ψ allows in principle the exact computation of all corresponding non-relativistic properties. However, the complexity of many-body wave functions increases exponentially with the number of particles N, as they depend on $3N$ spatial and N spin coordinates, with fermionic antisymmetry imposing additional nodal constraints. This exponential scaling renders exact solutions intractable beyond the simplest systems. Consequently, much of the research in quantum chemistry since the early 20th century has been devoted to developing approximations that yield numerically accurate solutions while rendering chemical systems computationally tractable across all relevant domains.

A natural starting point for many modern electronic-structure methods is the mean-field approximation introduced by Hartree[2] and Fock[3] in the late 1920s. Within this approximation, the overwhelmingly complex many-electron problem is simplified by treating each electron as moving independently in an average potential created by all others. The resulting quantum state is represented by a single Slater determinant,[4] forming the basis of Hartree–Fock (HF) theory. Despite its conceptual elegance and ability to capture the dominant part of the total electronic energy, often close to 99% of the exact value, the HF approximation remains inherently limited because it neglects the comparatively small but essential correlation effects arising from instantaneous electron–electron interactions. Accurately describing these correlation effects is therefore a central challenge and driving motivation for developing more sophisticated quantum-chemical methods.

A conceptually straightforward solution of the Schrödinger equation that goes beyond the mean-field approximation is provided by the configuration interaction (CI) expansion.[4–6] Constructing the many-electron wave function as a linear combination of configuration states allows the description of electron correlation effects. Considering all possible states, known as full CI (FCI), yields the exact non-relativistic solution of a quantum system within a given one-particle basis. Despite the advantage of its formal rigor, the FCI ex-

pansion suffers from an exponential growth in the number of possible configurations with system size, rendering the computational cost prohibitive even on the most powerful modern classical hardware, except for a few atoms and small molecules with modest basis set sizes. A more practical approach to capture electron correlation relies on perturbation theory,[7] which was already well-established in classical physics before the advent of quantum mechanics, for instance in the computation of planetary orbits[8] or the theory of sound.[9] Partitioning the Hamiltonian into an exactly solvable zeroth-order part, capturing the dominant physics of the wave function, and a small perturbation yields an approximate solution to the many-body problem. The most widely used variant is Møller–Plesset perturbation theory (MPn),[10] with second-order MPn (MP2) offering a computationally more affordable description of correlation effects, scaling as $\mathcal{O}(M^5)$ with system size M, albeit at the cost of reduced accuracy compared to FCI. The coupled-cluster (CC) ansatz[11–13] further improves accuracy by describing electron correlation through an exponential parametrization of progressively higher excited cluster operators. The so-called gold standard of quantum chemistry for single-reference systems, CCSD(T),[14] combines CC with single and double excitations (CCSD) and adds perturbatively treated triple excitations. This approach captures a large portion of the electron correlation energy, although it comes with a formal $\mathcal{O}(M^7)$ computational scaling.

Besides the steep formal scaling of most electron correlation methods, these approaches suffer from substantial basis set incompleteness error (BSIE),[15] meaning that large one-electron basis sets are required to properly capture the underlying physics. The origin of this slow convergence has been understood since Kato's seminal work in the late 1950s,[16] which demonstrated that the exact electronic wave function has a discontinuous first derivative at electron coalescence ($r_{12} = 0$). Near these points, the wave function depends linearly on the interelectronic distance r_{12}, leading to the well-known electron–electron cusp conditions. Modern quantum chemistry has developed several approaches that incorporate interelectronic distances into the wave function description,[17–28] thereby introducing explicit multi-electron interactions that are absent in traditional excitation-based correlation methods. By directly describing the correct cusp behavior, these explicitly correlated methods significantly reduce the BSIE, albeit at the cost of introducing additional complicated molecular integrals not present in traditional quantum chemistry, which require efficient decomposition strategies for their practical and efficient evaluation.

This cumulative thesis comprises the work of **Publication I–IV**, introducing an empirical scaling technique and decomposition schemes specifically designed to reduce the computational cost of explicitly correlated methods. In Chapter 2, basic principles are introduced, starting with the Schrödinger equation, Hartree–Fock theory, and the definition of all relevant orbital spaces, followed by a discussion of static and dynamic correlation, combined with a survey of important traditional electron correlation methods that serve as the foundation for subsequent derivations. Chapter 3 begins with a discussion of finite basis set effects and the electron–electron cusp behavior of the exact multi-electron wave function, followed by an introduction to several explicitly correlated approaches. These methods are typically employed for highly accurate computations, with some even serving as bench-

mark methods that reach up to pico-Hartree accuracy.[29] The main focus lies on R12/F12 explicitly correlated theory,[25–28,30] the most popular and widely used explicitly correlated ansatz, with particular emphasis on its application to second-order Møller–Plesset perturbation theory.[26,27,31,32] The general derivation of the resulting R12/F12 correction is discussed, leading to the major direct- and exchange-type intermediates. In **Publication I**, an empirically scaled version of the MP2-F12 correction is introduced, which reproduces the unscaled F12 contribution to a high degree of accuracy. The approach leverages the fact that the MP2-F12 correction can be expressed as a pair theory, analogous to the corresponding correlation method, allowing direct-type geminal–geminal F12 contributions to be scaled while omitting the most expensive and rate-determining exchange-type intermediates. In contrast to most other empirically scaled correlation schemes, basis-set-specific scaling factors compensate for the faster convergence of triplet contributions toward the complete basis set limit. Significant speedups can be achieved, particularly for medium- to large-sized molecular systems, and the underlying concept can be readily extended to other types of F12 pair corrections.

Beyond empirically scaled approaches, the theoretical basis of various highly efficient many-electron integral decomposition schemes[33–41] and their combination within F12 theory is discussed. These schemes drastically reduce the computational cost of the main bottlenecks in MP2-F12, namely the evaluation of (F12-type) Fock matrix elements spanning multiple orbital spaces and the computation of complicated multi-electron integrals. In **Publication II**, the application of two of these decomposition strategies resolves the first bottleneck by factorizing direct- and exchange-type F12-type Fock matrices, extending techniques well known from self-consistent field (SCF) approaches. Direct-type elements are evaluated via an integral-direct resolution-of-the-identity Coulomb (RI-J)[42] method employing the J-engine ansatz to further accelerate the computation, while the exchange-type contribution is efficiently treated using sn-LinK,[43] a highly effective seminumerical exchange method. Although very large orbital spaces are considered, highly accurate results are obtained using standard auxiliary basis sets and modest integration grid sizes. While an approximation-free evaluation is computationally demanding, the combination of both approaches yields a drastically improved performance, achieving over three orders of magnitude faster evaluations, which can be further accelerated by exploiting the massively parallel nature of graphics processing units.

In **Publication III**, the efficient decomposition of exchange-type six-center three-electron integrals via numerical quadrature is demonstrated for the most expensive exchange contribution in RI-MP2-F12 theory. Through a more favorable factorization, the previously formal $\mathcal{O}(M^5)$ term can be rewritten as a three-electron integral that can be evaluated with formal $\mathcal{O}(M^3)$ time complexity. Furthermore, an efficient batch-wise, distance-dependent integral screening exploits the short-range behavior of the operators appearing in F12 theory based on integral partition bounds,[44] drastically reducing the cost of the required three-center one-electron integrals. Combined with efficient block-sparse linear algebra,[45] this enables a linear-scaling, atomic-orbital-based evaluation. The errors introduced by these approximations are negligible, and even higher accuracy than in the previous approach can

be achieved by increasing the numerical grid size. Overall, remarkable speedups of up to four orders of magnitude are obtained.
Extending these findings, first the approximation-free evaluation of all major intermediates appearing in MP2-F12 theory is discussed, and subsequently highly efficient routes for computing both direct- and exchange-type contributions are outlined. While the classical formulation already provides good performance for direct-type terms, **Publication IV** introduces an efficient numerical-quadrature-based decomposition of exchange contributions. By factorizing as many of the arising operator combinations as possible into three-electron integrals, which can be readily computed using the techniques developed in **Publication III**, more compact intermediates are obtained that allow for an increased amount of shared computation. The reformulation yields more favorable products of four-center two-electron integrals, which can be factorized through a novel decomposition scheme combining density fitting[34] with numerical quadrature.[38] Efficient algorithms covering all exchange-type contributions are presented, including advantageous batching strategies. The resulting approach achieves mean errors below 0.01 kcal/mol for representative benchmark sets of non-covalent interactions and isomerization energies using only small to moderate grid sizes, with the accuracy remaining tunable to balance numerical precision and computational effort. Overall, the method reduces the formal scaling of the F12 correction from $\mathcal{O}(M^5)$ to $\mathcal{O}(M^4)$ and yields substantial speedups for medium- to large-sized molecular systems, reaching approximately an order of magnitude faster evaluations. Further refinements appear possible through the use of localized molecular orbitals[46–51] in combination with suitable integral screening techniques.[44,52–62]
Although the techniques and strategies presented in this thesis were developed and examined in the context of MP2-F12, the general framework is equally applicable to other F12 approaches and to a broader range of explicitly correlated wave function methodologies. The present work could therefore lay the groundwork for enhancing the practical applicability of these methods by offering significant speedups at virtually no loss in accuracy.

Chapter 2

Basic Principles

In this work, both explicit and implicit summation notation are employed. Implicit summation arises when indices appear exclusively on a single side of an equation. Additionally, both the "physicist's" (Dirac) and "chemist's" (Mulliken) notations for molecular integrals are used.[63] The Dirac integral notation is employed for molecular integrals involving any number of electrons. For instance, for two real-valued n-electron functions g and h and an n-electron operator $\hat{O}_{1\ldots n}$, the integral is written as:

$$\langle g|\hat{O}_{1\ldots n}|h\rangle = \int dx_1 \cdots \int dx_n \, g^*(x_1,\ldots,x_n)\, \hat{O}_{1\ldots n}\, h(x_1,\ldots,x_n)\,, \tag{2.1}$$

where x denotes a general integration variable representing spatial and/or spin coordinates. Products of one-electron functions $g_1,\ldots,g_n$ and $h_1,\ldots,h_n$ are written as:

$$\langle g_1 \cdots g_n|\hat{O}_{1\ldots n}|h_1 \cdots h_n\rangle = \int dx_1 \cdots \int dx_n \, g_1^*(x_1)\cdots g_n^*(x_n)\, \hat{O}_{1\ldots n}\, h_1(x_1)\cdots h_n(x_n)\,. \tag{2.2}$$

For two-electron integrals, Mulliken notation is frequently employed. For example, an integral over four one-electron functions p, q, r, s and a multiplicative two-electron operator $\hat{G}_{12}$ takes the form:

$$(pq|\hat{G}_{12}|rs) = \int dx_1 \int dx_2 \, p^*(x_1) q(x_1)\, \hat{G}_{12}(x_1,x_2)\, r^*(x_2) s(x_2)\,. \tag{2.3}$$

2.1 The Schrödinger Equation

The fundamental equation of motion in quantum mechanics, which fully describes a non-relativistic system of N_e electrons and N_n nuclei, is given by the time-dependent Schrödinger equation[1] (TDSE)

$$i\hbar \frac{\partial}{\partial t}\Psi(\tau,t) = \hat{\mathcal{H}}\Psi(\tau,t)\,, \tag{2.4}$$

where the particle coordinate $\tau = (\boldsymbol{r},\omega)$ is decomposed into spatial coordinates $\boldsymbol{r} \in \mathbb{R}^{3(N_e+N_n)}$ and the associated spin variable ω. This equation states that the time derivative

of the system's wave function $\Psi(\tau, t)$ is determined by the action of the Hamiltonian $\hat{\mathcal{H}}$, which encodes the total kinetic and potential energy of all particles. In atomic units, the molecular Hamiltonian reads

$$\hat{\mathcal{H}} = -\sum_{A}^{N_n} \frac{\Delta_A}{2m_A} + \sum_{A}^{N_n} \sum_{B>A}^{N_n} \frac{Z_A Z_B}{r_{AB}} - \frac{1}{2} \sum_{i}^{N_e} \Delta_i - \sum_{i}^{N_e} \sum_{A}^{N_n} \frac{Z_A}{r_{iA}} + \sum_{i}^{N_e} \sum_{j>i}^{N_e} \frac{1}{r_{ij}}, \tag{2.5}$$

where Δ_i and Δ_A are the one-particle Laplacians of electrons and nuclei, r_{AB}, r_{iA}, and r_{ij} denote interparticle distances, and Z_A and m_A are the nuclear charges and masses, respectively. For a stationary state, the time-independence of the Hamiltonian implies via Noether's theorem[64] that the wave function's time dependence reduces to a pure phase factor $e^{-iEt/\hbar}$. Therefore, the TDSE reduces via separation of variables to the time-independent Schrödinger equation

$$\hat{\mathcal{H}}\Psi(\tau) = E\Psi(\tau), \tag{2.6}$$

determining the system's energy levels and the corresponding spatial distribution of the particles for a given electronic configuration. To further simplify this problem, the Born–Oppenheimer approximation[65] treats the motions of nuclei and electrons separately, based on the assumption that, due to the large mass difference, the electrons adapt instantaneously to the motion of the nuclei. Within this framework, the electronic structure is described in the field of stationary nuclei, resulting in the eigenvalue equation

$$\hat{H}\Psi(\tau) = E\Psi(\tau), \tag{2.7}$$

with the electronic Hamiltonian

$$\hat{H} = -\frac{1}{2} \sum_{i}^{N_e} \Delta_i - \sum_{i}^{N_e} \sum_{A}^{N_n} \frac{Z_A}{r_{iA}} + \sum_{i}^{N_e} \sum_{j>i}^{N_e} \frac{1}{r_{ij}}, \tag{2.8}$$

neglecting the nuclear kinetic energy, while the nucleus–nucleus interaction is treated separately as a fixed classical potential evaluated from point charges.
In this context, the exact many-electron wave function $\Psi(r_1, r_2, \ldots, r_{N_e})$ can be expressed as a linear combination of a complete set of N_e basis functions $\{\Phi_a\}$, each of which belongs to the N_e-fold antisymmetrized tensor product of the one-particle Hilbert space:

$$\Psi(\tau_1, \tau_2, \ldots, \tau_{N_e}) = \sum_{a} c_a \Phi_a(\tau_1, \tau_2, \ldots, \tau_{N_e}), \tag{2.9}$$

enabling a systematic and mathematically rigorous description of the exact physics of the system. The one-particle Hilbert space is spanned by a complete set of orthonormal, square-integrable spin orbitals ϕ_α ($\alpha \in \mathbb{N}$), each dependent on the electronic coordinate τ of a single electron with

$$\langle \phi_\alpha | \phi_\beta \rangle = \int \phi_\alpha^*(\tau_1) \phi_\beta(\tau_1)\, d\tau_1 = \delta_{\alpha\beta}, \tag{2.10}$$

with the Kronecker delta $\delta_{\alpha\beta}$. These orbitals are separable into spatial and spin components:

$$\phi_\alpha(\tau_1) = \varphi_\alpha(\boldsymbol{r}_1) s_\alpha(\omega_1)\,, \tag{2.11}$$

where the spin functions s_α take one of two possible forms, $s_\alpha \in \{s_\uparrow, s_\downarrow\}$, satisfying

$$\int s_\uparrow^*(\omega) s_\uparrow(\omega)\, d\omega = \int s_\downarrow^*(\omega) s_\downarrow(\omega)\, d\omega = 1, \quad \int s_\uparrow^*(\omega) s_\downarrow(\omega)\, d\omega = 0\,. \tag{2.12}$$

To enforce the exact antisymmetry principle,[66,67] which generalizes Pauli's exclusion principle,[68] the many-electron wave function must be antisymmetric with respect to the exchange of any two electronic coordinates. Within a complete set of orthonormal spin-orbital basis functions, the antisymmetry requirement can be compactly represented by a single Slater determinant[4] as

$$\Phi_a(\tau_1, \tau_2, \ldots, \tau_{N_e}) = \frac{1}{\sqrt{N_e!}} \begin{vmatrix} \phi_{\alpha_1}(\tau_1) & \phi_{\alpha_1}(\tau_2) & \cdots & \phi_{\alpha_1}(\tau_{N_e}) \\ \phi_{\alpha_2}(\tau_1) & \phi_{\alpha_2}(\tau_2) & \cdots & \phi_{\alpha_2}(\tau_{N_e}) \\ \vdots & \vdots & \ddots & \vdots \\ \phi_{\alpha_{N_e}}(\tau_1) & \phi_{\alpha_{N_e}}(\tau_2) & \cdots & \phi_{\alpha_{N_e}}(\tau_{N_e}) \end{vmatrix}, \tag{2.13}$$

describing a specific configuration of spin orbitals. Solving for the exact many-electron wave function is extremely challenging, as the number of possible configurations grows combinatorially with the number of electrons, and an infinite basis cannot be realized in practice. Consequently, electronic structure calculations rely on various approximations, giving rise to a wide range of methods across quantum chemistry. Most of these approaches remain guided by the theoretical principles outlined above, aiming to reduce computational cost while trying to maintain accuracy. In particular, the choice of the one-electron basis is crucial to capture a sufficiently large portion of the Hilbert space and accurately describe the underlying physics.

2.2 Hartree–Fock Theory

Hartree–Fock (HF) theory[2,3,69] occupies a fundamental position in quantum chemistry as the simplest approach that rigorously incorporates wave function antisymmetry when solving the electronic Schrödinger equation (Eq. 2.7) for many-electron ground states. Beyond its intrinsic value, HF theory serves as the cornerstone for virtually all correlated methods that achieve higher accuracy. The central approximation in HF theory is the representation of the complex many-electron wave function by a single Slater determinant Φ_{HF}, constructed from N_e orthonormal spin-orbitals ϕ_i ($i \in \{1, \ldots, N_e\}$). Substituting this ansatz into the general expression for the expectation value of the electronic Hamiltonian

$$E = \langle \Psi | \hat{H} | \Psi \rangle = \int d\tau_1 \cdots \int d\tau_{N_e} \Psi^*(\tau_1, \ldots, \tau_{N_e}) \hat{H}\, \Psi(\tau_1, \ldots, \tau_{N_e})\,, \tag{2.14}$$

and employing the Slater–Condon rules for determinantal wave functions,[4,6] leads to the Hartree–Fock energy

$$E_{\mathrm{HF}} = \langle \Phi_{\mathrm{HF}} | \hat{H} | \Phi_{\mathrm{HF}} \rangle = \sum_{i}^{N_e} \langle \phi_i | \hat{h}_i | \phi_i \rangle + \sum_{i}^{N_e} \sum_{j>i}^{N_e} \Big[\langle ij|ij\rangle - \langle ij|ji\rangle \Big] , \tag{2.15}$$

where the one-electron Hamiltonian incorporates both the kinetic energy and nuclear attraction operators:

$$\hat{h}_i = -\frac{1}{2}\Delta_i - \sum_{A}^{N_n} \frac{Z_A}{r_{iA}} . \tag{2.16}$$

To determine the precise form of the molecular orbitals (MOs) employed in a Slater determinant ansatz, one minimizes the Hartree–Fock energy expression (Eq. 2.15) according to the variational principle while simultaneously ensuring MO orthonormality

$$\frac{\delta E_{\mathrm{HF}}}{\delta \phi_i} = 0 \quad \text{with} \quad \langle \phi_i | \phi_j \rangle = \delta_{ij} \tag{2.17}$$

using Lagrange's method of constrained optimization. This yields the general Hartree–Fock equations, which can be transformed into their canonical form by exploiting the invariance of the Fock operator $\hat{f}$ under unitary orbital transformations. By diagonalizing the Lagrange multiplier matrix $\boldsymbol{\varepsilon}$, one obtains the canonical Hartree–Fock equations:

$$\hat{f}\phi_i(\tau) = \varepsilon_i \phi_i(\tau) , \tag{2.18}$$

where ε_i denotes the orbital energy eigenvalues. The single-particle Fock operator

$$\hat{f} = \hat{t} + \hat{v} + \hat{j} - \hat{k} \tag{2.19}$$

consists of four operators: the kinetic energy operator $\hat{t}$, the nuclear attraction operator $\hat{v}$, and the mean-field Coulomb and exchange operators $\hat{j}$ and $\hat{k}$, whose action on a MO ϕ_i is given by

$$\hat{t}\phi_i(\tau_1) = -\frac{1}{2}\Delta_1 \, \phi_i(\tau_1) , \tag{2.20}$$

$$\hat{v}\phi_i(\tau_1) = -\sum_{A}^{N_n} Z_A \frac{\phi_i(\tau_1)}{r_{1A}} , \tag{2.21}$$

$$\hat{j}\,\phi_i(\tau_1) = \sum_{j}^{N_e} \left[\int d\tau_2 \frac{|\phi_j(\tau_2)|^2}{r_{12}} \right] \phi_i(\tau_1) , \tag{2.22}$$

$$\hat{k}\phi_i(\tau_1) = \sum_{j}^{N_e} \left[\int d\tau_2 \frac{\phi_j^*(\tau_2)\phi_i(\tau_2)}{r_{12}} \right] \phi_j(\tau_1) . \tag{2.23}$$

For a numerical solution of the canonical Hartree–Fock equations (Eq. 2.18), the spatial parts φ_i of the molecular orbitals $\phi_i = \varphi_i s_i$ are typically expanded in a fixed, generally non-orthogonal, atom-centered Gaussian-type basis set $\{\chi_\mu\}$ with N_b basis functions ($\mu \in \{1, \ldots, N_b\}$), according to the linear combination of atomic orbitals (LCAO) ansatz:

$$\varphi_i = \sum_\mu c_{\mu i}\, \chi_\mu \,, \tag{2.24}$$

with linear expansion coefficients $c_{\mu i}$. The canonical Hartree–Fock equations, when combined with the LCAO ansatz, transform into a generalized eigenvalue problem known as the Roothaan–Hall equations:[70]

$$\mathbf{FC} = \mathbf{SC}\boldsymbol{\varepsilon} \,, \tag{2.25}$$

where $\mathbf{S}$ denotes the overlap matrix and $\mathbf{F}$ the Fock matrix, with the corresponding matrix elements

$$S_{\mu\nu} = \langle \chi_\mu | \chi_\nu \rangle \,, \tag{2.26}$$

$$f_{\mu\nu} = \langle \chi_\mu | \hat{f} | \chi_\nu \rangle \,, \tag{2.27}$$

and coefficient matrix $\mathbf{C}$. To circumvent the issue of solving the Roothaan–Hall equations in a non-orthogonal basis, which complicates their direct solution, Löwdin symmetric orthogonalization[71] of the basis functions is typically introduced. This leads to the orthogonalized Fock matrix

$$\mathbf{F}' = \mathbf{S}^{-\frac{1}{2}} \mathbf{F} \mathbf{S}^{-\frac{1}{2}} \tag{2.28}$$

and the transformed coefficient matrix

$$\mathbf{C}' = \mathbf{S}^{\frac{1}{2}} \mathbf{C} \,, \tag{2.29}$$

such that the Roothaan–Hall equations reduce to a conventional eigenvalue problem in an orthonormal basis:

$$\mathbf{F}'\mathbf{C}' = \mathbf{C}'\boldsymbol{\varepsilon} \,, \tag{2.30}$$

where $\mathbf{C}'$ contains the MO coefficients in the orthogonalized spatial basis, and $\boldsymbol{\varepsilon}$ is the diagonal matrix of orbital energies. The associated molecular orbitals are obtained by combining the N_b spatial orbitals with their corresponding spin functions. Since the Coulomb and exchange operators, $\hat{\jmath}$ and $\hat{k}$, depend on the computed orbitals themselves, an iterative solution is required. In each iteration, the Fock operator is constructed from the orbitals obtained in the previous step, starting from a suitable initial guess, until a convergence criterion is met. This iterative procedure, which ensures mutual consistency between the orbitals and the Fock operator, is known as the self-consistent field (SCF) method. Upon convergence, the N_e lowest-energy spin-orbitals define the *occupied* space and provide the optimal single-determinant approximation to the wave function in the given basis, with the remaining *virtual* orbitals corresponding to unoccupied one-electron states that can be used to describe correlated ground-states as well as electronic excitations.

Within the SCF procedure, the $\mathcal{O}(N_b^4)$ evaluation of the Fock matrix $f_{\mu\nu}$ elements from the density matrix elements

$$P_{\mu\nu} = \sum_i c_{\mu i} c_{\nu i} \tag{2.31}$$

constitutes the principal computational bottleneck. Here, the construction of the Coulomb matrix elements

$$j_{\mu\nu} = \langle \chi_\mu | \hat{j} | \chi_\nu \rangle = \sum_{\lambda\sigma} P_{\lambda\sigma} (\mu\nu|\lambda\sigma) \tag{2.32}$$

and the elements of the exchange matrix

$$k_{\mu\nu} = \langle \chi_\mu | \hat{k} | \chi_\nu \rangle = \sum_{\lambda\sigma} P_{\lambda\sigma} (\mu\sigma|\lambda\nu) \tag{2.33}$$

are by far the most demanding steps. Consequently, a variety of efficient strategies have been devised to reduce the computational effort.[42,43,72–77] In **Publication II**, these concepts are extended to multiple orbital spaces spanning Fock matrix elements beyond HF theory, and the theoretical details are provided in Section 3.3.5.

2.3 Orbital Spaces

Table 2.1 summarizes the orbital notation employed throughout this thesis and provides a consistent reference, particularly important for the discussion of orbital spaces in Chapter 3 where different explicitly correlated approaches are examined. The atomic orbital space is spanned by non-orthogonal, atom-centered, Gaussian-type basis functions, whereas the molecular orbitals are orthogonal and constructed via the linear combination of atomic orbitals approach. A clear distinction between the Hartree–Fock AO and MO spaces and their corresponding complementary spaces, as well as their finite approximations, is essential for understanding explicitly correlated methods. The complementary AO $\{\underline{\mu}\}$ and MO $\{\underline{\alpha}\}$ spaces are formally defined by excluding the occupied Hartree–Fock orbitals $\{\mu\}$ (AO) and $\{p\}$ (MO) from the complete spaces $\{\overline{\mu}\}$ (AO) and $\{\overline{\alpha}\}$ (MO), respectively. In practice, these complementary spaces are approximated by finite auxiliary AO $\{\mu''\}$ and MO $\{p''\}$ basis sets. By including a sufficiently large set of auxiliary functions, one can achieve nearly complete coverage of the formally infinite complementary space, thereby reducing errors to negligible levels in the corresponding quantum chemical calculations.

Table 2.1: Orbital spaces and notation adopted throughout this thesis

Description	Indices	Cardinality
HF AO basis (non-orthogonal)	$\mu, \nu, \lambda, \sigma, \ldots$	$N_\mu = N_b$
Complete AO basis set (AO CBS, non-orthogonal)	$\overline{\mu}, \overline{\nu}, \overline{\lambda}, \overline{\sigma}, \ldots$	$N_{\overline{\mu}}$
Complement of the AO HF space in the AO CBS $\{\underline{\mu}\} = \{\overline{\mu}\} \backslash \{\mu\}$ (non-orthogonal)	$\underline{\mu}, \underline{\nu}, \underline{\lambda}, \underline{\sigma}, \ldots$	$N_{\underline{\mu}}$
Approximate AO complement-spanning auxiliary set (AO CABS, non-orthogonal)	$\mu'', \nu'', \lambda'', \sigma'', \ldots$	$N_{\mu''}$
Union of AO HF and AO CABS space $\{\mu'\} = \{\mu\} \cup \{\mu''\}$ (non-orthogonal)	$\mu', \nu', \lambda', \sigma', \ldots$	$N_{\mu'}$
Approximate AO CBS-spanning auxiliary set (non-orthogonal)	$P, Q, R, S, \ldots$	N_P
Arbitrary HF orbitals	$p, q, r, s, \ldots$	N_p
HF occupied orbitals (active)	i, j	$N_i = N_{\text{act.}}$
HF occupied orbitals	$k, l, m, n, \ldots$	$N_k = N_e$
HF virtual orbitals	$a, b, c, d, \ldots$	N_a
Complete one-electron basis set (CBS)	$\overline{\alpha}, \overline{\beta}, \overline{\gamma}, \overline{\delta}, \ldots$	$N_{\overline{\alpha}}$
Complement of HF space in CBS space $\text{span}(\{\underline{\alpha}\}) = \text{span}(\{\bar{\alpha}\}) \cap \text{span}(\{p\})^\perp$	$\underline{\alpha}, \underline{\beta}, \underline{\gamma}, \underline{\delta}, \ldots$	$N_{\underline{\alpha}}$
Approximate complement-spanning auxiliary set (CABS, orthogonal)	$p'', q'', r'', s'', \ldots$	$N_{p''}$
Union of HF and CABS space $\{p'\} = \{p\} \cup \{p''\}$ (orthogonal)	$p', q', r', s', \ldots$	$N_{p'}$

2.4 Electron Correlation

To capture the true nature of electron–electron interactions, a single-determinant approach such as Hartree–Fock theory proves insufficient. While the HF ansatz correctly accounts for the exchange (Fermi) correlation between electrons of the same spin through the antisymmetrization of the wave function, it fails to describe the instantaneous correlation arising from Coulomb repulsion between all electron pairs. The missing correlation energy, frequently defined as the difference between the exact non-relativistic energy and the Hartree–Fock limit, is entirely neglected by mean-field approximations.[63]

Electron correlation is commonly classified into two major types that mutually influence each other: *static* and *dynamic* correlation.[78] Static correlation (also known as non-dynamical or strong correlation) arises in systems where a single reference determinant fails to provide an adequate description of the electronic structure. This situation typically occurs in systems with (near-)degenerate electronic states, characterized by small gaps be-

tween the highest occupied molecular orbital (HOMO) and lowest unoccupied molecular orbital (LUMO), which arise for example in bond-breaking scenarios, diradical species, or transition metal complexes with partially filled *d*-orbitals. To account for the necessary physics, multiple reference determinants are required to construct a proper zeroth-order wave function. On the other hand, (short-ranged) dynamic correlation describes the spin-independent, instantaneous repulsion between electron pairs, manifested as Coulomb holes,[16,79] regions of reduced electron probability density. To overcome the limitations of the HF mean-field approach, so-called *excited* determinants are introduced, in which some of the occupied ground-state orbitals are replaced by virtual orbitals, allowing for a more flexible electronic structure that better captures the underlying physics. The following discussion primarily focuses on methods for an improved treatment of dynamic correlation, where a single determinant reference provides a suitable starting point. Nevertheless, many of the techniques and concepts presented can be extended to multi-reference approaches, thereby enhancing the description of electronic correlation in strongly correlated systems.

2.4.1 Configuration Interaction

The oldest systematic and conceptually most straightforward way to treat electron correlation in atoms and molecules is provided by a configuration interaction (CI) wave function ansatz,[4–6,70,80–82] which expands the electronic wave function as a linear combination of Slater determinants or, more generally, spin-adapted configuration state functions (CSFs). Following the Ritz variational principle,[83] expansion coefficients for each CSF are optimized to minimize the electronic energy. Since the canonical Hartree–Fock determinant already captures a substantial portion of the total energy and often provides a qualitatively correct description of the electronic structure, it is typically used as the starting point of a finite determinant expansion. The strength of the CI ansatz lies in its conceptual simplicity while allowing, in principle, for an exact solution of the many-electron problem in a given basis. Including all possible configuration state functions in the expansion leads to full configuration interaction (FCI), which can formally be written as

$$\Phi_{\mathrm{FCI}} = (1 + \sum_{ia} c_i^a \hat{a}_a^\dagger \hat{a}_i + \sum_{\substack{i<j \\ a<b}} c_{ij}^{ab} \hat{a}_a^\dagger \hat{a}_b^\dagger \hat{a}_j \hat{a}_i + \sum_{\substack{i<j<k \\ a<b<c}} c_{ijk}^{abc} \hat{a}_a^\dagger \hat{a}_b^\dagger \hat{a}_c^\dagger \hat{a}_k \hat{a}_j \hat{a}_i + \dots)\Phi_{\mathrm{HF}}\,, \tag{2.34}$$

with *annihilation* operator $\hat{a}_i$ removing an electron from the occupied orbital ϕ_i, *creation* operator $\hat{a}_a^\dagger$ adding an electron to the virtual orbital ϕ_a, and variationally determined optimal expansion coefficients $(c_i^a, c_{ij}^{ab}, c_{ijk}^{abc}, \dots)$. The resulting determinants are classified as singly, doubly, triply, ... excited determinants, where all possible excitations of the corresponding order are considered. Truncation of the expansion at a specific excitation level yields the systematic CI hierarchy of methods (CIS, CISD, CISDT, ...), which provides an increasingly accurate description of electron correlation. In practice, FCI becomes computationally intractable for all but very small systems within a given one-electron basis, as the number of determinants scales combinatorially as $\binom{2N_b}{N_e}$. For instance, already a system of 10 electrons with 100 spin orbitals (50 spatial basis functions) generates approximately

1.7×10^{13} possible Slater determinants when symmetry restrictions are neglected, rendering FCI calculations impractical for systems with more than a few atoms.

2.4.2 Second-Order Møller–Plesset Perturbation Theory

Within the framework of Rayleigh–Schrödinger perturbation theory (RSPT),[7,9] the approximate solution for a non-degenerate many-body quantum system is obtained by partitioning the system's Hamiltonian $\hat{H}$ into an exactly solvable zeroth-order Hamiltonian $\hat{H}_0$, which captures the dominant physics of the reference wave function, and a perturbation operator $\hat{V}$, which describes the residual interactions. Formally, this partitioning can be expressed as

$$\hat{H} = \hat{H}_0 + \lambda \hat{V}, \tag{2.35}$$

where λ is a formal perturbation parameter (typically set to unity) that allows for a systematic expansion of the energy and wave function in powers of the perturbation, given by the Taylor series:

$$E_0 = E_0^{(0)} + \lambda E_0^{(1)} + \lambda^2 E_0^{(2)} + \dots \tag{2.36}$$

$$\Phi_0 = \Phi_0^{(0)} + \lambda \Phi_0^{(1)} + \lambda^2 \Phi_0^{(2)} + \dots \tag{2.37}$$

Substituting Eq. 2.35 and Eqs. 2.36–2.37 into the Schrödinger equation yields

$$\begin{aligned} (\hat{H}_0 + \lambda \hat{V}) \Big(\Phi_0^{(0)} + \lambda \Phi_0^{(1)} + \lambda^2 \Phi_0^{(2)} + \dots \Big) \\ = \Big(E_0^{(0)} + \lambda E_0^{(1)} + \lambda^2 E_0^{(2)} + \dots \Big) \Big(\Phi_0^{(0)} + \lambda \Phi_0^{(1)} + \lambda^2 \Phi_0^{(2)} + \dots \Big) \end{aligned} \tag{2.38}$$

which allows for a systematic ordering according to powers of λ:

$$\hat{H}_0 \, |\Phi_0^{(0)}\rangle = E_0^{(0)} \, |\Phi_0^{(0)}\rangle \tag{2.39}$$

$$\hat{H}_0 \, |\Phi_0^{(1)}\rangle + \hat{V} \, |\Phi_0^{(0)}\rangle = E_0^{(0)} \, |\Phi_0^{(1)}\rangle + E_0^{(1)} \, |\Phi_0^{(0)}\rangle \tag{2.40}$$

$$\hat{H}_0 \, |\Phi_0^{(2)}\rangle + \hat{V} \, |\Phi_0^{(1)}\rangle = E_0^{(0)} \, |\Phi_0^{(2)}\rangle + E_0^{(1)} \, |\Phi_0^{(1)}\rangle + E_0^{(2)} \, |\Phi_0^{(0)}\rangle \tag{2.41}$$

$$\vdots$$

Applying intermediate normalization ($\langle \Phi_0^{(0)} | \Phi_0 \rangle = 1$ and $\langle \Phi_0^{(0)} | \Phi_0^{(k)} \rangle = 0$ for all $k \geq 1$) and projecting onto the zeroth-order wave function $\langle \Phi_0^{(0)}|$ results in the energy corrections for different orders:

$$E_0^{(0)} = \langle \Phi_0^{(0)} | \hat{H}_0 | \Phi_0^{(0)} \rangle \tag{2.42}$$

$$E_0^{(1)} = \langle \Phi_0^{(0)} | \hat{V} | \Phi_0^{(0)} \rangle \tag{2.43}$$

$$E_0^{(2)} = \langle \Phi_0^{(0)} | \hat{V} | \Phi_0^{(1)} \rangle \tag{2.44}$$

$$\vdots$$

The corresponding wave function corrections can generally be expanded via

$$\Phi_k^{(n)} = \sum_{m \neq k} c_m^{(n)} \, \Phi_m^{(0)} \,, \tag{2.45}$$

which simplifies for the first-order correction to

$$\Phi_0^{(1)} = \sum_{m \neq 0} c_m^{(1)} \, \Phi_m^{(0)} \quad \text{with} \quad c_m^{(1)} = -\frac{\langle \Phi_m^{(0)} | \hat{V} | \Phi_0^{(0)} \rangle}{E_m^{(0)} - E_0^{(0)}} \,, \tag{2.46}$$

leading to the second-order energy correction

$$E_0^{(2)} = \langle \Phi_0^{(0)} | \hat{V} | \Phi_0^{(1)} \rangle = \sum_{m \neq 0} \frac{\left| \langle \Phi_0^{(0)} | \hat{V} | \Phi_m^{(0)} \rangle \right|^2}{E_0^{(0)} - E_m^{(0)}} \,. \tag{2.47}$$

Extending the RSPT framework to the Slater determinant ansatz has proven highly successful for the treatment of many-electron systems.[78] This approach forms the basis of Møller–Plesset perturbation theory (MPn),[10] a standard method in quantum chemistry. Within this context, the zeroth-order Hamiltonian is typically chosen as the sum of Fock operators,

$$\hat{H}_0 = \sum_i^{N_e} \hat{f}_i \,, \tag{2.48}$$

while the perturbation operator accounts for the residual electron–electron interactions beyond the mean-field approximation

$$\hat{V} = \sum_{i<j}^{N_e} \frac{1}{r_{ij}} - \sum_i^{N_e} (\hat{\jmath}_i - \hat{k}_i) \,. \tag{2.49}$$

At zeroth order, the energy is given by the sum of the occupied orbital energies, and the addition of the first-order perturbative contribution reproduces the Hartree–Fock energy exactly

$$\langle \Phi_0^{(0)} | \hat{H}_0 + \hat{V} | \Phi_0^{(0)} \rangle = E_0^{(0)} + E_0^{(1)} = E_{\text{HF}} \,. \tag{2.50}$$

The first explicit treatment of dynamical correlation is then provided by the second-order correction, yielding the second-order Møller–Plesset (MP2) energy

$$E_{\text{MP2}} = \sum_a \frac{\left| \langle \Phi_{\text{HF}} | \hat{H} - \sum_k^{N_e} \hat{f}_k | \Phi_a \rangle \right|^2}{\left(\sum_i^{N_e} \varepsilon_i \right) - E_a} \,, \tag{2.51}$$

where a runs over all excited determinants Φ_a with zeroth-order eigenvalues (sums of orbital energies) E_a. Due to Brillouin's theorem,[84,85] contributions from singly excited determinants vanish, while the Slater–Condon rules ensure that matrix elements between determinants differing by more than two spin orbitals are strictly zero. As a result, only doubly excited determinants contribute to the MP2 energy, leading to the compact expression

$$E_{\text{MP2}} = -\tfrac{1}{2} \sum_{ijab} \frac{\left| \langle ij | r_{12}^{-1} | | ab \rangle \right|^2}{\varepsilon_a + \varepsilon_b - \varepsilon_i - \varepsilon_j} \,, \tag{2.52}$$

with $||ab\rangle$ denoting the antisymmetrized two-electron state $||ab\rangle = 2^{-1/2}(|ab\rangle - |ba\rangle)$. Equation 2.52 also shows that the MP2 correlation energy can be expressed as a sum of pair contributions, $E_{\mathrm{MP2}} = \sum_{ij} e_{ij}^{\mathrm{MP2}}$. The exact second-order pair energies e_{ij}^{exact} can be defined through the variational minimization of the Hylleraas pair functional[81,86]

$$J_{ij}^2[u_{ij}] = \langle u_{ij}| \hat{f}_1 + \hat{f}_2 - \varepsilon_i - \varepsilon_j |u_{ij}\rangle + 2\,\langle u_{ij}|\, r_{12}^{-1}||ij\rangle \ , \tag{2.53}$$

where u_{ij} is an abstract two-electron state. In the complete basis set limit, eqs. 2.52 and 2.53 become equivalent, since the first-order wave function can then be expanded exactly in terms of doubly excited determinants. The conventional MP2 expression is recovered by inserting the linear ansatz

$$|u_{ij}^{\mathrm{MP2}}\rangle = \sum_{a<b} t_{ij}^{ab}||ab\rangle \ , \tag{2.54}$$

where the amplitudes t_{ij}^{ab} are obtained as variational parameters minimizing J_{ij}^2. Expressing the MP2 energy through the Hylleraas pair functional provides the natural foundation for introducing explicit correlation into MP2 theory, as discussed in Section 3.3.1.

2.4.3 Coupled-Cluster Theory

The coupled-cluster (CC) ansatz[11–14,87,88] is widely regarded as the leading approach for highly accurate dynamical correlation calculations in single-reference systems. It provides near-exact results at a computational cost that, although demanding, remains manageable for systems of moderate size. This approach is based on describing dynamical correlation via so-called cluster functions, e.g., the two-electron cluster function

$$d_{ij}(\tau_m, \tau_n) = \sum_{a>b} t_{ij}^{ab}\phi_a(\tau_m)\phi_b(\tau_n) \tag{2.55}$$

with cluster amplitudes t_{ij}^{ab}, which go beyond the Hartree–Fock independent-particle approximation by accounting for simultaneous pair excitations from occupied orbitals i, j to virtual orbitals a, b, thereby capturing instantaneous electron–electron correlation effects neglected at the mean-field level. Inserting d_{ij} into the HF Slater determinant Φ_{HF} leads to a first description of a correlated wave function

$$\Phi_{\mathrm{corr.}} = |[\phi_i(\tau_1)\phi_j(\tau_2) + d_{ij}(\tau_1, \tau_2)]\ldots\phi_l(\tau_{N_e})\rangle \tag{2.56}$$

$$= \Phi_{\mathrm{HF}} + \sum_{a>b} t_{ij}^{ab}\,|\phi_a(\tau_1)\phi_b(\tau_2)\ldots\phi_l(\tau_{N_e})\rangle \ , \tag{2.57}$$

as a linear combination of doubly excited Slater determinants built upon the reference. Systematically including cluster functions involving different numbers of orbitals yields an increasingly accurate treatment of dynamical correlation. This motivates the formulation of cluster operators, which for single and double excitations are conveniently expressed in

second quantization as

$$\hat{T}_1 = \sum_{ia} t_i^a \, \hat{a}_a^\dagger \hat{a}_i \,, \tag{2.58}$$

$$\hat{T}_2 = \frac{1}{4} \sum_{ijab} t_{ij}^{ab} \, \hat{a}_a^\dagger \hat{a}_b^\dagger \hat{a}_j \hat{a}_i \,, \tag{2.59}$$

and more generally

$$\hat{T}_n = \frac{1}{(n!)^2} \sum_{ij\ldots ab\ldots} t_{ij\ldots}^{ab\ldots} \, \hat{a}_a^\dagger \hat{a}_b^\dagger \ldots \hat{a}_j \hat{a}_i \ldots \,, \tag{2.60}$$

representing the n-fold cluster operator. Exploiting the commutation properties of the cluster operators, the resulting terms then naturally form the power-series expansion of an exponential function.

$$e^{\hat{T}} = 1 + \hat{T} + \frac{1}{2!}\hat{T}^2 + \frac{1}{3!}\hat{T}^3 + \ldots \,, \tag{2.61}$$

with $\hat{T} = \sum_{n=1}^{N_e} \hat{T}_n$. Expanding the powers of $\hat{T}$ generates all possible excitations and their products, such as $\hat{T}_1^2$, $\hat{T}_1\hat{T}_2$, $\hat{T}_2^2$, etc. The coupled-cluster wave function can thus be written as

$$|\Psi_{\mathrm{CC}}\rangle = e^{\hat{T}} \, |\Phi_{\mathrm{HF}}\rangle \,, \tag{2.62}$$

which yields the exact solution within a given one-particle basis when the full cluster expansion is employed. Insertion into the electronic Schrödinger equation leads to the similarity-transformed form

$$e^{-\hat{T}} \hat{H} e^{\hat{T}} \, |\Phi_{\mathrm{HF}}\rangle = E_{\mathrm{CC}} \, |\Phi_{\mathrm{HF}}\rangle \,, \tag{2.63}$$

where the non-Hermitian operator $e^{-\hat{T}} \hat{H} e^{\hat{T}}$ ensures that the exponential parametrization can be handled algebraically. Projection onto the Hartree–Fock reference determinant gives the CC energy expression

$$E_{\mathrm{CC}} = \langle \Phi_{\mathrm{HF}} | \, e^{-\hat{T}} \hat{H} e^{\hat{T}} \, |\Phi_{\mathrm{HF}}\rangle \,. \tag{2.64}$$

In practice, the CC ansatz relies on truncation of the cluster operator $\hat{T}$ at a given excitation level to remain computationally tractable, defining a hierarchy of methods (CCS, CCSD, CCSDT, ...). In contrast to truncated configuration interaction (CI), these approximations retain both size consistency and size extensivity, as the exponential ansatz implicitly includes disconnected excitations. Amplitudes of determinants not explicitly contained in $\hat{T}$ are represented as products of lower-order amplitudes, allowing truncated methods such as CCSD to capture a substantial portion of the correlation energy efficiently. The corresponding cluster amplitudes are obtained by projection of the similarity-transformed Schrödinger equation onto the set of excited determinants

$$\langle \Phi_{ij\ldots}^{ab\ldots} | \, e^{-\hat{T}} \hat{H} e^{\hat{T}} \, |\Phi_{\mathrm{HF}}\rangle = 0 \,, \tag{2.65}$$

from which the amplitudes are determined iteratively. Since truncated CC methods are not variational, the resulting energy may occasionally lie slightly below the exact value, which is typically tolerated due to the remarkable accuracy achieved in practice, particularly for relative energies where systematic errors often partially cancel.[89]

Chapter 3

Explicit Correlation

3.1 Finite Basis Effects and the Electronic Cusps

The choice of the one-electron basis set is crucial for the accuracy of quantum-chemical methods and, consequently, for the predictive capability of calculated energies and properties. Since exact electronic wave functions can only be expressed in closed form for one-electron systems, all practical quantum-chemical applications necessarily rely on finite basis sets. This truncation introduces a systematic basis set incompleteness error (BSIE),[15] defined as the deviation from the complete basis set (CBS) limit, which ultimately constrains the attainable accuracy, as illustrated in Figure 3.1.

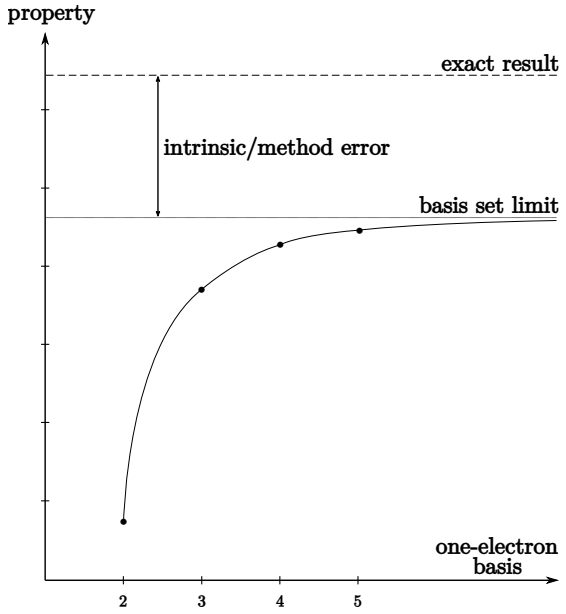

Figure 3.1: Qualitative illustration of the basis set incompleteness error (BSIE) for increasingly large finite one-electron basis sets (2, 3, 4, 5, ...), compared to the intrinsic/method error.

The magnitude of the BSIE differs notably between Hartree–Fock and correlated methods. While the HF energy converges relatively quickly with increasing basis set size, post-HF correlation methods (see Sections 2.4.1–2.4.3) exhibit much slower convergence, requiring prohibitively large basis sets to approach their CBS limit.[90] To systematically improve the completeness of a basis set, additional shells with higher total angular momentum L are added, allowing the wave function to relax more fully in Hilbert space and yielding a more accurate description of the electronic structure. For atoms, the correlation energy convergence was shown to follow an inverse cubic trend with $\mathcal{O}((L+1)^{-3})$,[91–97] reflecting a rather poor convergence rate.

This difference in BSIE convergence between Hartree–Fock and correlated methods originates from the underlying physical nature. The mean-field approximation in HF can be described accurately with a comparatively modest subset of basis functions, whereas correlated methods aim to approximate the exact eigenfunction of the electronic Hamiltonian, $\hat{H}$, requiring a more flexible and extensive basis set. The origin of this slow convergence has been understood since Kato's seminal work in the late 1950s,[16] which demonstrated that the exact electronic wave function exhibits a discontinuity in its first derivative at points of electron coalescence ($r_{12} = 0$). In the vicinity of these points, the wave function depends linearly on the interelectronic distance r_{12}, leading to the formulation of the electron–electron *cusp conditions*[16,98] for regions close to coalescence

$$\Psi^{(1)} = \frac{r_{12}}{2(s+1)}\,\Psi^{(0)} + \mathcal{O}(r_{12}^2)\,, \tag{3.1}$$

where $s = 0$ and $s = 1$ correspond to singlet (s-wave) and triplet (p-wave) spin states, respectively. Here, $\Psi^{(1)}$ denotes the first-order perturbative correction to the zeroth-order wave function $\Psi^{(0)}$, in which the purely electronic Coulomb interaction perturbs the nuclear Hamiltonian. The spin-dependent prefactor $\big(2(s+1)\big)^{-1}$ reflects the Pauli exclusion principle, with opposite-spin electrons in a singlet state exhibiting a steeper cusp with slope 1/2 and parallel-spin electrons in a triplet state displaying a shallower cusp with slope 1/4 due to their spatial antisymmetry. Although the electron–electron cusp can in principle be represented within a complete one-particle basis of Slater- or Gaussian-type orbitals, these functions are analytic in the interelectronic coordinates and therefore lack the derivative discontinuity at $r_{12} = 0$. Therefore, the cusp can only be approximated asymptotically by an infinite superposition of smooth functions, resulting in the exceedingly slow basis set convergence observed in correlated methods.

One strategy to overcome this drastic limitation and approach the CBS limit of correlation energies is to leverage the often systematic nature of basis set effects by employing extrapolation schemes[90,99–101] together with Dunning's correlation-consistent basis sets.[102] Alternatively, more physically motivated strategies that go beyond pure Slater determinant approaches attempt to directly recover the electron–electron cusp behavior by introducing terms in the wave function that explicitly depend on interelectronic distances r_{ij},[25,28,80] a straightforward idea that is nevertheless mathematically and technically challenging.

3.2 Explicitly Correlated Wave Function Approaches

From a historical perspective, the very first attempts to incorporate the interelectronic distance r_{12} into wave function descriptions predate even Kato's pioneering work on the electron–electron cusp (Section 3.1), originating with Slater in the late 1920s. In his initial work, Slater sought to construct a two-electron atomic wave function that would simultaneously reproduce the correct "core" behavior near the nucleus and the asymptotic Rydberg limit.[103] This approach was later combined with another wave function to investigate properties of the helium atom, such as its diamagnetic susceptibility.[104] During the same period, Hylleraas undertook a systematic study of the helium ground-state wave function,[80,81,105] aiming to reduce the remaining discrepancy between theory and experiment to less than 0.1 eV. By incorporating terms linearly dependent on r_{12} into his variational, two-electron CI-type wave function ansatz, he achieved remarkably accurate energies differing from the exact Born–Oppenheimer non-relativistic results by only 1.3 mE_h ($\sim$ 0.035 eV), a major breakthrough that provided strong support for the validity of quantum mechanics in its early days.[106] Modern quantum chemistry has developed several approaches that incorporate interelectronic distances into wave function descriptions beyond two-electron systems (Sections 3.2.1–3.2.3). This work primarily focuses on so-called R12/F12 methods (Section 3.3), which are considered the leading approach for systematically improving basis set convergence while maintaining computational tractability in medium- and large-sized systems.

3.2.1 Hylleraas Configuration Interaction

The extension of the classical Hylleraas wave function ansatz to systems with more than two electrons leads to multidimensional integrals over $3N_e$ spatial coordinates with explicit interelectronic distance dependencies, which are prohibitively difficult to evaluate due to their nonseparable nature. A simplified variant that retains Hylleraas' essential idea while limiting the complexity is the so-called Hylleraas configuration interaction (Hylleraas-CI) method,[17,18] where each term in the wave function expansion contains at most powers of one explicit r_{ij} dependence. In a linear combination of M_CSF configuration state functions $\{\Phi_m\}$ premultiplied by r_{ij}^k, the Hylleraas-CI wave function takes the form

$$\Psi_\text{Hy-CI} = \sum_{k=0}^{k_\mathrm{max}} \sum_{m=1}^{M_\mathrm{CSF}} c_{mk} \sum_{i<j}^{N_e} r_{ij}^k \Phi_m \,, \tag{3.2}$$

with variationally determined coefficients c_{mk}. The canonical CI ansatz is recovered for $k = 0$, whereas $k = 1$ introduces a linear r_{ij} dependence that captures electron–electron cusp behavior and ensures rapid basis set convergence. As a result, higher powers of r_{ij} are seldom included, thus avoiding the corresponding increase in computational complexity.
While typically combined with Slater-type orbitals to capture the correct electron–nucleus cusp, Hylleraas-CI represents one of the most powerful tools to obtain a highly accurate solution of the Schrödinger equation. It involves only up to four-electron integrals,[107–109] a

major simplification over the generalized Hylleraas method. These integrals can be evaluated analytically for atoms, but for molecular systems, numerical integration is generally required. However, the computational cost of Hylleraas-CI remains prohibitively high for medium- to large-sized systems, and it is therefore typically applied only to few-body systems. In this context, it is used to obtain highly precise reference energies, reaching up to pico-Hartree accuracy, which serve as benchmarks for quantum electrodynamic (QED) and relativistic corrections,[29,110,111] thereby aligning theoretical predictions with experimental results as closely as possible.

3.2.2 Explicitly Correlated Gaussian

An alternative highly accurate approach for few-particle systems goes back to the work of Boys[19] and Singer[20] in the explicitly correlated Gaussian (ECG) ansatz.[112,113] As the name indicates, explicit correlation is introduced by Gaussian correlation factors $e^{-\beta_{ij} r_{ij}^2}$ for electron pairs (often referred to as Gaussian geminals) in the wave function, which can be extended to a fully correlated wave function following a CI expansion (Section 2.4.1):

$$\Psi_{\mathrm{ECG}} = \sum_{m=1}^{M} c_m \, \mathcal{A}\{G_m(\boldsymbol{r}_1, \ldots, \boldsymbol{r}_{N_e}) \, \chi_{SM_S}\} \,, \tag{3.3}$$

$$G_m(\boldsymbol{r}_1, \ldots, \boldsymbol{r}_{N_e}) = \exp\Bigg(- \sum_{i=1}^{N_e} \alpha_i^m \big|\boldsymbol{r}_i - \boldsymbol{R}_i^{(m)}\big|^2 - \sum_{i=1}^{N_e} \sum_{j>i}^{N_e} \beta_{ij}^m \big|\boldsymbol{r}_i - \boldsymbol{r}_j\big|^2 \Bigg), \tag{3.4}$$

where $\mathcal{A}$ denotes the antisymmetrizer (or symmetrizer for bosonic systems) and χ_{SM_S} are the corresponding spin functions. Here, $\boldsymbol{R}_i^{(m)}$ are the orbital centers, α_i^m are the orbital exponents, and β_{ij}^m are the variationally optimized correlation factors. Although a Gaussian-based ansatz does not satisfy the cusp condition in Eq. 3.1 and shows incorrect behavior at very short or long interelectronic distances, a linear combination of Gaussian geminals can efficiently capture the electron–electron cusp, in a manner analogous to how combinations of one-electron Gaussian functions reproduce the electron–nucleus cusp. Since only Gaussian-type functions are employed, all multi-electron integrals can be evaluated analytically, even for molecular systems. Difficulties of the ECG ansatz typically arise from linear dependencies and from the steep scaling of the non-linear optimization of the correlation factors β_{ij}^m. Nevertheless, ECG wave functions have been successfully applied to few-particle systems, achieving extremely accurate results.[114]

3.2.3 Transcorrelated Hamiltonian

A conceptually alternative approach to introduce explicit correlation in quantum chemistry is provided by the family of transcorrelated (TC) methods originated by Boys and Handy,[21–24] in which the Hamiltonian is similarity transformed with a correlation factor[115] to directly incorporate dynamic correlation effects. While the resulting transcorrelated

Hamiltonian is not necessarily Hermitian, it remains formally isospectral to the original Hamiltonian, and its eigenfunctions and eigenvalues can be approximated more efficiently using small basis sets. The classical approach starts with a Jastrow ansatz[116] for the wave function

$$\Psi = e^J \Phi \,, \tag{3.5}$$

which, when inserted into the Schrödinger equation (Eq. 2.7), results in

$$\hat{H} e^J \Phi = E e^J \Phi \quad \rightarrow \quad \underbrace{e^{-J} \hat{H} e^J}_{\hat{H}_{\mathrm{TC}}} \Phi = E \Phi \,, \tag{3.6}$$

where $\hat{H}_{\mathrm{TC}}$ represents the transcorrelated Hamiltonian. Typically, a single Hartree–Fock Slater determinant Φ is chosen as the reference state, and the Jastrow operator J is defined as

$$J = \sum_{i<j}^{N_e} u(\boldsymbol{r}_i, \boldsymbol{r}_j) \,, \tag{3.7}$$

where $u(\boldsymbol{r}_i, \boldsymbol{r}_j) = u(\boldsymbol{r}_j, \boldsymbol{r}_i)$ is a symmetric two-electron correlation function. Using the Baker–Campbell–Hausdorff (BCH) expansion,[78] $\hat{H}_{\mathrm{TC}}$ truncates exactly at second order, yielding

$$\begin{aligned} \hat{H}_{\mathrm{TC}} = e^{-J} \hat{H} e^J &= \hat{H} + [\hat{H}, J] + \frac{1}{2}[[\hat{H}, J], J] \\ &= \hat{H} - \sum_{i<j}^{N_e} \hat{K}(\boldsymbol{r}_i, \boldsymbol{r}_j) - \sum_{i<j<k}^{N_e} \hat{L}(\boldsymbol{r}_i, \boldsymbol{r}_j, \boldsymbol{r}_k) \,. \end{aligned} \tag{3.8}$$

The additional operators $\hat{K}$ and $\hat{L}$ can be expressed using the shorthand notation $u(\boldsymbol{r}_i, \boldsymbol{r}_j) = u_{ij}$ as

$$\begin{aligned} \hat{K}(\boldsymbol{r}_i, \boldsymbol{r}_j) = &\frac{1}{2} \left[\nabla_i^2 u_{ij} + \nabla_j^2 u_{ij} + |\nabla_i u_{ij}|^2 + |\nabla_j u_{ij}|^2 \right] \\ &+ \nabla_i u_{ij} \cdot \nabla_i + \nabla_j u_{ij} \cdot \nabla_j, \end{aligned} \tag{3.9}$$

$$\hat{L}(\boldsymbol{r}_i, \boldsymbol{r}_j, \boldsymbol{r}_k) = \nabla_i u_{ij} \cdot \nabla_i u_{ik} + \nabla_j u_{ji} \cdot \nabla_j u_{jk} + \nabla_k u_{ki} \cdot \nabla_k u_{kj} \,. \tag{3.10}$$

The choice of J strongly affects the complexity of the resulting integrals. For generic Jastrow factors,[117] the coefficients are often determined via variational quantum Monte Carlo calculations, which allows the inclusion of electron–nucleus, electron–electron, electron–electron–nucleus, and electron–electron–nucleus–nucleus effects, requiring the evaluation of up to three-electron integrals.[118] Alternative approaches aim to directly incorporate the exact electron–electron cusp condition via Slater-type geminal correlation factors, as in F12 theory.[119,120] In this case, some of the resulting intermediates are identical to those in F12 methods, and techniques for efficient evaluation, as discussed in Sections 3.3, can be applied. A major drawback of TC methods is that, in practice, $\hat{H}_{\mathrm{TC}}$ is non-Hermitian, so the variational principle no longer strictly holds and the computed energy is not guaranteed

to be an upper bound. However, this rarely affects the accuracy, and combining TC with post-Hartree–Fock correlation methods such as CC[121] or CI[122] yields very accurate results for small systems.

3.3 The F12 Ansatz

Within the family of explicitly correlated methods, approaches built upon the F12 ansatz have emerged as the most prominent and widely adopted, providing explicit, often non-variational corrections that significantly reduce the BSIE across a range of electron correlation methods. Their success dates back to the seminal work of Kutzelnigg and Klopper on the so-called R12 corrections,[25–27] which introduced an r_{12}-dependent correlation factor into the wave function description and successfully employed the resolution-of-the-identity (RI) technique to approximate the resulting three- and four-electron integrals as sums of two-electron integrals involving auxiliary basis functions. In modern versions, the original linear r_{12} correlation factor, which exhibits unphysical behavior at very short and long electron–electron distances, has been replaced by a more suitable, general r_{12}-dependent correlation factor that correctly describes the electron–electron cusp, giving rise to what is today known as F12 theory.[28]
In the following, the primary focus lies on the application of the F12 ansatz to second-order Møller–Plesset perturbation theory (MP2-F12).[25–28,31,32,38,123–126] First, the derivation of the general MP2-F12 correction is revisited in Section 3.3.1, yielding the major intermediates. Subsequently, an empirically scaled version of MP2-F12 is introduced in Section 3.3.2 (**Publication I**), which reproduces the unscaled correction to a high degree of accuracy while neglecting the most computationally expensive exchange terms. The explicitly correlated F12 correction to coupled-cluster theory (CC-F12)[30,58,100,127–136] is then briefly discussed in Section 3.3.3, highlighting similarities to MP2-F12 and the reuse of intermediates. Additionally, efficient decomposition techniques for factorizing terms and reducing their computational cost are presented in Section 3.3.4, focusing on the most popular resolution-of-the-identity decomposition scheme,[33] density fitting (DF) techniques,[34,35] three-dimensional numerical quadrature[36–38] (NQ) combined with efficient distance-dependent integral screening (**Publication III**), and tensor hypercontraction (THC).[39–41] Building on this background, a reduced-scaling formulation of RI-MP2-F12 is presented in Section 3.3.5, enabling a highly efficient evaluation of Fock matrix elements spanning multiple orbital spaces in F12 theory (**Publication II**). Furthermore, the exact evaluation of the major $\mathcal{V}$, $\mathcal{X}$, and $\mathcal{B}$ intermediates is discussed, together with a detailed analysis of a highly efficient decomposition of direct- and exchange-type contributions, resulting in an overall efficient correction with formal $\mathcal{O}(M^4)$ scaling in the so-called NQ/DF/CABS-RI approach (**Publication IV**).

3.3.1 Explicitly Correlated Second-Order Møller–Plesset Perturbation Theory

Kutzelnigg and Klopper first introduced the R12/F12 ansatz in electron correlation methods for second-order Møller–Plesset perturbation theory, within the framework of the first-order wave function correction in the Hylleraas pair functional (Eq. 2.53).[27,81,86] While the conventional linear ansatz (Eq. 2.54) yields the standard MP2 energy, they introduced additional explicitly correlated terms to directly account for the electron–electron cusp[32,38] through

$$|u_{ij}^{\text{MP2-F12}}\rangle = |u_{ij}^{\text{MP2}}\rangle + |u_{ij}^{\text{F12}}\rangle \tag{3.11}$$

$$= \sum_{a<b} t_{ij}^{ab} |ab\rangle + \sum_{x<y} c_{ij}^{xy} \hat{Q}_{12} \hat{F}_{12} |\hat{S}_{xy} xy\rangle \ . \tag{3.12}$$

The additional functionals $|u_{ij}^{\text{F12}}\rangle$ are constructed as antisymmetrized geminal states, with the geminal-generating orbitals x, y, v, and w typically chosen to span the (active) Hartree–Fock occupied space in ground-state calculations, although other choices have been explored.[137–139] The correlation factor, $\hat{F}_{12}$, is represented by a Slater-type function that ensures the correct interelectronic cusp behavior, and, in combination with itself and the Coulomb operator, $\hat{g}_{12}$, it gives rise to four different distance-dependent operators appearing in MP2-F12 theory, commonly expressed as

$$\hat{F}_{12} = \frac{1}{\gamma} e^{-\gamma r_{12}} \tag{3.13}$$

$$\hat{g}_{12} = \frac{1}{r_{12}} \tag{3.14}$$

$$\hat{F}_{12}^2 = \frac{1}{\gamma^2} e^{-2\gamma r_{12}} \tag{3.15}$$

$$\hat{F}_{12}\hat{g}_{12} = \frac{1}{\gamma} e^{-\gamma r_{12}} \frac{1}{r_{12}} \, , \tag{3.16}$$

with γ as a fixed geminal exponent. In this context, the *strong orthogonality operator*

$$\hat{Q}_{12} = (1 - \hat{\text{o}}_1)(1 - \hat{\text{o}}_2)(1 - \hat{\text{v}}_1\hat{\text{v}}_2) \tag{3.17}$$

projects the explicitly correlated geminal functions out of the occupied and virtual Hartree–Fock orbital spaces, enforcing strong orthogonality conditions, which strictly separate the conventional and explicitly correlated contributions and prevent linear dependencies. Here, $\hat{\text{o}}_n$ and $\hat{\text{v}}_n$ are corresponding projectors of the n-th electron onto the occupied and virtual Hartree–Fock spaces, defined as

$$\hat{\text{o}}_n g(..., \boldsymbol{r}_n, ...) = \sum_i \phi_i(\boldsymbol{r}_n) \left(\int \phi_i(\boldsymbol{r}_n) g(..., \boldsymbol{r}_n, ...) d\boldsymbol{r}_n \right) \tag{3.18}$$

$$\hat{\text{v}}_n g(..., \boldsymbol{r}_n, ...) = \sum_a \phi_a(\boldsymbol{r}_n) \left(\int \phi_a(\boldsymbol{r}_n) g(..., \boldsymbol{r}_n, ...) d\boldsymbol{r}_n \right) . \tag{3.19}$$

The projector combination $(1-\hat{o}_1)(1-\hat{o}_2)$ ensures orthogonality to all single excitations as well as to the standard doubly excited determinants with respect to the occupied space. The additional projection onto the virtual space, $\hat{v}_1\hat{v}_2$, further decouples the MP2 and F12 corrections to the greatest extent. Here, the *rational generator* $\hat{S}_{xy}$ introduced by Ten-no[38] is applicable to both restricted and unrestricted first-order wave functions and ensures the simultaneous satisfaction of the s- and p-wave coalescence conditions. The operator $\hat{S}_{xy}$ is defined as

$$\hat{S}_{xy} = \frac{3}{8} + \frac{1}{8}\hat{P}_{xy}, \tag{3.20}$$

where the permutation operator $\hat{P}_{xy}$ exchanges spatial coordinates:

$$\hat{P}_{xy}\,\phi_x(\boldsymbol{r}_1,\omega_1)\phi_y(\boldsymbol{r}_2,\omega_2) = \phi_x(\boldsymbol{r}_2,\omega_1)\phi_y(\boldsymbol{r}_1,\omega_2). \tag{3.21}$$

The resulting MP2-F12 Hylleraas pair functional, $J^2_{ij}[u^{\text{MP2-F12}}_{ij}]$, depends on two sets of amplitudes, t^{ab}_{ij} and c^{xy}_{ij}, whose optimization leads to two weakly coupled amplitude equations:

$$\frac{\partial J^2_{ij}[u^{\text{MP2-F12}}_{ij}]}{\partial t^{ab}_{ij}} \overset{!}{=} 0 = g^{ab}_{ij} + f^a_c t^{cb}_{ij} + f^b_d t^{ad}_{ij} - t^{ab}_{kj} f^k_i - t^{ab}_{il} f^l_j + C^{ab}_{xy} c^{xy}_{ij}, \tag{3.22}$$

$$\frac{\partial J^2_{ij}[u^{\text{MP2-F12}}_{ij}]}{\partial c^{xy}_{ij}} \overset{!}{=} 0 = V^{xy}_{ij} + C^{\dagger xy}_{ab} t^{ab}_{ij} + B^{xy}_{vw} c^{vw}_{ij} - X^{xy}_{vw} c^{vw}_{kj} f^k_i - X^{xy}_{vw} c^{vw}_{il} f^l_j\,, \tag{3.23}$$

where the corresponding intermediates are defined as

$$B^{xy}_{vw} = \langle(\hat{S}_{xy}xy)|\,\hat{F}_{12}\hat{Q}_{12}(\hat{f}_1+\hat{f}_2)\hat{Q}_{12}\hat{F}_{12}||(\hat{S}_{vw}vw)\rangle \tag{3.24}$$

$$X^{xy}_{vw} = \langle(\hat{S}_{xy}xy)|\,\hat{F}_{12}\hat{Q}_{12}\hat{F}_{12}||(\hat{S}_{vw}vw)\rangle \tag{3.25}$$

$$X^{xy}_{ij} = \langle(\hat{S}_{xy}xy)|\,\hat{F}_{12}\hat{Q}_{12}\hat{g}_{12}||(\hat{S}_{vw}vw)\rangle \tag{3.26}$$

$$C^{ab}_{xy} = \langle ab|\,(\hat{f}_1+\hat{f}_2)\hat{Q}_{12}\hat{F}_{12}||(\hat{S}_{vw}vw)\rangle \tag{3.27}$$

$$g^{ab}_{ij} = \langle ab|\,\hat{g}_{12}||ij\rangle \tag{3.28}$$

$$f^p_q = \langle p|\hat{f}|q\rangle\ . \tag{3.29}$$

For amplitudes t^{ab}_{ij} and c^{xy}_{ij}, satisfying both Eq. 3.22 and Eq. 3.23, the MP2-F12 energy expression reduces to the simple form

$$E_{\text{MP2-F12}} = g^{\dagger ij}_{ab} t^{ab}_{ij} + V^{\dagger ij}_{xy} c^{xy}_{ij}. \tag{3.30}$$

However, the full optimization of the geminal amplitudes requires the computation of all listed quantities and increases the computational cost by an additional order of magnitude. Thus, the so-called *fixed-amplitude approach*[38] is often employed,

$$c^{xy}_{ij} = \delta_{ix}\delta_{jy}, \tag{3.31}$$

which restricts the geminal generating space to the (active) Hartree–Fock orbitals while still satisfying the electron–electron cusp condition, thereby yielding accurate results and significantly reducing the computational cost of the F12 correction.[106,140] Following the fixed-amplitude approach and employing canonical molecular orbitals in Eq. 3.22 yields the optimal double-excitation amplitudes

$$t_{ij}^{ab} = -\frac{g_{ij}^{ab} + C_{ij}^{ab}}{\varepsilon_a + \varepsilon_b - \varepsilon_i - \varepsilon_j}\,, \tag{3.32}$$

which, when inserted into Eq. 3.23, defines the residual

$$R_{ij}^{ij} = V_{ij}^{ij} - \frac{C_{ab}^{\dagger ij} g_{ij}^{ab} + C_{ab}^{\dagger ij} C_{ij}^{ab}}{\varepsilon_a + \varepsilon_b - \varepsilon_i - \varepsilon_j} + B_{ij}^{ij} - X_{kj}^{ij} f_i^k - X_{il}^{ij} f_j^l\,, \tag{3.33}$$

and the corresponding MP2-F12 energy is then given by

$$E_{\text{MP2-F12}}^{\text{fix.}} = -\frac{g_{ab}^{\dagger ij} g_{ij}^{ab} + 2 g_{ab}^{\dagger ij} C_{ij}^{ab} + C_{ab}^{\dagger ij} C_{ij}^{ab}}{\varepsilon_a + \varepsilon_b - \varepsilon_i - \varepsilon_j} + 2V_{ij}^{ij} + B_{ij}^{ij} - X_{kj}^{ij} f_i^k - X_{il}^{ij} f_j^l\,. \tag{3.34}$$

The fully analytical evaluation of the integral expressions arising in the intermediates is far from trivial, and in practice one typically relies on the resolution-of-the-identity (RI) technique (Section 3.3.4) to decompose the resulting terms. Within this framework, two approximations are commonly employed,[27] the *generalized Brillouin condition* (GBC), which assumes that Fock matrix elements between occupied orbitals and any auxiliary function $\underline{\alpha}$ outside the Hartree–Fock space (introduced through the RI expansion) vanish,

$$f_{\underline{i}}^{\underline{\alpha}} \approx 0\,, \tag{3.35}$$

whereas the *extended Brillouin condition* (EBC) imposes this restriction also on virtual orbitals,

$$f_{\underline{a}}^{\underline{\alpha}} \approx 0\,. \tag{3.36}$$

Although the GBC generally provides a more accurate approximation than the EBC, the accuracy of both improves as the Hartree–Fock orbital basis set is enlarged. The EBC is often employed in practical calculations since the elements of C_{ij}^{ab} vanish under this approximation, which simplifies Eq. 3.34 to

$$E_{\text{MP2-F12}}^{\text{EBC}} = -\frac{g_{ab}^{\dagger ij} g_{ij}^{ab}}{\varepsilon_a + \varepsilon_b - \varepsilon_i - \varepsilon_j} + 2V_{ij}^{ij} + B_{ij}^{ij} - X_{kj}^{ij} f_i^k - X_{il}^{ij} f_j^l\,. \tag{3.37}$$

Equation 3.37 represents one of the simplest explicitly correlated corrections and enables an efficient approach to MP2 results close to the complete basis set limit using moderately sized one-electron basis sets.[31] Nevertheless, MP2-F12 theory introduces a multitude of new integrals arising from the three major intermediates

$$\mathcal{V}_{kl}^{ij} = \langle ij|\, \hat{F}_{12}\hat{Q}_{12}\hat{g}_{12}\,|kl\rangle \tag{3.38}$$

$$\mathcal{X}_{kl}^{ij} = \langle ij|\, \hat{F}_{12}\hat{Q}_{12}\hat{F}_{12}\,|kl\rangle \tag{3.39}$$

$$\mathcal{B}_{kl}^{ij} = \langle ij|\, \hat{F}_{12}\hat{Q}_{12}(\hat{f}_1 + \hat{f}_2)\hat{Q}_{12}\hat{F}_{12}\,|kl\rangle\,, \tag{3.40}$$

which involve operator combinations that go beyond those encountered in traditional quantum chemistry.

3.3.2 Scaled MP2-F12 Theory

The general idea of scaling parallel- and antiparallel-spin pair correlation energies originates from Grimme's work[141] in the early 2000s on spin-component-scaled MP2 (SCS-MP2), in which same-spin (SS) and opposite-spin (OS) electron pair contributions to the MP2 correlation energy were investigated. The conventional MP2 correlation energy (Eq. 2.52) treats all electron-pair interactions on the same footing, without distinguishing between opposite- and same-spin contributions, although their physical nature differs significantly. Electrons with identical spin cannot occupy the same spatial position within a single Slater determinant, which increases their average interelectronic distance and reduces the magnitude of same-spin correlation. In contrast, opposite-spin pairs statistically attain shorter interelectronic distances, resulting in stronger correlation contributions. The SCS-MP2 energy accounts for these differences by introducing fixed, empirically determined scaling factors in the energy expression:

$$E_{\text{SCS-MP2}} = c_{\text{OS}} E^{\text{OS}}_{\text{MP2}} + c_{\text{SS}} E^{\text{SS}}_{\text{MP2}} \,, \tag{3.41}$$

with $c_{\text{OS}} = 6/5$ and $c_{\text{SS}} = 1/3$ obtained by fitting to a set of representative reaction energies.[141] For properties such as reaction energies of small organic molecules, vibrational frequencies, thermodynamic quantities, and π-stacking interactions, the original SCS ansatz significantly improves upon standard MP2 results and has inspired a series of alternative approaches, extending to both specific applications[142–145] and other correlation methods.[146–151] A particularly useful modification is the scaled-opposite-spin (SOS) approach,[152–158] which neglects the smaller same-spin contributions and compensates for them by scaling the opposite-spin correlation. Applied to MP2, this yields the energy expression

$$E_{\text{SOS-MP2}} = c_{\text{SOS}} E^{\text{OS}}_{\text{MP2}} \,, \tag{3.42}$$

with a scaling factor $c_{\text{SOS}} = 1.3$, resulting in only minor deviations from the full SCS ansatz.[152] By neglecting same-spin contributions, the computational cost of RI-MP2 scales as $\mathcal{O}(M^4)$ rather than $\mathcal{O}(M^5)$ with respect to the system size M, provided that Laplace-transform techniques are employed.[159]

Inspired by the SCS and SOS approaches, an alternative method is introduced in **Publication I** that circumvents the rate-determining F12 exchange contributions by empirically scaling spin-pair correlation energies. Analogous to standard MP2, the corresponding F12 correction can be derived within the framework of pair theory in a closed-shell, spin-adapted form as[123]

$$E_{\text{F12}} = \sum_{s=0,1} (2s+1) \sum_{ij} e^s_{ij} \,, \tag{3.43}$$

where e^s_{ij} denotes the singlet ($s = 0$) and triplet ($s = 1$) energy correction for a pair of spatial orbitals ($\phi_i \phi_j$). Following the fixed amplitude approach in conjunction with the

rational generator, the explicitly correlated pair contribution can be expressed as

$$e_{ij}^{s} = e_{ij,\bar{\mathcal{B}}}^{s} + e_{ij,\bar{\mathcal{V}}}^{s} \,. \tag{3.44}$$

Here, $e_{ij,\bar{\mathcal{B}}}^{s}$ and $e_{ij,\bar{\mathcal{V}}}^{s}$ comprise F12 integrals involving either one or two explicitly correlated geminals, respectively, and are defined as

$$e_{ij,\bar{\mathcal{B}}}^{s} = 2^{-(2s+2+\delta_{ij})}\left[\bar{\mathcal{B}}_{ij}^{ij} + (1-2s)\bar{\mathcal{B}}_{ji}^{ij}\right], \tag{3.45}$$

$$e_{ij,\bar{\mathcal{V}}}^{s} = 2^{-(s+\delta_{ij})}\left[\bar{\mathcal{V}}_{ij}^{ij} + (1-2s)\bar{\mathcal{V}}_{ji}^{ij}\right], \tag{3.46}$$

where δ_{ij} denotes the Kronecker delta. The combined intermediates are given by

$$\bar{\mathcal{B}}_{ij}^{ij} = \mathcal{B}_{ij}^{ij} - \mathcal{X}_{ij}^{ij}(\varepsilon_i + \varepsilon_j) - \frac{\mathcal{C}_{ab}^{\dagger ij}\mathcal{C}_{ij}^{ab}}{\varepsilon_a + \varepsilon_b - \varepsilon_i - \varepsilon_j}\,, \tag{3.47}$$

$$\bar{\mathcal{V}}_{ij}^{ij} = \mathcal{V}_{ij}^{ij} - \frac{\mathcal{C}_{ab}^{\dagger ij}\tilde{g}_{ij}^{ab}}{\varepsilon_a + \varepsilon_b - \varepsilon_i - \varepsilon_j}\,, \tag{3.48}$$

employing the three principal MP2-F12 intermediates $\mathcal{V}$ (Eq. 3.38), $\mathcal{X}$ (Eq. 3.39), and $\mathcal{B}$ (Eq. 3.40). The corresponding exchange-type expressions, $\bar{\mathcal{B}}_{ji}^{ij}$ and $\bar{\mathcal{V}}_{ji}^{ij}$, are obtained by interchanging $|ij\rangle$ and $|ji\rangle$, whereas the fractions involving $\mathcal{C}$ and $\tilde{g}$, which are derived from Eq. 3.27 and Eq. 3.28, vanish under the EBC. The resulting singlet and triplet F12 energy corrections from a given pair of spatial orbitals are then expressed as

$$e_{ij}^{0} = \frac{1}{8}\left(\bar{\mathcal{B}}_{ij}^{ij} + \bar{\mathcal{B}}_{ji}^{ij}\right) + \frac{1}{2}\left(\bar{\mathcal{V}}_{ij}^{ij} + \bar{\mathcal{V}}_{ji}^{ij}\right) \tag{3.49}$$

$$e_{ij}^{1} = \frac{1}{32}\left(\bar{\mathcal{B}}_{ij}^{ij} - \bar{\mathcal{B}}_{ji}^{ij}\right) + \frac{1}{4}\left(\bar{\mathcal{V}}_{ij}^{ij} - \bar{\mathcal{V}}_{ji}^{ij}\right), \tag{3.50}$$

and the total contribution is given by

$$e_{ij}^{0} + 3e_{ij}^{1} = \frac{7}{32}\bar{\mathcal{B}}_{ij}^{ij} + \frac{1}{32}\bar{\mathcal{B}}_{ji}^{ij} + \frac{5}{4}\bar{\mathcal{V}}_{ij}^{ij} - \frac{1}{4}\bar{\mathcal{V}}_{ji}^{ij}\,. \tag{3.51}$$

As outlined in Section 3.3.5, the computation of the exchange-type intermediate $\bar{\mathcal{B}}_{ji}^{ij}$ constitutes by far the most computationally demanding step in the MP2-F12 correction, despite contributing only a relatively small energy term, which is further scaled by a factor of 1/32. In scaled F12 theory, this evaluation is avoided by scaling the geminal–geminal triplet energy by a factor of 4/3 and introducing an empirically determined factor c_{SF12} to reproduce the standard MP2-F12 correction as closely as possible for non-covalent interactions (NCIs). The resulting scaled explicitly correlated F12 correction to second-order Møller–Plesset perturbation theory (MP2-SF12), developed in **Publication I**, for a pair of spatial orbitals can then be expressed as

$$c_{\mathrm{SF12}}\left(e_{ij,\bar{\mathcal{B}}}^{0} + 4e_{ij,\bar{\mathcal{B}}}^{1}\right) + e_{ij,\bar{\mathcal{V}}}^{0} + 3e_{ij,\bar{\mathcal{V}}}^{1} = c_{\mathrm{SF12}}\frac{1}{4}\bar{\mathcal{B}}_{ij}^{ij} + \frac{5}{4}\bar{\mathcal{V}}_{ij}^{ij} - \frac{1}{4}\bar{\mathcal{V}}_{ji}^{ij}\,. \tag{3.52}$$

Møller–Plesset perturbation theory, and consequently the corresponding F12 correction, exhibits strong basis set dependence, with triplet correlation energies converging more rapidly toward the complete basis set limit than singlet contributions.[97,100] While other empirical scaling approaches typically neglect this behavior, the additional scaling of the geminal–geminal correction via c_{SF12} in SF12 theory is adjusted to account for its diminishing impact with increasing basis set size. Accordingly, optimal c_{SF12} values can be determined by fitting to a small representative set of molecular systems for any given basis set, with recommended scaling factors of 0.935, 0.95, and 0.96 for the cc-pVXZ-F12 family (X = D, T, Q), respectively.
Overall, MP2-SF12 reproduces the unscaled MP2-F12 correction with high accuracy for the tested non-covalent interactions, while significantly reducing the computational cost, yielding calculations that are several times faster for medium- to large-sized systems compared to the standard MP2-F12 ansatz.
The SF12 approach holds further potential for other explicitly correlated F12 methods and enables simplified F12 analytical derivatives,[160–163] potentially facilitating the evaluation of molecular properties. Dynamic simulations may additionally benefit from determining an optimal c_{SF12} factor once, or updating it periodically, maintaining high accuracy while substantially lowering the computational cost.

3.3.3 Explicitly Correlated Coupled-Cluster Theory

The R12/F12 methodology introduced in the previous section can be extended to virtually any wave function-based method[164–175] and has also been applied to density functional theory,[176,177] enabling highly accurate calculations approaching the CBS limit. The F12 ansatz has proven particularly successful when combined with coupled-cluster methods (Section 2.4.3), establishing itself as a widely adopted and reliable standard reference in both benchmark studies[178,179] and applications demanding high precision.[180–182] As in MP2-F12 approaches, the wave function in explicitly correlated coupled-cluster theory is augmented by an additional (geminal) operator $\hat{R}$, which correctly accounts for the electron–electron cusp behavior. This leads to the parametrization of the CC wave function as

$$\Psi_{\text{CC-F12}} = e^{\hat{T}^{(n)}_{\text{CC-F12}}} \left|\Phi_{\text{HF}}\right\rangle , \tag{3.53}$$

with

$$\hat{T}^{(n)}_{\text{CC-F12}} = \hat{T}_1 + \hat{T}_2 + \cdots + \hat{T}_n + \hat{R} . \tag{3.54}$$

The excitation operators $\hat{T}_1, \ldots, \hat{T}_n$ are defined as in standard CC methodology (Eq. 2.60), where the explicitly correlated excitation operator is given by

$$\hat{R} = \frac{1}{4} \sum_{ijxy} c^{ij}_{xy} \hat{\gamma}^{xy}_{ij} , \tag{3.55}$$

with c^{ij}_{xy} denoting the geminal amplitudes, and the geminal operator $\hat{\gamma}^{xy}_{ij}$ generating orthogonalized geminal configurations by replacing the occupied orbital pair ij:

$$\hat{\gamma}^{xy}_{ij} \left|ij\right\rangle = \hat{Q}_{12} \hat{F}_{12} \left|\left(\hat{S}_{xy} xy\right)\right\rangle . \tag{3.56}$$

The original CC-R12/F12 expressions are obtained by inserting the CC-F12 wave function definition (Eq. 3.53) in the time-independent Schrödinger equation and multiplying from the left with $e^{-\hat{T}^{(n)}_{\text{CC-F12}}}$ to obtain

$$e^{-\hat{T}^{(n)}_{\text{CC-F12}}}\hat{H}e^{\hat{T}^{(n)}_{\text{CC-F12}}}\left|\Phi_{\text{HF}}\right\rangle = \hat{H}_{\text{CC-F12}}\left|\Phi_{\text{HF}}\right\rangle = E_{\text{CC-F12}}\left|\Phi_{\text{HF}}\right\rangle \,, \tag{3.57}$$

with the similarity-transformed CC-F12 Hamiltonian $\hat{H}_{\text{CC-F12}}$. Additional projection of the reference, excited, and geminal determinants onto Eq. 3.57 yields the energy, as well as the corresponding amplitude and geminal equations. The most common choice for $\hat{T}^{(n)}_{\text{CC-F12}}$ is $n=2$, leading to the CCSD-F12 approach,[30,127,130,183] which includes only singly and doubly excited determinants, although higher excitation levels have also been considered.[132,184] The CCSD-F12 method employs the same major intermediates (V, X, C, and B) as MP2-F12, while introducing additional intermediates whose computational complexity is comparable to or exceeds that of the B intermediate.[106] As a result, the evaluation of explicitly correlated terms factored via RI shares the same computational scaling of $\mathcal{O}(M^6)$ with system size M as standard CCSD. However, the computational cost of CCSD-F12, in terms of both the number of operations and required storage, is significantly higher than that of CCSD. Early work motivated the introduction of the so-called *standard approximation*,[30] which greatly simplifies the evaluation by neglecting terms involving some form of RI. Over the years, several alternative approaches within the CCSD-F12 framework have been proposed to reduce computational complexity while maintaining high accuracy,[106,129,133,134,136,140,185–189] with some schemes relying solely on the intermediates introduced in MP2-F12. In general, the strategies for factorizing F12 terms introduced in **Publication III** and **Publication IV** for MP2-F12 theory, as discussed in Section 3.3.4, can also be applied to terms arising in explicitly correlated CC-F12 theory. This may further enhance the applicability of F12 corrections to CC theory, where the relative cost of the F12 correction is already more favorable than for MP2 theory, thereby reinforcing their practical utility for high-accuracy applications.

3.3.4 Low-Rank Integral Decomposition Techniques

Already at the MP2-F12 level, an exact, approximation-free evaluation (see Section 3.3.5) involves high-order tensors ranging from four-center two-electron (4c2e) integrals and their products to six-center three-electron (6c3e) and eight-center four-electron (8c4e) integrals. The computational effort, memory requirements, and contraction complexity of these expressions render them infeasible for all but the smallest systems. For instance, the evaluation of the 8c4e integrals formally scales as $\mathcal{O}(M^8)$ in the AO basis, imposing a computational burden that exceeds standard CCSD calculations by two orders of magnitude. For CC-F12 methods, the computational demands are even more severe, depending on the level of theory. Simply increasing computational resources in a brute-force manner, whether through longer runtimes on faster processors, larger memory, or extended parallelization, yields only disappointingly small gains in treatable system sizes at substantial computational cost. Practical implementations therefore rely heavily on decomposition

techniques to reduce formal scaling and memory requirements while maintaining high accuracy. Generally, a large variety of integral factorization schemes have been developed for quantum chemical calculations, most of which work by reducing a higher-rank tensor in an *a posteriori* or *a priori* manner into contributions of lower-rank tensors.[72,190–197] Furthermore, integral screening techniques[44,198–202] allow to leverage integral sparsity and can further enhance performance. This discussion focuses on techniques particularly well-suited for the F12 ansatz, presenting historically important approaches as well as newly derived combinations exemplified for generic cases. These methods are used to significantly reduce the formal scaling of the F12 ansatz, as illustrated for MP2-F12 in Section 3.3.5.

Resolution-of-the-Identity in F12 Theory

The resolution-of-the-identity (RI) methodology[198,203–206] has been key to the success of the R12/F12 ansatz, as it allows the decomposition of complicated 6c3e and 8c4e integrals into tractable products of 4c2e integrals. By definition, RI inserts the identity operator $\hat{1}$ of the one-electron function space, which can be exactly resolved with respect to an electron n via the CBS projector:

$$\hat{\bar{\alpha}}\, g(..., \boldsymbol{r}_n, ...) = \sum_{\bar{\alpha}} \bar{\alpha}(\boldsymbol{r}_n) \left(\int \bar{\alpha}(\boldsymbol{r}_n) g(..., \boldsymbol{r}_n, ...)\, d\boldsymbol{r}_n \right). \tag{3.58}$$

Especially in F12 approaches, the advantageous partitioning of spaces via

$$\mathrm{span}(\{\underline{\alpha}\}) = \mathrm{span}(\{\bar{\alpha}\}) \cap \mathrm{span}(\{p\})^{\perp}, \tag{3.59}$$

which defines a complementary auxiliary space $\{\underline{\alpha}\}$, ensures that the HF space is always included in the auxiliary RI space. Compared to other partitioning schemes, this inclusion guarantees the exact representability of integral contributions involving only HF orbital products, while the additional complementary auxiliary space $\{\underline{\alpha}\}$ serves exclusively to improve the description of electron correlation through the explicitly correlated geminals. In practice, $\{\underline{\alpha}\}$ needs to be approximated by a finite complementary auxiliary basis set (CABS) $\{p''\}$,[33] typically constructed from an auxiliary set of atom-centered Gaussian-type AOs. An orthonormal set of auxiliary AO basis functions, $\{\mu_0''\}$, is then obtained, e.g., via Löwdin orthogonalization:[71]

$$\mu_0''(\boldsymbol{r}) = \sum_{\nu''} \left[\mathbf{S}^{-1/2}\right]_{\nu''}^{\mu''} \nu''(\boldsymbol{r}), \tag{3.60}$$

where $\mathbf{S}$ is the overlap matrix of the auxiliary AO basis set. The functions $\{p''\}$ are defined as

$$|p''\rangle = \sum_{\mu_0''} c_{\mu_0''}^{p''} |\mu_0''\rangle, \tag{3.61}$$

with corresponding coefficients $c_{\mu_0''}^{p''}$. Following Eq. 3.59, the overlap between $\{p''\}$ and $\{p\}$ is required to vanish,

$$\langle p''|p\rangle = 0, \quad \forall p'' \in \{p''\},\ \forall p \in \{p\}. \tag{3.62}$$

Inserting Eq. 3.61 into Eq. 3.62 gives

$$\sum_{\mu_0''} c_{p''}^{\mu_0''} \langle \mu_0'' | p \rangle = 0 \,, \quad \forall p'' \in \{p''\},\ \forall p \in \{p\} \tag{3.63}$$

with the orthonormality condition on $\{p''\}$ imposed as

$$\sum_{\mu_0''} \sum_{\nu_0''} c_{p''}^{\mu_0''} c_{\nu_0''}^{q''} \langle \mu_0'' | \nu_0'' \rangle = \delta_{q''}^{p''} \,, \quad \forall p'', q'' \in \{p''\} \,. \tag{3.64}$$

A numerically robust method for determining the expansion coefficients $c_{\mu_0''}^{p''}$ is provided by a singular value decomposition (SVD). Eq. 3.63 can be written in matrix form as

$$\mathbf{S}_{12}\mathbf{C} = 0 \,, \tag{3.65}$$

where $\mathbf{S}_{12}$ is the overlap matrix between $\{p''\}$ and $\{p\}$. The null space of $\mathbf{S}_{12}$ is then obtained via SVD:

$$\mathbf{U}_1^\dagger \mathbf{\Sigma}_{12} \mathbf{V}_2 \mathbf{C} = 0 \,, \tag{3.66}$$

with $\mathbf{U}_1^\dagger$ and $\mathbf{V}_2$ being orthogonal matrices of dimensions N_p and $N_{p''}$, respectively. $\mathbf{\Sigma}_{12}$ denotes a rectangular diagonal $N_p \times N_{p''}$ matrix of singular values, under the assumption $N_{p''} > N_p$, so that $\mathrm{rank}(\mathbf{S}_{12}) \leq N_p$. Consequently, $\mathbf{V}_2$ can be partitioned as

$$\mathbf{V}_2 = \begin{pmatrix} \mathbf{V}_2^{\mathrm{R}} \\ \mathbf{V}_2^{\mathrm{N}} \end{pmatrix} \,, \tag{3.67}$$

where the two blocks contain $\mathrm{rank}(\mathbf{S}_{12})$ and $N_{p''} - \mathrm{rank}(\mathbf{S}_{12})$ rows, respectively. The desired coefficients $\mathbf{C}$ are then obtained by transposing $\mathbf{V}_2^{\mathrm{N}}$, which satisfies

$$\mathbf{U}_1^\dagger \mathbf{\Sigma}_{12} \mathbf{V}_2 \mathbf{V}_2^{\mathrm{N}} = 0 \,. \tag{3.68}$$

After a backward transformation to the original non-orthogonal $\{\mu''\}$ basis, the corresponding CABS coefficients are obtained. Hereafter, the acronym RI denotes the use of a MO completeness relation, either in the approximated full space or in the corresponding complementary auxiliary space.

Density Fitting

A closely related approach to the RI methodology is density fitting (DF),[34,35,207] which approximates the product of two atomic or molecular orbitals, depending on the context, as a linear combination of atom-centered auxiliary basis functions $\{P\}$:

$$|\mu\nu) \approx |\widetilde{\mu\nu}) = \sum_P C_{\mu\nu}^P |P) \,. \tag{3.69}$$

Using Eq. 3.69, a 4c2e integral over an arbitrary distance-dependent two-electron operator (e.g., Eqs. 3.13–3.16) can be decomposed as:

$$(\mu\nu|\hat{O}_{12}|\lambda\sigma) \approx (\widetilde{\mu\nu}|\hat{O}_{12}|\widetilde{\lambda\sigma}) = \sum_{PQ} C^P_{\mu\nu}(P|\hat{O}_{12}|Q)C^Q_{\lambda\sigma}\,, \tag{3.70}$$

where minimizing the metric corresponding to the operator $\hat{O}_{12}$, such as the Coulomb metric for $\hat{g}_{12}$, with respect to the coefficients $C^P_{\mu\nu}$ as

$$\frac{\partial}{\partial C^P_{\mu\nu}}(\mu\nu - \widetilde{\mu\nu}|\hat{O}_{12}|\mu\nu - \widetilde{\mu\nu}) \stackrel{!}{=} 0\,, \tag{3.71}$$

$$\frac{\partial}{\partial C^P_{\mu\nu}}\left[(\mu\nu|\hat{O}_{12}|\mu\nu) - 2\sum_R C^R_{\mu\nu}(\mu\nu|\hat{O}_{12}|R) + \sum_{RS} C^R_{\mu\nu}C^S_{\mu\nu}(R|\hat{O}_{12}|S)\right] \stackrel{!}{=} 0\,, \tag{3.72}$$

results in

$$C^P_{\mu\nu} = \sum_Q (P|\hat{O}_{12}|Q)^{-1}(\mu\nu|\hat{O}_{12}|Q)\,. \tag{3.73}$$

Inserting Eq. 3.73 into Eq. 3.70 yields the advantageous partitioning

$$(\mu\nu|\hat{O}_{12}|\lambda\sigma) \approx \sum_{PQRS} (\mu\nu|\hat{O}_{12}|R)(R|\hat{O}_{12}|P)^{-1}(P|\hat{O}_{12}|Q)(Q|\hat{O}_{12}|S)^{-1}(S|\hat{O}_{12}|\lambda\sigma) \tag{3.74}$$

$$= \sum_{PQ} (\mu\nu|\hat{O}_{12}|P)(P|\hat{O}_{12}|Q)^{-1}(Q|\hat{O}_{12}|\lambda\sigma)\,, \tag{3.75}$$

reducing the formal scaling for the evaluation of direct-type 4c2e integrals evaluated in the AO basis from $\mathcal{O}(M^4)$ to $\mathcal{O}(M^3)$. For products of 4c2e integrals, DF achieves a similar reduction in formal scaling for direct-type products, from $\mathcal{O}(M^5)$ to $\mathcal{O}(M^4)$, via

$$\mathcal{W}^{ij}_{kl}\mathcal{Y}^{kl}_{ij} = \langle ij|\,\hat{W}_{12}\,|kl\rangle\,\langle kl|\,\hat{Y}_{12}\,|ij\rangle \approx \mathcal{W}^{ik}_P\tilde{\mathcal{W}}^P_Q\mathcal{W}^Q_{jl}\mathcal{Y}^{ki}_R\tilde{\mathcal{Y}}^R_S\mathcal{Y}^S_{lj}\,, \tag{3.76}$$

where $\hat{W}_{12} = W(|\boldsymbol{r}_1 - \boldsymbol{r}_2|)$ and $\hat{Y}_{12} = Y(|\boldsymbol{r}_1 - \boldsymbol{r}_2|)$ represent generic distance-dependent operators, and the corresponding three-center two-electron (3c2e) and two-center two-electron (2c2e) integrals are defined as

$$\mathcal{Y}^{ki}_R = (ki|\hat{Y}_{12}|R)\,, \tag{3.77}$$

$$\tilde{\mathcal{Y}}^R_S = \left[\mathcal{Y}^{-1}\right]^R_S\,, \tag{3.78}$$

$$\mathcal{Y}^R_S = (R|\hat{Y}_{12}|S)\,. \tag{3.79}$$

and analogously for $\hat{W}_{12}$. Applying DF exclusively to the decomposition of exchange-type integrals does not change the formal scaling of the method. Nevertheless, DF greatly reduces both the computational prefactor and the associated memory requirements, for example, by avoiding the computation and storage of the full set of 4c2e integrals. Overall, DF is essential for the efficient evaluation of integrals in F12 theory, offering a highly effective partitioning scheme that significantly outperforms the decomposition-free approach while preserving high accuracy.

Numerical Quadrature

A potent and versatile decomposition technique that is well suited for the factorization of exchange-type integrals in quantum chemistry is provided by three-dimensional numerical quadrature (NQ).[36,37,43,76,208–210] Especially in density functional theory (DFT), the use of NQ is essential, since a closed-form evaluation of the exchange–correlation functional is generally not possible. This motivated the development of highly efficient numerical integration schemes that rely on molecular grids[211,212] composed of three-dimensional grid points $\boldsymbol{r}_g$ together with their associated weights w_g. However, NQ itself is not limited to DFT but allows for the numerical integration of any sufficiently well-behaved function $f : \mathbb{R}^3 \to \mathbb{R}$ (or $\mathbb{C}$), such as the electron density or spatial orbitals, as

$$\int f(\boldsymbol{r})\, d\boldsymbol{r} \approx \sum_g w_g f(\boldsymbol{r}_g). \tag{3.80}$$

To achieve maximum accuracy, grids are typically constructed by combining spherical atomic grids that respect the spherical symmetry of the electronic structure around each nucleus, with the accuracy improving as the number of grid points N_g increases. For the purpose of F12 theory,[38,125,213–215] the application of numerical quadrature to two-electron integrals over a general distance-dependent two electron operator (e.g., Eqs. 3.13–3.16) allows for the factorization

$$\iint f(\boldsymbol{r}_1, \boldsymbol{r}_2) d\boldsymbol{r}_1 d\boldsymbol{r}_2 = \iint \chi_\mu(\boldsymbol{r}_1)\chi_\nu(\boldsymbol{r}_1)\hat{O}_{12}\chi_\lambda(\boldsymbol{r}_2)\chi_\sigma(\boldsymbol{r}_2)\, d\boldsymbol{r}_1 d\boldsymbol{r}_2 \tag{3.81}$$

$$\approx \int \chi_\mu(\boldsymbol{r}_1)\chi_\nu(\boldsymbol{r}_1) \sum_g w_g \hat{O}_{1g}\chi_\lambda(\boldsymbol{r}_g)\chi_\sigma(\boldsymbol{r}_g)\, d\boldsymbol{r}_1 \tag{3.82}$$

where the interelectronic distance $r_{12} = |\boldsymbol{r}_1 - \boldsymbol{r}_2|$ is replaced by the distance to the grid point $r_{1g} = |\boldsymbol{r}_1 - \boldsymbol{r}_g|$. In shorthand notation this factorization allows an efficient decomposition of exchange-type four-center two-electron integrals, which occur, for example, in HF and F12 theory, as

$$\langle ij|\, \hat{O}_{12}\, |ji\rangle \approx w_g c_{\mu i} \chi^g_\mu c_{\nu j} \chi^g_\nu c_{\lambda i} c_{\sigma j} (g|\hat{O}_{1g}|\lambda\sigma) \tag{3.83}$$

$$= w_g P_{\mu\lambda} P_{\nu\sigma} \chi^g_\mu \chi^g_\nu (g|\hat{O}_{1g}|\lambda\sigma) \tag{3.84}$$

with $\chi^g_\mu = \chi_\mu(\boldsymbol{r}_g)$ and the associated AO three-center one-electron (3c1e) integrals

$$(g|\hat{O}_{1g}|\lambda\sigma) = \int \hat{O}_{1g}\chi_\lambda(\boldsymbol{r}_1)\chi_\sigma(\boldsymbol{r}_1)\, d\boldsymbol{r}_1\,. \tag{3.85}$$

A major advantage of using NQ to factorize exchange-type four-center two-electron integrals, as opposed to relying exclusively on DF techniques, is the reduction in formal computational scaling. Whereas DF merely reduces the prefactor, NQ allows the energy

contribution to be evaluated through three steps with reduced scaling:

$$\text{step 1:} \quad \bar{\chi}^g_\lambda = P_{\mu\lambda}\chi^g_\mu \qquad (N_g N_\mu^2) \tag{3.86}$$
$$\text{step 2:} \quad O^g_\sigma = w_g(g|\hat{O}_{1g}|\lambda\sigma)\bar{\chi}^g_\lambda \qquad (N_g N_\mu^2) \tag{3.87}$$
$$\text{step 3:} \quad E_{\{O^{ij}_{ji}\}} = O^g_\sigma \bar{\chi}^g_\sigma \qquad (N_g N_\mu) \tag{3.88}$$

where the formal scaling is indicated. Numerical quadrature can be applied not only to efficiently reduce the scaling of exchange-type 4c2e integrals, but also to 6c3e and 8c4e integrals, provided that all involved operators share a common spatial coordinate. For example, an exchange-type 6c3e integral involving arbitrary interelectronic distance-dependent operators $\hat{W}_{12}$ and $\hat{Y}_{12}$ can be factorized as:

$$\langle ijk|\,\hat{W}_{12}\hat{Y}_{23}\,|kij\rangle \approx w_g\, c_{\mu j}\chi^g_\mu\, c_{\nu i}\chi^g_\nu\, c_{\lambda i}c_{\sigma k}(g|\hat{W}_{1g}|\lambda\sigma)\, c_{\delta k}c_{\varepsilon j}(g|\hat{Y}_{1g}|\delta\varepsilon) \tag{3.89}$$
$$= w_g P_{\mu\varepsilon}P_{\nu\lambda}P_{\sigma\delta}\,\chi^g_\mu\chi^g_\nu\,(g|\hat{W}_{1g}|\lambda\sigma)\,(g|\hat{Y}_{1g}|\delta\varepsilon), \tag{3.90}$$

allowing for an efficient stepwise low-scaling evaluation via:

$$\text{step 1:} \quad \bar{\chi}^g_\varepsilon = P_{\mu\varepsilon}\chi^g_\mu \qquad (N_g N_\mu^2) \tag{3.91}$$
$$\text{step 2:} \quad \mathcal{W}^g_\sigma = \bar{\chi}^g_\lambda(g|\hat{W}_{1g}|\lambda\sigma) \qquad (N_g N_\mu^2) \tag{3.92}$$
$$\text{step 3:} \quad \mathcal{Y}^g_\delta = \bar{\chi}^g_\varepsilon(g|\hat{Y}_{1g}|\delta\varepsilon) \qquad (N_g N_\mu^2) \tag{3.93}$$
$$\text{step 4:} \quad E_{\{\mathcal{W}\mathcal{Y}^{ijk}_{kij}\}} = w_g P_{\sigma\delta}\mathcal{W}^g_\sigma\mathcal{Y}^g_\delta\,. \qquad (N_g N_\mu^2)\,. \tag{3.94}$$

Regardless of whether 4c2e, 6c3e, or 8c4e integrals are considered, their evaluation via NQ formally scales as $\mathcal{O}(M^3)$ with system size M. In this context, an efficient implementation employs a batch-wise scheme, processing only a subset of grid points at a time. For steps involving matrix–matrix multiplications, batch-local quantities can be combined using block-sparse matrix algebra,[45] reducing the asymptotic scaling to linear. The by far most demanding step remains the computation of the 3c1e integrals (Eq. 3.85). To drastically lower their computational cost, an efficient batch-wise distance-dependent screening of F12-type 3c1e integrals (Figure 3.2) is introduced in **Publication III**, exploiting the local character of the involved operators whose contributions fall below 10^{-10} already at short interelectronic distances. The absolute contribution of a single 3c1e integral within a shell pair $\dot{\mu}\dot{\nu}$ (dotted indices correspond to shells rather than individual AO basis functions), exemplified in the following for the correlation factor $\hat{F}_{12}$, is bounded by

$$|(\mu\nu|\hat{F}_{1g}|g)| \leq \overset{\bullet}{S}_{\dot{\mu}\dot{\nu}}\hat{F}_{12}\big(\dot{r}_{1g} - r^{\dot{\mu}\dot{\nu}}_{\text{ext.}}(\vartheta_{\text{dist.}})\big) + \mathring{S}_{\dot{\mu}\dot{\nu}} \qquad \forall\mu,\nu\in\dot{\mu} \tag{3.95}$$

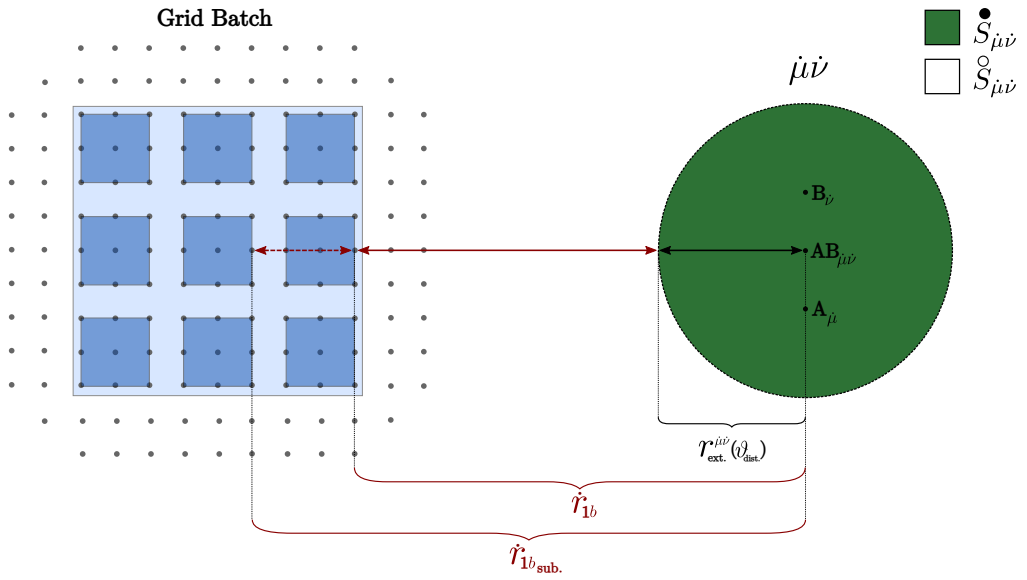

Figure 3.2: Schematic illustration of the batch-wise, distance-dependent screening of 3c1e integrals present in F12 theory.

with

$$S_{\dot{\mu}\dot{\nu}} \geq \int |\Omega_{\mu\nu}(\boldsymbol{r})| d\boldsymbol{r} \qquad \forall \mu, \nu \in \dot{\mu} \tag{3.96}$$

$$\overset{\bullet}{S}_{\dot{\mu}\dot{\nu}} \geq \int_{\bullet} |\Omega_{\mu\nu}(\boldsymbol{r})| d\boldsymbol{r} \qquad \forall \mu, \nu \in \dot{\mu} \tag{3.97}$$

$$\overset{\circ}{S}_{\dot{\mu}\dot{\nu}} \geq \int_{\circ} |\Omega_{\mu\nu}(\boldsymbol{r})| d\boldsymbol{r} \qquad \forall \mu, \nu \in \dot{\mu} \tag{3.98}$$

$$\overset{\circ}{S}_{\dot{\mu}\dot{\nu}} \leq \vartheta_{\text{dist.}} \tag{3.99}$$

$$\Omega_{\mu\nu}(\boldsymbol{r}) = \chi_{\mu}(\boldsymbol{r})\chi_{\nu}(\boldsymbol{r}) \tag{3.100}$$

$$\dot{r}_{1g} = |\boldsymbol{r}_{\dot{\mu}\dot{\nu}} - \boldsymbol{r}_g| \,, \tag{3.101}$$

where $\boldsymbol{r}_{\dot{\mu}\dot{\nu}}$ denotes the center of the shell pair $\dot{\mu}\dot{\nu}$. The integration domain $\boldsymbol{r}$ of the shell pair overlap $S_{\dot{\mu}'\dot{\nu}}$ is divided into an inner ($\bullet$) and an outer ($\circ$) region relative to the shell pair extent $r_{\text{ext.}}^{\dot{\mu}\dot{\nu}}(\vartheta_{\text{dist.}})$, as illustrated in Fig. 3.2. The extent $r_{\text{ext.}}^{\dot{\mu}\dot{\nu}}(\vartheta_{\text{dist.}})$ defines a spherical integration domain (a ball) centered at $\boldsymbol{r}_{\dot{\mu}\dot{\nu}}$ and bounded by $\overset{\circ}{S}_{\dot{\mu}\dot{\nu}}$, ensuring that all contributions below the distance-screening threshold $\vartheta_{\text{dist.}}$ are excluded. A set of optimal extents covering the full range of relevant $\vartheta_{\text{dist.}}$ values, commonly referred to as integral partition bounds (IPBs),[44] is evaluated only once using the extent equations and subsequently pre-tabulated for each shell pair. The overlap contribution inside the ball is then tightly bounded by

$$S_{\dot{\mu}\dot{\nu}} \geq \overset{\bullet}{S}_{\dot{\mu}\dot{\nu}} \,, \tag{3.102}$$

noting that both contributions differ by at most $\vartheta_{\text{dist.}}$.
In practical applications, even sharper bounds can be achieved by incorporating all com-

ponents that affect the expression of interest. Here, the associated grid weights w_g are incorporated in the form of the relative grid weights $\sqrt{w_g/w_{\text{avg.}}}$, where $w_{\text{avg.}}$ denotes the average weight over all grid points. The square root is convenient for 6c3e integrals and equally applicable to 4c2e integrals, since in most cases $w_g < 1$ and therefore $\sqrt{w_g} > w_g$. Normalization with the average weight is key to render the resulting screening procedure largely independent of the total grid size. Without this adjustment, the screening would become progressively looser on finer grids, where individual contributions decrease in magnitude. To provide a reasonable estimate for the computational cost of a shell pair, the corresponding number of primitive Cartesian basis functions $N_{\dot{\mu}\dot{\nu}}^{\text{Cart.}}$ is incorporated, directly reflecting the associated computational workload. Furthermore, the contracted AOs on the grid, $\bar{\chi}_{\dot{\gamma}}^{g}$, are exploited as an additional source of sparsity, since they are obtained as the product of the density matrix $\mathbf{P}$ and the batch-local AOs on the grid, χ_{μ}^{g}. Inclusion of these factors allows the significance $\sigma_{\dot{\mu}\dot{\nu}g}$ of an individual integral to be estimated as

$$\sigma_{\dot{\mu}\dot{\nu}g} = \frac{1}{N_{\dot{\mu}\dot{\nu}}^{\text{Cart.}}} \sqrt{\frac{w_g}{w_{\text{avg.}}}} \bar{\chi}_{\dot{\nu}}^{g} S_{\dot{\mu}\dot{\nu}} \hat{F}_{12}(r_{1g} - r_{\text{ext.}}^{\dot{\mu}\dot{\nu}}(\vartheta_{\text{dist.}})) \leq \vartheta_{\text{F12}}, \tag{3.103}$$

where ϑ_{F12} is a fixed, predefined threshold specifying the desired accuracy, and

$$\bar{\chi}_{\dot{\nu}}^{g} = \sqrt{\sum_{\nu \in \dot{\nu}} |\bar{\chi}_{\nu}^{g}|^2}\,. \tag{3.104}$$

Reformulating Eq. 3.103 by incorporating all pre-factors on the right-hand side leads to the screening condition

$$S_{\dot{\mu}\dot{\nu}} \hat{F}_{12}(\dot{r}_{1g} - r_{\text{ext.}}^{\dot{\mu}\dot{\nu}}) \leq N_{\dot{\mu}\dot{\nu}}^{\text{Cart.}} \sqrt{\frac{w_{\text{avg.}}}{w_g}} \frac{1}{\bar{\chi}_{\dot{\nu}}^{g}} \vartheta_{\text{F12}} \equiv \vartheta_{\dot{\mu}\dot{\nu}g}^{\text{F12}}, \tag{3.105}$$

resulting in an adjusted, tighter threshold $\vartheta_{\dot{\mu}\dot{\nu}g}^{\text{F12}}$, which is employed instead of $\vartheta_{\text{dist.}}$ to reduce the shell pair extent $r_{\text{ext.}}^{\dot{\mu}\dot{\nu}}(\vartheta_{\text{dist.}})$. To maximize efficiency, the screening is carried out over batches of spatially adjacent grid points, as illustrated in Figure 3.2. After construction of optimal batches b of grid points,[212] a batch-wise screening condition can be formulated as

$$S_{\dot{\mu}\dot{\nu}} \hat{F}_{12}(\dot{r}_{1b} - r_{\text{ext.}}^{\dot{\mu}\dot{\nu}}(\vartheta_{\text{dist.}})) \leq N_{\dot{\mu}\dot{\nu}}^{\text{Cart.}} \frac{1}{\tilde{\chi}_{\dot{\nu}}^{b}} \vartheta_{\text{F12}} \equiv \vartheta_{\dot{\mu}\dot{\nu}b}^{\text{F12}}, \tag{3.106}$$

with

$$\dot{r}_{1b} \leq \min_{g \in b}(\dot{r}_{1g}) \tag{3.107}$$

$$\tilde{\chi}_{\dot{\nu}}^{b} = \frac{1}{\sqrt{w_{\text{avg.}}}} \max_{g \in b}(\sqrt{w_g} \bar{\chi}_{\dot{\nu}}^{b}). \tag{3.108}$$

In practice, the number of grid points per batch depends on whether NQ is combined with DF techniques for some or all terms involving the operator under consideration. For a pure

NQ decomposition, organizing the grid into larger batches and smaller subbatches (with $b_{\text{sub.}} \to \dot{r}_{1b_{\text{sub.}}}$) can further enhance the efficiency of the screening procedure, whereas smaller batch sizes are recommended when combined with DF to reduce memory requirements. The screening condition in Eq. 3.106 ensures that exchange-type 4c2e and 6c3e integrals, as well as certain 8c4e integrals appearing in MP2-F12 theory, can be evaluated with linear time complexity. In total, it incorporates three powerful sources of sparsity: the decay of the shell-pair overlap $S_{\dot{\mu}\dot{\nu}}$, the short-range nature of the operators, and the decay of the density matrix for systems with a significant HOMO–LUMO gap. Overall, NQ is a highly effective tool that can be adapted and combined with other decomposition techniques to further reduce the formal scaling of the evaluation.

Numerical Quadrature + Density Fitting

A novel combination of numerical quadrature and density fitting techniques for practical calculations is proposed in **Publication IV** for the decomposition of exchange-type products of 4c2e integrals in F12 theory. This approach reduces the formal scaling of the total evaluation to $\mathcal{O}(M^4)$ with system size M and is not limited to F12 theory, but can also be applied to other correlation methods. In particular, the exchange-type product of two 4c2e integrals can be represented as

$$\langle ij|\,\hat{W}_{12}\,|kl\rangle\,\langle kl|\,\hat{Y}_{12}\,|ji\rangle \approx w_g\,\phi_i^g\phi_k^g\,(g|\hat{W}_{1g}|jl)\,\mathcal{Y}_R^{kj}\tilde{\mathcal{Y}}_S^R\mathcal{Y}_{li}^S\,, \tag{3.109}$$

which can be stepwise computed via

$$\text{step 1:} \quad \tilde{\mathcal{Y}}_{li}^R = \tilde{\mathcal{Y}}_S^R\mathcal{Y}_{li}^S \qquad (N_P^2N_kN_i) \tag{3.110}$$

$$\text{step 2:} \quad \tilde{\mathcal{Y}}_{lg}^R = \phi_i^g\,\tilde{\mathcal{Y}}_{li}^R \qquad (N_gN_PN_kN_i) \tag{3.111}$$

$$\text{step 3:} \quad \mathcal{Y}_R^{gj} = \phi_k^g\,\mathcal{Y}_R^{kj} \qquad (N_gN_PN_kN_i) \tag{3.112}$$

$$\text{step 4:} \quad \mathcal{Y}_{gjl} = \tilde{\mathcal{Y}}_{lg}^R\,\mathcal{Y}_R^{gj} \qquad (N_gN_PN_kN_i) \tag{3.113}$$

$$\text{step 5:} \quad E_{\{\mathcal{W}\mathcal{Y}_{ji}^{ij}\}} = w_g(g|\hat{W}_{1g}|jl)\mathcal{Y}_{gjl} \qquad (N_gN_kN_i)\,. \tag{3.114}$$

The NQ/DF ansatz offers considerable flexibility, as the spatial coordinate corresponding to a specific electron at which the numerical quadrature is inserted can be freely chosen. This is particularly advantageous, since the largest MO space can then be contracted early in the evaluation in a $\mathcal{O}(M^3)$ step, simplifying all subsequent computations. Furthermore, the ansatz can be easily extended to include additional products of multiple orbital spaces spanning Fock or exchange matrix elements, whose highly efficient evaluation is discussed in **Publication II**. The NQ/DF ansatz can also be employed to reduce the overall scaling of MP2 (Section 2.4.2) theory to $\mathcal{O}(M^4)$. Here, the bottleneck is the exchange-type contribution, which can be expressed in the AO formalism using the Laplace transformation[159] of the energy denominator in combination with NQ/DF as

$$E_{\text{MP2/exch.}}^{\text{AO}} = \sum_{\Gamma}\sum_{\mu\nu\lambda\sigma}\sum_{\gamma\delta\epsilon\eta} \underline{P}_{\mu\eta}^{\Gamma}\overline{P}_{\nu\gamma}^{\Gamma}\underline{P}_{\lambda\delta}^{\Gamma}\overline{P}_{\sigma\epsilon}^{\Gamma}\chi_\mu^g\chi_\nu^g(g|\hat{g}_{1g}|\lambda\sigma)\mathcal{G}_P^{\gamma\delta}\tilde{\mathcal{G}}_Q^P\mathcal{G}_{\epsilon\eta}^Q\,. \tag{3.115}$$

The occupied and virtual pseudo-densities for each Laplace point Γ are defined as

$$\underline{P}^{\Gamma}_{\mu\eta} = (w^{\Gamma})^{\frac{1}{4}} \sum_{i} c_{\mu i} e^{\varepsilon_i t^{\Gamma}} c_{\eta i} \tag{3.116}$$

$$\overline{P}^{\Gamma}_{\nu\gamma} = (w^{\Gamma})^{\frac{1}{4}} \sum_{a} c_{\nu a} e^{\varepsilon_a t^{\Gamma}} c_{\gamma a} \tag{3.117}$$

with corresponding Laplace weights w^{Γ}. These pseudo-densities are then decomposed using Cholesky decomposition as in CDD-MP2,[51] i.e.,

$$\underline{P}_{\mu\eta} = \underline{L}_{\mu i} \underline{L}_{\eta i} \tag{3.118}$$

$$\overline{P}_{\nu\gamma} = \overline{L}_{\nu a} \overline{L}_{\gamma a} \,. \tag{3.119}$$

Subsequently, the three-center two-electron integrals are transformed from the AO to the MO basis and contracted with the square root of $\tilde{\mathcal{G}}$:

$$\mathcal{G}^{\gamma \underline{j}}_{P} = \mathcal{G}^{\gamma\delta}_{P} \underline{L}_{\delta j} \qquad (N_P N_\mu^2 N_i) \tag{3.120}$$

$$\mathcal{G}^{\overline{a}\underline{j}}_{P} = \mathcal{G}^{\gamma \underline{j}}_{P} \overline{L}_{\gamma a} \qquad (N_P N_\mu N_a N_i) \tag{3.121}$$

$$\tilde{\mathcal{G}}^{\overline{a}\underline{j}}_{R} = \mathcal{G}^{\overline{a}\underline{j}}_{P} \left[\tilde{\mathcal{G}}^{\frac{1}{2}}\right]^{R}_{P} \qquad (N_P^2 N_a N_i) \,, \tag{3.122}$$

which yields the transformed quantities $\tilde{\mathcal{G}}^{\overline{a}\underline{j}}_{R}$ and $\tilde{\mathcal{G}}^{R}_{\overline{b}\underline{i}}$. The MP2 exchange energy is then evaluated stepwise as follows:

step 1:	$\underline{\chi}^{g}_{i}$	$= \chi^{g}_{\mu} \underline{L}_{\mu i}$	$(N_g N_\mu N_i)$	(3.123)
	$\overline{\chi}^{g}_{a}$	$= \chi^{g}_{\nu} \overline{L}_{\nu a}$	$(N_g N_\mu N_a)$	(3.124)
step 2:	$(g\vert\hat{g}_{1g}\vert\underline{j}\sigma)$	$= (g\vert\hat{g}_{1g}\vert\lambda\sigma)\underline{L}_{\lambda j}$	$(N_g N_\mu^2 N_i)$	(3.125)
	$(g\vert\hat{g}_{1g}\vert\underline{j}\overline{b})$	$= (g\vert\hat{g}_{1g}\vert\underline{j}\sigma)\overline{L}_{\sigma b}$	$(N_g N_\mu N_a N_i)$	(3.126)
step 3:	$\tilde{\mathcal{G}}^{g\underline{j}}_{R}$	$= \tilde{\mathcal{G}}^{\overline{a}\underline{j}}_{R} \overline{\chi}^{g}_{a}$	$(N_g N_P N_a N_i)$	(3.127)
	$\tilde{\mathcal{G}}^{R}_{\overline{b}g}$	$= \tilde{\mathcal{G}}^{R}_{\overline{b}\underline{i}} \underline{\chi}^{g}_{i}$	$(N_g N_P N_a N_i)$	(3.128)
step 4:	$\overset{\square}{\mathcal{G}}_{g\underline{j}\overline{b}}$	$= \tilde{\mathcal{G}}^{g\underline{j}}_{R} \tilde{\mathcal{G}}^{R}_{\overline{b}g}$	$(N_g N_P N_a N_i)$	(3.129)
step 5:	$E_{\mathrm{MP2/exch.}}$	$= \overset{\square}{\mathcal{G}}_{g\underline{j}\overline{b}} (g\vert\hat{g}_{1g}\vert\underline{j}\overline{b}) \,.$	$(N_g N_a N_i)$	(3.130)

The number of Laplace quadrature points N_Γ is typically chosen between 5 and 10, and thus does not affect the overall scaling behavior.

Tensor Hypercontraction

Numerical quadrature is not limited to a single insertion but can also be applied to both spatial coordinates in a 4c2e integral. A possible stepwise derivation, connecting RI or

DF approximations with NQ, starts by decomposing a 4c2e integral via a finite auxiliary completeness relation, inserted before and after an operator $\hat{O}_{12}$:

$$(\mu\nu|\hat{O}_{12}|\lambda\sigma) \approx (\mu\nu P)(P|\hat{O}_{12}|Q)(Q\lambda\sigma)\,, \tag{3.131}$$

where the three-center overlap integrals are given by

$$(\mu\nu P) = \int \chi_\mu(\boldsymbol{r})\chi_\nu(\boldsymbol{r})\chi_P(\boldsymbol{r})\,d\boldsymbol{r}\,. \tag{3.132}$$

In contrast to density fitting techniques, the auxiliary functions are defined as Dirac delta functions in physical space, $\delta(\boldsymbol{r}-\boldsymbol{r}_P)$,[36,37,208,209] which reduces the integral to

$$w_{\dot{P}}w_{\dot{Q}}\chi_\mu(\boldsymbol{r}_{\dot{P}})\chi_\nu(\boldsymbol{r}_{\dot{P}})\hat{O}_{\dot{P}\dot{Q}}\chi_\lambda(\boldsymbol{r}_{\dot{Q}})\chi_\sigma(\boldsymbol{r}_{\dot{Q}}) = X_\mu^{\dot{P}}X_\nu^{\dot{P}}\hat{O}_{\dot{P}\dot{Q}}X_\lambda^{\dot{Q}}X_\sigma^{\dot{Q}}\,, \tag{3.133}$$

where $\dot{P}$ and $\dot{Q}$ denote discrete grid points, and

$$X_\mu^{\dot{P}} = \sqrt{w_{\dot{P}}}\,\chi_\mu(\boldsymbol{r}_{\dot{P}})\,. \tag{3.134}$$

However, the decomposition of a 4c2e integral via Eq. 3.133 has certain drawbacks. In particular, its application to the classical Coulomb operator introduces singularities for any finite quadrature grid when $\boldsymbol{r}_{\dot{P}} = \boldsymbol{r}_{\dot{Q}}$. This issue can be avoided by employing an alternative operator, such as the attenuated Coulomb metric,[216] which regularizes the short-range behavior at the cost of some accuracy. A more severe limitation arises from the requirement of a sufficiently dense numerical grid, which must be applied twice in this approach. For direct-type 4c2e integrals, a decomposition via DF is more efficient, whereas for exchange-type 4c2e integrals, a single NQ insertion yields better performance. Although the decomposition of products of 4c2e integrals may be promising in certain cases, it introduces significant memory demands, particularly for exchange-type products when standard DFT molecular grids are employed ($N_{\dot{P}} = N_g$).
An alternative approach closely related to the 4c2e integral decomposition in Eq. 3.133 is tensor hypercontraction (THC),[39–41,217–220] which likewise decouples the orbital indices. In the following, its least-squares formulation (LS-THC) is considered. Minimizing the L^2-norm estimator

$$O = \frac{1}{2}\big\|(\mu\nu|\lambda\sigma) - X_\mu^{\dot{P}}X_\nu^{\dot{P}}Z_{\hat{O}_{12}}^{\dot{P}\dot{Q}}X_\lambda^{\dot{Q}}X_\sigma^{\dot{Q}}\big\|_2^2 \tag{3.135}$$

yields the renormalized Z representation of an arbitrary operator $\hat{O}_{12}$, with

$$Z_{\hat{O}_{12}}^{\dot{P}\dot{Q}} = [\mathbf{S}^{-1}]^{\dot{P}\dot{P}'}E_{\hat{O}_{12}}^{\dot{P}'\dot{Q}'}[\mathbf{S}^{-1}]^{\dot{Q}\dot{Q}'}\,. \tag{3.136}$$

The grid metric $S^{\dot{P}\dot{P}'}$ is defined as

$$S^{\dot{P}\dot{P}'} = X_{\mu'}^{\dot{P}}X_{\mu'}^{\dot{P}'}X_{\nu'}^{\dot{P}}X_{\nu'}^{\dot{P}'}\,, \tag{3.137}$$

and the grid-projected 4c2e integral tensor is given by

$$E_{\hat{O}_{12}}^{\dot{P}'\dot{Q}'} = X_\mu^{\dot{P}'}X_\nu^{\dot{P}'}\mathcal{I}_{\mu\nu\lambda\sigma}X_\lambda^{\dot{Q}'}X_\sigma^{\dot{Q}'}\,, \tag{3.138}$$

where $\mathcal{I}_{\mu\nu\lambda\sigma}$ denotes either the classical 4c2e integral tensor or a doubly density-fitted RI approximation. Depending on the application, the fitting can be performed either in the AO or MO representation. For energy expressions, the MO formalism is typically preferred, as the considered MO spaces are usually smaller, which reduces the number of required quadrature points or allows higher accuracy for the same grid size. Further details on an efficient fitting of $Z^{\dot{P}\dot{Q}}_{\hat{O}_{12}}$ are available in the literature.[41]
One major advantage of THC is that the required numerical grids are typically much smaller than standard DFT grids, with $N_{\dot{P}} \approx 3\,N_P$. Furthermore, after the fitting process, THC allows for computing direct-type products of 4c2e integrals as

$$\langle ij|\,\hat{W}_{12}\,|kl\rangle\,\langle kl|\,\hat{Y}_{12}\,|ij\rangle \approx X^{\dot{P}}_i X^{\dot{P}}_k Z^{\dot{P}\dot{Q}}_{\hat{W}_{12}} X^{\dot{Q}}_j X^{\dot{Q}}_l X^{\dot{R}}_k X^{\dot{R}}_i Z^{\dot{R}\dot{S}}_{\hat{Y}_{12}} X^{\dot{S}}_l X^{\dot{S}}_j \tag{3.139}$$

with formal $\mathcal{O}(M^3)$ time complexity, evaluated stepwise as:

$$\begin{aligned}
\text{step 1:}\quad & \bar{X}^{\dot{P}\dot{R}} &&= X^{\dot{P}}_i X^{\dot{R}}_i && (N^2_{\dot{P}} N_i) && (3.140)\\
& \tilde{X}^{\dot{P}\dot{R}} &&= X^{\dot{P}}_k X^{\dot{R}}_k && (N^2_{\dot{P}} N_k) && (3.141)\\
\text{step 2:}\quad & \bar{Z}^{\dot{R}\dot{Q}}_{\hat{W}_{12}} &&= \bar{X}^{\dot{P}\dot{R}} \tilde{X}^{\dot{P}\dot{R}} Z^{\dot{P}\dot{Q}}_{\hat{W}_{12}} && (N^3_{\dot{P}}) && (3.142)\\
& \bar{Z}^{\dot{R}\dot{Q}}_{\hat{Y}_{12}} &&= \bar{X}^{\dot{Q}\dot{S}} \tilde{X}^{\dot{Q}\dot{S}} Z^{\dot{R}\dot{S}}_{\hat{Y}_{12}} && (N^3_{\dot{P}}) && (3.143)\\
\text{step 3:}\quad & E_{\{\mathcal{W}\mathcal{Y}^{ij}_{ij}\}} &&= \bar{Z}^{\dot{R}\dot{Q}}_{\hat{W}_{12}} \bar{Z}^{\dot{R}\dot{Q}}_{\hat{Y}_{12}} && (N^2_{\dot{P}})\,. && (3.144)
\end{aligned}$$

Factorization of the corresponding exchange-type products of 4c2e integrals using THC yields formal $\mathcal{O}(M^4)$ scaling, comparable to the DF/NQ ansatz. As far as can be ascertained, the NQ/DF approach was first introduced in practical calculations in **Publication IV**, which makes a clear assessment of their relative performance difficult. While DF/NQ is potentially more accurate due to the use of highly refined DFT grids, THC may offer a smaller computational prefactor, reduced memory requirements, and a more unified and potentially faster evaluation. Overall, both methodologies exhibit considerable promise in quantum chemistry and can be combined with localized representations[46–51] and integral-screening techniques[44,52–62] to further reduce their computational cost.

3.3.5 Reduced Scaling MP2-F12 Theory

To reduce the scaling and computational cost of explicitly correlated F12 corrections, the decomposition strategies presented in Section 3.3.4 can be employed to target the principal bottlenecks, outlined here for the example of MP2-F12 theory. The discussion begins with the highly efficient computation of Fock matrix elements spanning multiple orbital spaces, which arise from the CABS-RI ansatz. Subsequently, the approximation-free evaluation of the three major $\mathcal{V}$, $\mathcal{X}$, and $\mathcal{B}$ intermediates (Eqs. 3.38–3.40) in MP2-F12 theory is introduced, along with a detailed analysis of their most efficient evaluation using decomposition techniques for direct- and exchange-type contributions.

Multiple Orbital Spaces Spanning Fock Matrix Elements

In contrast to Hartree–Fock theory (Section 2.2), F12 approaches give rise to F12-type Fock matrix elements that span multiple orbital spaces due to the decomposition of 6c3e and 8c4e integrals via CABS-RI (Section 3.3.4), as illustrated in Fig. 3.3 for the AO and MO spaces.

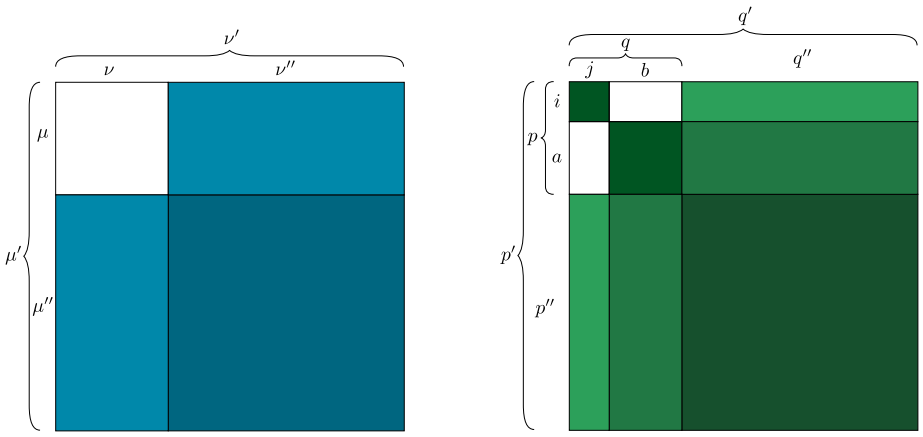

a) AO b) MO

Figure 3.3: Graphical representation of the AO (a) and MO (b) spaces present in RI-MP2-F12, covered by F12-type Fock matrix elements.

In the AO formalism, these elements are written as

$$f_{\mu'\nu'} = h^{\text{core}}_{\mu'\nu'} + j_{\mu'\nu'} - \tfrac{1}{2} k_{\mu'\nu'} \,, \tag{3.145}$$

where $h^{\text{core}}_{\mu'\nu'}$, $j_{\mu'\nu'}$, and $k_{\mu'\nu'}$ denote the core-Hamiltonian, Coulomb, and exchange matrix elements in the combined orbital spaces, respectively. While the computation of $h^{\text{core}}_{\mu'\nu'}$ is straightforward and incurs negligible cost, the Coulomb and exchange elements are evaluated as

$$j_{\mu'\nu'} = P_{\lambda\sigma}(\mu'\nu'|\lambda\sigma) \,, \tag{3.146}$$

$$k_{\mu'\nu'} = P_{\lambda\sigma}(\mu'\sigma|\lambda\nu') \,, \tag{3.147}$$

with $P_{\lambda\sigma}$ denoting the density matrix of the converged HF calculation. Subsequently, the AO F12-type Fock matrix is transformed into the MO basis by contraction with the final SCF MO and precomputed CABS coefficients, which incurs only minor computational cost. In contrast, the approximation-free evaluation of $j_{\mu'\nu'}$ and $k_{\mu'\nu'}$ is considerably more demanding and represents one of the computationally dominant contributions to the overall cost of the corresponding F12 correction. This is attributed to the large CABS space, which typically includes basis functions with higher angular momentum quantum numbers than the corresponding HF space, making F12-type Fock matrix constructions significantly more expensive than standard SCF Fock builds.

In **Publication II**, two highly efficient approaches are adapted from HF/DFT for the direct and exchange-type contributions of F12-type Fock matrix elements, significantly reducing their computational cost. Coulomb matrix elements are evaluated by extending the RI-J procedure[42,75,77] to multiple orbital spaces given by

$$j_{\mu'\nu'} \approx P_{\lambda\sigma}(\mu'\nu'|P)(P|Q)^{-1}(Q|\lambda\sigma)\,, \tag{3.148}$$

which enables a stepwise integral-direct algorithm:

$$\text{step 1:} \quad J_Q = (Q|\lambda\sigma)\,P_{\lambda\sigma}\,, \tag{3.149}$$

$$\text{step 2:} \quad \tilde{J}_P = (P|Q)^{-1}J_Q\,, \tag{3.150}$$

$$\text{step 3:} \quad j_{\mu'\nu'} = (\mu'\nu'|P)\tilde{J}_P\,. \tag{3.151}$$

In step 2, the explicit matrix inversion is avoided by solving the Coulomb-metric $(P|Q)\,x = J_Q$ directly, yielding $x = (P|Q)^{-1}J_Q \equiv \tilde{J}_P$, for which a Cholesky decomposition of $(P|Q)$ is employed. The rate-determining steps 1 and 3 are accelerated by a J-engine algorithm.[73,221] Here, the density(-like) matrix and the integrals are transformed into the Hermite basis, allowing the omission of all intermediate Hermite coefficients that do not contribute to the representation of the auxiliary basis functions during their contraction. Together, these techniques enable a highly efficient evaluation of the $j_{\mu'\nu'}$ elements.
For exchange matrix elements, numerical quadrature is employed, extending the sn-LinK methodology[43,222] to multiple orbital spaces, leading to

$$\bar{k}_{\mu'\nu'} \approx \frac{1}{2}\big[w_g P_{\lambda\sigma}\chi^g_{\mu'}\chi^g_\sigma(g|\lambda\nu') + \text{transpose}\big]\,, \tag{3.152}$$

where again a stepwise evaluation gives

$$\text{step 1:} \quad \bar{\chi}^g_\lambda = P_{\lambda\sigma}\,\chi^g_\sigma \tag{3.153}$$

$$\text{step 2:} \quad \mathcal{G}^g_{\nu'} = w_g\,(g|\lambda\nu')\bar{\chi}^g_\lambda \tag{3.154}$$

$$\text{step 3:} \quad \bar{k}_{\mu'\nu'} = \mathcal{G}^g_{\nu'}\bar{\chi}^g_{\mu'}\,. \tag{3.155}$$

To improve the precision of NQ for small grid sizes, the slight violation of symmetry in $\bar{k}_{\mu'\nu'}$ is corrected in the final exchange matrix by

$$k_{\mu'\nu'} \approx \frac{\bar{k}_{\mu'\nu'} + \bar{k}_{\nu'\mu'}}{2}\,. \tag{3.156}$$

The formal $\mathcal{O}(N_g N^2_{\mu'})$ scaling can be further reduced by employing batch-local quantities and integral screening strategies, as discussed in Section 3.3.4.
In general, RI-J and sn-LinK drastically improve the performance of Fock matrix evaluations spanning multiple orbital spaces in F12 theory while maintaining high accuracy. Compared to fully analytic Fock builds, speedups exceeding three orders of magnitude can be achieved, which can be further enhanced by exploiting the massively parallel capabilities of graphics processing units (GPUs). Both approaches perform even more efficiently in F12 calculations than in conventional HF theory, as the typically larger orbital spaces make the decomposition more effective. By applying these techniques, the Fock matrix construction, previously a major bottleneck in RI-MP2-F12 calculations, becomes effectively negligible.

$\mathcal{V}$ and $\mathcal{X}$ Intermediate

Both the $\mathcal{V}$ and $\mathcal{X}$ intermediates (Eqs. 3.38 and 3.39) share similar structural features, allowing for an analogous treatment of both terms. Within the fixed-amplitude approach, using the definition of the strong orthogonality operator $\hat{Q}_{12}$ in Eq. 3.17 and assuming the use of canonical molecular orbitals for the Fock matrix elements f_i^k and f_j^l leads directly to their approximation-free direct-type representation:

$$\mathcal{V}_{ij}^{ij} = \mathcal{FG}_{ij}^{ij} + \mathcal{F}_{kl}^{ij}\mathcal{G}_{ij}^{kl} - \mathcal{F}_{ab}^{ij}\mathcal{G}_{ij}^{ab} - \langle ijk|\hat{F}_{12}\hat{g}_{23}|kji\rangle - \langle jik|\hat{F}_{12}\hat{g}_{23}|kij\rangle \tag{3.157}$$

$$\mathcal{X}_{ij}^{ij} = \mathcal{FF}_{ij}^{ij} + \mathcal{F}_{kl}^{ij}\mathcal{F}_{ij}^{kl} - \mathcal{F}_{ab}^{ij}\mathcal{F}_{ij}^{ab} - \langle ijk|\hat{F}_{12}\hat{F}_{23}|kji\rangle - \langle jik|\hat{F}_{12}\hat{F}_{23}|kij\rangle \ , \tag{3.158}$$

with

$$\mathcal{G}_{rs}^{pq} = \langle pq|\hat{g}_{12}|rs\rangle \tag{3.159}$$

$$\mathcal{F}_{rs}^{pq} = \langle pq|\hat{F}_{12}|rs\rangle \tag{3.160}$$

$$\mathcal{FG}_{rs}^{pq} = \langle pq|\hat{F}_{12}\hat{g}_{12}|rs\rangle \tag{3.161}$$

$$\mathcal{FF}_{rs}^{pq} = \langle pq|\hat{F}_{12}\hat{F}_{12}|rs\rangle \ . \tag{3.162}$$

The corresponding exchange-type intermediates are obtained by interchanging i and j in the ket on the right-hand side, e.g.,

$$\langle ijk|\hat{F}_{12}\hat{g}_{23}|kji\rangle \quad \underset{\text{direct}}{\overset{\text{exchange}}{\rightleftarrows}} \quad \langle ijk|\hat{F}_{12}\hat{g}_{23}|kij\rangle \ . \tag{3.163}$$

Direct-type terms are typically evaluated using an alternative formulation of $\hat{Q}_{12}$ (here denoted as approximation a1),[31] in which the complete orbital space is approximated by the union of the HF and CABS-RI spaces, yielding

$$\hat{Q}_{12}^{\mathrm{a1}} = 1 - \hat{\mathrm{p}}_1\hat{\mathrm{p}}_2 - \hat{\mathrm{o}}_1\hat{\mathrm{p}}_2'' - \hat{\mathrm{p}}_1''\hat{\mathrm{o}}_2 \, . \tag{3.164}$$

The resulting intermediates can then be expressed as

$$\mathcal{V}_{ij}^{ij} = \mathcal{FG}_{ij}^{ij} - \mathcal{F}_{kp''}^{ij}\mathcal{G}_{ij}^{kp''} - \mathcal{F}_{p''k}^{ij}\mathcal{G}_{ij}^{p''k} - \mathcal{F}_{pq}^{ij}\mathcal{G}_{ij}^{pq} \tag{3.165}$$

$$\mathcal{X}_{ij}^{ij} = \mathcal{FF}_{ij}^{ij} - \mathcal{F}_{kp''}^{ij}\mathcal{F}_{ij}^{kp''} - \mathcal{F}_{p''k}^{ij}\mathcal{F}_{ij}^{p''k} - \mathcal{F}_{pq}^{ij}\mathcal{F}_{ij}^{pq} \, , \tag{3.166}$$

where further decomposition through DF, as discussed in Section 3.3.4, reduces the formal scaling to $\mathcal{O}(M^4)$. The form of $\hat{Q}_{12}$ in Eq. 3.164 circumvents the explicit computation of direct-type 6c3e integrals. Although these integrals can, in principle, also be factorized using NQ with $\mathcal{O}(M^4)$ scaling, this comes at the cost of a considerably larger prefactor. Following Eqs. 3.165 and 3.166 enables the reuse of quantities occurring during the decomposition of the $\mathcal{B}$ intermediate. For small molecular systems, this route remains the most efficient strategy for the corresponding exchange-type intermediates, albeit with formal $\mathcal{O}(M^5)$ scaling.

For medium- to large-sized systems, the strategies presented in **Publication III** and **Publication IV** enable an efficient evaluation of $\mathcal{V}_{ji}^{ij}$ and $\mathcal{X}_{ji}^{ij}$ with an overall formal $\mathcal{O}(M^4)$ scaling, working directly with the approximation-free formulation of $\hat{Q}_{12}$ defined in Eq. 3.17. The exact exchange-type expressions are given by

$$\mathcal{V}_{ji}^{ij} = \mathcal{FG}_{ji}^{ij} + \mathcal{F}_{kl}^{ij}\mathcal{G}_{ji}^{kl} - \mathcal{F}_{ab}^{ij}\mathcal{G}_{ji}^{ab} - \langle ijk|\hat{F}_{12}\hat{g}_{23}|kij\rangle - \langle jik|\hat{F}_{12}\hat{g}_{23}|kji\rangle \tag{3.167}$$

$$\mathcal{X}_{ji}^{ij} = \mathcal{FF}_{ji}^{ij} + \mathcal{F}_{kl}^{ij}\mathcal{F}_{ji}^{kl} - \mathcal{F}_{ab}^{ij}\mathcal{F}_{ji}^{ab} - \langle ijk|\hat{F}_{12}\hat{F}_{23}|kij\rangle - \langle jik|\hat{F}_{12}\hat{F}_{23}|kji\rangle \ , \tag{3.168}$$

where each intermediate consists of one 4c2e integral, two products of 4c2e integrals, and two identical 6c3e exchange-type integrals. The contribution of the $\mathcal{V}_{ji}^{ij}$ intermediate can be decomposed as

$$\mathcal{FG}_{ji}^{ij} \approx w_g P_{\mu\sigma} P_{\nu\lambda} \chi_\mu^g \chi_\nu^g (g|\hat{F}_{1g}\hat{g}_{1g}|\lambda\sigma) \quad (N_g N_\mu^2) \tag{3.169}$$

$$\mathcal{F}_{kl}^{ij}\mathcal{G}_{ji}^{kl} \approx \mathcal{F}_P^{ik}\tilde{\mathcal{F}}_Q^P\mathcal{F}_{jl}^Q w_g \phi_k^g \phi_j^g (g|\hat{g}_{1g}|li) \quad (N_g N_P N_k N_i) \tag{3.170}$$

$$\mathcal{F}_{ab}^{ij}\mathcal{G}_{ji}^{ab} \approx \mathcal{F}_P^{ia}\tilde{\mathcal{F}}_Q^P\mathcal{F}_{jb}^Q w_g \phi_a^g \phi_j^g (g|\hat{g}_{1g}|bi) \quad (N_g N_P N_a N_i) \tag{3.171}$$

$$\langle ijk|\hat{F}_{12}\hat{g}_{23}|kij\rangle \approx w_g P_{\mu\varepsilon} P_{\nu\lambda} P_{\sigma\delta}\, \chi_\mu^g \chi_\nu^g\, (g|\hat{F}_{1g}|\lambda\sigma)\, (g|\hat{g}_{1g}|\delta\varepsilon) \quad (N_g N_\mu^2)\,. \tag{3.172}$$

The AO formalism is applied wherever it ensures optimal efficiency, and the formal time complexity is indicated for each term. The $\mathcal{X}_{ji}^{ij}$ intermediate can be evaluated in an analogous manner:

$$\mathcal{FF}_{ji}^{ij} \approx w_g P_{\mu\sigma} P_{\nu\lambda} \chi_\mu^g \chi_\nu^g (g|\hat{F}_{1g}^2|\lambda\sigma) \quad (N_g N_\mu^2) \tag{3.173}$$

$$\mathcal{F}_{kl}^{ij}\mathcal{F}_{ji}^{kl} \approx \mathcal{F}_P^{ik}\tilde{\mathcal{F}}_Q^P\mathcal{F}_{jl}^Q w_g \phi_k^g \phi_j^g (g|\hat{F}_{1g}|li) \quad (N_g N_P N_k N_i) \tag{3.174}$$

$$\mathcal{F}_{ab}^{ij}\mathcal{G}_{ji}^{ab} \approx \mathcal{F}_P^{ia}\tilde{\mathcal{F}}_Q^P\mathcal{F}_{jb}^Q w_g \phi_a^g \phi_j^g (g|\hat{F}_{1g}|bi) \quad (N_g N_P N_a N_i) \tag{3.175}$$

$$\langle ijk|\hat{F}_{12}\hat{F}_{23}|kij\rangle \approx w_g P_{\mu\varepsilon} P_{\nu\lambda} P_{\sigma\delta}\, \chi_\mu^g \chi_\nu^g\, (g|\hat{F}_{1g}|\lambda\sigma)\, (g|\hat{F}_{1g}|\delta\varepsilon) \quad (N_g N_\mu^2)\,. \tag{3.176}$$

In Eqs. 3.170 and 3.171, numerical quadrature is applied to the 4c2e integrals containing the classical Coulomb operator $\hat{g}_{12}$, rather than to those involving the correlation factor $\hat{F}_{12}$. This approach eliminates the need for additional 3c2e or 2c2e integrals, since the required 3c1e integrals for $\hat{g}_{12}$ are already used in Eq. 3.172, thus reducing memory requirements. In addition to lowering the formal scaling, a major benefit of using the exact form of $\hat{Q}_{12}$ is that the evaluation remains completely CABS-RI free, avoiding both approximation errors and the corresponding computational overhead.

$\mathcal{B}$ Intermediate

The $\mathcal{B}$ intermediate constitutes by far the most intricate and computationally demanding contribution in RI-MP2-F12 theory, as it involves Fock operators together with the strong orthogonality operator $\hat{Q}_{12}$ in the arising integral expressions. Fortunately, the symmetry of $\hat{F}_{12}$ and $\hat{Q}_{12}$ under the exchange of electron labels allows $\hat{f}_1$ and $\hat{f}_2$ to be treated equivalently. Interchanging the indices $1 \leftrightarrow 2$ yields

$$\langle ij|\hat{F}_{12}\hat{Q}_{12}\hat{f}_2\hat{Q}_{12}\hat{F}_{12}|ij\rangle = \langle ji|\hat{F}_{12}\hat{Q}_{12}\hat{f}_1\hat{Q}_{12}\hat{F}_{12}|ji\rangle \ , \tag{3.177}$$

such that only $\hat{Q}_{12}\hat{f}_1\hat{Q}_{12}$ needs to be evaluated. Inserting $\hat{Q}_{12}$ as given in Eq. 3.17 leads to a set of distinct operator and projector combinations:

$$\begin{array}{rrrrr}
\hat{f}_1 & -\hat{f}_1\hat{o}_1 & -\hat{f}_1\hat{o}_2 & \hat{f}_1\hat{o}_1\hat{o}_2 & -\hat{f}_1\hat{v}_1\hat{v}_2 \\
-\hat{o}_1\hat{f}_1 & \hat{o}_1\hat{f}_1\hat{o}_1 & \hat{o}_1\hat{f}_1\hat{o}_2 & -\hat{o}_1\hat{f}_1\hat{o}_1\hat{o}_2 & \hat{o}_1\hat{f}_1\hat{v}_1\hat{v}_2 \\
-\hat{o}_2\hat{f}_1 & \hat{o}_2\hat{f}_1\hat{o}_1 & \hat{o}_2\hat{f}_1\hat{o}_2 & -\hat{o}_2\hat{f}_1\hat{o}_1\hat{o}_2 & \hat{o}_2\hat{f}_1\hat{v}_1\hat{v}_2 \\
\hat{o}_1\hat{o}_2\hat{f}_1 & -\hat{o}_1\hat{o}_2\hat{f}_1\hat{o}_1 & -\hat{o}_1\hat{o}_2\hat{f}_1\hat{o}_2 & \hat{o}_1\hat{o}_2\hat{f}_1\hat{o}_1\hat{o}_2 & -\hat{o}_1\hat{o}_2\hat{f}_1\hat{v}_1\hat{v}_2 \\
-\hat{v}_1\hat{v}_2\hat{f}_1 & \hat{v}_1\hat{v}_2\hat{f}_1\hat{o}_1 & \hat{v}_1\hat{v}_2\hat{f}_1\hat{o}_2 & -\hat{v}_1\hat{v}_2\hat{f}_1\hat{o}_1\hat{o}_2 & \hat{v}_1\hat{v}_2\hat{f}_1\hat{v}_1\hat{v}_2
\end{array} \tag{3.178}$$

Here, the idempotency of the projectors, the commutation properties of the operators, and the identities

$$\hat{o}_n\hat{v}_n = \hat{v}_n\hat{o}_n = \hat{o}_n\hat{f}_n\hat{v}_n = \hat{v}_n\hat{f}_n\hat{o}_n = 0\,, \tag{3.179}$$

together with the removal of canceling terms in the third and fourth rows, allow (3.178) to be reduced to:

$$\begin{array}{rrrrr}
\hat{f}_1 & -\hat{f}_1\hat{o}_1 & -\hat{f}_1\hat{o}_2 & \hat{f}_1\hat{o}_1\hat{o}_2 & -\hat{f}_1\hat{v}_1\hat{v}_2 \\
-\hat{o}_1\hat{f}_1 & \hat{o}_1\hat{f}_1\hat{o}_1 & \hat{o}_1\hat{o}_2\hat{f}_1 & -\hat{o}_1\hat{f}_1\hat{o}_1\hat{o}_2 & 0 \\
0 & 0 & 0 & 0 & 0 \\
0 & 0 & 0 & 0 & 0 \\
-\hat{v}_1\hat{v}_2\hat{f}_1 & 0 & 0 & 0 & \hat{v}_1\hat{f}_1\hat{v}_1\hat{v}_2
\end{array} \tag{3.180}$$

Consequently, $\hat{Q}_{12}\hat{f}_1\hat{Q}_{12}$ can be compactly written as

$$\hat{Q}_{12}\hat{f}_1\hat{Q}_{12} = \hat{f}_1 - \hat{f}_1\hat{o}_2 + \hat{\Pi}(-\hat{f}_1\hat{o}_1 + \hat{f}_1\hat{o}_1\hat{o}_2 - \hat{f}_1\hat{v}_1\hat{v}_2) + \hat{o}_1\hat{f}_1\hat{o}_1 - \hat{o}_1\hat{f}_1\hat{o}_1\hat{o}_2 + \hat{v}_1\hat{f}_1\hat{v}_1\hat{v}_2\,, \tag{3.181}$$

where the linear operator $\hat{\Pi}$ generates the transposed term, i.e., $\hat{\Pi}(\hat{f}_1\hat{o}_1) = \hat{f}_1\hat{o}_1 + \hat{o}_1\hat{f}_1$, thereby grouping identical terms due to the symmetry of the integrals. The operator and projector combinations in Eq. 3.181 can be evaluated in various ways. In the following, the exact evaluation, which involves complicated 4c2e, 6c3e, and 8c4e integrals, is discussed. Alternative approaches are presented subsequently, distinguishing between routes for the efficient evaluation of direct and exchange contributions.

The approximation-free evaluation of Eq. 3.181 yields the following integrals, with terms involving standard Fock matrix elements separated from those where individual contributions to the Fock operator must be evaluated separately. Terms involving only standard Fock matrix elements originate from operator combinations $\hat{o}_1\hat{f}_1\hat{o}_1$, $\hat{o}_1\hat{f}_1\hat{o}_1\hat{o}_2$, and $\hat{v}_1\hat{f}_1\hat{v}_1\hat{v}_2$, and can be evaluated as

$$\langle ij|\hat{F}_{12}\hat{o}_1\hat{f}_1\hat{o}_1\hat{F}_{12}|ij\rangle = \langle ijk|\hat{F}_{12}\hat{F}_{23}|lji\rangle\, f_k^l \tag{3.182}$$

$$\langle ij|\hat{F}_{12}\hat{o}_1\hat{f}_1\hat{o}_1\hat{o}_2\hat{F}_{12}|ij\rangle = \mathcal{F}_{lm}^{ij} f_k^l \mathcal{F}_{ij}^{km} \tag{3.183}$$

$$\langle ij|\hat{F}_{12}\hat{v}_1\hat{f}_1\hat{v}_1\hat{v}_2\hat{F}_{12}|ij\rangle = \mathcal{F}_{ab}^{ij} f_c^a \mathcal{F}_{ij}^{cb}\,. \tag{3.184}$$

The remaining combinations involve non-standard Fock matrix elements, including the kinetic energy, nuclear attraction, Coulomb, and exchange operators. Terms that give rise

to at most 4c2e integrals are computed as

$$\langle ij|\hat{F}_{12}\hat{t}_1\hat{F}_{12}|ij\rangle = \frac{1}{2}\langle ij|(\nabla_1\hat{F}_{12}\cdot\nabla_1\hat{F}_{12})|ij\rangle - \frac{1}{2}\langle ij|\hat{F}_{12}^2|(\Delta i)j\rangle \tag{3.185}$$

$$\langle ij|\hat{F}_{12}\hat{v}_1\hat{F}_{12}|ij\rangle = -\sum_A Z_A\langle ij|\hat{F}_{12}^2\hat{g}_{1A}|ij\rangle \tag{3.186}$$

$$\langle ij|\hat{F}_{12}\hat{t}_1(\hat{o}_1\hat{o}_2-\hat{v}_1\hat{v}_2)\hat{F}_{12}|ij\rangle = -\frac{1}{2}\langle ij|\hat{F}_{12}|(\Delta k)l\rangle\mathcal{F}_{ij}^{kl} + \frac{1}{2}\langle ij|\hat{F}_{12}|(\Delta a)b\rangle\mathcal{F}_{ij}^{ab} \tag{3.187}$$

$$\langle ij|\hat{F}_{12}\hat{v}_1(\hat{o}_1\hat{o}_2-\hat{v}_1\hat{v}_2)\hat{F}_{12}|ij\rangle = -\sum_A\langle ij|\hat{F}_{12}\hat{g}_{1A}|kl\rangle\mathcal{F}_{ij}^{kl} + \sum_A\langle ij|\hat{F}_{12}\hat{g}_{1A}|ab\rangle\mathcal{F}_{ij}^{ab}\,. \tag{3.188}$$

Terms leading up to 6c3e integrals are given by

$$\langle ij|\hat{F}_{12}\hat{j}_1\hat{F}_{12}|ij\rangle = \langle ijk|\hat{F}_{12}^2\hat{g}_{13}|ijk\rangle \tag{3.189}$$

$$\langle ij|\hat{F}_{12}\hat{k}_1\hat{F}_{12}|ij\rangle = \langle ijk|\hat{F}_{12}\hat{F}_{23}\hat{g}_{13}|kji\rangle \tag{3.190}$$

$$\langle ij|\hat{F}_{12}\hat{t}_1\hat{o}_1\hat{F}_{12}|ij\rangle = -\frac{1}{2}\langle ijk|\hat{F}_{12}\hat{F}_{23}|(\Delta k)ji\rangle \tag{3.191}$$

$$\langle ij|\hat{F}_{12}\hat{v}_1\hat{o}_1\hat{F}_{12}|ij\rangle = -\sum_A Z_A\langle ijk|\hat{F}_{12}\hat{F}_{23}\hat{g}_{1A}|kji\rangle \tag{3.192}$$

$$\langle ij|\hat{F}_{12}\hat{t}_1\hat{o}_2\hat{F}_{12}|ij\rangle = -\frac{1}{2}\langle ijk|\hat{F}_{12}\Delta_1\hat{F}_{13}|ikj\rangle \tag{3.193}$$

$$= -\frac{1}{2}\langle ijk|\hat{F}_{12}(\Delta_1\hat{F}_{13})|ikj\rangle \tag{3.194}$$

$$-\langle ijk|\hat{F}_{12}\nabla_1\hat{F}_{13}\cdot|(\nabla i)kj\rangle \tag{3.195}$$

$$-\frac{1}{2}\langle ijk|\hat{F}_{12}\hat{F}_{13}|(\Delta i)kj\rangle \tag{3.196}$$

$$\langle ij|\hat{F}_{12}\hat{v}_1\hat{o}_2\hat{F}_{12}|ij\rangle = -\sum_A Z_A\langle ijk|\hat{F}_{12}\hat{F}_{13}\hat{g}_{1A}|ikj\rangle \tag{3.197}$$

$$\langle ij|\hat{F}_{12}\hat{j}_1(\hat{o}_1\hat{o}_2-\hat{v}_1\hat{v}_2)\hat{F}_{12}|ij\rangle = \langle ijm|\hat{F}_{12}\hat{g}_{13}|klm\rangle\,\mathcal{F}_{ij}^{kl} + \langle ijk|\hat{F}_{12}\hat{g}_{13}|abk\rangle\,\mathcal{F}_{ij}^{ab} \tag{3.198}$$

$$\langle ij|\hat{F}_{12}\hat{k}_1(\hat{o}_1\hat{o}_2-\hat{v}_1\hat{v}_2)\hat{F}_{12}|ij\rangle = \langle ijm|\hat{F}_{12}\hat{g}_{13}|mlk\rangle\,\mathcal{F}_{ij}^{kl} + \langle ijk|\hat{F}_{12}\hat{g}_{13}|kba\rangle\,\mathcal{F}_{ij}^{ab}\,. \tag{3.199}$$

The remaining operator combinations give rise to 8c4e integrals

$$\langle ij|\hat{F}_{12}\hat{j}_1\hat{o}_1\hat{F}_{12}|ij\rangle = \langle ijkl|\hat{F}_{12}\hat{F}_{23}\hat{g}_{14}|kjil\rangle \tag{3.200}$$

$$\langle ij|\hat{F}_{12}\hat{k}_1\hat{o}_1\hat{F}_{12}|ij\rangle = \langle ijkl|\hat{F}_{12}\hat{F}_{23}\hat{g}_{14}|ljik\rangle \tag{3.201}$$

$$\langle ij|\hat{F}_{12}\hat{j}_1\hat{o}_2\hat{F}_{12}|ij\rangle = \langle ijkl|\hat{F}_{12}\hat{F}_{13}\hat{g}_{14}|ikjl\rangle \tag{3.202}$$

$$\langle ij|\hat{F}_{12}\hat{k}_1\hat{o}_2\hat{F}_{12}|ij\rangle = \langle ijkl|\hat{F}_{12}\hat{F}_{34}\hat{g}_{14}|lkji\rangle\,. \tag{3.203}$$

Several of these integrals closely resemble those arising in Hylleraas-CI (Section 3.2.1),[223–226] and can be evaluated with different approaches.[28,227–232] In practice, decomposition techniques (Section 3.3.4) are commonly employed to reduce the cost of the demanding 6c3e and 8c4e integrals, thereby enabling multiple computational strategies.

The evaluation of direct-type $\mathcal{B}_{ij}^{ij}$ contributions follows the general exact separation of (3.181) in combination with Eq. 3.177 given by

$$\mathcal{B}_{ij}^{ij} = \mathcal{A}_{ij}^{ij} + \mathcal{A}_{ji}^{ji} - \mathcal{Z}_{ij}^{ij} - \mathcal{Z}_{ji}^{ji} - \mathcal{F}_{ab}^{ij}\mathcal{C}_{ij}^{ab} - \mathcal{F}_{ab}^{ji}\mathcal{C}_{ji}^{ab}\,, \tag{3.204}$$

where

$$\mathcal{A}_{ij}^{ij} = \langle ij|\hat{F}_{12}\hat{f}_1\hat{Q}_{12}\hat{F}_{12}|ij\rangle\ , \tag{3.205}$$

$$\mathcal{Z}_{ij}^{ij} = \langle ij|\hat{F}_{12}\hat{\mathrm{o}}_1\hat{f}_1\hat{Q}_{12}\hat{F}_{12}|ij\rangle\ , \tag{3.206}$$

$$\mathcal{C}_{ij}^{ab} = \langle ab|\hat{f}_1(1-\hat{\mathrm{v}}_1)\hat{F}_{12}|ij\rangle\ . \tag{3.207}$$

Defining $\hat{Q}_{12}^{\mathrm{a1}} = 1 - \hat{P}_{12}$ (see Eq. 3.164), allows $\mathcal{A}_{ij}^{ij}$ to be split into two individual contributions

$$\mathcal{A}_{ij}^{ij} = \mathcal{M}_{ij}^{ij} - \mathcal{N}_{ij}^{ij} = \langle ij|\hat{F}_{12}\hat{f}_1\hat{F}_{12}|ij\rangle - \langle ij|\hat{F}_{12}\hat{f}_1\hat{P}_{12}\hat{F}_{12}|ij\rangle\ , \tag{3.208}$$

where

$$\hat{P}_{12} = -\hat{\mathrm{p}}_1\hat{\mathrm{p}}_2 - \hat{\mathrm{o}}_1\hat{\mathrm{p}}_2'' + \hat{\mathrm{p}}_1''\hat{\mathrm{o}}_2\,, \tag{3.209}$$

results in

$$\langle ij|\hat{F}_{12}\hat{f}_1\hat{P}_{12}\hat{F}_{12}|ij\rangle = \langle ij|\hat{F}_{12}\hat{f}_1|pq\rangle\mathcal{F}_{ij}^{pq} + \langle ij|\hat{F}_{12}\hat{f}_1|kp''\rangle\mathcal{F}_{ij}^{kp''} + \langle ij|\hat{F}_{12}\hat{f}_1|p''k\rangle\mathcal{F}_{ij}^{p''k}\,. \tag{3.210}$$

Additionally, approximating the projector on the complete MO space via $\hat{\bar{\alpha}}_1 \approx \hat{\mathrm{p}}_1'$ for $\mathcal{N}_{ij}^{ij}$ gives rise to products of 4c2e integrals with multiple orbital spaces spanning Fock matrix elements (Section 3.3.5):

$$\langle ij|\hat{F}_{12}\hat{\bar{\alpha}}_1\hat{f}_1|pq\rangle\mathcal{F}_{ij}^{pq} \approx \mathcal{F}_{r'q}^{ij}f_p^{r'}\mathcal{F}_{ij}^{pq} \tag{3.211}$$

$$\langle ij|\hat{F}_{12}\hat{\bar{\alpha}}_1\hat{f}_1|kp''\rangle\mathcal{F}_{ij}^{kp''} \approx \mathcal{F}_{r'p''}^{ij}f_k^{r'}\mathcal{F}_{ij}^{kp''} \tag{3.212}$$

$$\langle ij|\hat{F}_{12}\hat{\bar{\alpha}}_1\hat{f}_1|p''k\rangle\mathcal{F}_{ij}^{p''k} \approx \mathcal{F}_{r'k}^{ij}f_{p''}^{r'}\mathcal{F}_{ij}^{p''k} \tag{3.213}$$

Contributions arising from $\mathcal{Z}_{ij}^{ij}$ and $\mathcal{C}_{ij}^{ab}$ are comparatively small and vanish under the GBC and ECB approximations, respectively. For the computation of $\mathcal{Z}_{ij}^{ij}$, the projector $\hat{Q}_{12}^{\mathrm{a1}}$ (Eq. 3.164) is further approximated (denoted as a2) by an additional RI insertion of the form $1 \approx \hat{\mathrm{p}}_1'\hat{\mathrm{p}}_2'$:

$$\hat{Q}_{12}^{\mathrm{a2}} = \hat{\mathrm{p}}_1''\hat{\mathrm{p}}_2'' + \hat{\mathrm{v}}_1\hat{\mathrm{p}}_2'' + \hat{\mathrm{p}}_1''\hat{\mathrm{v}}_2\,, \tag{3.214}$$

leading to

$$\langle ij|\hat{F}_{12}\hat{\mathrm{o}}_1\hat{f}_1\hat{Q}_{12}^{\mathrm{a2}}\hat{F}_{12}|ij\rangle = \mathcal{F}_{kq''}^{ij}f_{p''}^{k}\mathcal{F}_{ij}^{p''q''} + \mathcal{F}_{ka}^{ij}f_{p''}^{k}\mathcal{F}_{ij}^{p''a}\,. \tag{3.215}$$

In the case of $\mathcal{C}_{ij}^{ab}$, the difference between the complete and virtual orbital space is approximated as $1 - \hat{\mathrm{v}}_1 \approx \hat{\mathrm{o}}_1 + \hat{\mathrm{p}}_1''$, yielding

$$\mathcal{C}_{ij}^{ab} \approx \langle ab|\hat{f}_1(\hat{\mathrm{o}}_1 + \hat{\mathrm{p}}_1'')\hat{F}_{12}|ij\rangle = f_{p''}^{a}\mathcal{F}_{ij}^{p''b}\,, \tag{3.216}$$

where for Eqs. 3.215 and 3.216 Brillouin's condition $f_i^a = 0$ is employed.[84,85] Factorization of the remaining $\mathcal{M}_{ij}^{ij}$ contribution via a triple full-space RI insertion is possible:

$$\langle ij|\hat{F}_{12}\hat{\bar{\alpha}}_1\hat{f}_1\hat{\bar{\alpha}}_1\hat{\bar{\alpha}}_2\hat{F}_{12}|ij\rangle \approx \mathcal{F}_{p'q'}^{ij} f_{r'}^{p'} \mathcal{F}_{ij}^{r'q'}, \tag{3.217}$$

but the resulting errors have been shown to converge slowly with the size of the RI basis, motivating the alternative, more efficient *commutator relation*.[25,27] Here, the commuting behavior of the $\hat{v}_1$ and $\hat{j}_1$ operators with the correlation factor $\hat{F}_{12}$ is exploited to obtain

$$\hat{F}_{12}\hat{f}_1\hat{F}_{12} = \frac{1}{2}\big[[\hat{F}_{12},\hat{t}_1],\hat{F}_{12}\big] - \hat{F}_{12}\hat{k}_1\hat{F}_{12} + \frac{1}{2}\big((\hat{f}_1+\hat{k}_1)\hat{F}_{12}^2 + \hat{F}_{12}^2(\hat{f}_1+\hat{k}_1)\big)\,, \tag{3.218}$$

noting that $\hat{f}_1 + \hat{k}_1 = \hat{t}_1 + \hat{v}_1 + \hat{j}_1$. The first term in Eq. 3.218 can be further transformed using the product rules for the Laplacian Δ_1 and the gradient operator ∇_1 as

$$\big[[\hat{F}_{12},\hat{t}_1],\hat{F}_{12}\big] = (\nabla_1\hat{F}_{12}\cdot\nabla_1\hat{F}_{12})\,, \tag{3.219}$$

allowing to write

$$\langle ij|(\nabla_1\hat{F}_{12}\cdot\nabla_1\hat{F}_{12})|ji\rangle \approx \gamma^2 \mathcal{FF}_{ij}^{ij}\,, \tag{3.220}$$

with γ as a fixed geminal exponent. The last two terms in Eq. 3.218 are identical due to the symmetry of the integrals and can be treated using a single full-space RI insertion:

$$\langle ij|(\hat{f}_1+\hat{k}_1)\hat{\bar{\alpha}}_1\hat{F}_{12}^2|ij\rangle \approx (f+k)_{p'}^{i}\mathcal{FF}_{ij}^{p'j}, \tag{3.221}$$

$$\langle ij|\hat{F}_{12}^2\hat{\bar{\alpha}}_1(\hat{f}_1+\hat{k}_1)|ij\rangle \approx \mathcal{FF}_{p'j}^{ij}(f+k)_{i}^{p'}. \tag{3.222}$$

The remaining terms involving the exchange operator are evaluated analogously to Eq. 3.217 using a triple RI insertion:

$$\langle ij|\hat{F}_{12}\hat{\bar{\alpha}}_1\hat{k}_1\hat{\bar{\alpha}}_1\hat{\bar{\alpha}}_2\hat{F}_{12}|ij\rangle \approx \mathcal{F}_{p'q'}^{ij} k_{r'}^{p'} \mathcal{F}_{ij}^{r'q'}\,, \tag{3.223}$$

where, due to the smaller energy contribution of the $\hat{k}_1$ operator, the resulting errors are considered acceptable. Further decomposition of the resulting 4c2e integral products via density fitting, as discussed in Section 3.3.4, is essential for efficient evaluation, reducing the formal scaling of these direct-type integrals from $\mathcal{O}(M^5)$ to $\mathcal{O}(M^4)$ with system size M. Moreover, exploiting canceling subspaces and reusing intermediate quantities across all integrals leads to optimal performance.

For the exchange-type $\mathcal{B}_{ji}^{ij}$ intermediate, a novel approach employing numerical quadrature is presented in **Publication IV**, requiring fewer RI insertions. This formalism decomposes certain operator and projector combinations from Eq. 3.181 into 6c3e integrals, which can be evaluated highly efficiently as detailed in **Publication III**, and allows for a more efficient application of DF/NQ to the remaining 4c2e integral products. While a purely DF-based evaluation retains $\mathcal{O}(M^5)$ scaling, the proposed strategy reduces this to formal $\mathcal{O}(M^4)$ scaling.

As for the direct-type counterparts, the *commutator relation* (Eq. 3.218) is employed, where the $(\nabla_1 \hat{F}_{12} \cdot \nabla_1 \hat{F}_{12})$ operator combination can be efficiently decomposed via a single NQ insertion in the AO formalism:

$$\langle ij|(\nabla_1 \hat{F}_{12} \cdot \nabla_1 \hat{F}_{12})|ji\rangle \approx \gamma^2 w_g P_{\mu\sigma} P_{\nu\lambda} \chi^g_\mu \chi^g_\nu (g|\hat{F}^2_{1g}|\lambda\sigma) \quad (N_g N^2_\mu)\,, \tag{3.224}$$

where again the formal scaling is reported. The corresponding exchange-type counterparts to the identical terms in Eqs. 3.221 and 3.222 similarly require only a single additional NQ insertion for efficient evaluation:

$$\langle ij|(\hat{f}_1 + \hat{k}_1)\hat{\tilde{\alpha}}_1 \hat{F}^2_{12}|ji\rangle \approx w_g P_{\mu\lambda} P_{\nu\sigma} P_{\varepsilon'\delta'} \chi^g_\mu \chi^g_{\varepsilon'} (g|\hat{F}^2_{1g}|\nu\lambda)(f+k)^{\delta'}_\sigma \quad (N_g N_{\mu'} N_\mu)\,, \tag{3.225}$$

with most of the computational effort of Eqs. 3.224 and 3.225 being shared with expressions arising in the $\mathcal{X}^{ij}_{ji}$ intermediate. The operator combinations $\hat{f}_1\hat{o}_1$ and $\hat{o}_1\hat{f}_1\hat{o}_1$ from Eq. 3.181, as well as $\hat{k}_1$ (Eq. 3.218), either inherently yield or can be transformed into exchange-type 6c3e integrals via full RI insertions $\hat{\tilde{\alpha}}$, with the AO formalism allowing for near-linear-scaling evaluation:

$$\begin{aligned}
\hat{k}_1 \to \hat{\tilde{\alpha}}_1 \hat{k}_1 \hat{\tilde{\alpha}}_1 : \ \langle ijp'|\hat{F}_{12}\hat{F}_{23}|q'ij\rangle\, k^{p'}_{q'} &\approx w_g P_{\mu\lambda} P_{\nu\sigma} P_{\delta'\gamma'} P_{\varepsilon'\zeta'} \chi^g_\mu \chi^g_\nu \\
&\quad \times (g|\hat{F}_{1g}|\lambda\delta')(g|\hat{F}_{1g}|\sigma\varepsilon')k^{\zeta'}_{\gamma'} && (3.226)\\
\hat{f}_1\hat{o}_1 \to \hat{\tilde{\alpha}}_1 \hat{f}_1 \hat{o}_1 : \langle ijp'|\hat{F}_{12}\hat{F}_{23}|lij\rangle\, f^{p'}_l &\approx w_g P_{\mu\lambda} P_{\nu\sigma} P_{\delta\gamma} P_{\varepsilon'\zeta'} \chi^g_\mu \chi^g_\nu \\
&\quad \times (g|\hat{F}_{1g}|\lambda\delta)(g|\hat{F}_{1g}|\sigma\varepsilon')f^{\zeta'}_\gamma && (3.227)\\
\hat{o}_1\hat{f}_1\hat{o}_1 : \qquad \langle ijk|\hat{F}_{12}\hat{F}_{23}|lij\rangle\, f^k_l &\approx w_g P_{\mu\lambda} P_{\nu\sigma} P_{\delta\gamma} P_{\varepsilon\zeta} \chi^g_\mu \chi^g_\nu \\
&\quad \times (g|\hat{F}_{1g}|\lambda\delta)(g|\hat{F}_{1g}|\sigma\varepsilon)f^{\zeta}_\gamma && (3.228)
\end{aligned}$$

Apart from the exchange and Fock matrix elements contracted in a final step, Eqs. 3.227 and 3.228 span only subspaces of Eq. 3.226. Most parts of these three expressions can therefore be evaluated simultaneously at no additional computational cost, while the overall $\mathcal{O}(N_g N^2_{\mu'})$ scaling is preserved. The remaining operator combinations $\hat{f}_1\hat{o}_2$, $\hat{f}_1\hat{o}_1\hat{o}_2$, $\hat{o}_1\hat{f}_1\hat{o}_1\hat{o}_2$, $\hat{f}_1\hat{v}_1\hat{v}_2$, and $\hat{v}_1\hat{f}_1\hat{v}_1\hat{v}_2$ in Eq. 3.181 can be factorized as products of 4c2e integrals multiplied by F12-type Fock matrix elements. Due to the reduced orbital space, the MO representation provides optimal performance, requiring at most a double full space RI insertion combined with DF and NQ, which leads to:

$$\begin{aligned}
\hat{f}_1\hat{o}_2 \to \hat{\tilde{\alpha}}_1\hat{f}_1\hat{\tilde{\alpha}}_1\hat{o}_2 : \quad \mathcal{F}^{ij}_{p'm} f^{p'}_{r'} \mathcal{F}^{r'm}_{ji} &\approx w_g \phi^g_i \phi^g_{p'} (g|\hat{F}_{1g}|jm)\, \mathcal{F}^{r'j}_R \tilde{\mathcal{F}}^R_S \mathcal{F}^S_{mi} f^{p'}_{r'} && (3.229)\\
\hat{f}_1\hat{o}_1\hat{o}_2 \to \hat{\tilde{\alpha}}_1\hat{f}_1\hat{o}_1\hat{o}_2 : \quad \mathcal{F}^{ij}_{p'm} f^{p'}_l \mathcal{F}^{lm}_{ji} &\approx w_g \phi^g_i \phi^g_{p'} (g|\hat{F}_{1g}|jm)\, \mathcal{F}^{lj}_R \tilde{\mathcal{F}}^R_S \mathcal{F}^S_{mi} f^{p'}_l && (3.230)\\
\hat{o}_1\hat{f}_1\hat{o}_1\hat{o}_2 : \quad \mathcal{F}^{ij}_{km} f^k_l \mathcal{F}^{lm}_{ji} &\approx w_g \phi^g_i \phi^g_k (g|\hat{F}_{1g}|jm)\, \mathcal{F}^{lj}_R \tilde{\mathcal{F}}^R_S \mathcal{F}^S_{mi} f^k_l && (3.231)\\
\hat{f}_1\hat{v}_1\hat{v}_2 \to \hat{\tilde{\alpha}}_1\hat{f}_1\hat{v}_1\hat{v}_2 : \quad \mathcal{F}^{ij}_{p'c} f^{p'}_b \mathcal{F}^{bc}_{ji} &\approx w_g \phi^g_i \phi^g_{p'} (g|\hat{F}_{1g}|jc)\, \mathcal{F}^{bj}_R \tilde{\mathcal{F}}^R_S \mathcal{F}^S_{ci} f^{p'}_b && (3.232)\\
\hat{v}_1\hat{f}_1\hat{v}_1\hat{v}_2 : \quad \mathcal{F}^{ij}_{ac} f^a_b \mathcal{F}^{bc}_{ji} &\approx w_g \phi^g_i \phi^g_a (g|\hat{F}_{1g}|jc)\, \mathcal{F}^{bj}_R \tilde{\mathcal{F}}^R_S \mathcal{F}^S_{ci} f^a_b\,, && (3.233)
\end{aligned}$$

where Eq. 3.230 and Eq. 3.231 span the same subspaces as Eq. 3.229, while Eq. 3.233 shares those of Eq. 3.232. Consequently, terms spanning the same orbital spaces can be

evaluated together by scaling the shared subspaces just once, which can be easily achieved by appropriately modifying the corresponding p'-th MO on the grid, $\phi^g_{p'}$. This enables the definition of two new intermediates:

$$\mathcal{U}^{ij}_{ji} = w_g\, \phi^g_i\, \phi^g_{p',\{\mathcal{U}\}} (g|\hat{F}_{1g}|jm)\, \mathcal{F}^{r'j}_R \tilde{\mathcal{F}}^R_S \mathcal{F}^S_{mi} f^{p'}_{r'} \qquad (N_g N_P N_{p'} N_i) \tag{3.234}$$

$$\mathcal{T}^{ij}_{ji} = w_g\, \phi^g_i\, \phi^g_{p',\{\mathcal{T}\}} (g|\hat{F}_{1g}|jc)\, \mathcal{F}^{bj}_R \tilde{\mathcal{F}}^R_S \mathcal{F}^S_{ci} f^{p'}_b \qquad (N_g N_P N_a N_i) \tag{3.235}$$

where $\phi^g_{p',\{\mathcal{U}\}}$ and $\phi^g_{p',\{\mathcal{T}\}}$ correspond to the scaled MOs on the grid. While the evaluation of exchange-type 4c2e and 6c3e integrals requires negligible effort, products of 4c2e integrals dominate the overall computational cost. The reformulation of terms leading to $\mathcal{U}^{ij}_{ji}$ and $\mathcal{T}^{ij}_{ji}$ differs from the direct-integral decomposition starting from Eq. 3.204 and enables a more homogeneous evaluation via numerical quadrature and density fitting (NQ/DF/CABS-RI), with greater reuse of intermediate quantities and formal $\mathcal{O}(M^4)$ scaling. The NQ/DF/CABS-RI approach is particularly beneficial for medium- to large-sized molecular systems, significantly reducing computational cost compared to decompositions relying solely on RI and DF. The numerical grid size can be adjusted to balance precision and efficiency. For large systems, speedups of approximately one order of magnitude are achieved for the rate-determining steps with virtually no loss of accuracy. This improvement is especially pronounced for systems with a delocalized electronic structure, where the ratio of active orbitals to numerical grid points is favorable. Overall, NQ/DF/CABS-RI substantially narrows the computational gap between the explicitly correlated F12 correction and conventional RI-MP2 calculations using the same basis set. For systems with significant HOMO–LUMO gaps, further performance gains appear feasible through localized MO representations[46–51] in combination with integral-screening techniques.[44,52–62,198–202]

Chapter 4

Publications

4.1 Publication I

A scaled explicitly correlated F12 correction to second-order Møller–Plesset perturbation theory

L. Urban, T. H. Thompson, and C. Ochsenfeld,
J. Chem. Phys. **2021**, *154*, 044101

Abstract:

An empirically scaled version of the explicitly correlated F12 correction to second-order Møller–Plesset perturbation theory (MP2-F12) is introduced. The scaling eliminates the need for many of the most costly terms of the F12 correction while reproducing the unscaled explicitly correlated F12 interaction energy correction to a high degree of accuracy. The method requires a single, basis set dependent scaling factor that is determined by fitting to a set of test molecules. We present factors for the cc-pVXZ-F12 (X = D, T, Q) basis set family obtained by minimizing interaction energies of the S66 set of small- to medium-sized molecular complexes and show that our new method can be applied to accurately describe a wide range of systems. Remarkably good explicitly correlated corrections to the interaction energy are obtained for the S22 and L7 test sets, with mean percentage errors for the double-zeta basis of 0.60% for the F12 correction to the interaction energy, 0.05% for the total electron correlation interaction energy, and 0.03% for the total interaction energy, respectively. Additionally, mean interaction energy errors introduced by our new approach are below 0.01 kcal mol^{-1} for each test set and are thus negligible for second-order perturbation theory based methods. The efficiency of the new method compared to the unscaled F12 correction is shown for all considered systems, with distinct speedups for medium- to large-sized structures.

The Journal of Chemical Physics ARTICLE scitation.org/journal/jcp

A scaled explicitly correlated F12 correction to second-order Møller–Plesset perturbation theory

Cite as: J. Chem. Phys. 154, 044101 (2021); doi: 10.1063/5.0033411
Submitted: 15 October 2020 • Accepted: 17 December 2020 •
Published Online: 22 January 2021

L. Urban,[1,2] T. H. Thompson,[1] and C. Ochsenfeld[1,2,a)]

AFFILIATIONS

[1] Department of Chemistry, Ludwig-Maximilians-University Munich (LMU Munich), D-81377 Munich, Germany
[2] Max Planck Institute for Solid State Research, D-70569 Stuttgart, Germany

[a)] Author to whom correspondence should be addressed: c.ochsenfeld@fkf.mpg.de

ABSTRACT

An empirically scaled version of the explicitly correlated F12 correction to second-order Møller–Plesset perturbation theory (MP2-F12) is introduced. The scaling eliminates the need for many of the most costly terms of the F12 correction while reproducing the unscaled explicitly correlated F12 interaction energy correction to a high degree of accuracy. The method requires a single, basis set dependent scaling factor that is determined by fitting to a set of test molecules. We present factors for the cc-pVXZ-F12 (X = D, T, Q) basis set family obtained by minimizing interaction energies of the S66 set of small- to medium-sized molecular complexes and show that our new method can be applied to accurately describe a wide range of systems. Remarkably good explicitly correlated corrections to the interaction energy are obtained for the S22 and L7 test sets, with mean percentage errors for the double-zeta basis of 0.60% for the F12 correction to the interaction energy, 0.05% for the total electron correlation interaction energy, and 0.03% for the total interaction energy, respectively. Additionally, mean interaction energy errors introduced by our new approach are below 0.01 kcal mol^{-1} for each test set and are thus negligible for second-order perturbation theory based methods. The efficiency of the new method compared to the unscaled F12 correction is shown for all considered systems, with distinct speedups for medium- to large-sized structures.

I. INTRODUCTION

It is well-known that the computation and evaluation of electron correlation effects are critical for the accurate and quantitative description of chemical systems. One of the simplest *ab initio* wave function based correlation methods is second-order Møller–Plesset perturbation theory (MP2).[1] Since its first formulation in 1934, several extensions and simplifications have been proposed to improve its accuracy and decrease its computational cost: The resolution of the identity (RI) approximation[2–4] and the related pseudospectral approach[5] can be used to significantly reduce the computational prefactor of the method, while local orbital or atomic orbital (AO) based formulations (see, e.g., Refs. 6 and 7) are able to lower the asymptotic computational scaling with the system size to as low as linear. In addition, complete basis set (CBS) extrapolation[8,9] and explicitly correlated R12/F12 methods[10–15] have been introduced to overcome the basis set incompleteness error (BSIE). The latter incorporates explicitly coupled two-electron terms (geminals) into the wave function to better describe short-ranged correlation and satisfy electronic cusp conditions,[16] leading to much faster convergence with respect to the size of the one-electron basis set.

To improve accuracy for non-covalent interactions (NCIs), some authors have introduced a scaling of the correlation energy with an empirically determined factor.[17,18] In 2003, Grimme[19] established the spin-component-scaled MP2 (SCS-MP2) method, which employs separate scaling factors for the same-spin (SS) and the opposite-spin (OS) energy contributions,

$$E_{\text{SCS-MP2}} = c_{\text{OS}} E^{\text{OS}}_{\text{MP2}} + c_{\text{SS}} E^{\text{SS}}_{\text{MP2}}, \quad (1)$$

where $c_{OS} = \frac{6}{5}$ and $c_{SS} = \frac{1}{3}$ are the fixed OS and SS scaling factors, respectively. In particular, the description of stacked unsaturated complexes and the computation of thermochemical properties benefit by using SCS-MP2 instead of MP2, where for general NCIs, no superior results are obtained.[20] However, several variations of this ansatz[21–25] could improve its accuracy and have been applied to other correlation methods within the context of configuration interaction[26,27] and coupled cluster[28,29] theories. One popular variation of the SCS-MP2 method is Jung *et al.*'s[30] scaled-opposite-spin MP2 (SOS-MP2) method, which focuses on the opposite-spin MP2 energy contribution and completely neglects the same-spin part, leading to the energy expression

$$E_{\text{SOS-MP2}} = c_{\text{SOS}} E^{\text{OS}}_{\text{MP2}}. \tag{2}$$

The choice of $c_{\text{SOS}} = 1.3$ as a scaling factor results in small differences to SCS-MP2 and improved reaction and atomization energies compared to standard MP2. The use of SOS-MP2 is beneficial in terms of efficiency since it allows for a reduction in the computational scaling of the method with the system size M from $\mathcal{O}(M^5)$ for standard MP2 and SCS-MP2 to $\mathcal{O}(M^4)$ when SOS-MP2 is combined with Laplace-transform methods.[30,31]

Besides SCS-MP2 and SOS-MP2, the hybrid supermolecular MP2 *coupled* (MP2C) approach by Pitoňák and Heßelmann[32] has become popular in the last decade for the calculation of NCIs. It focuses on correcting the MP2 dispersion interactions of complexes by neglecting and replacing the uncoupled Hartree–Fock (UCHF) dispersion energy with a more accurate time-dependent density-functional theory (TDDFT) based quantity, resulting in

$$E^{\text{MP2C}}_{\text{IE}} = E^{\text{MP2}}_{\text{IE}} - E^{\text{UCHF}}_{\text{Disp}} + E^{\text{TDDFT}}_{\text{Disp}}, \tag{3}$$

as interaction energy expression, and a notably improved description of all kinds of NCIs. In general, MP2, SCS-MP2, and MP2C suffer from large BSIEs and are improved when an explicitly correlated F12 correction is applied, allowing for the use of smaller double-zeta basis sets.[33] However, the F12 correction introduces significant overhead, especially for MP2 theory and its variation, and its computation is by far the most expensive step in the correlation calculation.

In this paper, we address this issue of the computationally demanding F12 correction by using the general SOS idea in the context of explicitly correlated second-order Møller–Plesset perturbation theory. Our new method does not require the computationally expensive geminal–geminal exchange-type integrals and thus drastically reduces the prefactor of MP2-F12 calculations, especially for small basis sets. We have determined scaling factors designed to reproduce the standard explicitly correlated MP2-F12 correction to the interaction energy as accurately as possible for a wide range of organic and biologically relevant systems.

II. THEORY

A. Fixed-amplitude Fl 2 correction

Consider the closed-shell, spin-adapted explicitly correlated second-order F12 correction to the correlation energy,

$$E_{\text{F12}} = \sum_{s=0,1} (2s+1) \sum_{ij} e^s_{ij}, \tag{4}$$

where e^s_{ij} is the singlet ($s = 0$) or triplet ($s = 1$) energy contribution for a pair of spatial orbitals $(\phi_i\phi_j)$. In the popular diagonal, orbital-invariant formulation of Ten-no,[15,34,35] which satisfies Kato's cusp condition[16] without the need for geminal amplitude optimization, the pair contributions can be written as

$$e^s_{ij} = e^s_{ij,\tilde{B}} + e^s_{ij,\tilde{V}}, \tag{5}$$

where $e^s_{ij,\tilde{V}}$ represents the contributions of all terms involving one explicitly correlated geminal (orbital-geminal) and $e^s_{ij,\tilde{B}}$ contains all terms involving two geminals (geminal–geminal). The explicitly correlated pair energies are

$$e^s_{ij,\tilde{B}} = 2^{-(2s+2+\delta_{ij})}\left(\tilde{B}^{ij}_{ij} + (1-2s)\tilde{B}^{ji}_{ij}\right), \tag{6}$$

$$e^s_{ij,\tilde{V}} = 2^{-(s+\delta_{ij})}\left(\tilde{V}^{ij}_{ij} + (1-2s)\tilde{V}^{ji}_{ij}\right), \tag{7}$$

with Kronecker delta δ_{ij},

$$\tilde{B}^{ij}_{ij} = B^{ij}_{ij} - X^{ij}_{ij}(\epsilon_i + \epsilon_j) - (C^{ab}_{ij})^\dagger C^{ab}_{ij}\varepsilon^{ab}_{ij}, \tag{8}$$

$$\tilde{V}^{ij}_{ij} = V^{ij}_{ij} - (C^{ab}_{ij})^\dagger g^{ij}_{ab}\varepsilon^{ab}_{ij}, \tag{9}$$

and

$$B^{ij}_{ij} = \langle\phi_i\phi_j|\hat{F}_{12}\hat{Q}_{12}(\hat{f}_1+\hat{f}_2)\hat{Q}_{12}\hat{F}_{12}|\phi_i\phi_j\rangle, \tag{10}$$

$$X^{ij}_{ij} = \langle\phi_i\phi_j|\hat{F}_{12}\hat{Q}_{12}\hat{F}_{12}|\phi_i\phi_j\rangle, \tag{11}$$

$$V^{ij}_{ij} = \langle\phi_i\phi_j|\hat{F}_{12}\hat{Q}_{12}r_{12}^{-1}|\phi_i\phi_j\rangle, \tag{12}$$

$$C^{ij}_{ab} = \langle\phi_a\phi_b|(\hat{f}_1+\hat{f}_2)\hat{Q}_{12}\hat{F}_{12}|\phi_i\phi_j\rangle, \tag{13}$$

$$g^{ij}_{ab} = \langle\phi_a\phi_b|r_{12}^{-1}|\phi_i\phi_j\rangle, \tag{14}$$

$$\varepsilon^{ab}_{ij} = (\epsilon_a + \epsilon_b - \epsilon_i - \epsilon_j)^{-1}. \tag{15}$$

Here, $\hat{f}_1$ and $\hat{f}_2$ are the one-electron Fock-operators, ϵ_i and ϵ_a are occupied and virtual orbital energies, respectively, $\hat{F}_{12}$ is the correlation factor, and $\hat{Q}_{12}$ is the strong orthogonality operator,

$$\hat{Q}_{12} = (1-\hat{o}_1)(1-\hat{o}_2)(1-\hat{v}_1\hat{v}_2). \tag{16}$$

The exchange-type expressions for $\tilde{B}^{ji}_{ij}$ and $\tilde{V}^{ji}_{ij}$ are simply obtained by switching $|\phi_i\phi_j\rangle$ to $|\phi_j\phi_i\rangle$ in Eqs. (10)–(14). More details on the computation and derivation of these intermediates can be found in the literature.[36–38] The singlet and triplet F12 energy corrections are

$$e^0_{ij} = \frac{1}{8}(\tilde{B}^{ij}_{ij} + \tilde{B}^{ji}_{ij}) + \frac{1}{2}(\tilde{V}^{ij}_{ij} + \tilde{V}^{ji}_{ij}), \tag{17}$$

$$e^1_{ij} = \frac{1}{32}(\tilde{B}^{ij}_{ij} - \tilde{B}^{ji}_{ij}) + \frac{1}{4}(\tilde{V}^{ij}_{ij} - \tilde{V}^{ji}_{ij}), \tag{18}$$

and the contribution from one pair of spatial orbitals is thus

$$e_{ij}^{0} + 3e_{ij}^{1} = \frac{7}{32}\tilde{B}_{ij}^{ij} + \frac{1}{32}\tilde{B}_{ij}^{ji} + \frac{5}{4}\tilde{V}_{ij}^{ij} - \frac{1}{4}\tilde{V}_{ij}^{ji}. \quad (19)$$

B. Empirical scaling of geminal–geminal terms

We aim to avoid the need to calculate the $\mathcal{O}(M^5)$ scaling exchange-type term $\tilde{B}_{ij}^{ji}$ since it is by far the most costly[37] and also contributes relatively little to the final F12 correction. Therefore, we introduce a scaling of the geminal–geminal triplet energy by a factor of 4/3 and an empirically determined scaling factor c_{SF12} used to fit the resulting energy to the standard MP2-F12 interaction energy values. The resulting explicitly correlated total pair energy correction then becomes

$$c_{\mathrm{SF12}}\left(e_{ij,\tilde{B}}^{0} + 4e_{ij,\tilde{B}}^{1}\right) + e_{ij,\tilde{V}}^{0} + 3e_{ij,\tilde{V}}^{1} = c_{\mathrm{SF12}}\frac{1}{4}\tilde{B}_{ij}^{ij} + \frac{5}{4}\tilde{V}_{ij}^{ij} - \frac{1}{4}\tilde{V}_{ij}^{ji}, \quad (20)$$

where summation over all pairs of spatial orbitals in combination with the MP2 energy leads to the definition of our scaled explicitly correlated second-order Møller–Plesset perturbation energy denoted as MP2-SF12.

C. Basis set dependence of c_{SF12}

Because triplet correlation energies converge faster than singlet energies,[39] the F12 triplet correction vanishes earlier in the complete basis set limit than the singlet correction. For this reason, the initial scaling of the triplet geminal–geminal correction by 4/3 becomes increasingly negligible as the size of the basis set increases, and the ideal c_{SF12} factor changes accordingly. Thus, it is necessary to determine an optimal factor for each basis set. This is not a problem in practice since the determination of good factors can be performed quite cheaply by fitting to a set of small molecules (see below). In any case, the F12 correction is designed to deliver accurate energies with smaller basis sets, which become necessary for calculations of larger systems where the SF12 approximation allows for sizable speedups.

D. Effect of SF12 scaling on the computational cost

In explicitly correlated second-order F12 theory, the use of RI in the form of Valeev's CABS approach[13] leads to MP2 like expressions involving products of two-electron integrals, which scale as $\mathcal{O}(M^5)$ with the size of the system M. Through the use of density fitting (DF) techniques,[40,41] the scaling of direct-type terms ($\tilde{B}_{ij}^{ij}$, $\tilde{V}_{ij}^{ij}$) can be reduced to fourth-order, while the fifth-order scaling remains for the exchange-type terms, albeit with a significantly reduced prefactor. Both RI and DF require auxiliary basis sets μ' and μ'', and such sets have been specifically designed for both cases.[42,43] Although the computational scaling is not worse than for MP2 itself, the sheer number of terms involved in the F12 correction, along with the appearance of the very large CABS basis set in the most expensive terms, means that it is significantly more costly than an MP2 calculation when using the same one-electron basis set. The SF12 approximation reduces the number of $\mathcal{O}(M)$ terms substantially, leading to significant cost savings for larger systems.

During testing, we noted that the size of the one-electron basis set used has an effect on the computational cost-saving, with slightly smaller speedups seen for larger basis sets (see below). Since the expensive steps of the F12 calculation (integral calculation, integral transformation, and integral contraction) all scale as $\mathcal{O}(N^3)$ with the size of the one-electron basis sets N for a given system, one could expect that speedups should stay roughly the same as the size of these basis sets increases. The decrease in computational advantage for larger basis sets occurs due to the fact that the computational steps saved through the SF12 approximation involve only orthogonalized basis sets in which linear dependencies within the given atomic orbitals have been removed. The number of linear dependencies can become quite large in the CABS method so that expensive $\mathcal{O}(M^4)$ scaling steps involving overdetermined atomic orbitals (integral calculation and integral transformation), which are largely unaffected by our SF12 approximation, gain more importance with increasing atomic orbital basis sets. This, however, is not a problem in practice since the intended goal of the SF12 approximation is to reduce the computational overhead for calculation of large systems with relatively small basis sets.

III. COMPUTATIONAL DETAILS

All reported MP2-SF12 and MP2-F12 energy calculations were performed in our program package `FermiONs++`.[44–48] Besides the necessary use of Ten-no's fixed amplitude ansatz,[15] we applied the extended Brillouin condition (EBC)[11] and thus neglect the last term in Eqs. (8) and (9). A fixed Slater type geminal (STG) correlation factor[14,49] of the form $\hat{F}_{12} = \frac{1}{\gamma}[1 - \exp(-\gamma r_{12})]$, with $\gamma = 1.3$, was utilized in the 3*C variant[36] of the explicitly correlated F12 correction. Furthermore, we employed the cc-pVXZ-F12[50–52] basis set family, with the corresponding RI cc-pVXZ-F12/OptRI+[42] and DF cc-pVXZ-F12/MP2fit[43] basis sets.

IV. RESULTS

A. Determination of c_{SF12}

In order to obtain reliable, well-balanced c_{SF12} factors for each member of the cc-pVXZ-F12 (X = D, T, Q) basis set family, which are capable of reproducing the F12 correction to the interaction energy to a high degree of accuracy, we decided to employ the S66 complexes[53] for parameterization. The small- to medium-sized S66 dimers cover a broad range of organic and biologically relevant systems and incorporate different kinds of noncovalent interactions (NCIs). With 23 systems representing frequently occurring hydrogen bond donor and acceptor groups, 23 structures dominated by dispersion effects, and 20 with mixed dispersion and electrostatic interactions, respectively, we consider the S66 complexes as suitable reference for fitting SF12 energies to NCIs.

First, the MP2-F12 interaction energies for each basis set and S66 complex were once evaluated via Boys and Bernardi counterpoise correction,[54] and the total and intermediate energy results of these calculations were saved. These data were subsequently used in a minimization procedure to reduce the mean percentage error (MPE) between the SF12 and F12 corrections of the S66 complexes. Starting with initial guesses of 0.9 and 1.0 for c_{SF12} to avoid potential local minima, the factors were stepwise increased and decreased with a systematic reduction in the stepsize close to the minimum value. Figure 1 visualizes the minimization procedure for the MPE

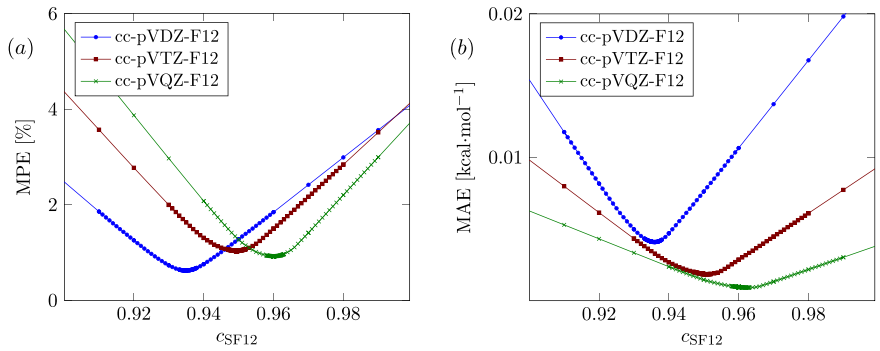

FIG. 1. Visualization of the minimization procedure for the cc-pVXZ-F12 (X = D, T, Q) basis set family using S66 complexes. (a) MPE minimization between the MP2-F12 and MP2-SF12 corrections to the interaction energy and (b) corresponding MAEs (kcal mol^{-1}).

and the corresponding mean absolute errors (MAE), demonstrating very small errors for all basis sets. We determined for the double-, triple-, and quadruple-zeta basis sets factors of 0.935, 0.95, and 0.96, respectively.

B. SFI 2 non-covalent interaction energies

1. Accuracy

The main results of the F12 and SF12 interaction energy corrections using our c_{SF12} factors are reported in Table I, showing MAEs, maximum errors (MAX), and MPEs for the S66 fitting set and two validation sets S22[8] and L7.[55] Together, S22 and L7 cover a broad range of small- to medium-sized (S22) as well as large-sized structures (L7) with up to 112 atoms, including single, double, and triple bonds. In combination, a scope of NCIs such as dispersion interactions like π–π stacking, hydrogen bonds, mixed electrostatic-dispersion effects, and interaction of aliphatic hydrocarbons is represented. In general, excellent MAEs for all test and basis sets were obtained, with values of 0.004 kcal mol^{-1}, 0.002 kcal mol^{-1}, and 0.007 kcal mol^{-1} (S66, S22, L7) for a cc-pVDZ-F12 basis. Even for the large L7 complexes, highly accurate results were obtained, which indicates no size limitation of our SF12 method using the determined c_{SF12} factors. Only a few small aliphatic S66 hydrocarbons lead to outlying larger deviations to F12, which are visualized in Fig. 2 alongside with the errors for each system basis set combination. In total, almost no error variations are observed supporting the general applicability of SF12.

The MPEs are considerably below 1% for the cc-pVDZ-F12 basis set and show almost no error. For larger basis sets, only S66 and S22 were employed (since some L7 complexes were too large for their computation). Here, absolute errors decrease and MPEs moderately increase. Again, SF12 introduces insignificant errors, which leads to negligible percentage errors in the correlation and total interaction energy of 0.05% and 0.03% for a cc-pVDZ-F12 basis.

Overall, the additional mean absolute errors introduced by SF12 are two orders of magnitude smaller than MP2-F12, SCS-MP2-F12, and MP2C-F12 errors compared to the CCSD(T)/aug-cc-pVTQZ (gold standard) for the S22 complexes. The most accurate of these stated methods for the S22 complexes is the MP2C-F12 approach, which results in MAEs of 0.18 kcal mol^{-1}, 0.15 kcal mol^{-1}, and 0.16 kcal mol^{-1} for the comparable aug-cc-pVXZ (X = D, T, Q) basis sets.[33] Our SF12 approach introduces additional errors for all these methods of 0.002 kcal mol^{-1}, 0.002 kcal mol^{-1}, and 0.001 kcal mol^{-1}, which are thus completely negligible.

TABLE I. MAEs, MAXs, and MPEs of the S66, S22, and L7 explicitly correlated F12 correction to the interaction energy using cc-pVXZ-F12 (X = D, T, Q) basis sets.

Test set	Basis set	c_{SF12}	MAE (kcal mol^{-1})	MAX (kcal mol^{-1})	MPE (%)
S66	cc-pVDZ-F12	0.935	0.004 12	0.082 22	0.627 31
S22	cc-pVDZ-F12	0.935	0.002 42	0.007 79	0.342 08
L7	cc-pVDZ-F12	0.935	0.007 29	0.011 29	0.475 16
S66	cc-pVTZ-F12	0.95	0.001 86	0.023 41	1.036 43
S22	cc-pVTZ-F12	0.95	0.001 92	0.010 77	0.535 26
S66	cc-pVQZ-F12	0.96	0.000 95	0.011 36	0.924 76
S22	cc-pVQZ-F12	0.96	0.001 18	0.005 33	0.692 09

2. Speedup

For comparison of the computational costs for the second-order SF12 and F12 corrections and associated therewith the applicability of our SF12 approach, the required computational times for both methods were measured for the adenine–thymine Watson–Crick complex from the S22 set, the L7 complexes, and additionally for a set of linear alkanes and amylose chains. The adenine–thymine Watson–Crick complex was calculated on 2 × Intel© Xeon© processor E5-2620 CPUs (12 cores, 2.00 GHz), while the L7 complexes as well as the linear alkanes and amylose chains were computed on 2 × Intel Xeon CPU E5-2667 v4 (16 cores, 3.20 GHz).

Table II reports the results of the S22 adenine–thymine Watson–Crick and the L7 complexes for a cc-pVDZ-F12 basis. The SF12 calculation of the explicitly correlated terms for the medium-sized adenine–thymine complex is 1.79 times faster than F12, which reduces to 1.53 and 1.14 times, for a cc-pVTZ-F12 and cc-pVQZ-F12 basis, respectively. As expected, the computation of larger systems like the L7 systems experiences a substantial speedup employing SF12. On average, the calculations of the explicitly correlated terms for these structures are by a factor of 2.41 times faster using in MP2-SF12 instead of MP2-F12, which

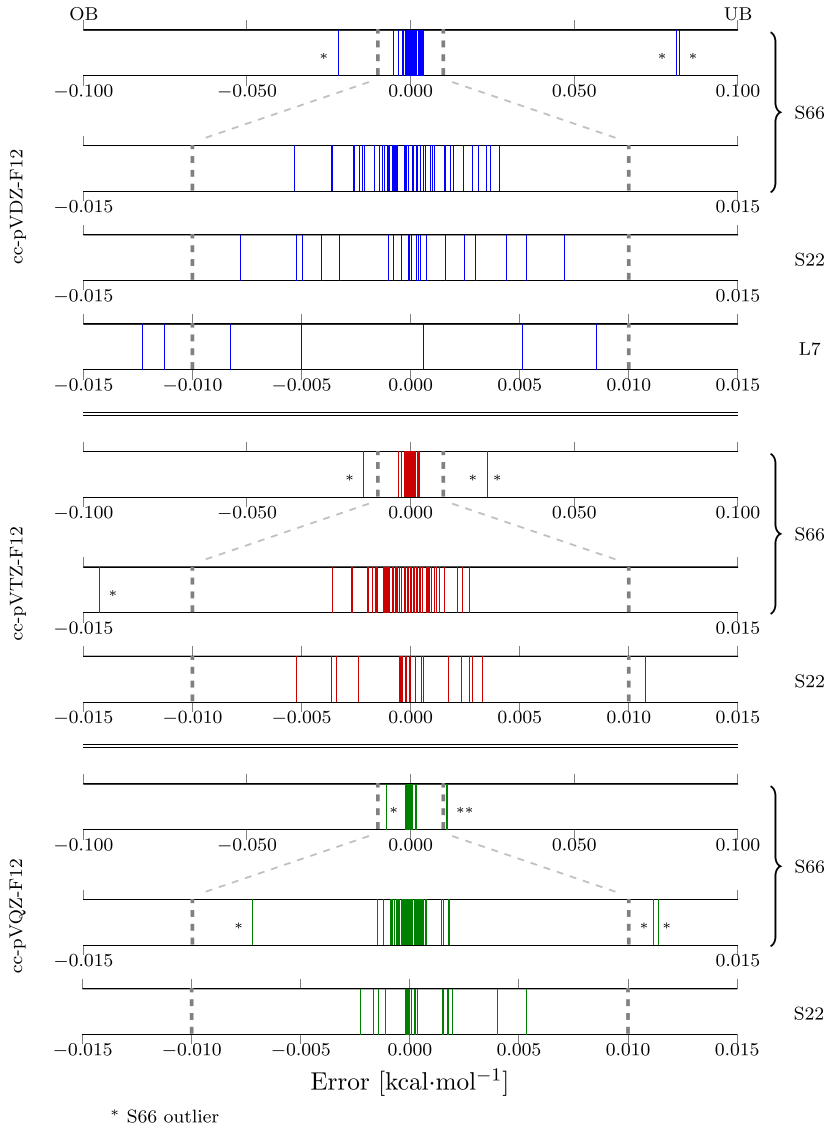

FIG. 2. SF12 Errors with respect to F12 for the S66, S22, and L7 complexes using cc-pVXZ-F12 (X = D, T, Q) basis sets and our c_{SF12} factors. Dashed guidelines are at ±0.01 kcal mol^{-1}, where negative values note overbinding (OB) and positive values note underbinding (UB).

has considerable effects on the total post Hartree–Fock computational time, e.g., the total MP2-SF12 correlation calculation with additional evaluation of the CABS+ singles correction requires for the L7 octadecane-dimer only 60% of the time MP2-F12 needs. In general, the SF12 approach combines distinct speedups with accurate explicitly correlated corrections to the interaction energy. Thus, its usage becomes highly attractive for medium- to large-sized structures.

To make quantitative scaling assessments and investigate the properties of SF12 and F12 for a series of systematically increasing structures, the timings for the explicitly correlated terms for linear alkanes and amylose chains were measured for a cc-pVDZ-F12 basis, showing good speedups that increase with the molecule size. For the largest members of both sets, $C_{60}H_{122}$ and an amylose chain out of four D-glucose monomers, SF12 performs 3.60 and

TABLE II. Ratios of the MP2-F12 and MP2-SF12 timings of the explicitly correlated F12 terms for the S22 adenine–thymine Watson–Crick and L7 complexes using a cc-pVDZ-F12 basis.

Complex	t_{F12} (h)	t_{SF12} (h)	$\frac{t_{F12}}{t_{SF12}}$
Adenine–thymin Watson–Crick	0.19	0.11	1.79
Octadecane-dimer	3.20	1.03	3.10
Guanine-trimer	0.56	0.25	2.19
Circumcoronene-adenine	7.94	2.74	2.90
Circumcoronene-guanine-cytosine	11.06	4.35	2.54
Phenylalanineresidues-trimer	2.40	1.07	2.24
Coronene-dimer	1.74	0.81	2.15
Guanine-cytosin–guanine-cytosin stack	0.85	0.48	1.76

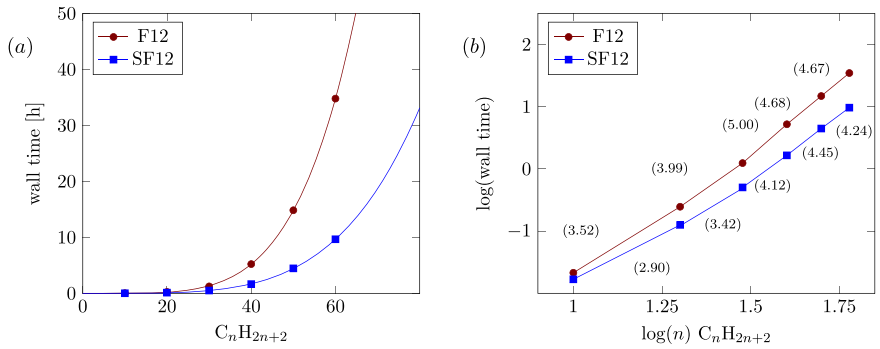

FIG. 3. Linear plot (a) and corresponding log–log plot (b) of the wall times for the explicitly correlated F12 and SF12 corrections of linear *n*-alkanes (C_nH_{2n+2}, $n \in \{10, 20, 30, 40, 50, 60\}$) for a cc-pVDZ-F12 basis. The numbers in brackets correspond to scaling exponents between two neighboring structures.

2.83 times faster than F12. This has, in practice, distinct effects on the computational cost, e.g., the F12 calculation of $C_{60}H_{122}$ requires 34.78 h, which drops to 9.66 h for SF12. Since our c_{SF12} are fitted to interaction energy corrections, larger deviations to F12 absolute energy corrections are expected. Regardless, our factors have proven to accurately treat all kinds of NCIs, and going to chemically related complexes of these polymers such as L7 octadecan–dimer complex, SF12 results in a negligible interaction energy correction error of 0.000 65 kcal mol^{-1}.

All evaluated F12 and SF12 timings of the alkane and amyloses are visualized in Figs. 3 and 4 as linear and log–log plots, and the scaling behavior with the system size M was determined by linear regression of the wall times between two neighboring members of the test sets. SF12 shows a noticeably decreased scaling behavior with $\mathcal{O}(M^{4.24})$ and $\mathcal{O}(N^{3.60})$ for the largest systems, where F12 leads to $\mathcal{O}(M^{4.67})$ and $\mathcal{O}(M^{4.10})$, respectively. The observed scaling of the explicitly correlated SF12 terms is smaller than the formal $\mathcal{O}(M^5)$ scaling of F12 and SF12 in the 3*C variant.[37] Lower scaling terms dominate the calculation due to the neglect of the exchange-type B terms even for large systems and thus lower the measured scaling exponent. Considering the beneficial performance enhancement and the achieved precision of SF12, which was demonstrated even for large systems, highly accurate results are expectable, and its usage enables the computation of chemical relevant systems very close to the level of F12 but in remarkably less time.

V. CONCLUSION AND OUTLOOK

A simple extension to the 3*C variant of the explicitly correlated F12 correction to the second-order Møller–Plesset perturbation theory is introduced, which noticeably reduces its computational demand, especially for medium- to large-sized molecules, while retaining accurately to the MP2-F12 interaction energy reference. By scaling of the Coulomb type geminal–geminal contributions to the F12 correction and additional neglect of exchange-type integrals, we achieved a substantial computational cost reduction.

In order to determine the necessary c_{SF12} factors of each cc-pVXZ-F12 (X = D, T, Q) basis set, a minimization procedure was employed to reduce the mean percentage error between S66 MP2-F12 and MP2-SF12 Boys and Bernardi counterpoise corrected F12 interaction energy corrections. The obtained general c_{SF12} has shown some remarkably good results for the S66, S22, and L7 test set with a very low MAE of 0.004 kcal mol^{-1}, 0.002 kcal mol^{-1}, and 0.007 kcal mol^{-1} for a cc-pVDZ-F12 basis. Supported by small MPE for the explicitly correlated interaction correction, the correlation interaction energy, and the total interaction energy with values of 0.60%, 0.05%, and 0.03% for a cc-pVDZ-F12 basis, MP2-SF12 allows the computation of non-covalent interactions for all kinds of chemically relevant systems close to the level of MP2-F12. Besides the good accuracy, a noticeable computational cost reduction was observed as demonstrated for L7 complexes, linear alkanes, and amylose chains.

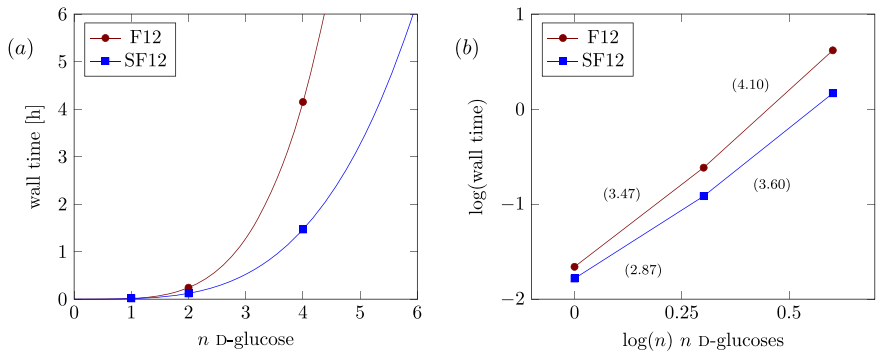

FIG. 4. Linear plot (a) and corresponding log–log plot (b) of the wall times for MP2-F12 and MP2-SF12 explicitly correlated F12 correction calculations of linear amyloses (n D-glucose, $n \in \{1, 2, 4\}$) for a cc-pVDZ-F12 basis. The numbers in brackets correspond to scaling exponents between two neighboring structures.

For medium- to large-sized systems, a speedup of the explicitly correlated F12 correction to the correlation calculation by a factor of 2 and more compared to MP2-F12 are expectable using a cc-pVDZ-F12 basis.

In total, our SF12 correction is recommended for large systems and molecular complexes with a cc-pVDZ-F12 basis to incorporate the full potential of F12 theory. Future work will focus on applying our SF12 approach to dynamical studies to investigate novel chemical problems. Furthermore, we are planning to combine SF12 with different theories and fitting references to reproduce high quality, explicitly correlated quantum chemical interaction energies, e.g., the reproduction of CCSD(T)-F12 interaction energies.

SUPPLEMENTARY MATERIAL

See the supplementary material for energy data and timings of all test set calculations.

ACKNOWLEDGMENTS

Financial support is gratefully acknowledged from the DFG Excellence Cluster, Grant No. EXC 2111-390814868 (Munich Center for Quantum Science and Technology—MCQST). C.O. further acknowledges financial support as Max-Planck-Fellow of the MPI-FKF Stuttgart.

DATA AVAILABILITY

The data that support the findings of this study are available within the article and its supplementary material.

REFERENCES

[1] C. Møller and M. S. Plesset, Phys. Rev. **46**, 618 (1934).
[2] M. Feyereisen, G. Fitzgerald, and A. Komornicki, Chem. Phys. Lett. **208**, 359 (1993).
[3] O. Vahtras, J. Almlöf, and M. W. Feyereisen, Chem. Phys. Lett. **213**, 514 (1993).
[4] F. Weigend, M. Häser, H. Patzelt, and R. Ahlrichs, Chem. Phys. Lett. **294**, 143 (1998).
[5] R. A. Friesner, R. B. Murphy, M. D. Beachy, M. N. Ringnalda, W. T. Pollard, B. D. Dunietz, and Y. Cao, J. Phys. Chem. A **103**, 1913–1928 (1999).
[6] M. Schütz, G. Hetzer, and H.-J. Werner, J. Chem. Phys. **111**, 5691 (1999).
[7] B. Doser, D. S. Lambrecht, J. Kussmann, and C. Ochsenfeld, J. Chem. Phys. **130**, 064107 (2009).
[8] P. Jurečka, J. Šponer, J. Černý, and P. Hobza, Phys. Chem. Chem. Phys. **8**, 1985–1993 (2006).
[9] T. H. Dunning, J. Chem. Phys. **90**, 1007 (1989).
[10] W. Kutzelnigg, Theor. Chem. Acc. **68**, 445 (1985).
[11] W. Kutzelnigg and W. Klopper, J. Chem. Phys. **94**, 1985 (1991).
[12] F. R. Manby, H.-J. Werner, T. B. Adler, and A. J. May, J. Chem. Phys. **124**, 094103 (2006).
[13] E. F. Valeev, Chem. Phys. Lett. **395**, 190 (2004).
[14] S. Ten-no, Chem. Phys. Lett. **398**, 56 (2004).
[15] S. Ten-no, J. Chem. Phys. **121**, 117 (2004).
[16] T. Kato, Commun. Pure Appl. Math. **10**, 151 (1957).
[17] M. S. Gordon and D. G. Truhlar, J. Am. Chem. Soc. **108**, 5412–5419 (1986).
[18] P. E. M. Siegbahn, M. R. A. Blomberg, and M. Svensson, Chem. Phys. Lett. **223**, 35 (1994).
[19] S. Grimme, J. Chem. Phys. **118**, 9095 (2003).
[20] S. Grimme, L. Goerigk, and R. F. Fink, Wiley Interdiscip. Rev.: Comput. Mol. Sci. **2**, 886 (2012).
[21] R. C. Lochan, Y. Jung, and M. Head-Gordon, J. Phys. Chem. A **109**, 7598 (2005).
[22] R. C. Lochan and M. Head-Gordon, J. Chem. Phys. **126**, 164101 (2007).
[23] Y. Jung and M. Head-Gordon, Phys. Chem. Chem. Phys. **8**, 2831–2840 (2006).
[24] Á. Szabados, J. Chem. Phys. **125**, 214105 (2006).
[25] R. A. Distasio and M. Head-Gordon, Mol. Phys. **105**, 1073–1083 (2007).
[26] Y. M. Rhee and M. Head-Gordon, J. Phys. Chem. A **111**, 5314–5326 (2007).
[27] D. Casanova, Y. M. Rhee, and M. Head-Gordon, J. Chem. Phys. **128**, 164106 (2008).
[28] T. Takatani, E. G. Hohenstein, and D. C. Sherrill, J. Chem. Phys. **128**, 124111 (2008).
[29] A. Hellweg, S. A. Grün, and C. Hättig, Phys. Chem. Chem. Phys. **10**, 4119–4127 (2008).
[30] Y. Jung, R. C. Lochan, A. D. Dutoi, and M. Head-Gordon, J. Chem. Phys. **121**, 9793 (2004).
[31] J. Almlöf, Chem. Phys. Lett. **181**, 319 (1991).
[32] M. Pitoňák and A. Heßelmann, J. Chem. Theory Comput. **6**, 168 (2010).
[33] L. A. Burns, M. S. Marshall, and C. D. Sherrill, J. Chem. Phys. **141**, 234111 (2014).
[34] F. A. Bischoff, S. Höfener, A. Glöß, and W. Klopper, Theor. Chem. Acc. **121**, 11 (2008).
[35] W. Klopper and C. C. M. Samson, J. Chem. Phys. **116**, 6397 (2002).
[36] H.-J. Werner, T. B. Adler, and F. R. Manby, J. Chem. Phys. **126**, 164102 (2007).
[37] R. A. Bachorz, F. A. Bischoff, A. Glöß, C. Hättig, S. Höfener, W. Klopper, and D. P. Tew, J. Comput. Chem. **32**, 2492 (2011).
[38] Y. M. Wang, C. Hättig, S. Reine, E. Valeev, T. Kjærgaard, and K. Kristensen, J. Chem. Phys. **144**, 204112 (2016).
[39] W. Klopper, Mol. Phys. **99**, 481 (2001).
[40] F. R. Manby, J. Chem. Phys. **119**, 4607 (2003).
[41] A. J. May and F. R. Manby, J. Chem. Phys. **121**, 4479 (2004).
[42] R. A. Shaw and J. Grant Hill, J. Chem. Theory Comput. **13**, 1691–1698 (2017).
[43] S. Kritikou and J. Grant Hill, J. Chem. Theory Comput. **11**, 5269–5276 (2015).
[44] J. Kussmann and C. Ochsenfeld, J. Chem. Phys. **138**, 134114 (2013).
[45] J. Kussmann and C. Ochsenfeld, J. Chem. Theory Comput. **11**, 918 (2015).
[46] J. Kussmann and C. Ochsenfeld, J. Chem. Theory Comput. **13**, 2712 (2017).
[47] J. Kussmann and C. Ochsenfeld, J. Chem. Theory Comput. **13**, 3153 (2017).
[48] T. H. Thompson and C. Ochsenfeld, J. Chem. Phys. **150**, 044101 (2019).
[49] S. Ten-no, J. Chem. Phys. **126**, 014108 (2007).
[50] K. A. Peterson, T. B. Adler, and H.-J. Werner, J. Chem. Phys. **128**, 084102 (2008).
[51] J. Grant Hill and K. A. Peterson, Phys. Chem. Chem. Phys. **12**, 10460–10468 (2010).
[52] J. Grant Hill and K. A. Peterson, J. Chem. Phys. **141**, 094106 (2014).
[53] J. Řezáč, K. E. Riley, and P. Hobza, J. Chem. Theory Comput. **7**, 2427 (2011).
[54] S. F. Boys and F. Bernardi, Mol. Phys. **19**, 553 (1970).
[55] R. Sedlak, T. Janowski, M. Pitoňák, J. Řezáč, P. Pulay, and P. Hobza, J. Chem. Theory Comput. **9**, 3364 (2013).

A Scaled Explicitly Correlated F12 Correction to Second-Order Møller-Plesset Perturbation Theory: Supplementary Material

L. Urban,[1,2] T. H. Thompson,[1] and C. Ochsenfeld[1,2]

[1)] *Department of Chemistry, Ludwig-Maximilians-University Munich (LMU Munich), D-81377 Munich, Germany*

[2)] *Max Planck Institute for Solid State Research, D-70569 Stuttgart, Germany;*

(Dated: 15 October 2020)

TABLE I. DF-MP2-F12/cc-pVDZ-F12 and DF-MP2-SF12/cc-pVDZ-F12 explicitly correlated F12 interaction energy corrections of the S66 test set. c_{SF12} = 0.935; MAE [kcal·mol^{-1}] = 0.004; MPE [%] = 0.62731; MPE of the correlation interaction energy [%] = 0.04445; MPE of the total interaction energy [%] = 0.02618.

S66-Structure	$E_{Int.\ F12}$ [H]	$E_{Int.\ SF12}$ [H]	c_{SF12}	Err. [H]	Err. [%]	corr. Int. Err. [%]	tot. Int. Error [%]
01WaterWater	-0.000673	-0.000672	0.93313	0.000001	0.15002	0.05215	0.01297
02WaterMeOH	-0.000824	-0.000822	0.93294	0.000001	0.16324	0.04531	0.01513
03WaterMeNH2	-0.000922	-0.000925	0.93914	0.000003	0.31334	0.07742	0.02606
04WaterPeptide	-0.001152	-0.001151	0.93366	0.000001	0.10504	0.03636	0.00963
05MeOHMeOH	-0.000804	-0.000802	0.93182	0.000002	0.25410	0.05887	0.02246
06MeOHMeNH2	-0.001001	-0.001003	0.93697	0.000001	0.14655	0.02786	0.01217
07MeOHPeptide	-0.001149	-0.001147	0.93244	0.000002	0.19826	0.05234	0.01796
08MeOHWater	-0.000654	-0.000652	0.93181	0.000002	0.25799	0.07294	0.02140
09MeNH2MeOH	-0.000477	-0.000477	0.93362	0.000000	0.09374	0.01393	0.00959
10MeNH2MeNH2	-0.000663	-0.000664	0.93610	0.000000	0.06961	0.00907	0.00705
11MeNH2Peptide	-0.000884	-0.000883	0.93335	0.000001	0.10803	0.01584	0.01137
12MeNH2Water	-0.001025	-0.001027	0.93706	0.000002	0.15300	0.03466	0.01336
13PeptideMeOH	-0.000803	-0.000803	0.93478	0.000000	0.01616	0.00270	0.00132
14PeptideMeNH2	-0.000924	-0.000928	0.93987	0.000003	0.33695	0.04834	0.02602
15PeptidePeptide	-0.001076	-0.001077	0.93625	0.000001	0.09082	0.01603	0.00726
16PeptideWater	-0.000593	-0.000594	0.93604	0.000000	0.08027	0.01826	0.00591
17UracilUracilBP	-0.002063	-0.002069	0.93832	0.000006	0.26759	0.08577	0.02054
18WaterPyridine	-0.000838	-0.000841	0.93952	0.000003	0.34736	0.07302	0.02633
19MeOHPyridine	-0.000870	-0.000871	0.93738	0.000002	0.18197	0.03031	0.01320
20AcOHAcOH	-0.002678	-0.002679	0.93533	0.000001	0.02759	0.01494	0.00248
21AcNH2AcNH2	-0.002047	-0.002052	0.93781	0.000005	0.22217	0.08060	0.01801
22AcOHUracil	-0.002415	-0.002419	0.93694	0.000004	0.16097	0.07167	0.01280
23AcNH2Uracil	-0.002228	-0.002234	0.93862	0.000007	0.29219	0.11639	0.02174
24BenzeneBenzenepipi	-0.000517	-0.000513	0.91612	0.000004	0.80636	0.03160	0.06091
25PyridinePyridinepipi	-0.000698	-0.000693	0.92269	0.000004	0.59663	0.02935	0.04695
26UracilUracilpipi	-0.001596	-0.001588	0.92593	0.000008	0.52912	0.04907	0.05078
27BenzenePyridinepipi	-0.000620	-0.000616	0.92059	0.000004	0.66347	0.02990	0.05126
28BenzeneUracilpipi	-0.001018	-0.001012	0.92375	0.000006	0.56861	0.03492	0.05215
29PyridineUracilpipi	-0.001104	-0.001098	0.92527	0.000006	0.51567	0.03535	0.04443
30BenzeneEthene	-0.000342	-0.000339	0.90913	0.000003	0.98555	0.04332	0.10478
31UracilEthene	-0.000592	-0.000590	0.92873	0.000002	0.32328	0.02376	0.03284

S66-Structure	$E_{Int.\ F12}$ [H]	$E_{Int.\ SF12}$ [H]	c_{SF12}	Err. [H]	Err. [%]	corr. Int. Err. [%]	tot. Int. Error [%]
32UracilEthyne	-0.000628	-0.000627	0.93009	0.000002	0.23997	0.02143	0.02345
33PyridineEthene	-0.000402	-0.000398	0.91451	0.000003	0.84388	0.04135	0.08461
34PentanePentane	-0.000630	-0.000629	0.93173	0.000001	0.17017	0.00956	0.01835
35NeopentanePentane	-0.000432	-0.000432	0.93556	0.000000	0.02983	0.00168	0.00323
36NeopentaneNeopentane	-0.000269	-0.000270	0.94210	0.000001	0.39467	0.02014	0.04040
37CyclopentaneNeopentane	-0.000418	-0.000418	0.93683	0.000000	0.09906	0.00562	0.01118
38CyclopentaneCyclopentane	-0.000490	-0.000489	0.93352	0.000000	0.07923	0.00442	0.00832
39BenzeneCyclopentane	-0.000598	-0.000596	0.92870	0.000002	0.31452	0.01654	0.02759
40BenzeneNeopentane	-0.000482	-0.000482	0.93389	0.000000	0.05837	0.00321	0.00523
41UracilPentane	-0.000895	-0.000891	0.92710	0.000004	0.42033	0.02788	0.04706
42UracilCyclopentane	-0.000737	-0.000734	0.92592	0.000003	0.47410	0.02926	0.05076
43UracilNeopentane	-0.000603	-0.000601	0.92967	0.000002	0.28251	0.01839	0.02857
44EthenePentane	-0.000307	-0.000272	1.25412	0.000035	11.47364	0.01099	0.01955
45EthynePentane	-0.002448	-0.002579	1.01607	0.000131	5.35302	0.25798	0.02285
46PeptidePentane	-0.000792	-0.000790	0.92894	0.000003	0.32984	0.02361	0.03949
47BenzeneBenzeneTS	-0.000512	-0.000512	0.93432	0.000000	0.03625	0.00235	0.00333
48PyridinePyridineTS	-0.000640	-0.000640	0.93562	0.000000	0.03590	0.00289	0.00350
49BenzenePyridineTS	-0.000578	-0.000579	0.93660	0.000001	0.08949	0.00667	0.00826
50BenzeneEthyneCHpi	-0.000517	-0.000519	0.94081	0.000002	0.33108	0.03566	0.03316
51EthyneEthyneTS	-0.001970	-0.002100	1.02773	0.000129	6.57183	0.23223	0.02237
52BenzeneAcOHOHpi	-0.000887	-0.000887	0.93526	0.000000	0.01638	0.00215	0.00185
53BenzeneAcNH2NHpi	-0.000760	-0.000761	0.93867	0.000002	0.23210	0.03090	0.02485
54BenzeneWaterOHpi	-0.000603	-0.000604	0.93609	0.000000	0.06908	0.01012	0.00780
55BenzeneMeOHOHpi	-0.000733	-0.000731	0.93220	0.000001	0.16614	0.01659	0.01710
56BenzeneMeNH2NHpi	-0.000582	-0.000581	0.93084	0.000001	0.22327	0.01755	0.02290
57BenzenePeptideNHpi	-0.000840	-0.000840	0.93421	0.000000	0.04595	0.00379	0.00412
58PyridinePyridineCHN	-0.000641	-0.000646	0.94675	0.000005	0.77825	0.10309	0.07413
59EthyneWaterCHO	-0.000356	-0.000359	0.94458	0.000002	0.69636	0.26032	0.05552
60EthyneAcOHOHpi	-0.000875	-0.000877	0.93941	0.000003	0.28755	0.07253	0.03298
61PentaneAcOH	-0.000601	-0.000600	0.92977	0.000002	0.28401	0.02217	0.03910
62PentaneAcNH2	-0.000703	-0.000701	0.93009	0.000002	0.27446	0.02204	0.03624
63BenzeneAcOH	-0.000727	-0.000726	0.93257	0.000001	0.13390	0.01118	0.01454
64PeptideEthene	-0.000571	-0.000570	0.93449	0.000000	0.02953	0.00305	0.00362
65PyridineEthyne	-0.000458	-0.000464	0.95415	0.000006	1.26978	0.23252	0.08905
66MeNH2Pyridine	-0.000680	-0.000679	0.93086	0.000002	0.24209	0.02183	0.02426

TABLE II. DF-MP2-F12/cc-pVTZ-F12 and DF-MP2-SF12/cc-pVTZ-F12 explicitly correlated F12 interaction energy corrections of the S66 test set. c_{SF12} = 0.950; MAE [kcal·mol^{-1}] = 0.002; MPE [%] = 1.03643; MPE of the correlation interaction energy [%] = 0.02309; MPE of the total interaction energy [%] = 0.01759.

S66-Structure	$E_{Int.\ F12}$ [H]	$E_{Int.\ SF12}$ [H]	c_{SF12}	Err. [H]	Err. [%]	corr. Int. Err. [%]	tot. Int. Error [%]
01WaterWater	-0.000290	-0.000291	0.95170	0.000000	0.14847	0.02128	0.00548
02WaterMeOH	-0.000354	-0.000354	0.95032	0.000000	0.02805	0.00319	0.00110
03WaterMeNH2	-0.000400	-0.000402	0.95567	0.000002	0.48175	0.04951	0.01715
04WaterPeptide	-0.000502	-0.000502	0.94994	0.000000	0.00487	0.00068	0.00019
05MeOHMeOH	-0.000348	-0.000348	0.94958	0.000000	0.03693	0.00355	0.00139
06MeOHMeNH2	-0.000436	-0.000437	0.95355	0.000001	0.29722	0.02363	0.01057
07MeOHPeptide	-0.000498	-0.000497	0.94904	0.000000	0.08266	0.00887	0.00317
08MeOHWater	-0.000285	-0.000285	0.95071	0.000000	0.06193	0.00730	0.00221
09MeNH2MeOH	-0.000199	-0.000199	0.94859	0.000000	0.11354	0.00672	0.00469
10MeNH2MeNH2	-0.000272	-0.000272	0.94907	0.000000	0.07213	0.00371	0.00291
11MeNH2Peptide	-0.000365	-0.000364	0.94612	0.000001	0.31040	0.01786	0.01300
12MeNH2Water	-0.000439	-0.000440	0.95322	0.000001	0.27164	0.02525	0.00999
13PeptideMeOH	-0.000342	-0.000342	0.95022	0.000000	0.01865	0.00128	0.00064
14PeptideMeNH2	-0.000387	-0.000389	0.95475	0.000002	0.39174	0.02282	0.01247
15PeptidePeptide	-0.000461	-0.000461	0.95184	0.000001	0.15609	0.01126	0.00524
16PeptideWater	-0.000255	-0.000255	0.95312	0.000001	0.26885	0.02523	0.00839
17UracilUracilBP	-0.000907	-0.000910	0.95466	0.000004	0.41997	0.05601	0.01397
18WaterPyridine	-0.000379	-0.000380	0.95538	0.000002	0.45814	0.04196	0.01546
19MeOHPyridine	-0.000394	-0.000395	0.95365	0.000001	0.30953	0.02258	0.01002
20AcOHAcOH	-0.001201	-0.001203	0.95222	0.000002	0.20388	0.04550	0.00809
21AcNH2AcNH2	-0.000883	-0.000887	0.95431	0.000003	0.38590	0.05672	0.01329
22AcOHUracil	-0.001073	-0.001076	0.95352	0.000003	0.32171	0.05924	0.01118
23AcNH2Uracil	-0.000973	-0.000978	0.95492	0.000004	0.44511	0.07254	0.01428
24BenzeneBenzenepipi	-0.000245	-0.000242	0.92911	0.000003	1.24246	0.02244	0.04207
25PyridinePyridinepipi	-0.000313	-0.000310	0.93450	0.000003	1.01052	0.02162	0.03401
26UracilUracilpipi	-0.000656	-0.000651	0.93864	0.000006	0.87126	0.03171	0.03287
27BenzenePyridinepipi	-0.000284	-0.000281	0.93281	0.000003	1.08021	0.02160	0.03650
28BenzeneUracilpipi	-0.000438	-0.000433	0.93555	0.000004	0.99394	0.02529	0.03728
29PyridineUracilpipi	-0.000476	-0.000472	0.93735	0.000004	0.89605	0.02548	0.03172
30BenzeneEthene	-0.000169	-0.000167	0.92255	0.000003	1.48334	0.03107	0.07149
31UracilEthene	-0.000265	-0.000263	0.93886	0.000002	0.75257	0.02364	0.03204

S66-Structure	$E_{Int.\ F12}$ [H]	$E_{Int.\ SF12}$ [H]	c_{SF12}	Err. [H]	Err. [%]	corr. Int. Err. [%]	tot. Int. Error [%]
32UracilEthyne	-0.000288	-0.000286	0.93968	0.000002	0.65890	0.02558	0.02787
33PyridineEthene	-0.000190	-0.000187	0.92643	0.000003	1.35648	0.03030	0.05990
34PentanePentane	-0.000274	-0.000273	0.94312	0.000001	0.48333	0.01147	0.02140
35NeopentanePentane	-0.000189	-0.000188	0.94733	0.000000	0.19167	0.00459	0.00864
36NeopentaneNeopentane	-0.000124	-0.000124	0.95326	0.000000	0.23535	0.00540	0.01087
37CyclopentaneNeopentane	-0.000184	-0.000184	0.94864	0.000000	0.09881	0.00240	0.00470
38CyclopentaneCyclopentane	-0.000214	-0.000214	0.94449	0.000001	0.39132	0.00931	0.01723
39BenzeneCyclopentane	-0.000258	-0.000256	0.93972	0.000002	0.70344	0.01546	0.02542
40BenzeneNeopentane	-0.000211	-0.000210	0.94436	0.000001	0.39512	0.00922	0.01480
41UracilPentane	-0.000377	-0.000374	0.93876	0.000003	0.81666	0.02203	0.03629
42UracilCyclopentane	-0.000311	-0.000309	0.93748	0.000003	0.90092	0.02271	0.03833
43UracilNeopentane	-0.000261	-0.000259	0.94060	0.000002	0.67103	0.01824	0.02778
44EthenePentane	0.000138	0.000161	1.07375	0.000023	16.41575	0.00706	0.01266
45EthynePentane	-0.000446	-0.000483	1.02122	0.000037	8.36203	0.07574	0.00653
46PeptidePentane	-0.000334	-0.000332	0.94017	0.000002	0.71529	0.02081	0.03407
47BenzeneBenzeneTS	-0.000216	-0.000215	0.94393	0.000001	0.43286	0.01146	0.01606
48PyridinePyridineTS	-0.000268	-0.000267	0.94506	0.000001	0.36991	0.01201	0.01439
49BenzenePyridineTS	-0.000240	-0.000239	0.94639	0.000001	0.26591	0.00794	0.00976
50BenzeneEthyneCHpi	-0.000205	-0.000205	0.95005	0.000000	0.00385	0.00016	0.00015
51EthyneEthyneTS	-0.000250	-0.000287	1.04599	0.000037	14.91334	0.06840	0.00646
52BenzeneAcOHOHpi	-0.000351	-0.000350	0.94849	0.000000	0.11936	0.00585	0.00508
53BenzeneAcNH2NHpi	-0.000309	-0.000309	0.95017	0.000000	0.01324	0.00068	0.00055
54BenzeneWaterOHpi	-0.000239	-0.000239	0.94938	0.000000	0.04866	0.00265	0.00207
55BenzeneMeOHOHpi	-0.000290	-0.000289	0.94534	0.000001	0.35302	0.01331	0.01372
56BenzeneMeNH2NHpi	-0.000234	-0.000233	0.94264	0.000001	0.52888	0.01600	0.02064
57BenzenePeptideNHpi	-0.000336	-0.000335	0.94671	0.000001	0.24984	0.00794	0.00861
58PyridinePyridineCHN	-0.000280	-0.000281	0.95606	0.000001	0.49269	0.02754	0.02002
59EthyneWaterCHO	-0.000152	-0.000153	0.95685	0.000001	0.57240	0.08680	0.01928
60EthyneAcOHOHpi	-0.000369	-0.000370	0.95161	0.000000	0.12717	0.01249	0.00594
61PentaneAcOH	-0.000254	-0.000252	0.94089	0.000002	0.66110	0.02089	0.03567
62PentaneAcNH2	-0.000298	-0.000296	0.94103	0.000002	0.65596	0.02143	0.03445
63BenzeneAcOH	-0.000307	-0.000305	0.94267	0.000002	0.53012	0.01790	0.02296
64PeptideEthene	-0.000243	-0.000242	0.94377	0.000001	0.45724	0.01915	0.02260
65PyridineEthyne	-0.000201	-0.000203	0.96307	0.000002	1.05783	0.08207	0.03204
66MeNH2Pyridine	-0.000282	-0.000280	0.94283	0.000002	0.53547	0.01918	0.02121

TABLE III. DF-MP2-F12/cc-pVQZ-F12 and DF-MP2-SF12/cc-pVQZ-F12 explicitly correlated F12 interaction energy corrections of the S66 test set. $c_{SF12} = 0.960$; MAE [kcal·mol^{-1}] = 0.001; MPE [%] = 0.92476; MPE of the correlation interaction energy [%] = 0.01306; MPE of the total interaction energy [%] = 0.00850.

S66-Structure	$E_{Int.\ F12}$ [H]	$E_{Int.\ SF12}$ [H]	c_{SF12}	Err. [H]	Err. [%]	corr. Int. Err. [%]	tot. Int. Error [%]
01WaterWater	-0.000142	-0.000142	0.96311	0.000000	0.29776	0.02060	0.00535
02WaterMeOH	-0.000170	-0.000171	0.96225	0.000000	0.21425	0.01159	0.00402
03WaterMeNH2	-0.000195	-0.000197	0.96624	0.000001	0.57870	0.02874	0.01002
04WaterPeptide	-0.000238	-0.000239	0.96219	0.000000	0.20922	0.01371	0.00387
05MeOHMeOH	-0.000166	-0.000166	0.96179	0.000000	0.17195	0.00776	0.00306
06MeOHMeNH2	-0.000208	-0.000209	0.96460	0.000001	0.42640	0.01605	0.00722
07MeOHPeptide	-0.000233	-0.000233	0.96174	0.000000	0.16722	0.00826	0.00298
08MeOHWater	-0.000137	-0.000138	0.96246	0.000000	0.23681	0.01330	0.00405
09MeNH2MeOH	-0.000093	-0.000093	0.95957	0.000000	0.03919	0.00107	0.00075
10MeNH2MeNH2	-0.000127	-0.000127	0.95957	0.000000	0.03878	0.00092	0.00072
11MeNH2Peptide	-0.000166	-0.000166	0.95802	0.000000	0.18073	0.00467	0.00341
12MeNH2Water	-0.000212	-0.000213	0.96420	0.000001	0.38880	0.01733	0.00690
13PeptideMeOH	-0.000162	-0.000162	0.96107	0.000000	0.10198	0.00326	0.00164
14PeptideMeNH2	-0.000186	-0.000187	0.96434	0.000001	0.40012	0.01110	0.00609
15PeptidePeptide	-0.000216	-0.000217	0.96283	0.000001	0.26871	0.00898	0.00421
16PeptideWater	-0.000125	-0.000125	0.96305	0.000000	0.29074	0.01319	0.00442
17UracilUracilBP	-0.000437	-0.000440	0.96564	0.000002	0.54928	0.03485	0.00878
18WaterPyridine	-0.000184	-0.000185	0.96641	0.000001	0.59609	0.02625	0.00975
19MeOHPyridine	-0.000189	-0.000190	0.96514	0.000001	0.48008	0.01660	0.00740
20AcOHAcOH	-0.000570	-0.000573	0.96509	0.000003	0.50517	0.05282	0.00949
21AcNH2AcNH2	-0.000425	-0.000427	0.96548	0.000002	0.53682	0.03750	0.00887
22AcOHUracil	-0.000513	-0.000516	0.96549	0.000003	0.54264	0.04723	0.00900
23AcNH2Uracil	-0.000469	-0.000472	0.96599	0.000003	0.58881	0.04560	0.00906
24BenzeneBenzenepipi	-0.000103	-0.000101	0.94181	0.000001	1.38153	0.01032	0.01905
25PyridinePyridinepipi	-0.000135	-0.000134	0.94678	0.000001	1.06196	0.00967	0.01506
26UracilUracilpipi	-0.000293	-0.000291	0.95077	0.000002	0.82776	0.01324	0.01368
27BenzenePyridinepipi	-0.000121	-0.000120	0.94522	0.000001	1.16152	0.00979	0.01634
28BenzeneUracilpipi	-0.000192	-0.000190	0.94747	0.000002	1.04644	0.01152	0.01679
29PyridineUracilpipi	-0.000209	-0.000207	0.94904	0.000002	0.93345	0.01145	0.01421
30BenzeneEthene	-0.000068	-0.000067	0.93539	0.000001	1.74834	0.01447	0.03248
31UracilEthene	-0.000115	-0.000114	0.95017	0.000001	0.81053	0.01086	0.01466

S66-Structure	$E_{Int.\ F12}$ [H]	$E_{Int.\ SF12}$ [H]	c_{SF12}	Err. [H]	Err. [%]	corr. Int. Err. [%]	tot. Int. Error [%]
32UracilEthyne	-0.000126	-0.000125	0.94983	0.000001	0.81098	0.01342	0.01457
33PyridineEthene	-0.000078	-0.000077	0.93928	0.000001	1.53916	0.01384	0.02681
34PentanePentane	-0.000114	-0.000114	0.95439	0.000001	0.47754	0.00469	0.00868
35NeopentanePentane	-0.000082	-0.000082	0.95759	0.000000	0.20690	0.00213	0.00399
36NeopentaneNeopentane	-0.000055	-0.000055	0.96166	0.000000	0.14138	0.00144	0.00283
37CyclopentaneNeopentane	-0.000081	-0.000081	0.95861	0.000000	0.11803	0.00125	0.00242
38CyclopentaneCyclopentane	-0.000091	-0.000091	0.95545	0.000000	0.38552	0.00386	0.00706
39BenzeneCyclopentane	-0.000112	-0.000111	0.95111	0.000001	0.73950	0.00697	0.01135
40BenzeneNeopentane	-0.000093	-0.000093	0.95500	0.000000	0.41712	0.00428	0.00682
41UracilPentane	-0.000163	-0.000161	0.94997	0.000001	0.87276	0.01005	0.01645
42UracilCyclopentane	-0.000133	-0.000132	0.94882	0.000001	0.96914	0.01033	0.01733
43UracilNeopentane	-0.000113	-0.000112	0.95165	0.000001	0.71489	0.00831	0.01256
44EthenePentane	0.000083	0.000094	1.05905	0.000012	13.90074	0.00357	0.00643
45EthynePentane	-0.000278	-0.000295	1.01759	0.000018	6.38766	0.03617	0.00310
46PeptidePentane	-0.000144	-0.000143	0.95152	0.000001	0.73550	0.00909	0.01476
47BenzeneBenzeneTS	-0.000096	-0.000096	0.95525	0.000000	0.40281	0.00470	0.00652
48PyridinePyridineTS	-0.000120	-0.000120	0.95642	0.000000	0.31207	0.00448	0.00537
49BenzenePyridineTS	-0.000109	-0.000109	0.95749	0.000000	0.21545	0.00289	0.00355
50BenzeneEthyneCHpi	-0.000097	-0.000097	0.96061	0.000000	0.05227	0.00099	0.00092
51EthyneEthyneTS	-0.000204	-0.000222	1.03578	0.000018	8.86503	0.03336	0.00314
52BenzeneAcOHOHpi	-0.000165	-0.000165	0.95957	0.000000	0.03881	0.00088	0.00077
53BenzeneAcNH2NHpi	-0.000145	-0.000145	0.96003	0.000000	0.00300	0.00007	0.00006
54BenzeneWaterOHpi	-0.000113	-0.000113	0.96084	0.000000	0.07486	0.00189	0.00149
55BenzeneMeOHOHpi	-0.000134	-0.000133	0.95731	0.000000	0.23729	0.00407	0.00419
56BenzeneMeNH2NHpi	-0.000105	-0.000105	0.95463	0.000000	0.45732	0.00614	0.00788
57BenzenePeptideNHpi	-0.000155	-0.000155	0.95815	0.000000	0.16257	0.00236	0.00256
58PyridinePyridineCHN	-0.000132	-0.000133	0.96541	0.000001	0.49111	0.01275	0.00935
59EthyneWaterCHO	-0.000075	-0.000076	0.96583	0.000000	0.53420	0.03840	0.00881
60EthyneAcOHOHpi	-0.000173	-0.000174	0.96232	0.000000	0.20912	0.00944	0.00453
61PentaneAcOH	-0.000109	-0.000108	0.95152	0.000001	0.73721	0.00990	0.01677
62PentaneAcNH2	-0.000129	-0.000128	0.95197	0.000001	0.70186	0.00980	0.01560
63BenzeneAcOH	-0.000137	-0.000136	0.95408	0.000001	0.50485	0.00749	0.00957
64PeptideEthene	-0.000107	-0.000106	0.95492	0.000000	0.44083	0.00797	0.00936
65PyridineEthyne	-0.000100	-0.000101	0.97052	0.000001	0.93117	0.03495	0.01390
66MeNH2Pyridine	-0.000126	-0.000125	0.95471	0.000001	0.46350	0.00730	0.00805

TABLE IV. DF-MP2-F12/cc-pVDZ-F12 and DF-MP2-SF12/cc-pVDZ-F12 explicitly correlated F12 interaction energy corrections of the S22 test set. $c_{\mathrm{SF12}} = 0.935$; MAE [kcal·mol^{-1}] = 0.002; MPE [%] = 0.34208; MPE of the correlation interaction energy [%] = 0.04616; MPE of the total interaction energy [%] = 0.03212.

S22-Structure	$E_{\mathrm{Int.\ F12}}$ [H]	$E_{\mathrm{Int.\ SF12}}$ [H]	c_{SF12}	Err. [H]	Err. [%]	corr. Int. Err. [%]	tot. Int. Error [%]
BenzenedimerTshaped	-0.000540	-0.000540	0.93463	0.000000	0.02001	0.00138	0.00198
IndolebenzeneTshapecomplex	-0.000898	-0.000898	0.93507	0.000000	0.00411	0.00033	0.00035
Phenoldimer	-0.001080	-0.001078	0.93296	0.000002	0.15002	0.01806	0.01360
Ammoniadimer	-0.000482	-0.000483	0.93737	0.000001	0.15086	0.02786	0.01490
Waterdimer	-0.000705	-0.000704	0.93279	0.000001	0.17616	0.06045	0.01598
BenzeneMethanecomplex	-0.000319	-0.000318	0.93095	0.000001	0.20439	0.01448	0.02472
Formicaciddimer	-0.002786	-0.002787	0.93548	0.000001	0.04057	0.02438	0.00390
Formamidedimer	-0.002135	-0.002140	0.93780	0.000005	0.22036	0.08908	0.01905
Uracildimerhbonded	-0.002234	-0.002241	0.93886	0.000007	0.31507	0.11591	0.02198
2pyridoxine2aminopyridinecomplex	-0.002031	-0.002039	0.94047	0.000008	0.41596	0.08052	0.03109
AdeninethymineWatsonCrickcomplex	-0.002093	-0.002105	0.94212	0.000011	0.53731	0.11473	0.04352
Methanedimer	-0.000090	-0.000090	0.93147	0.000000	0.14035	0.01018	0.01915
Ethenedimer	-0.000346	-0.000346	0.93717	0.000000	0.11545	0.01119	0.01778
Benzenedimerparalleldisplaced	-0.000713	-0.000708	0.91922	0.000005	0.72831	0.03307	0.07233
Pyrazinedimer	-0.001019	-0.001013	0.92261	0.000007	0.63785	0.03890	0.06454
Uracildimerstack	-0.001518	-0.001510	0.92606	0.000008	0.51847	0.04737	0.04747
Indolebenzenecomplexstack	-0.001023	-0.001014	0.91721	0.000008	0.81834	0.03620	0.07055
Adeninethyminecomplexstack	-0.001953	-0.001940	0.92349	0.000012	0.63552	0.04523	0.05598
Etheneethynecomplex	-0.000242	-0.000245	0.95253	0.000003	1.06487	0.14395	0.10408
Benzenewatercomplex	-0.000553	-0.000554	0.93656	0.000001	0.09841	0.01431	0.01025
Benzeneammoniacomplex	-0.000415	-0.000415	0.93544	0.000000	0.02454	0.00242	0.00259
BenzeneHCNcomplex	-0.000781	-0.000785	0.94322	0.000004	0.50872	0.08549	0.05076

TABLE V. DF-MP2-F12/cc-pVTZ-F12 and DF-MP2-SF12/cc-pVTZ-F12 explicitly correlated F12 interaction energy corrections of the S22 test set. $c_{\mathrm{SF12}} = 0.950$; MAE [kcal·mol^{-1}] = 0.002; MPE [%] = 0.53526; MPE of the correlation interaction energy [%] = 0.02981; MPE of the total interaction energy [%] = 0.02661.

S22-Structure	$E_{\mathrm{Int.\ F12}}$ [H]	$E_{\mathrm{Int.\ SF12}}$ [H]	c_{SF12}	Err. [H]	Err. [%]	corr. Int. Err. [%]	tot. Int. Error [%]
BenzenedimerTshaped	-0.000220	-0.000219	0.94522	0.000001	0.35036	0.00953	0.01356
IndolebenzeneTshapecomplex	-0.000347	-0.000347	0.94761	0.000001	0.18267	0.00554	0.00576
Phenoldimer	-0.000465	-0.000464	0.94787	0.000001	0.18088	0.00907	0.00689
Ammoniadimer	-0.000196	-0.000196	0.95013	0.000000	0.01009	0.00072	0.00040
Waterdimer	-0.000303	-0.000303	0.95145	0.000000	0.12674	0.01782	0.00488
BenzeneMethanecomplex	-0.000137	-0.000136	0.94114	0.000001	0.61011	0.01789	0.02983
Formicaciddimer	-0.001256	-0.001258	0.95242	0.000003	0.22285	0.05502	0.00950
Formamidedimer	-0.000921	-0.000924	0.95446	0.000004	0.40047	0.06525	0.01470
Uracildimerhbonded	-0.000981	-0.000985	0.95506	0.000005	0.46088	0.07015	0.01397
2pyridoxine2aminopyridinecomplex	-0.000883	-0.000887	0.95555	0.000004	0.48503	0.03953	0.01556
AdeninethymineWatsonCrickcomplex	-0.000916	-0.000922	0.95657	0.000005	0.57302	0.05171	0.02006
Methanedimer	-0.000042	-0.000042	0.93837	0.000000	0.66283	0.02122	0.03835
Ethenedimer	-0.000155	-0.000154	0.94441	0.000001	0.38027	0.01568	0.02421
Benzenedimerparalleldisplaced	-0.000323	-0.000319	0.93169	0.000004	1.17023	0.02337	0.04933
Pyrazinedimer	-0.001163	-0.001180	0.96637	0.000017	1.47530	0.10022	0.17499
Uracildimerstack	-0.000626	-0.000621	0.93871	0.000005	0.86081	0.03096	0.03115
Indolebenzenecomplexstack	-0.000450	-0.000444	0.93027	0.000006	1.28805	0.02437	0.04599
Adeninethyminecomplexstack	-0.000798	-0.000789	0.93623	0.000008	1.04045	0.02914	0.03567
Etheneethynecomplex	-0.000102	-0.000103	0.96009	0.000001	0.76188	0.04111	0.03018
Benzenewatercomplex	-0.000219	-0.000219	0.94973	0.000000	0.02145	0.00116	0.00085
Benzeneammoniacomplex	-0.000166	-0.000166	0.94720	0.000000	0.20558	0.00772	0.00824
BenzeneHCNcomplex	-0.000301	-0.000302	0.95385	0.000001	0.30573	0.01856	0.01131

TABLE VI. DF-MP2-F12/cc-pVQZ-F12 and DF-MP2-SF12/cc-pVQZ-F12 explicitly correlated F12 interaction energy corrections of the S22 test set. $c_{\mathrm{SF12}} = 0.960$; MAE [kcal·mol^{-1}] = 0.001; MPE [%] = 0.69209; MPE of the correlation interaction energy [%] = 0.01519; MPE of the total interaction energy [%] = 0.00947.

S22-Structure	$E_{\mathrm{Int.\ F12}}$ [H]	$E_{\mathrm{Int.\ SF12}}$ [H]	c_{SF12}	Err. [H]	Err. [%]	corr. Int. Err. [%]	tot. Int. Error [%]
BenzenedimerTshaped	-0.000100	-0.000100	0.95645	0.000000	0.30733	0.00376	0.00533
IndolebenzeneTshapecomplex	-0.000164	-0.000164	0.95850	0.000000	0.13239	0.00188	0.00199
Phenoldimer	-0.000217	-0.000217	0.95977	0.000000	0.02180	0.00050	0.00038
Ammoniadimer	-0.000093	-0.000093	0.96107	0.000000	0.09578	0.00320	0.00177
Waterdimer	-0.000148	-0.000148	0.96296	0.000000	0.28317	0.01919	0.00530
BenzeneMethanecomplex	-0.000059	-0.000059	0.95304	0.000000	0.57810	0.00722	0.01190
Formicaciddimer	-0.000594	-0.000597	0.96524	0.000003	0.52212	0.06012	0.01050
Formamidedimer	-0.000443	-0.000445	0.96559	0.000002	0.54745	0.04231	0.00964
Uracildimerhbonded	-0.000474	-0.000476	0.96600	0.000003	0.59139	0.04291	0.00863
2pyridoxine2aminopyridinecomplex	-0.000429	-0.000431	0.96573	0.000002	0.54965	0.02156	0.00852
AdeninethymineWatsonCrickcomplex	-0.000443	-0.000446	0.96644	0.000003	0.61617	0.02659	0.01038
Methanedimer	-0.000017	-0.000017	0.94763	0.000000	0.89729	0.01132	0.01990
Ethenedimer	0.000235	0.000229	0.87590	0.000006	2.73059	0.01158	0.00087
Benzenedimerparalleldisplaced	-0.000140	-0.000139	0.94427	0.000002	1.24393	0.01065	0.02221
Pyrazinedimer	-0.000520	-0.000528	0.98192	0.000008	1.63460	0.00183	0.01810
Uracildimerstack	-0.000279	-0.000277	0.95081	0.000002	0.81884	0.01292	0.01297
Indolebenzenecomplexstack	-0.000196	-0.000194	0.94322	0.000003	1.34737	0.01101	0.02063
Adeninethyminecomplexstack	-0.000354	-0.000351	0.94849	0.000004	1.02321	0.01257	0.01536
Etheneethynecomplex	-0.000050	-0.000051	0.96794	0.000000	0.66716	0.01726	0.01276
Benzenewatercomplex	-0.000103	-0.000104	0.96110	0.000000	0.09827	0.00246	0.00181
Benzeneammoniacomplex	-0.000077	-0.000077	0.95831	0.000000	0.14519	0.00247	0.00264
BenzeneHCNcomplex	-0.000146	-0.000147	0.96419	0.000001	0.37409	0.01086	0.00666

TABLE VII. DF-MP2-F12/cc-pVDZ-F12 and DF-MP2-SF12/cc-pVDZ-F12 explicitly correlated F12 interaction energy corrections of the L7 test set. $c_{\mathrm{SF12}} = 0.935$; MAE [kcal·mol$_1$] = 0.007; MPE [%] = 0.47516; MPE of the correlation interaction energy [%] = 0.02150; MPE of the total interaction energy [%] = 0.03864.

L7-Structure	$E_{\mathrm{Int.\ F12}}$ [H]	$E_{\mathrm{Int.\ SF12}}$ [H]	c_{SF12}	Err. [H]	Err. [%]	corr. Int. Err. [%]	tot. Int. Error [%]
octadecanedimer	-0.001159	-0.001160	0.93658	0.000001	0.07900	0.00310	0.00503
guaninetrimer	-0.001451	-0.001433	0.90194	0.000018	1.24065	0.04674	0.17026
circumcoroneneadenine	-0.001978	-0.001964	0.92174	0.000013	0.66486	0.02339	0.03166
circumcoroneneGCbasepair	-0.007038	-0.007030	0.93325	0.000008	0.11326	0.00739	0.00657
phenylalanineresiduestrimer	-0.005308	-0.005322	0.93839	0.000014	0.25529	0.03344	0.01662
coronenedimer	-0.002292	-0.002272	0.91566	0.000020	0.85442	0.02332	0.03345
GCGCbasepairstack	-0.006916	-0.006924	0.93673	0.000008	0.11867	0.01312	0.00691

TABLE VIII. DF-MP2-F12/cc-pVDZ-F12 and DF-MP2-SF12/cc-pVDZ-F12 absolute explicitly correlated F12 energy corrections of the S66 test set. $c_{\mathrm{SF12}} = 0.935$; MAE [kcal·mol^{-1}] = 3.744; MPE [%] = 2.27553; $\varnothing \frac{t_{\mathrm{F12}}}{t_{\mathrm{SF12}}} = 1.25849$.

S66-Structure	E_{F12} [H]	E_{SF12} [H]	Err. [H]	Err. [%]	t_{F12}	t_{SF12}	$\frac{t_{\mathrm{F12}}}{t_{\mathrm{SF12}}}$
01WaterWater	-0.106652	-0.108788	0.002136	2.00260	2.06	2.52	0.8175
02WaterMeOH	-0.134150	-0.136962	0.002812	2.09599	5.38	5.12	1.0508
03WaterMeNH2	-0.122135	-0.124911	0.002776	2.27279	6.08	5.82	1.0447
04WaterPeptide	-0.220731	-0.225449	0.004718	2.13754	28.16	24.48	1.1503
05MeOHMeOH	-0.161549	-0.165034	0.003485	2.15734	10.59	9.70	1.0918
06MeOHMeNH2	-0.149574	-0.153021	0.003446	2.30399	12.47	11.66	1.0695
07MeOHPeptide	-0.247989	-0.253380	0.005392	2.17412	45.02	38.10	1.1816
08MeOHWater	-0.134063	-0.136873	0.002809	2.09537	5.56	5.01	1.1098
09MeNH2MeOH	-0.149337	-0.152788	0.003451	2.31099	12.49	11.66	1.0712
10MeNH2MeNH2	-0.137300	-0.140713	0.003413	2.48571	14.68	13.18	1.1138
11MeNH2Peptide	-0.235730	-0.241088	0.005358	2.27288	48.92	41.09	1.1906
12MeNH2Water	-0.122174	-0.124948	0.002774	2.27086	6.38	6.24	1.0224
13PeptideMeOH	-0.247716	-0.253113	0.005398	2.17899	46.15	38.66	1.1937
14PeptideMeNH2	-0.235677	-0.241037	0.005360	2.27435	48.79	45.37	1.0754
15PeptidePeptide	-0.334253	-0.341558	0.007305	2.18556	130.88	94.91	1.3790
16PeptideWater	-0.220451	-0.225174	0.004724	2.14266	28.37	24.24	1.1704
17UracilUracilBP	-0.529434	-0.539842	0.010407	1.96572	335.49	200.95	1.6695
18WaterPyridine	-0.210700	-0.215355	0.004655	2.20924	30.64	28.24	1.0850
19MeOHPyridine	-0.238078	-0.243405	0.005327	2.23730	47.40	40.30	1.1762
20AcOHAcOH	-0.303336	-0.309311	0.005975	1.96977	46.56	40.57	1.1476
21AcNH2AcNH2	-0.279510	-0.285457	0.005947	2.12780	55.33	43.45	1.2734
22AcOHUracil	-0.416446	-0.424639	0.008192	1.96722	139.20	98.11	1.4188
23AcNH2Uracil	-0.404615	-0.412793	0.008178	2.02126	151.94	114.53	1.3266
24BenzeneBenzenepipi	-0.297263	-0.304340	0.007077	2.38082	173.29	128.82	1.3452
25PyridinePyridinepipi	-0.314376	-0.321539	0.007163	2.27862	152.15	113.81	1.3369
26UracilUracilpipi	-0.528595	-0.538984	0.010389	1.96546	387.11	223.49	1.7321
27BenzenePyridinepipi	-0.305811	-0.312931	0.007120	2.32828	163.93	122.16	1.3419
28BenzeneUracilpipi	-0.412892	-0.421626	0.008734	2.11522	253.72	171.87	1.4762
29PyridineUracilpipi	-0.421507	-0.430285	0.008778	2.08257	238.52	167.39	1.4249
30BenzeneEthene	-0.201777	-0.206744	0.004967	2.46143	54.82	45.84	1.1959
31UracilEthene	-0.317496	-0.324126	0.006630	2.08828	85.36	66.74	1.2790

S66-Structure	E_{F12} [H]	E_{SF12} [H]	Err. [H]	Err. [%]	t_{F12}	t_{SF12}	$\frac{t_{F12}}{t_{SF12}}$
32UracilEthyne	-0.312246	-0.318641	0.006395	2.04816	73.04	58.45	1.2496
33PyridineEthene	-0.210298	-0.215307	0.005009	2.38201	50.52	43.80	1.1534
34PentanePentane	-0.283965	-0.291403	0.007437	2.61914	233.29	169.08	1.3798
35NeopentanePentane	-0.283713	-0.291132	0.007419	2.61496	230.92	165.30	1.3970
36NeopentaneNeopentane	-0.283510	-0.290911	0.007401	2.61048	236.55	162.20	1.4584
37CyclopentaneNeopentane	-0.280379	-0.287562	0.007183	2.56189	208.54	152.35	1.3688
38CyclopentaneCyclopentane	-0.277375	-0.284340	0.006965	2.51117	183.31	136.58	1.3421
39BenzeneCyclopentane	-0.287261	-0.294280	0.007019	2.44356	186.43	140.03	1.3314
40BenzeneNeopentane	-0.290354	-0.297593	0.007239	2.49325	204.29	147.10	1.3888
41UracilPentane	-0.406140	-0.415056	0.008916	2.19520	318.40	196.00	1.6245
42UracilCyclopentane	-0.402807	-0.411487	0.008680	2.15486	259.20	182.01	1.4241
43UracilNeopentane	-0.405956	-0.414856	0.008900	2.19239	290.92	195.03	1.4917
44EthenePentane	-0.195036	-0.200149	0.005113	2.62173	68.07	57.02	1.1938
45EthynePentane	-0.192013	-0.197058	0.005045	2.62741	55.35	47.13	1.1744
46PeptidePentane	-0.308910	-0.316276	0.007366	2.38466	189.08	138.25	1.3677
47BenzeneBenzeneTS	-0.297387	-0.304473	0.007085	2.38257	165.40	118.64	1.3941
48PyridinePyridineTS	-0.314513	-0.321685	0.007172	2.28048	149.10	106.53	1.3996
49BenzenePyridineTS	-0.305924	-0.313053	0.007129	2.33025	155.14	118.59	1.3082
50BenzeneEthyneCHpi	-0.196430	-0.201162	0.004733	2.40939	44.75	38.11	1.1742
51EthyneEthyneTS	-0.096997	-0.099507	0.002510	2.58811	5.67	5.35	1.0598
52BenzeneAcOHOHpi	-0.300077	-0.306615	0.006538	2.17883	94.46	72.00	1.3119
53BenzeneAcNH2NHpi	-0.288403	-0.294926	0.006523	2.26186	99.35	84.96	1.1694
54BenzeneWaterOHpi	-0.202174	-0.206787	0.004612	2.28126	34.71	30.21	1.1490
55BenzeneMeOHOHpi	-0.229499	-0.234782	0.005283	2.30175	55.35	45.81	1.2083
56BenzeneMeNH2NHpi	-0.217307	-0.222553	0.005246	2.41392	60.59	50.39	1.2024
57BenzenePeptideNHpi	-0.315667	-0.322858	0.007191	2.27801	154.55	111.35	1.3880
58PyridinePyridineCHN	-0.314535	-0.321714	0.007179	2.28253	137.13	98.98	1.3854
59EthyneWaterCHO	-0.100858	-0.103119	0.002261	2.24184	3.40	3.29	1.0334
60EthyneAcOHOHpi	-0.199149	-0.203337	0.004188	2.10314	19.27	16.91	1.1396
61PentaneAcOH	-0.293303	-0.300019	0.006716	2.28969	121.11	89.53	1.3527
62PentaneAcNH2	-0.281479	-0.288173	0.006694	2.37813	127.38	98.29	1.2960
63BenzeneAcOH	-0.299968	-0.306504	0.006536	2.17897	95.27	74.53	1.2783
64PeptideEthene	-0.220096	-0.225177	0.005080	2.30825	46.23	39.13	1.1814
65PyridineEthyne	-0.204895	-0.209676	0.004781	2.33333	38.12	33.95	1.1228
66MeNH2Pyridine	-0.225967	-0.231257	0.005290	2.34101	54.41	45.39	1.1987

TABLE IX. DF-MP2-F12/cc-pVTZ-F12 and DF-MP2-SF12/cc-pVTZ-F12 absolute explicitly correlated F12 energy corrections of the S66 test set. $c_{\mathrm{SF12}} = 0.950$; MAE [kcal·mol^{-1}] = 1.677; MPE [%] = 2.12916; $\varnothing \frac{t_{\mathrm{F12}}}{t_{\mathrm{SF12}}} = 1.17926$.

S66-Structure	E_{F12} [H]	E_{SF12} [H]	Err. [H]	Err. [%]	t_{F12}	t_{SF12}	$\frac{t_{\mathrm{F12}}}{t_{\mathrm{SF12}}}$
01WaterWater	-0.051301	-0.052217	0.000915	1.78450	6.85	6.69	1.0239
02WaterMeOH	-0.064770	-0.066009	0.001238	1.91188	19.63	18.83	1.0425
03WaterMeNH2	-0.059540	-0.060797	0.001256	2.11007	24.23	23.07	1.0503
04WaterPeptide	-0.105646	-0.107735	0.002088	1.97671	106.35	97.32	1.0928
05MeOHMeOH	-0.078239	-0.079800	0.001561	1.99470	43.45	40.76	1.0660
06MeOHMeNH2	-0.072993	-0.074570	0.001577	2.16038	51.32	48.30	1.0625
07MeOHPeptide	-0.119034	-0.121444	0.002411	2.02507	178.84	154.91	1.1545
08MeOHWater	-0.064782	-0.066020	0.001238	1.91048	19.71	18.72	1.0529
09MeNH2MeOH	-0.072972	-0.074551	0.001580	2.16513	50.36	48.24	1.0439
10MeNH2MeNH2	-0.067666	-0.069262	0.001596	2.35821	58.31	53.89	1.0820
11MeNH2Peptide	-0.113723	-0.116153	0.002429	2.13610	199.71	176.18	1.1336
12MeNH2Water	-0.059527	-0.060783	0.001255	2.10869	24.99	23.76	1.0518
13PeptideMeOH	-0.118962	-0.121375	0.002413	2.02880	181.14	159.18	1.1380
14PeptideMeNH2	-0.113677	-0.116108	0.002431	2.13830	197.18	173.29	1.1379
15PeptidePeptide	-0.159801	-0.163065	0.003264	2.04275	478.49	380.68	1.2569
16PeptideWater	-0.105600	-0.107692	0.002092	1.98077	105.88	97.35	1.0876
17UracilUracilBP	-0.245791	-0.250223	0.004432	1.80313	1090.76	780.73	1.3971
18WaterPyridine	-0.099864	-0.101918	0.002054	2.05703	120.02	109.34	1.0977
19MeOHPyridine	-0.113308	-0.115684	0.002376	2.09673	198.24	166.24	1.1925
20AcOHAcOH	-0.143009	-0.145577	0.002568	1.79584	185.67	150.71	1.2320
21AcNH2AcNH2	-0.132841	-0.135465	0.002624	1.97525	205.40	183.18	1.1213
22AcOHUracil	-0.194401	-0.197902	0.003501	1.80077	481.79	377.10	1.2776
23AcNH2Uracil	-0.189340	-0.192868	0.003528	1.86333	509.84	394.55	1.2922
24BenzeneBenzenepipi	-0.141839	-0.145028	0.003189	2.24848	663.99	530.62	1.2513
25PyridinePyridinepipi	-0.148262	-0.151451	0.003189	2.15085	580.57	502.54	1.1553
26UracilUracilpipi	-0.245632	-0.250058	0.004427	1.80221	1239.10	906.43	1.3670
27BenzenePyridinepipi	-0.145037	-0.148226	0.003189	2.19866	618.88	505.73	1.2237
28BenzeneUracilpipi	-0.193711	-0.197519	0.003808	1.96556	915.45	709.15	1.2909
29PyridineUracilpipi	-0.196985	-0.200794	0.003808	1.93339	846.33	664.90	1.2729
30BenzeneEthene	-0.097589	-0.099857	0.002268	2.32392	218.37	193.63	1.1278
31UracilEthene	-0.149500	-0.152389	0.002889	1.93265	316.44	271.86	1.1640

S66-Structure	E_{F12} [H]	E_{SF12} [H]	Err. [H]	Err. [%]	t_{F12}	t_{SF12}	$\frac{t_{F12}}{t_{SF12}}$
32UracilEthyne	-0.146479	-0.149238	0.002759	1.88372	273.80	243.13	1.1261
33PyridineEthene	-0.100774	-0.103042	0.002267	2.25007	204.57	180.60	1.1327
34PentanePentane	-0.140921	-0.144439	0.003517	2.49590	940.98	724.68	1.2985
35NeopentanePentane	-0.140546	-0.144055	0.003509	2.49684	918.22	726.57	1.2638
36NeopentaneNeopentane	-0.140203	-0.143703	0.003501	2.49680	909.19	737.41	1.2330
37CyclopentaneNeopentane	-0.137763	-0.141141	0.003378	2.45185	841.14	665.57	1.2638
38CyclopentaneCyclopentane	-0.135369	-0.138625	0.003255	2.40482	736.22	597.42	1.2323
39BenzeneCyclopentane	-0.138560	-0.141782	0.003221	2.32497	693.79	557.49	1.2445
40BenzeneNeopentane	-0.140986	-0.144331	0.003345	2.37236	782.78	625.08	1.2523
41UracilPentane	-0.193228	-0.197200	0.003973	2.05591	1079.75	807.24	1.3376
42UracilCyclopentane	-0.190441	-0.194283	0.003842	2.01736	958.85	742.80	1.2909
43UracilNeopentane	-0.192898	-0.196864	0.003965	2.05562	1138.09	798.10	1.4260
44EthenePentane	-0.096840	-0.099251	0.002412	2.49035	285.70	242.17	1.1797
45EthynePentane	-0.094462	-0.096804	0.002343	2.47997	230.83	204.96	1.1262
46PeptidePentane	-0.150284	-0.153672	0.003388	2.25439	703.38	551.89	1.2745
47BenzeneBenzeneTS	-0.141902	-0.145095	0.003192	2.24970	593.95	482.54	1.2309
48PyridinePyridineTS	-0.148310	-0.151502	0.003192	2.15227	526.35	429.55	1.2254
49BenzenePyridineTS	-0.145081	-0.148273	0.003192	2.20033	576.08	490.04	1.1756
50BenzeneEthyneCHpi	-0.094431	-0.096569	0.002139	2.26485	176.50	157.09	1.1236
51EthyneEthyneTS	-0.047055	-0.048177	0.001122	2.38465	21.61	20.34	1.0624
52BenzeneAcOHOHpi	-0.142428	-0.145313	0.002885	2.02559	350.14	304.77	1.1489
53BenzeneAcNH2NHpi	-0.137415	-0.140327	0.002911	2.11873	368.02	304.02	1.2105
54BenzeneWaterOHpi	-0.096622	-0.098676	0.002054	2.12631	139.40	133.05	1.0477
55BenzeneMeOHOHpi	-0.110007	-0.112382	0.002375	2.15875	221.98	197.81	1.1222
56BenzeneMeNH2NHpi	-0.104728	-0.107120	0.002393	2.28468	241.95	215.67	1.1219
57BenzenePeptideNHpi	-0.150717	-0.153943	0.003226	2.14074	575.49	466.51	1.2336
58PyridinePyridineCHN	-0.148432	-0.151627	0.003196	2.15301	490.41	398.12	1.2318
59EthyneWaterCHO	-0.049096	-0.050097	0.001001	2.03895	13.24	12.13	1.0915
60EthyneAcOHOHpi	-0.095006	-0.096837	0.001831	1.92740	74.17	66.81	1.1102
61PentaneAcOH	-0.142027	-0.145075	0.003049	2.14643	496.89	385.87	1.2877
62PentaneAcNH2	-0.136888	-0.139960	0.003072	2.24428	518.78	398.47	1.3019
63BenzeneAcOH	-0.142433	-0.145317	0.002884	2.02473	370.65	315.28	1.1756
64PeptideEthene	-0.106507	-0.108812	0.002305	2.16407	181.72	169.79	1.0703
65PyridineEthyne	-0.097682	-0.099822	0.002141	2.19173	149.22	134.07	1.1130
66MeNH2Pyridine	-0.107982	-0.110375	0.002393	2.21600	217.25	193.24	1.1242

TABLE X. DF-MP2-F12/cc-pVQZ-F12 and DF-MP2-SF12/cc-pVQZ-F12 absolute explicitly correlated F12 energy corrections of the S66 test set. $c_{\mathrm{SF12}} = 0.960$; MAE [kcal·mol^{-1}] = 0.791; MPE [%] = 1.93330; $\varnothing \frac{t_{\mathrm{F12}}}{t_{\mathrm{SF12}}} = 1.07904$.

S66-Structure	E_{F12} [H]	E_{SF12} [H]	Err. [H]	Err. [%]	t_{F12}	t_{SF12}	$\frac{t_{\mathrm{F12}}}{t_{\mathrm{SF12}}}$
01WaterWater	-0.026438	-0.026926	0.000488	1.84742	35.16	34.62	1.0156
02WaterMeOH	-0.033340	-0.033972	0.000632	1.89680	109.67	107.61	1.0191
03WaterMeNH2	-0.030854	-0.031466	0.000613	1.98573	128.70	126.04	1.0211
04WaterPeptide	-0.054667	-0.055696	0.001029	1.88148	578.11	543.11	1.0644
05MeOHMeOH	-0.040242	-0.041018	0.000776	1.92866	233.20	227.38	1.0256
06MeOHMeNH2	-0.037740	-0.038496	0.000756	2.00231	280.39	271.85	1.0314
07MeOHPeptide	-0.061543	-0.062715	0.001172	1.90484	898.57	817.65	1.0990
08MeOHWater	-0.033348	-0.033980	0.000632	1.89562	106.04	104.15	1.0181
09MeNH2MeOH	-0.037757	-0.038514	0.000757	2.00504	273.94	266.29	1.0287
10MeNH2MeNH2	-0.035230	-0.035966	0.000736	2.08934	311.57	305.25	1.0207
11MeNH2Peptide	-0.059020	-0.060173	0.001153	1.95283	1005.45	949.07	1.0594
12MeNH2Water	-0.030847	-0.031459	0.000612	1.98465	132.50	130.45	1.0157
13PeptideMeOH	-0.061545	-0.062719	0.001174	1.90699	903.81	852.76	1.0599
14PeptideMeNH2	-0.059032	-0.060185	0.001153	1.95378	1002.01	941.72	1.0640
15PeptidePeptide	-0.082863	-0.084433	0.001570	1.89459	2171.55	1941.72	1.1184
16PeptideWater	-0.054698	-0.055729	0.001030	1.88357	558.71	536.81	1.0408
17UracilUracilBP	-0.127701	-0.129905	0.002204	1.72577	4362.59	3624.17	1.2037
18WaterPyridine	-0.051908	-0.052882	0.000974	1.87626	645.83	624.67	1.0339
19MeOHPyridine	-0.058798	-0.059915	0.001117	1.90016	945.55	892.17	1.0598
20AcOHAcOH	-0.073801	-0.075116	0.001315	1.78191	844.89	790.70	1.0685
21AcNH2AcNH2	-0.069008	-0.070291	0.001283	1.85965	1005.57	935.17	1.0753
22AcOHUracil	-0.100753	-0.102512	0.001760	1.74647	2157.96	1981.66	1.0890
23AcNH2Uracil	-0.098348	-0.100092	0.001743	1.77264	2305.53	2020.86	1.1409
24BenzeneBenzenepipi	-0.073899	-0.075336	0.001437	1.94508	3092.66	2819.64	1.0968
25PyridinePyridinepipi	-0.077254	-0.078710	0.001456	1.88514	2777.64	2554.76	1.0872
26UracilUracilpipi	-0.127514	-0.129716	0.002201	1.72636	5523.54	4627.45	1.1936
27BenzenePyridinepipi	-0.075574	-0.077021	0.001447	1.91447	2938.61	2691.19	1.0919
28BenzeneUracilpipi	-0.100690	-0.102509	0.001819	1.80652	4160.42	3683.62	1.1294
29PyridineUracilpipi	-0.102385	-0.104214	0.001829	1.78625	4059.84	3480.49	1.1665
30BenzeneEthene	-0.050784	-0.051804	0.001020	2.00806	1151.15	1102.09	1.0445
31UracilEthene	-0.077589	-0.078992	0.001403	1.80785	1612.58	1499.62	1.0753

S66-Structure	E_{F12} [H]	E_{SF12} [H]	Err. [H]	Err. [%]	t_{F12}	t_{SF12}	$\frac{t_{F12}}{t_{SF12}}$
32UracilEthyne	-0.076089	-0.077434	0.001345	1.76758	1365.64	1282.28	1.0650
33PyridineEthene	-0.052454	-0.053483	0.001029	1.96197	1060.23	1015.31	1.0442
34PentanePentane	-0.073253	-0.074838	0.001584	2.16283	4289.21	3780.57	1.1345
35NeopentanePentane	-0.073241	-0.074822	0.001581	2.15930	4217.26	3690.82	1.1426
36NeopentaneNeopentane	-0.073180	-0.074757	0.001578	2.15578	4074.70	3684.98	1.1058
37CyclopentaneNeopentane	-0.071831	-0.073356	0.001525	2.12260	3835.73	3437.50	1.1158
38CyclopentaneCyclopentane	-0.070524	-0.071996	0.001472	2.08740	3516.33	3262.91	1.0777
39BenzeneCyclopentane	-0.072182	-0.073636	0.001454	2.01482	3339.06	3091.36	1.0801
40BenzeneNeopentane	-0.073503	-0.075010	0.001507	2.05047	3609.94	3212.41	1.1237
41UracilPentane	-0.100382	-0.102275	0.001893	1.88620	4846.59	4215.52	1.1497
42UracilCyclopentane	-0.098991	-0.100828	0.001837	1.85596	4306.23	3801.60	1.1327
43UracilNeopentane	-0.100343	-0.102233	0.001890	1.88388	4676.01	3996.72	1.1700
44EthenePentane	-0.050297	-0.051380	0.001082	2.15213	1383.61	1299.20	1.0650
45EthynePentane	-0.049192	-0.050247	0.001055	2.14413	1180.34	1144.94	1.0309
46PeptidePentane	-0.077985	-0.079561	0.001576	2.02047	3258.98	2921.82	1.1154
47BenzeneBenzeneTS	-0.073928	-0.075367	0.001439	1.94628	2785.02	2522.28	1.1042
48PyridinePyridineTS	-0.077322	-0.078781	0.001458	1.88608	2466.08	2298.57	1.0729
49BenzenePyridineTS	-0.075628	-0.077076	0.001449	1.91560	2641.25	2394.94	1.1028
50BenzeneEthyneCHpi	-0.049197	-0.050159	0.000962	1.95503	927.41	871.74	1.0639
51EthyneEthyneTS	-0.024657	-0.025161	0.000504	2.04390	112.61	110.73	1.0170
52BenzeneAcOHOHpi	-0.073842	-0.075221	0.001379	1.86747	1721.46	1567.97	1.0979
53BenzeneAcNH2NHpi	-0.071509	-0.072872	0.001363	1.90632	1735.37	1598.64	1.0855
54BenzeneWaterOHpi	-0.050172	-0.051136	0.000964	1.92150	760.96	719.08	1.0582
55BenzeneMeOHOHpi	-0.057025	-0.058132	0.001107	1.94091	1155.39	1095.81	1.0544
56BenzeneMeNH2NHpi	-0.054534	-0.055621	0.001087	1.99299	1236.72	1192.29	1.0373
57BenzenePeptideNHpi	-0.078296	-0.079800	0.001503	1.92001	2685.55	2439.86	1.1007
58PyridinePyridineCHN	-0.077399	-0.078860	0.001460	1.88656	2224.32	1992.65	1.1163
59EthyneWaterCHO	-0.025480	-0.025967	0.000488	1.91421	65.03	64.24	1.0123
60EthyneAcOHOHpi	-0.049166	-0.050068	0.000903	1.83568	379.17	373.71	1.0146
61PentaneAcOH	-0.073539	-0.074991	0.001452	1.97466	2180.46	2000.02	1.0902
62PentaneAcNH2	-0.071127	-0.072562	0.001435	2.01723	2376.86	2152.14	1.1044
63BenzeneAcOH	-0.073828	-0.075207	0.001378	1.86682	1844.50	1686.94	1.0934
64PeptideEthene	-0.055212	-0.056298	0.001086	1.96609	928.76	881.32	1.0538
65PyridineEthyne	-0.050961	-0.051934	0.000973	1.90957	754.34	718.84	1.0494
66MeNH2Pyridine	-0.056264	-0.057361	0.001097	1.94914	1137.00	1057.04	1.0756

TABLE XI. DF-MP2-F12/cc-pVDZ-F12 and DF-MP2-SF12/cc-pVDZ-F12 absolute explicitly correlated F12 energy corrections of the S22 test set. $c_{\mathrm{SF12}} = 0.935$; MAE [kcal·mol^{-1}] = 3.989; MPE [%] = 2.27496; $\varnothing \frac{t_{\mathrm{F12}}}{t_{\mathrm{SF12}}} = 1.30713$.

S22-Structure	E_{F12} [H]	E_{SF12} [H]	Err. [H]	Err. [%]	t_{F12}	t_{SF12}	$\frac{t_{F12}}{t_{SF12}}$
BenzenedimerTshaped	-0.297367	-0.304452	0.007085	2.38261	167.17	119.93	1.3939
IndolebenzeneTshapecomplex	-0.380023	-0.388723	0.008701	2.28947	342.59	227.98	1.5027
Phenoldimer	-0.395790	-0.404425	0.008635	2.18179	265.86	179.81	1.4786
Ammoniadimer	-0.082000	-0.084044	0.002043	2.49204	2.91	2.97	0.9798
Waterdimer	-0.106694	-0.108830	0.002136	2.00152	2.13	1.98	1.0758
BenzeneMethanecomplex	-0.180131	-0.184606	0.004475	2.48438	40.88	35.14	1.1633
Formicaciddimer	-0.247363	-0.251943	0.004580	1.85141	15.64	13.93	1.1228
Formamidedimer	-0.223536	-0.228091	0.004554	2.03747	20.40	17.71	1.1519
Uracildimerhbonded	-0.529564	-0.539973	0.010408	1.96548	332.59	200.32	1.6603
2pyridoxine2aminopyridinecomplex	-0.401458	-0.410156	0.008698	2.16663	253.11	167.20	1.5138
AdeninethymineWatsonCrickcomplex	-0.587519	-0.599450	0.011931	2.03082	690.83	386.08	1.7893
Methanedimer	-0.062632	-0.064495	0.001863	2.97464	4.28	4.06	1.0542
Ethenedimer	-0.105914	-0.108766	0.002852	2.69310	10.66	9.91	1.0757
Benzenedimerparalleldisplaced	-0.297282	-0.304355	0.007074	2.37954	174.53	142.26	1.2268
Pyrazinedimer	-0.331360	-0.338603	0.007243	2.18584	138.13	103.10	1.3398
Uracildimerstack	-0.528575	-0.538965	0.010391	1.96577	357.62	229.54	1.5580
Indolebenzenecomplexstack	-0.379656	-0.388339	0.008684	2.28721	374.80	245.79	1.5249
Adeninethyminecomplexstack	-0.586234	-0.598135	0.011900	2.02998	727.47	436.74	1.6657
Etheneethynecomplex	-0.100671	-0.103291	0.002620	2.60230	7.60	7.33	1.0368
Benzenewatercomplex	-0.202158	-0.206771	0.004613	2.28179	33.79	30.17	1.1200
Benzeneammoniacomplex	-0.189744	-0.194308	0.004564	2.40553	36.82	32.18	1.1442
BenzeneHCNcomplex	-0.203397	-0.208197	0.004800	2.35976	41.43	35.15	1.1787

TABLE XII. DF-MP2-F12/cc-pVTZ-F12 and DF-MP2-SF12/cc-pVTZ-F12 absolute explicitly correlated F12 energy corrections of the S22 test set. $c_{\mathrm{SF12}} = 0.950$; MAE [kcal·mol^{-1}] = 1.759; MPE [%] = 2.12241; $\varnothing \frac{t_{\mathrm{F12}}}{t_{\mathrm{SF12}}} = 1.18062$.

S22-Structure	E_{F12} [H]	E_{SF12} [H]	Err. [H]	Err. [%]	t_{F12}	t_{SF12}	$\frac{t_{F12}}{t_{SF12}}$
BenzenedimerTshaped	-0.141881	-0.145073	0.003192	2.25002	606.05	482.54	1.2560
IndolebenzeneTshapecomplex	-0.179487	-0.183369	0.003882	2.16273	1188.60	888.35	1.3380
Phenoldimer	-0.186800	-0.190596	0.003795	2.03181	931.99	708.45	1.3155
Ammoniadimer	-0.040562	-0.041510	0.000948	2.33821	10.94	11.31	0.9673
Waterdimer	-0.051320	-0.052236	0.000916	1.78390	7.07	9.39	0.7529
BenzeneMethanecomplex	-0.087573	-0.089631	0.002058	2.34996	166.04	151.47	1.0962
Formicaciddimer	-0.115646	-0.117566	0.001921	1.66077	59.94	55.79	1.0744
Formamidedimer	-0.105485	-0.107462	0.001978	1.87488	80.89	70.72	1.1438
Uracildimerhbonded	-0.245794	-0.250226	0.004432	1.80322	1087.50	765.54	1.4206
2pyridoxine2aminopyridinecomplex	-0.188264	-0.192085	0.003821	2.02965	887.98	697.76	1.2726
AdeninethymineWatsonCrickcomplex	-0.272364	-0.277513	0.005148	1.89016	2160.79	1413.85	1.5283
Methanedimer	-0.033155	-0.034077	0.000923	2.78257	15.65	15.38	1.0176
Ethenedimer	-0.053095	-0.054439	0.001345	2.53246	42.94	40.57	1.0584
Benzenedimerparalleldisplaced	-0.141812	-0.144999	0.003187	2.24747	651.75	535.67	1.2167
Pyrazinedimer	-0.155311	-0.158514	0.003203	2.06249	496.27	424.22	1.1698
Uracildimerstack	-0.245635	-0.250062	0.004427	1.80246	1237.17	907.13	1.3638
Indolebenzenecomplexstack	-0.179344	-0.183217	0.003874	2.15991	1272.43	1016.46	1.2518
Adeninethyminecomplexstack	-0.271816	-0.276951	0.005135	1.88927	2438.86	1826.83	1.3350
Etheneethynecomplex	-0.050045	-0.051262	0.001217	2.43084	29.45	27.88	1.0563
Benzenewatercomplex	-0.096627	-0.098682	0.002055	2.12664	138.69	127.05	1.0916
Benzeneammoniacomplex	-0.091229	-0.093300	0.002071	2.27015	155.60	137.30	1.1333
BenzeneHCNcomplex	-0.096965	-0.099111	0.002146	2.21351	163.65	146.96	1.1136

TABLE XIII. DF-MP2-F12/cc-pVQZ-F12 and DF-MP2-SF12/cc-pVQZ-F12 absolute explicitly correlated F12 energy corrections of the S22 test set. $c_{\mathrm{SF12}} = 0.960$; MAE [kcal·mol^{-1}] = 0.831; MPE [%] = 1.91368; $\varnothing \frac{t_{\mathrm{F12}}}{t_{\mathrm{SF12}}} = 1.05154$.

S22-Structure	E_{F12} [H]	E_{SF12} [H]	Err. [H]	Err. [%]	t_{F12}	t_{SF12}	$\frac{t_{F12}}{t_{SF12}}$
BenzenedimerTshaped	-0.073924	-0.075363	0.001439	1.94621	2898.42	2585.34	1.1211
IndolebenzeneTshapecomplex	-0.093683	-0.095447	0.001763	1.88220	1902.35	1791.35	1.0620
Phenoldimer	-0.096944	-0.098733	0.001789	1.84527	1528.42	1433.98	1.0659
Ammoniadimer	-0.021303	-0.021750	0.000447	2.09909	23.54	23.38	1.0068
Waterdimer	-0.026445	-0.026934	0.000488	1.84680	14.87	15.88	0.9364
BenzeneMethanecomplex	-0.045548	-0.046473	0.000925	2.03080	357.23	346.43	1.0312
Formicaciddimer	-0.059596	-0.060618	0.001022	1.71475	134.46	132.45	1.0152
Formamidedimer	-0.054833	-0.055824	0.000991	1.80667	168.64	167.11	1.0092
Uracildimerhbonded	-0.127688	-0.129892	0.002204	1.72584	1614.14	1474.32	1.0948
2pyridoxine2aminopyridinecomplex	-0.098141	-0.099936	0.001795	1.82860	1460.25	1300.88	1.1225
AdeninethymineWatsonCrickcomplex	-0.141999	-0.144479	0.002480	1.74667	2834.34	2485.24	1.1405
Methanedimer	-0.017142	-0.017553	0.000411	2.39919	37.68	37.50	1.0048
Ethenedimer	-0.027560	-0.028161	0.000601	2.18117	99.95	98.62	1.0135
Benzenedimerparalleldisplaced	-0.073866	-0.075302	0.001436	1.94423	1240.35	1198.72	1.0347
Pyrazinedimer	-0.081442	-0.082934	0.001492	1.83246	3059.72	2778.41	1.1012
Uracildimerstack	-0.127506	-0.129708	0.002202	1.72664	2039.21	1897.78	1.0745
Indolebenzenecomplexstack	-0.093559	-0.095318	0.001759	1.88022	2207.44	2051.22	1.0762
Adeninethyminecomplexstack	-0.141629	-0.144102	0.002474	1.74668	3835.15	3352.21	1.1441
Etheneethynecomplex	-0.026075	-0.026619	0.000544	2.08775	68.49	68.08	1.0060
Benzenewatercomplex	-0.050178	-0.051142	0.000964	1.92179	311.75	305.79	1.0195
Benzeneammoniacomplex	-0.047614	-0.048557	0.000943	1.98121	337.84	331.57	1.0189
BenzeneHCNcomplex	-0.050654	-0.051630	0.000976	1.92661	362.44	350.22	1.0349

TABLE XIV. DF-MP2-F12/cc-pVDZ-F12 and DF-MP2-SF12/cc-pVDZ-F12 absolute explicitly correlated F12 energy corrections of the L7 test set. $c_{\mathrm{SF12}} = 0.935$; MAE [kcal·mol^{-1}] = 17.635; MPE [%] = 2.17262; $\varnothing \frac{t_{\mathrm{F12}}}{t_{\mathrm{SF12}}} = 2.41254$.

L7-Structure	E_{F12} [H]	E_{SF12} [H]	Err. [H]	Err. [%]	t_{F12}	t_{SF12}	$\frac{t_{\mathrm{F12}}}{t_{\mathrm{SF12}}}$
octadecanedimer	-0.998084	-1.023572	0.025488	2.55370	11522.09	3714.16	3.1022
guaninetrimer	-1.030340	-1.050766	0.020426	1.98246	2025.41	922.95	2.1945
circumcoroneneadenine	-1.551431	-1.584857	0.033426	2.15454	28596.10	9853.87	2.9020
circumcoroneneGCbasepair	-1.850909	-1.890201	0.039292	2.12285	39812.82	15659.73	2.5424
phenylalanineresiduestrimer	-1.333442	-1.362366	0.028924	2.16911	8631.32	3857.86	2.2373
coronenedimer	-1.134823	-1.160120	0.025298	2.22922	6246.69	2907.62	2.1484
GCGCbasepairstack	-1.195569	-1.219438	0.023869	1.99645	3043.12	1728.11	1.7610

TABLE XV. DF-MP2-F12/cc-pVDZ-F12 and DF-MP2-SF12/cc-pVDZ-F12 absolute explicitly correlated F12 energy corrections for linear alkane chains. $c_{\mathrm{SF12}} = 0.935$; MAE [kcal·mol^{-1}] = 15.413; MPE [%] = 2.53732; $\varnothing \frac{t_{\mathrm{F12}}}{t_{\mathrm{SF12}}} = 2.66348$.

Alkanes	E_{F12} [H]	E_{SF12} [H]	Err. [H]	Err. [%]	t_{F12}	t_{SF12}	$\frac{t_{\mathrm{F12}}}{t_{\mathrm{SF12}}}$
alkan10	-0.280126	-0.287317	0.007191	2.56701	76.68	60.52	1.2670
alkan20	-0.556218	-0.570357	0.014139	2.54205	887.62	451.69	1.9651
alkan30	-0.832320	-0.853408	0.021088	2.53360	4827.21	1815.42	2.6590
alkan40	-1.108425	-1.136461	0.028036	2.52935	18807.86	5947.59	3.1623
alkan50	-1.384527	-1.419511	0.034984	2.52680	53423.46	16059.35	3.3266
alkan60	-1.660627	-1.702560	0.041933	2.52510	125226.71	34776.93	3.6009

TABLE XVI. DF-MP2-F12/cc-pVDZ-F12 and DF-MP2-SF12/cc-pVDZ-F12 absolute explicitly correlated F12 energy corrections for linear amylose chains. $c_{\mathrm{SF12}} = 0.935$; MAE [kcal·mol^{-1}] = 12.176; MPE [%] = 1.94653; $\varnothing \frac{t_{\mathrm{F12}}}{t_{\mathrm{SF12}}} = 2.04934$.

Amylose Chain	E_{F12} [H]	E_{SF12} [H]	Err. [H]	Err. [%]	t_{F12}	t_{SF12}	$\frac{t_{\mathrm{F12}}}{t_{\mathrm{SF12}}}$
adglucose	-0.458471	-0.467404	0.008933	1.94834	78.91	59.56	1.3249
amylose2	-0.862493	-0.879279	0.016786	1.94619	870.31	436.57	1.9935
amylose4	-1.670437	-1.702928	0.032491	1.94505	14938.01	5279.18	2.8296

4.2 Publication II

Highly Efficient and Accurate Computation of Multiple Orbital Spaces Spanning Fock Matrix Elements on Central and Graphics Processing Units for Application in F12 Theory

L. Urban, H. Laqua, and C. Ochsenfeld,
J. Chem. Theory Comput. **2022**, *18*, 4218

Abstract:

We employ our recently published highly efficient seminumerical exchange (sn-LinK) [Laqua, H.; Thompson, T. H.; Kussmann, J.; Ochsenfeld, C. *J. Chem. Theory Comput.* **2020**, *16*, 1456–1468] and integral-direct resolution of the identity Coulomb (RI-J) [Kussmann, J.; Laqua, H.; Ochsenfeld, C. *J. Chem. Theory Comput.* **2021**, *17*, 1512–1521] methods to significantly accelerate the computation of the demanding multiple orbital spaces spanning Fock matrix elements present in R12/F12 theory on central and graphics processing units. The errors introduced by RI-J and sn-LinK into the RI-MP2-F12 energy are thoroughly assessed for a variety of basis sets and integration grids. We find that these numerical errors are always below "chemical accuracy" ($\sim$1 mH) even for the coarsest settings and can easily be reduced below 1 μH by employing only moderately large integration grids and RI-J basis sets. Since the number of basis functions of the multiple orbital spaces is notably larger compared with conventional Hartree–Fock theory, the efficiency gains from the superior basis scaling of RI-J and sn-LinK ($\mathcal{O}(N_{\text{bas}}^2)$ instead of $\mathcal{O}(N_{\text{bas}}^4$ for both) are even more significant, with maximum speedup factors of 37000 for RI-J and 4500 for sn-LinK. In total, the multiple orbital spaces spanning Fock matrix evaluation of the largest tested structure using a triple-ζ F12 basis set (5058 AO basis functions, 9267 CABS basis functions) is accelerated over 1575$\times$ using CPUs and over 4155$\times$ employing GPUs.

JCTC Journal of Chemical Theory and Computation

pubs.acs.org/JCTC Article

Highly Efficient and Accurate Computation of Multiple Orbital Spaces Spanning Fock Matrix Elements on Central and Graphics Processing Units for Application in F12 Theory

Lars Urban, Henryk Laqua, and Christian Ochsenfeld*

Cite This: J. Chem. Theory Comput. 2022, 18, 4218−4228 Read Online

ACCESS | Metrics & More | Article Recommendations | Supporting Information

ABSTRACT: We employ our recently published highly efficient seminumerical exchange (sn-LinK) [Laqua, H.; Thompson, T. H.; Kussmann, J.; Ochsenfeld, C. *J. Chem. Theory Comput.* **2020**, *16*, 1456−1468] and integral-direct resolution of the identity Coulomb (RI-J) [Kussmann, J.; Laqua, H.; Ochsenfeld, C. *J. Chem. Theory Comput.* **2021**, *17*, 1512−1521] methods to significantly accelerate the computation of the demanding multiple orbital spaces spanning Fock matrix elements present in R12/F12 theory on central and graphics processing units. The errors introduced by RI-J and sn-LinK into the RI-MP2-F12 energy are thoroughly assessed for a variety of basis sets and integration grids. We find that these numerical errors are always below "chemical accuracy" (∼1 mH) even for the coarsest settings and can easily be reduced below 1 μH by employing only moderately large integration grids and RI-J basis sets. Since the number of basis functions of the multiple orbital spaces is notably larger compared with conventional Hartree−Fock theory, the efficiency gains from the superior basis scaling of RI-J and sn-LinK ($O(N_{bas}^2)$ instead of $O(N_{bas}^4)$ for both) are even more significant, with maximum speedup factors of 37 000 for RI-J and 4500 for sn-LinK. In total, the multiple orbital spaces spanning Fock matrix evaluation of the largest tested structure using a triple-ζ F12 basis set (5058 AO basis functions, 9267 CABS basis functions) is accelerated over 1575× using CPUs and over 4155× employing GPUs.

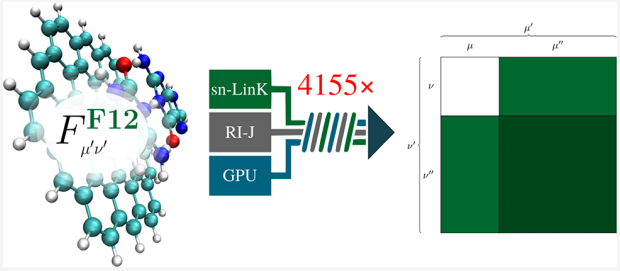

1. INTRODUCTION

Over the last decades, considerable efforts[1] have been devoted to accelerate the computation and contraction of direct- and exchange-type four-center−two-electron (4c-2e) integrals present in Hartree−Fock[2−5] (HF) and Kohn−Sham[6] (KS) theory, which in their conventional formulation show an unfavorable scaling of $O(N_{bas}^4)$ with the number atomic orbital (AO) basis functions N_{bas}. Among these aspirations are methods focusing on the efficient contraction of 4c-2e integrals[7−9] and attempts like the resolution of the identity (RI) approximation,[10−12] a frequently used approach to reduce the computational prefactor substantially. Especially the application of the RI technique for Coulomb contributions (RI-J)[13,14] yields significant speedups, which are additionally improved when RI-J is combined with the J-engine algorithm.[15−17] Here, our recently published[18] integral-direct RI-J version additionally accelerates the evaluation of the occurring three-center−two-electron (3c-2e) integrals, reducing the number of floating-point operations (FLOPs) and required local memory, which makes the method more efficient for both central processing units (CPUs) as well as graphics processing units (GPUs).

However, the relative RI efficiency for exchange contributions (RI-K)[12,19−21] succumbs to advanced RI-J algorithms due to the comparable formal $O(N_{occ}N_{aux}N_{bas}^2)$ scaling as the conventional evaluation when not combined with local approximations.[22,23] Here, seminumerical integration,[24−35] where one electronic coordinate of the 4c-2e integrals is represented numerically on real-space integration grids while the other one remains in its analytical representation, provides a promising alternative. For maximal performance, the number of grid points N_{grid} has to be as small as possible, and the computationally demanding evaluation of the necessary three-center−one-electron (3c-1e) integrals needs to be as efficient as possible. Recent efforts by our group systematically refined both of these aspects by introducing revised molecular integration grids[36−38] and a more effective batchwise integral screening method (sn-LinK).[39−41] Moreover, the possibility to parallelize over the grid index within the numerical integration combined with the reduced demand for local storage (e.g., L1 cache) to evaluate the 3c-1e integrals compared with the 4c-2e

Received: March 2, 2022
Published: June 8, 2022

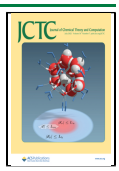

https://doi.org/10.1021/acs.jctc.2c00215
J. Chem. Theory Comput. 2022, 18, 4218−4228

integrals makes this method for computing exchange contributions particularly well suited for GPU acceleration.

Besides HF and KS theory, the computation of Fock matrix elements is essential for R12/F12 methods,[42−47] which are powerful tools to overcome the basis set incompleteness error (BSIE). These elements, denoted in the following as F12-type Fock matrix elements, need to be evaluated for multiple orbital spaces introduced by the strong orthogonality operator $\hat{Q}_{12}$, which notably increases the number of required basis functions. In general, the formally quartic-scaling evaluation of the direct and exchange contributions to F12-type Fock matrices is thus substantially more demanding than the evaluation of normal Fock matrices and frequently represents an extremely expensive step in applications of F12 theory.[44,48,49] Efficient evaluation is thus highly beneficial since a series of theories require these elements, among them the complementary auxiliary basis set (CABS) singles correction,[48,50] explicitly correlated second-order Møller−Plesset perturbation theory (MP2-R12/F12),[43,44,49,51−57] coupled cluster-F12 (CC-F12),[48,50,58−64] multireference-F12 (MR-F12),[65−72] and other explicitly correlated approaches.[73−75] Previous works applied RI[49,51,53,54,72] and seminumerical integral[76] approaches but focused primarily on other aspects of F12 theory, not the investigation of their influence on accuracy and efficiency. Motivated by these circumstances, we transferred our recently introduced RI-J and sn-LinK methods to F12 theory. Both of these are well-suited because of the improved formal $O(N_{\mathrm{bas}}{}^2)$ scaling with respect to the AO basis set size compared with the conventional $O(N_{\mathrm{bas}}{}^4)$ scaling, which is particularly relevant in view of the substantially larger size of the combined CABS (N_{CABS}) and AO basis.

The paper is structured as follows: We present the necessary underlying formulas for extending RI-J and sn-LinK to F12 theory in section 2, followed by the most important findings regarding accuracy in section 4.1 and efficiency in section 4.2 (additional data are provided in the Supporting Information).

2. THEORY

2.1. Approximation-Free Evaluation of F12-Type Fock Matrix Elements. In contrast to HF theory, Fock matrix elements in explicitly correlated F12 theory span the additional orbital spaces given in Table 1. The AO representation of the F12-type Fock matrix, visualized in Figure 1a, differs from the standard HF/KS approach by evaluation of $\{\mu'\}$, the union of the atomic orbitals $\{\mu\}$ and the CABS atomic orbitals $\{\mu''\}$, as given by

Table 1. Summary of Orbital Spaces and Indexing Conventions

orbital space	indices
AO space	$\mu, \nu, \lambda, \sigma$
AO complementary auxiliary space	$\mu'', \nu'', \lambda'', \sigma''$
combined AO space ($\{\mu\} \cup \{\mu''\}$)	$\mu', \nu', \lambda', \sigma'$
MO occupied space	i, j, k, l
MO virtual space	a, b, c, d
MO occupied + virtual space ($\{i\} \cup \{a\}$)	p, q, r, s
MO complementary auxiliary space	p'', q'', r'', s''
combined MO CABS/HF space ($\{p\} \cup \{p''\}$)	p', q', r', s'
RI-J auxiliary space	P, Q

$$F_{\mu'\nu'} = H^{\mathrm{core}}_{\mu'\nu'} + J_{\mu'\nu'} - \frac{1}{2}K_{\mu'\nu'} \tag{1}$$

where $H^{\mathrm{core}}_{\mu'\nu'}$, $J_{\mu'\nu'}$, and $K_{\mu'\nu'}$ are elements of the core-Hamiltonian matrix, Coulomb matrix, and exchange matrix of the combined orbital space, respectively. While $H^{\mathrm{core}}_{\mu'\nu'}$ contributions are trivial to evaluate with insignificant computational cost, the $J_{\mu'\nu'}$ and $K_{\mu'\nu'}$ elements are calculated via

$$J_{\mu'\nu'} = \sum_{\lambda\sigma} P_{\lambda\sigma}(\mu'\nu'|\lambda\sigma) \tag{2}$$

$$K_{\mu'\nu'} = \sum_{\lambda\sigma} P_{\lambda\sigma}(\mu'\sigma|\lambda\nu') \tag{3}$$

where $P_{\lambda\sigma}$ are the elements of the density matrix of the final SCF iteration in the AO space, and the computationally demanding 4c-2e integrals are given by

$$(\mu'\nu'|\lambda\sigma) = \int\int \mathrm{d}\mathbf{r}_1\, \mathrm{d}\mathbf{r}_2\, \chi_{\mu'}(\mathbf{r}_1)\chi_{\nu'}(\mathbf{r}_1)\frac{1}{|\mathbf{r}_1 - \mathbf{r}_2|}\chi_{\lambda}(\mathbf{r}_2)\chi_{\sigma}(\mathbf{r}_2) \tag{4}$$

After construction of the AO F12-type Fock matrix, the transformation into the molecular orbital (MO) space is achieved by contraction with the MO coefficients from the final SCF iteration and precomputed CABS coefficients.[46] Figure 1b visualizes the different MO spaces present in F12 theory and the resulting F12-type Fock matrix elements. The MO transformation and the determination of the required CABS coefficients require only minor computational effort. In contrast, the evaluations of the **J** and **K** matrices are computationally intensive procedures. The usually large CABS space further increases the cost of the direct- and exchange-type matrix element evaluation, leading to about an order of magnitude longer runtimes for computations using the F12-type Fock matrix compared with the standard SCF Fock matrix. Increasing the angular momentum quantum number (l) amplifies this effect, making more efficient methods having reduced time complexity with respect to the basis set size highly desirable.

2.2. An Integral-Direct J-Engine-Based Resolution of the Identity Coulomb Method. In this section, we briefly summarize the necessary theory for the integral-direct RI-J method that we employ for the F12-type Fock matrix element evaluation. For more insights and illustrative calculations, we refer the reader to the original literature.[17,18] Applying the RI approximation to the Coulomb potential leads to

$$\begin{aligned} J_{\mu'\nu'} &= \sum_{\lambda\sigma} P_{\lambda\sigma}(\mu'\nu'|\lambda\sigma) \\ &\approx \sum_{\lambda\sigma}\sum_{PQ} P_{\lambda\sigma}(\mu'\nu'|P)(P|Q)^{-1}(Q|\lambda\sigma) \end{aligned} \tag{5}$$

where for an integral-direct algorithm three consecutive steps are executed:

$$\text{step 1:}\quad J_P = \sum_{\lambda\sigma}(P|\lambda\sigma)P_{\lambda\sigma} \tag{6}$$

$$\text{step 2:}\quad J'_Q = \sum_{P}(Q|P)^{-1}J_P \tag{7}$$

$$\text{step 3:}\quad J_{\mu'\nu'} = \sum_{Q}(\mu'\nu'|Q)J'_Q \tag{8}$$

https://doi.org/10.1021/acs.jctc.2c00215
J. Chem. Theory Comput. 2022, 18, 4218−4228

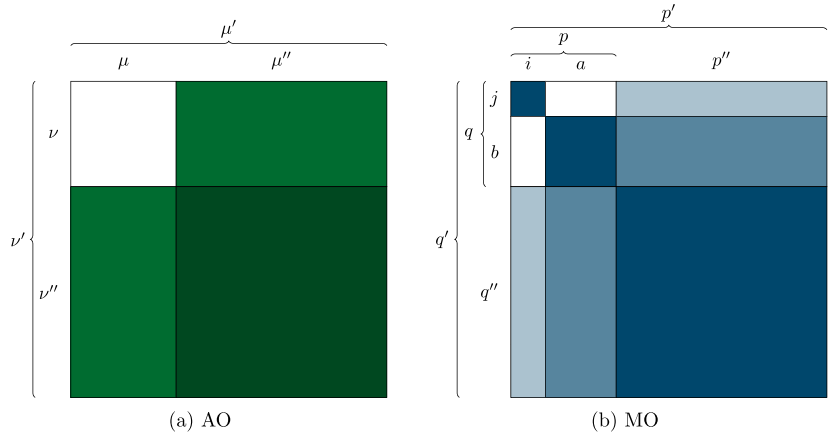

Figure 1. Representations of (a) the AO and (b) the MO spaces present in F12 theory covered by F12-type Fock matrix elements.

Several techniques allow the efficient evaluation of these formulas. For step 2, the well-known Coulomb fitting method of Mintmire and Dunlap[77] avoids the matrix inversion step for the two-center integrals by a direct evaluation of the Coulomb metric $(Q|P)x = J_P$, leading to $x = (Q|P)^{-1}J_P = J'_Q$, for which we employ a Cholesky decomposition of $(Q|P)$. The typically rate-determining steps 1 and 3 requiring 3c-2e integrals are accelerated by a J-engine[15,16] algorithm: First, the AO (step 1) and auxiliary (step 3) density(-like) matrices are transformed in a preprocessing computation into the Hermite basis. Subsequently, the resulting intermediates are contracted with the 3c-2e integrals to form the Coulomb potential in the Hermite basis, representing by far the most expensive step within the J-engine algorithm due to its asymptotic quadratic scaling. In the final postprocessing, the Coulomb potential is back-transformed into the AO (step 3) or auxiliary (step 1) basis, respectively.

Since some intermediate Hermite factors (i.e., all odd l quantum numbers) are not necessary for the representation of the auxiliary basis functions, these contributions can be omitted, leading to further efficiency gains (cf. section 2.1 of ref 18). Combining all of these aspects results in a highly efficient evaluation of the **J** matrix, especially when the massively parallel behavior of GPUs is utilized to compute the expensive Coulomb potential in the Hermite basis.

2.3. Seminumerical Exchange: sn-LinK. The general integration scheme for seminumerical integral evaluation[39,41,78] results in the symmetrical decomposition of the 4c-2e integrals as

$$\begin{aligned}(\mu\sigma|\lambda\nu) &\approx \frac{1}{2}[((\mu\sigma)^{\text{num}}|(\nu\lambda)^{\text{ana}}) + ((\mu\sigma)^{\text{ana}}|(\nu\lambda)^{\text{num}})] \\ &\equiv \frac{1}{2}\left[\sum_g w_g\chi_\mu(\mathbf{r}_g)\chi_\sigma(\mathbf{r}_g)\int \mathrm{d}\mathbf{r}\,\frac{\chi_\lambda(\mathbf{r})\chi_\nu(\mathbf{r})}{|\mathbf{r}_g-\mathbf{r}|}\right. \\ &\quad \left. + \sum_g w_g\int \mathrm{d}\mathbf{r}\,\frac{\chi_\mu(\mathbf{r})\chi_\sigma(\mathbf{r})}{|\mathbf{r}_g-\mathbf{r}|}\chi_\lambda(\mathbf{r}_g)\chi_\nu(\mathbf{r}_g)\right] \end{aligned} \tag{9}$$

where Becke-type molecular integration grids[36−38] with grid points $\mathbf{r}_g$ and associated weights w_g are employed. Application of this ansatz to the AO representation of the approximation-free F12-type exchange matrix results in

$$\begin{aligned}K_{\mu'\nu'} &= \sum_{\lambda\sigma} P_{\lambda\sigma}(\mu'\sigma|\lambda\nu') \\ &\approx \frac{1}{2}\left[\sum_g w_g\sum_{\lambda\sigma}\chi_{\mu'}(\mathbf{r}_g)\int \mathrm{d}\mathbf{r}\,\frac{\chi_\lambda(\mathbf{r})\chi_{\nu'}(\mathbf{r})}{|\mathbf{r}-\mathbf{r}_g|}\chi_\sigma(\mathbf{r}_g)P_{\lambda\sigma}\right. \\ &\quad \left. + \text{transpose}\right] \end{aligned} \tag{10}$$

which is computed in three consecutive steps:

$$\text{step 1:}\quad F_{\lambda g} = \sum_\sigma \chi_\sigma(\mathbf{r}_g)P_{\lambda\sigma} \tag{11}$$

$$\text{step 2:}\quad G_{\nu' g} = \sum_\lambda w_g A_{\lambda\nu' g}F_{\lambda g} \tag{12}$$

$$\text{step 3:}\quad \bar{K}_{\mu'\nu'} = \sum_g \chi_{\mu'}(\mathbf{r}_g)G_{\nu' g} \tag{13}$$

where $A_{\lambda\nu' g}$ are mixed-basis 3c-1e integrals, given by

$$A_{\lambda\nu' g} = \int \frac{\chi_\lambda(\mathbf{r})\chi_{\nu'}(\mathbf{r})}{|\mathbf{r}_g-\mathbf{r}|}\,\mathrm{d}\mathbf{r} \tag{14}$$

Finally, the F12-type exchange matrix is obtained via the symmetrization

$$K_{\mu'\nu'} = \frac{1}{2}(\bar{K}_{\mu'\nu'} + \bar{K}_{\nu'\mu'}) \tag{15}$$

to take care of the transpose in eq 10. Steps 1 (eq 11) and 3 (eq 13) are implemented as dense matrix−matrix multiplications, whereas step 2 (eq 12) requires on-the-fly evaluation of the 3c-1e integrals (eq 14). The matrix−matrix multiplications in steps 1 and 3 utilize batch-local matrices with asymptotically constant size computed via BLAS-3 libraries to achieve the best performance, as described in detail in ref 41. However, the evaluation of the 3c-1e integrals in step 2 is generally the most computationally demanding part in the seminumerical integral evaluation, requiring an efficient integral screening procedure for optimal performance. Practical approaches to determine the significance of a 3c-1e integral $A_{\lambda\nu' g}$ are screening for the F12-type exchange energy $\epsilon^E_{\lambda\nu' g}$ and the final F12-type exchange matrix contributions $\epsilon^K_{\lambda\nu' g}$, given by

https://doi.org/10.1021/acs.jctc.2c00215
J. Chem. Theory Comput. 2022, 18, 4218−4228

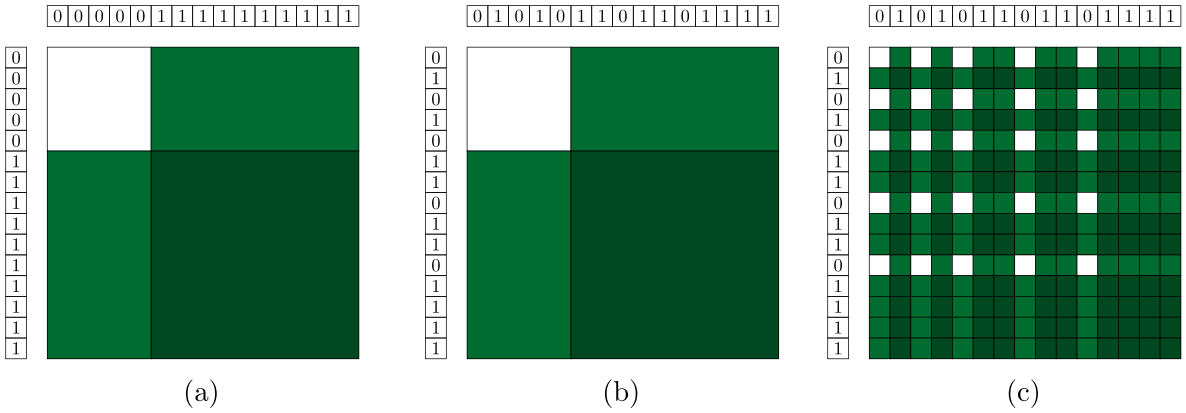

Figure 2. (a) Standard representation of the orbital spaces leading to separate blocks. (b) Construction of new shell-pair data. (c) Mixed pattern of the resulting orbital spaces.

$$\epsilon^{E}_{\lambda\nu' g} = \left| w_g \sum_{\mu\sigma} \chi_\mu(\mathbf{r}_g) P_{\mu\nu} A_{\lambda\nu' g} P_{\lambda\sigma} \chi_\sigma(\mathbf{r}_g) \right| = \left| w_g^{1/2} F_{\nu g} A_{\lambda\nu' g} w_g^{1/2} F_{\lambda g} \right| \tag{16}$$

$$\begin{aligned} \epsilon^{K}_{\lambda\nu' g} &= |w_g| \max\left(\sum_{\mu\sigma'} |\chi_\mu(\mathbf{r}_g)| |P_{\mu\nu}| |A_{\lambda\nu' g}| |\chi_{\sigma'}(\mathbf{r}_g)|, \right. \\ &\quad \left. \sum_{\mu'\sigma} |\chi_{\mu'}(\mathbf{r}_g)| |A_{\lambda\nu' g}| |P_{\lambda\sigma}| |\chi_\sigma(\mathbf{r}_g)| \right) \\ &\leq |w_g| \max(|F_{\nu g}|, |F_{\lambda g}|) |A_{\lambda\nu' g}| \sum_{\mu'} |\chi_{\mu'}(\mathbf{r}_g)| \end{aligned} \tag{17}$$

In accordance with ref 41, integrals are considered to be significant if either one or both of these values are above a given threshold, i.e.,

$$\epsilon^{E}_{\lambda\nu' g} \geq \vartheta_E \quad \text{or/and} \quad \epsilon^{K}_{\lambda\nu' g} \geq \vartheta_K \tag{18}$$

Details regarding the evaluation of the required integral bounds

$$\mathcal{V}_{\nu'\lambda} \leq \max_{\mathbf{r}_g \in \mathbb{R}^3} \left(\int \frac{|\chi'_\nu(\mathbf{r}) \chi_\lambda(\mathbf{r})|}{|\mathbf{r}_g - \mathbf{r}|} \, \mathrm{d}\mathbf{r} \right) \tag{19}$$

are provided in ref 40.

2.4. Adoption of RI-J/sn-LinK for F12-Type Fock Matrices. Our previous approximation-free reference implementation for the F12-type Fock matrix is based on the blockwise computation represented in Figure 2a, where elements of the different AO spaces are calculated via separate integral routines. The evaluation of the $F_{\mu''\nu}$ and $F_{\mu''\nu''}$ blocks requires additional implementational work, e.g., support for mixed shell-pairs.

In this present study, however, we avoid this extra effort by merging the AO basis and the CABS basis into one combined basis according to atom and angular momentum quantum numbers, represented by zeros and ones in Figure 2b. Capitalizing on this computationally inexpensive transformation from two separate basis sets to one combined basis set allows the direct use of standard integral routines as well as RI-J and sn-LinK. Back-transformation of the resulting F12-type Fock matrix (Figure 2c) to a blockwise representation is easily possible.

Since only the AO elements of the density matrix $P_{\lambda\sigma}$ are nonzero, a large number of irrelevant contributions are included within the combined basis set, which could in principle lead to substantial inefficiencies. However, all of those zero elements in $P_{\lambda'\sigma'}$ are excluded early on by the density-including integral screening techniques within both RI-J and sn-LinK, resulting in virtually no overhead in practice. In this way, our advanced RI-J[18] and sn-LinK[41] methods with all of their benefits (e.g., GPU acceleration) are directly applicable to the evaluation of F12-type Fock matrix elements.

3. COMPUTATIONAL DETAILS

All of the reported calculations were performed with our FermiONs++ program package,[79−82] where the grids[38] summarized in Table 2 and the cc-pVYZ-JKfit[12] (Y = D, T, Q, 5) RI-J basis sets were employed for sn-LinK and RI-J, respectively. As proposed in ref 38, SCF- and F12-type exchange matrices were computed using the smaller gX grid, whereas the final energy evaluation utilized a larger gX+2 grid (compressed in a shorthand multigrid gm[X+2/X] notation). As a reference we set our approximation-free code using the Obara−Saika recursion scheme[83] for the 4c-2e integrals. Throughout the following, the F12 correction refers to the explicitly correlated F12 energy correction to second-order Møller-Plesset perturbation theory in the 3*C variant,[51] where we employed Ten-no's fixed-amplitude ansatz[84] in combination with the extended Brillouin condition (EBC).[44] A fixed Slater-type geminal (STG) correlation factor[45,65] of the form $\hat{F}_{12} = \frac{1}{\gamma}[1 - \exp(-\gamma r_{12})]$ with $\gamma = 1.3$ was used together with

Table 2. Definition of the Employed Grids with Separation into Inner, Medium, and Outer Regions for the Example of the C Atom

grid	n_{rad}	n_{ang}(inner/medium/outer)	$n_{\mathrm{tot,C}}$
g0	30	14/38/74	1654
g1	35	14/50/110	2586
g2	40	26/74/194	5056
g3	50	38/110/302	9564
g4	55	50/194/434	15526
g5	60	50/194/590	21330
g6	70	86/302/974	40838
g7	80	110/434/1454	68770

https://doi.org/10.1021/acs.jctc.2c00215
J. Chem. Theory Comput. 2022, 18, 4218−4228

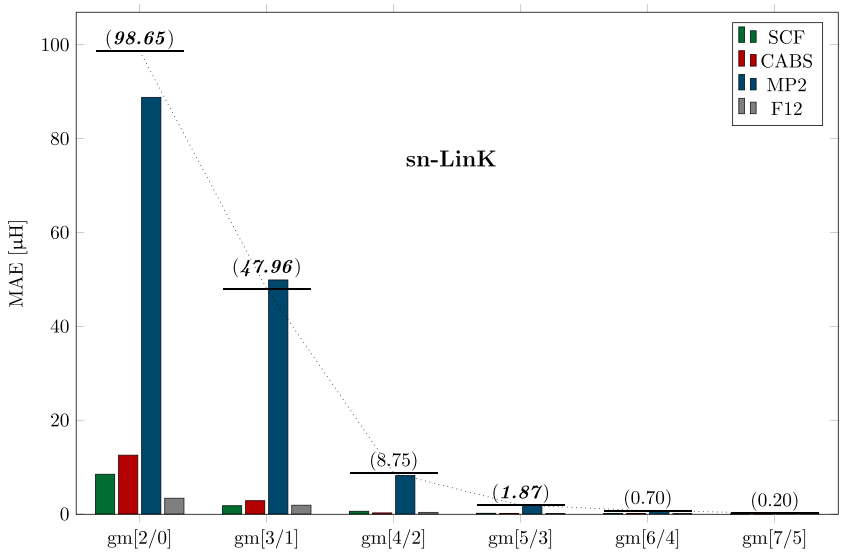

Figure 3. Visualization of HF, CABS singles, MP2, F12 correction, and total sn-LinK NCI MAEs (numbers in parentheses) in dependence on the grid size for the L7 test set, employing a cc-pVDZ-F12 AO basis and a cc-pVDZ-F12/OptRI+ CABS basis.

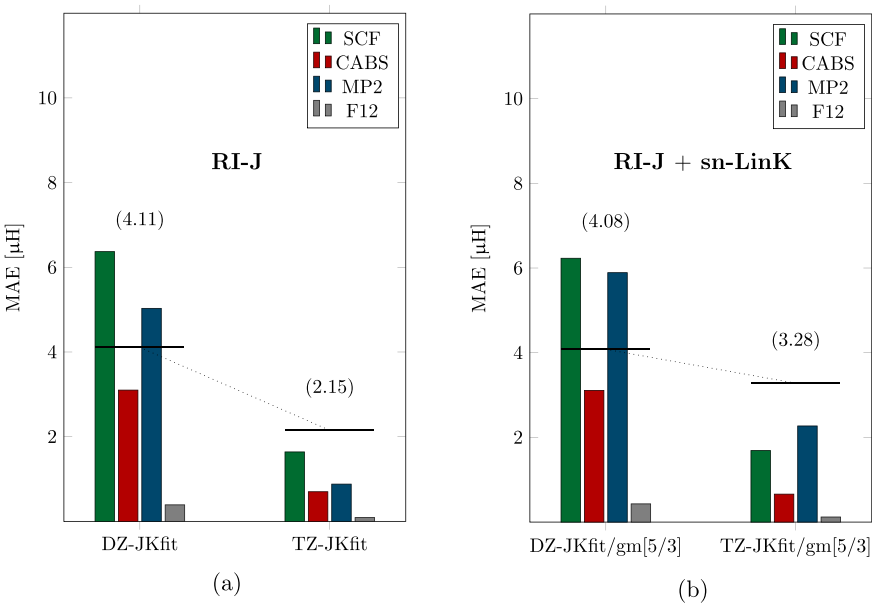

Figure 4. Visualization of L7 HF, CABS singles, MP2, F12 correction, and total NCI MAEs (numbers in parentheses) for (a) RI-J and (b) RI-J/sn-LinK, employing a cc-pVDZ-F12 AO basis set, a cc-pVDZ-F12/OptRI+ CABS basis set, and two different cc-pVYZ-JKfit (Y = D, T) RI-J basis sets.

the cc-pVXZ-F12[85−87] basis set family and corresponding CABS cc-pVXZ-F12/OptRI+[88] and density fitting (DF) cc-pVXZ-F12/MP2fit[89] basis sets (X = D, T, Q).

For optimal performance, the integral kernels were compiled with the Intel Compiler 19.1.0[90] (flags: -Ofast -march=cascadelake) and the OpenCL GPU kernels with ROCm-3.8.0[91] (flags: -O3 -cl-mad-enable -cl-finite-math-only -cl-no-signed-zeros). The performance was assessed on two Intel Xeon Silver 4216 processors (32 cores/64 threads; 2.1 GHz) and 4 AMD Radeon VII cards to ensure a fair comparison between CPU and GPU (roughly equal acquisition cost of hardware). For the conventionel 4c-2e and RI-J 3c-2e integrals, we set a threshold of 10^{-13}, and for sn-LinK we chose $\vartheta_K = 10^{-10}$ and $\vartheta_E = 10^{-13}$, employing mixed single- and double-precision 3c-1e integral evaluation[78] on CPUs. The SCF was converged to within 10^{-7} of the DIIS commutator norm ($\|\mathbf{FPS} - \mathbf{SPF}\|$),[92,93] and interaction energies were counterpoise-corrected[94] to take the basis set superposition error (BSSE) into account.

4. RESULTS

In the following, we summarize the most essential and representative findings of a benchmark study on the accuracy and efficiency of the F12-type Fock matrix element evaluation using varying sn-LinK and RI-J settings for prominent test sets.[95−98] Since the results are qualitatively identical among the test sets, here we focus on the L7 non-covalent interaction (NCI) energies[98] and refer the reader to the Supporting Information (SI) for more insights and detailed data on the remaining systems (the S22, S66, and ISO34 test sets), including deviations in isomerization and absolute energies as well as conventional RI-JK results.

https://doi.org/10.1021/acs.jctc.2c00215
J. Chem. Theory Comput. 2022, 18, 4218−4228

Table 3. RI-J/sn-LinK (cc-pVYZ-JKt/gm[2/0]; Y = X) Speedups on CPUs (S_{CPU}) and GPUs (S_{GPU}) for the Full F12-Type Fock Build for Each Member of the L7 Test Set (cc-pVXZ-F12; X = D, T, Q); Additional RI-JK (cc-pVDZ-JKfit) Results ($S_{CPU}^{RI\text{-}JK}$) Are Given for a cc-pVDZ-F12 Basis

	cc-pVDZ-F12					cc-pVTZ-F12				cc-pVQZ-F12		
L7 structure[a]	N_{bas}	N_{CABS}	$S_{CPU}^{RI\text{-}JK}$	S_{CPU}	S_{GPU}	N_{bas}	N_{CABS}	S_{CPU}	S_{GPU}	N_{bas}	N_{CABS}	S_{CPU}[b]
L1	1836	5288	19	209	528	3676	7804	639	1627	6996	9700	1551
L2	1191	3426	29	251	469	2331	4311	733	1550	4281	5229	1488
L3	2255	6486	41	517	1340	4405	8044	1423	3403	8065	9733	2761
L4	2588	7444	47	584	1635	5058	9267	1575	4155	9268	11220	2710
L5	1818	5232	31	316	742	3588	6999	976	2017	6678	8574	2024
L6	1752	5044	48	446	1072	3432	6384	1308	2884	6312	7752	2548
L7	1396	4016	33	331	682	2736	5106	939	1880	5036	6204	1918

[a]L7 test set structures: L1, octadecane dimer; L2, guanine trimer; L3, circumcoronene−adenine dimer; L4, circumcoronene−guanine−cytosine trimer; L5, phenylalanine residues trimer; L6, coronene dimer; L7, guanine−cytosine−guanine−cytosine tetramer. [b]Reference extrapolated from double- and triple-ζ F12 timings.

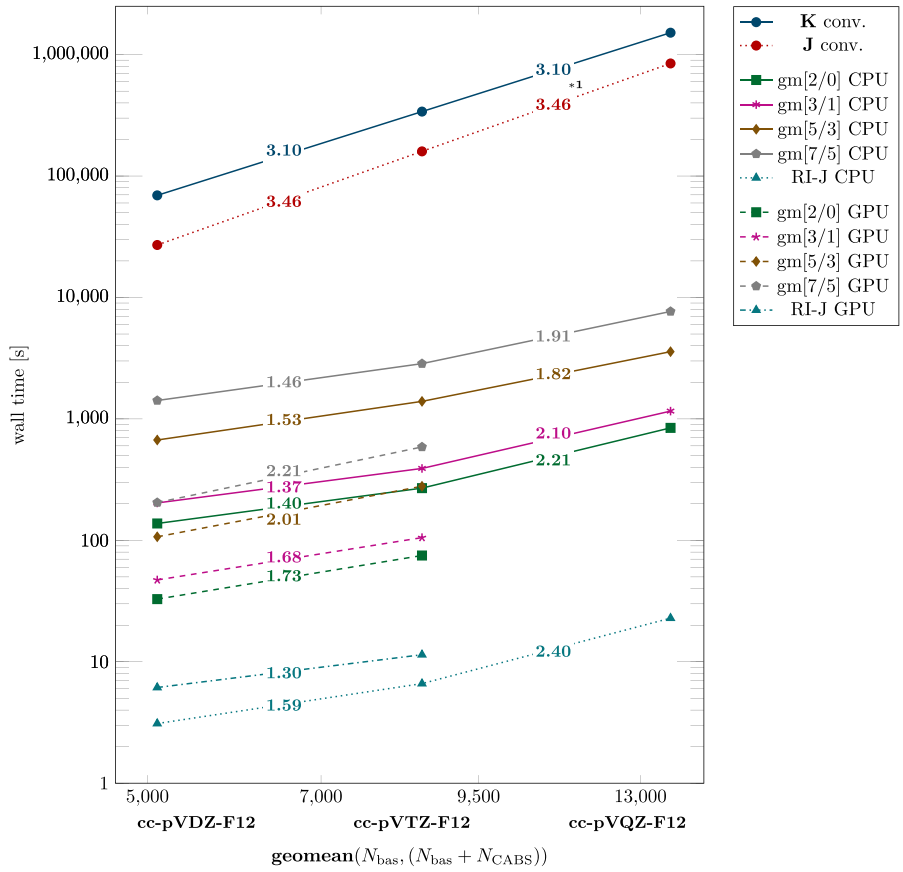

Figure 5. Log−log plot of the wall times for the L7 circumcoronene−guanine−cytosine trimer $J_{\mu'\nu'}$ and $K_{\mu'\nu'}$ matrix element evaluation employing an approximation-free reference code, RI-J, and sn-LinK for a cc-pVXZ-F12 AO basis set and a cc-pVXZ-F12/OptRI+ CABS basis set (X = D, T, Q) on CPUs and GPUs. sn-LinK and RI-J timings are reported for various gm[X+2/X] multigrid sizes and a cc-pVYZ-JKfit RI-J basis set (Y = X). Scaling coefficients are given within the lines. *1 extrapolated from double- and triple-ζ timings.

4.1. Accuracy. Starting with the main bottleneck of computing the F12-type Fock matrix elements, the evaluation of the exchange-type matrix $K_{\mu'\nu'}$, we explore the behavior of sn-LinK for different gm[X+2/X] multigrids for the cc-pVDZ-F12 AO basis set, with qualitatively identical results for triple- and quadruple-ζ F12 calculations given in the SI. We investigate the accuracy of HF, CABS singles, MP2, F12 correction, and total energies for counterpoise-corrected NCI of the L7 test set compared with an approximation-free reference code visualized in Figure 3. As expected, higher accuracy is achieved with increasing grid size, with total mean absolute errors (MAEs) ranging from 100 to 0.2 μH from the smallest to the largest multigrid, which is always substantially below the MP2 method error (>10 mH). With regard to the individual error contributions, the MP2 deviations dominate the total MAE, matching observations in ref 41. This error is only caused by a slight imperfection in the self-consistently converged Fock and density matrices due to the finite grid error in the SCF.

https://doi.org/10.1021/acs.jctc.2c00215
J. Chem. Theory Comput. 2022, 18, 4218−4228

Table 4. Absolute Timings for the F12-Type Fock Build Using Our Original Implementation, RI-JK (cc-pVDZ-JKfit), RI-J/sn-LinK (cc-pVDZ-JKt/gm[2/0]), and the Total MP2-F12 Correlation Calculation Excluding the F12-Type Fock Build (t_{corr}) for Each Member of the L7 Test Set (cc-pVDZ-F12) with the Corresponding Ratios of Fock Build Time to Remaining Correlation Time

L7 structure[a]	$t^{ref}_{F12\text{-}Fock}$ [s]	$t^{RI\text{-}JK}_{F12\text{-}Fock}$ [s]	$t^{RI\text{-}J/sn\text{-}LinK}_{F12\text{-}Fock}$ [s]	t_{corr} [s]	$\frac{R_{ref}}{corr}$ [%]	$\frac{R_{RI\text{-}JK}}{corr}$ [%]	$\frac{R_{RI\text{-}J/sn\text{-}LinK}}{corr}$ [%]
L1	13894	715	66	12854	108.1	5.6	0.5
L2	6584	225	26	2606	252.6	8.6	1.0
L3	61013	1459	118	29729	205.2	4.9	0.4
L4	96379	2044	165	57095	168.8	3.5	0.3
L5	22381	701	71	13568	164.9	5.2	0.5
L6	34536	725	77	9930	347.8	7.3	0.8
L7	12412	372	40	4925	252.0	7.6	0.8

[a]L7 test set structures: L1, octadecane dimer; L2, guanine trimer; L3, circumcoronene−adenine dimer; L4, circumcoronene−guanine−cytosine trimer; L5, phenylalanine residues trimer; L6, coronene dimer; L7, guanine−cytosine−guanine−cytosine tetramer.

To investigate the accuracy of RI-J for the L7 system, we utilized the cc-pVYZ-JKfit (Y = D, T) RI-J basis set family together with an AO cc-pVDZ-F12 basis set for both the SCF cycle and the F12-type Fock matrix evaluation. Following the same pattern as for sn-LinK, the MAEs show excellent accuracy with negligible deviations of roughly 4 μH even for a double-ζ RI-J basis set (Figure 4a). With a triple-ζ auxiliary basis set, even more precise values are possible, reducing the errors by a factor of approximately 2 compared with the double-ζ evaluation. For the combination of sn-LinK and RI-J, we employed the gm[5/3] multigrid because of the comparable errors of the two methods (Figure 4b). The actual RI-J/sn-LinK combination experiences some form of error cancellation with a MAE close to the RI-J errors and less than the sum of the individual-method MAEs. In practice, the errors of only 3−4 μH for RI-J/sn-LinK relative to the exact analytical treatment are virtually irrelevant.

4.2. Peformance Comparison. To demonstrate the full potential of our sn-LinK and RI-J methods, we focus on timings for the largest and consequently computationally most expensive member of the L7 test set (L4 in Table 3): a circumcoronene−guanine−cytosine trimer with 102 atoms. Figure 5 compares the performance of sn-LinK and RI-J for increasing AO and CABS basis sets employing the corresponding (DZ/TZ/QZ) RI-J basis sets and a variety of multigrids with the exact analytical treatment for increasing AO and CABS basis sets on CPUs and GPUs.

Because of the decreasing N_{bas} to N_{CABS} ratio for larger cardinal numbers X, we decided to plot the geometric mean $[N_{bas}(N_{bas} + N_{CABS})]^{1/2}$ against the required time to ensure a fair comparison between the different AO basis set sizes and the formal $N_{bas+CABS}{}^2 N_{bas}{}^2$ scaling of the reference. Quadruple-zeta F12 reference values were extrapolated from double- and triple-ζ results. GPU calculations for quadruple-ζ F12 calculations are currently not feasible due to numerical problems regarding the GPU execution of some integrals for h (l = 5) functions.

The observed time complexity with respect to the basis set size roughly matches the theoretical $O(N_{bas}{}^4)$ or $O(N_{bas}{}^2)$ scaling for the analytical or sn-LinK/RI-J treatment, respectively. The observed variations around these theoretical values, i.e, $O(N_{bas}{}^{3.10})$ to $O(N_{bas}{}^{3.46})$ instead of $O(N_{bas}{}^4)$ for the exact treatment and $O(N_{bas}{}^{1.30})$ to $O(N_{bas}{}^{2.40})$ instead of $O(N_{bas}{}^2)$ for RI-J/sn-LinK, are expected given that the average cost of evaluating one integral and the effectiveness of integral screening methods vary substantially among the basis sets because of, e.g., different l quantum numbers or the addition of diffuse functions. Moreover, the amount of parallel workload, which significantly affects GPU performance, also increases with larger basis sets. The choice of the multigrid contributes approximately as a constant prefactor (largely independent of the basis set). As a result of this reduced basis set scaling in combination with the large size of the CABS basis sets, tremendous speedups are achieved. For example, using only CPUs, sn-LinK with a gm[2/0] multigrid provides speedups ranging from 500× to 1800× (DZ-F12 to QZ-F12, respectively), and RI-J gives speedups ranging from 8700× to 37000×. Employing GPUs improves the performance of sn-LinK even further, with accelerations ranging from 3200× to 4500× (DZ-F12 to TZ-F12, respectively). In contrast, RI-J does not benefit from GPU acceleration due to a lack of parallel workload in this case (cf. discussion in ref 18). However, this is not a concern in practice because of the comparatively low cost of the RI-J part regardless.

To further illustrate the profound efficiency improvement of sn-LinK and RI-J, in Table 3 we summarize the total speedups for the full F12-type Fock build (**J**, **K**, core Hamiltonian, and ordering algorithm) for each member of the L7 benchmark set for a gm[2/0] integration grid (results for larger multigrids are given in the SI) alongside RI-JK double-ζ results (see details of our RI-K implementation in the SI).

While RI-JK yields good accelerations with, on average, 35× faster computations compared with our conventional implementation, double- and triple-ζ results were not feasible because of the vast memory demand of the required three-center integrals in RI-K. Generally, the steep $O(N_{occ}N_{aux}N_{bas}{}^2)$ scaling of RI-K makes it unfavorable for medium- to large-sized structures compared with the alternative of sn-LinK.

Our RI-J/sn-LinK methods proposed in this work result in excellent speedups, surpassing RI-JK with on average 379× faster computation for a double-ζ basis, with the performance gains over all basis sets (DZ−QZ) ranging between 209× and 4155×. For example, the total runtime for one triple-ζ F12-type Fock build for the circumcoronene−guanine−cytosine complex (L4) is reduced by a factor of 4155 from ∼6 days (analytically) to only ∼2 min (RI-J/sn-LinK).

To illustrate the importance of a fast F12-type Fock matrix evaluation, in Table 4 we compare timings for our conventional reference, RI-JK, and RI-J/sn-LinK for the L7 test set

https://doi.org/10.1021/acs.jctc.2c00215
J. Chem. Theory Comput. 2022, 18, 4218−4228

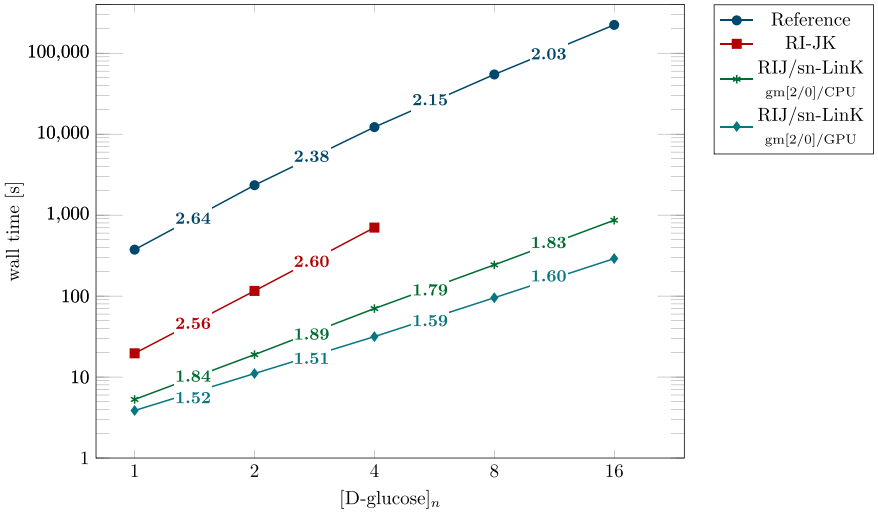

Figure 6. Log−log plot of the wall times against the length of increasing amylose chains for the evaluation of the corresponding F12-type Fock matrix elements, employing cc-pVDZ-F12 AO and cc-pVDZ-F12/OptRI+ CABS basis sets together with our reference, RI-JK (cc-pVDZ-JKfit), and RI-J/sn-LinK (cc-pVDZ-JKt/gm[2/0]) on CPUs and GPUs. Scaling coefficients are given within the lines.

(cc-pVDZ-F12) with our RI-MP2-F12 implementation excluding the F12-type Fock build. Our reference represents by far the most expensive step in the total correlation calculations for all L7 members, requiring on average 214.2% more time than the remaining terms, including the standard MP2 correction. For RI-JK, this ratio continues to be significant at 6.1%, whereas RI-J/sn-LinK lowers this ratio to a desirable 0.6%.

Finally, to demonstrate the behavior for a fixed basis set and increasing molecule sizes, we examined systematically increasing amylose chain lengths[99] using our reference code, RI-JK, RI-J/sn-LinK (CPU), and RI-J/sn-LinK (GPU) in combination with a double-ζ F12 basis. The results are shown in Figure 6. RI-JK decreases the required time by a factor of roughly 20, where memory limitations restrict the computation to a chain length of four D-glucose subunits, e.g., the 3c-2e RI-K integrals for eight subunits require 538 GB of storage, which increases to 4.21 TB for 16 subunits, matching its $O(M^{3.0})$ memory scaling with the molecule size (M). RI-J/sn-LinK leads once again to excellent speedups with scaling coefficients between $O(N_{\text{glucose}}{}^{2})$ and $O(N_{\text{glucose}}{}^{1.5})$, matching the asymptotic $O(M^2)$ and $O(M)$ scalings of RI-J and sn-LinK with the molecule size for systems with local electronic structure. For the largest chain length (16 D-glucose subunits), we observed 768× faster evaluation using our GPUs, reducing the required time from ∼2.6 days to less than 5 min.

5. CONCLUSION

We employed our recently published highly efficient RI-J[18] and sn-LinK[41] methods to overcome the two major bottlenecks of the **J** and **K** matrix computation in the evaluation of F12-type Fock matrices. We tested the accuracy of the methods for multiple benchmark sets covering non-covalent interactions and isomerization energies (also see the Supporting Information). Even for the smallest grids and RI-J basis sets, the mean absolute errors are always below 0.43 mH and are easily reducible to below 5 μH for slightly larger integration grids.

Moreover, since both methods lower the formal scaling with respect to the basis set size from $O(N_{\text{bas}}{}^{4})$ to $O(N_{\text{bas}}{}^{2})$, impressive performance improvements of up to 37000× for the direct (Coulomb) contribution and 1800× for the exchange contribution were achieved, and the latter could be improved even further to over 4500× faster execution when GPU acceleration was employed. In total, RI-J/sn-LinK combines remarkable efficiency with high accuracy for evaluation of the F12-type Fock matrix, leading to tremendous time savings with over 3 orders of magnitude faster computations. We therefore expect wide applicability in F12 theories.

■ ASSOCIATED CONTENT

Supporting Information

The Supporting Information is available free of charge at https://pubs.acs.org/doi/10.1021/acs.jctc.2c00215.

Detailed individual and total NCI, isomerization, and total energy data for all test sets (L7, S22, S66, ISO34) and methods employing a cc-pVXZ-F12 (X = D, T, Q) AO basis and additional timings for the L7 structures, and an outline of our RI-K implementation (PDF)

■ AUTHOR INFORMATION

Corresponding Author

Christian Ochsenfeld − *Chair of Theoretical Chemistry, Department of Chemistry, University of Munich (LMU), D-81377 Munich, Germany; Max Planck Institute for Solid State Research, D-70569 Stuttgart, Germany;* orcid.org/0000-0002-4189-6558; Email: christian.ochsenfeld@uni-muenchen.de

Authors

Lars Urban − *Chair of Theoretical Chemistry, Department of Chemistry, University of Munich (LMU), D-81377 Munich, Germany; Max Planck Institute for Solid State Research, D-70569 Stuttgart, Germany;* orcid.org/0000-0001-9891-3577

Henryk Laqua − *Chair of Theoretical Chemistry, Department of Chemistry, University of Munich (LMU), D-81377 Munich, Germany*

Complete contact information is available at: https://pubs.acs.org/10.1021/acs.jctc.2c00215

https://doi.org/10.1021/acs.jctc.2c00215
J. Chem. Theory Comput. 2022, 18, 4218−4228

Notes

The authors declare no competing financial interest.

■ ACKNOWLEDGMENTS

The authors thank F. H. Bangerter (LMU Munich) and V. Drontschenko (LMU Munich) for helpful discussions and J. Kussmann (LMU Munich) for providing a development version of the FermiONs++ program package.[79−82] Financial support was provided by the Excellence Cluster EXC2111-390814868 at the Munich Center for Quantum Science and Technology (MCQST) by the Deutsche Forschungsgemeinschaft (DFG). C.O acknowledges, in addition, financial support as Max Planck Fellow of MPI-FKF Stuttgart.

■ REFERENCES

(1) Kussmann, J.; Beer, M.; Ochsenfeld, C. Linear-scaling self-consistent field methods for large molecules. *Wiley Interdiscip. Rev.: Comput. Mol. Sci.* **2013**, *3*, 614−636.
(2) Hartree, D. R. The Wave Mechanics of an Atom with a Non-Coulomb Central Field Part I Theory and Methods. *Math. Proc. Camb. Philos. Soc.* **1928**, *24*, 89−110.
(3) Fock, V. Näherungsmethode zur Lösung des quantenmechanischen Mehrkörperproblems. *Z. Phys.* **1930**, *61*, 126−148.
(4) Roothaan, C. C. J. New developments in molecular orbital theory. *Rev. Mod. Phys.* **1951**, *23*, 69−89.
(5) Hall, G. G. The molecular orbital theory of chemical valency VIII. A method of calculating ionization potentials. *Proc. R. Soc. London, Ser. A* **1951**, *205*, 541−552.
(6) Kohn, W.; Sham, L. J. Self-consistent equations including exchange and correlation effects. *Phys. Rev.* **1965**, *140*, A1133−A1138.
(7) White, C. A.; Johnson, B. G.; Gill, P. M.; Head-Gordon, M. The continuous fast multipole method. *Chem. Phys. Lett.* **1994**, *230*, 8−16.
(8) Strain, M. C.; Scuseria, G. E.; Frisch, M. J. Achieving linear scaling for the electronic quantum coulomb problem. *Science* **1996**, *271*, 51−53.
(9) Ochsenfeld, C.; White, C. A.; Head-Gordon, M. Linear and sublinear scaling formation of Hartree-Fock-type exchange matrices. *J. Chem. Phys.* **1998**, *109*, 1663−1669.
(10) Whitten, J. L. Coulombic potential energy integrals and approximations. *J. Chem. Phys.* **1973**, *58*, 4496−4501.
(11) Dunlap, B. I.; Connolly, J. W. D.; Sabin, J. R. On some approximations in applications of Xα theory. *J. Chem. Phys.* **1979**, *71*, 3396−3402.
(12) Weigend, F. A fully direct RI-HF algorithm: Implementation, optimized auxiliary basis sets, demonstration of accuracy and efficiency. *Phys. Chem. Chem. Phys.* **2002**, *4*, 4285−4291.
(13) Eichkorn, K.; Treutler, O.; Öhm, H.; Häser, M.; Ahlrichs, R. Auxiliary basis sets to approximate Coulomb potentials. *Chem. Phys. Lett.* **1995**, *240*, 283−290.
(14) Eichkorn, K.; Weigend, F.; Treutler, O.; Ahlrichs, R. Auxiliary basis sets for main row atoms and transition metals and their use to approximate Coulomb potentials. *Theor. Chem. Acc.* **1997**, *97*, 119−124.
(15) Reza Ahmadi, G.; Almlöf, J. The Coulomb operator in a Gaussian product basis. *Chem. Phys. Lett.* **1995**, *246*, 364−370.
(16) White, C. A.; Head-Gordon, M. A J matrix engine for density functional theory calculations. *J. Chem. Phys.* **1996**, *104*, 2620−2629.
(17) Neese, F. An improvement of the resolution of the identity approximation for the formation of the Coulomb matrix. *J. Comput. Chem.* **2003**, *24*, 1740−1747.
(18) Kussmann, J.; Laqua, H.; Ochsenfeld, C. Highly Efficient Resolution-of-Identity Density Functional Theory Calculations on Central and Graphics Processing Units. *J. Chem. Theory Comput.* **2021**, *17*, 1512−1521.
(19) Früchtl, H. A.; Kendall, R. A.; Harrison, R. J.; Dyall, K. G. An Implementation of RI-SCF on Parallel Computers. *Int. J. Quantum Chem.* **1997**, *64*, 63−69.
(20) Hamel, S.; Casida, M. E.; Salahub, D. R. Assessment of the quality of orbital energies in resolution-of-the-identity Hartree-Fock calculations using deMon auxiliary basis sets. *J. Chem. Phys.* **2001**, *114*, 7342−7350.
(21) Weigend, F. Hartree−Fock exchange fitting basis sets for H to Rn. *J. Comput. Chem.* **2008**, *29*, 167−175.
(22) Polly, R.; Werner, H.-J.; Manby, F. R.; Knowles, P. J. Fast Hartree-Fock theory using local density fitting approximations. *Mol. Phys.* **2004**, *102*, 2311−2321.
(23) Köppl, C.; Werner, H.-J. Parallel and low-order scaling implementation of Hartree-Fock exchange using local density fitting. *J. Chem. Theory Comput.* **2016**, *12*, 3122−3134.
(24) Friesner, R. A. Solution of self-consistent field electronic structure equations by a pseudospectral method. *Chem. Phys. Lett.* **1985**, *116*, 39−43.
(25) Friesner, R. A. Solution of the Hartree-Fock equations by a pseudospectral method: Application to diatomic molecules. *J. Chem. Phys.* **1986**, *85*, 1462−1468.
(26) Friesner, R. A. Solution of the Hartree-Fock equations for polyatomic molecules by a pseudospectral method. *J. Chem. Phys.* **1987**, *86*, 3522−3531.
(27) Ringnalda, M. N.; Belhadj, M.; Friesner, R. A. Pseudospectral Hartree-Fock theory: Applications and algorithmic improvements. *J. Chem. Phys.* **1990**, *93*, 3397−3407.
(28) Neese, F.; Wennmohs, F.; Hansen, A.; Becker, U. Efficient, approximate and parallel Hartree-Fock and hybrid DFT calculations. A 'chain-of-spheres' algorithm for the Hartree-Fock exchange. *Chem. Phys.* **2009**, *356*, 98−109.
(29) Plessow, P.; Weigend, F. Seminumerical calculation of the Hartree-Fock exchange matrix: Application to two-component procedures and efficient evaluation of local hybrid density functionals. *J. Comput. Chem.* **2012**, *33*, 810−816.
(30) Bahmann, H.; Kaupp, M. Efficient self-consistent implementation of local hybrid functionals. *J. Chem. Theory Comput* **2015**, *11*, 1540−1548.
(31) Maier, T. M.; Bahmann, H.; Kaupp, M. Efficient Seminumerical Implementation of Global and Local Hybrid Functionals for Time-Dependent Density Functional Theory. *J. Chem. Theory Comput.* **2015**, *11*, 4226−4237.
(32) Klawohn, S.; Bahmann, H.; Kaupp, M. Implementation of Molecular Gradients for Local Hybrid Density Functionals Using Seminumerical Integration Techniques. *J. Chem. Theory Comput.* **2016**, *12*, 4254−4262.
(33) Liu, F.; Kong, J. Efficient Computation of Exchange Energy Density with Gaussian Basis Functions. *J. Chem. Theory Comput.* **2017**, *13*, 2571−2580.
(34) Holzer, C. An improved seminumerical Coulomb and exchange algorithm for properties and excited states in modern density functional theory. *J. Chem. Phys.* **2020**, *153*, 184115.
(35) Helmich-Paris, B.; de Souza, B.; Neese, F.; Izsák, R. An improved chain of spheres for exchange algorithm. *J. Chem. Phys.* **2021**, *155*, 104109.
(36) Becke, A. D. A multicenter numerical integration scheme for polyatomic molecules. *J. Chem. Phys.* **1988**, *88*, 2547−2553.
(37) Treutler, O.; Ahlrichs, R. Efficient molecular numerical integration schemes. *J. Chem. Phys.* **1995**, *102*, 346−354.
(38) Laqua, H.; Kussmann, J.; Ochsenfeld, C. An improved molecular partitioning scheme for numerical quadratures in density functional theory. *J. Chem. Phys.* **2018**, *149*, 204111.
(39) Laqua, H.; Kussmann, J.; Ochsenfeld, C. Efficient and Linear-Scaling Seminumerical Method for Local Hybrid Density Functionals. *J. Chem. Theory Comput.* **2018**, *14*, 3451−3458.
(40) Thompson, T. H.; Ochsenfeld, C. Integral partition bounds for fast and effective screening of general one-, two-, and many-electron integrals. *J. Chem. Phys.* **2019**, *150*, 044101.
(41) Laqua, H.; Thompson, T. H.; Kussmann, J.; Ochsenfeld, C. Highly Efficient, Linear-Scaling Seminumerical Exact-Exchange Method for Graphic Processing Units. *J. Chem. Theory Comput.* **2020**, *16*, 1456−1468.

https://doi.org/10.1021/acs.jctc.2c00215
J. Chem. Theory Comput. 2022, 18, 4218−4228

(42) Kutzelnigg, W. r_{12}-Dependent terms in the wave function as closed sums of partial wave amplitudes for large *l*. *Theor. Chim. Acta.* **1985**, *68*, 445−469.
(43) Klopper, W.; Kutzelnigg, W. Møller-plesset calculations taking care of the correlation CUSP. *Chem. Phys. Lett.* **1987**, *134*, 17−22.
(44) Kutzelnigg, W.; Klopper, W. Wave functions with terms linear in the interelectronic coordinates to take care of the correlation cusp. I. General theory. *J. Chem. Phys.* **1991**, *94*, 1985−2001.
(45) Ten-no, S. Initiation of explicitly correlated Slater-type geminal theory. *Chem. Phys. Lett.* **2004**, *398*, 56−61.
(46) Valeev, E. F. Improving on the resolution of the identity in linear R12 ab initio theories. *Chem. Phys. Lett.* **2004**, *395*, 190−195.
(47) Kato, T. On the eigenfunctions of many-particle systems in quantum mechanics. *Commun. Pure Appl. Math.* **1957**, *10*, 151−177.
(48) Noga, J.; Šimunek, J. On the one-particle basis set relaxation in R12 based theories. *Chem. Phys.* **2009**, *356*, 1−6.
(49) Bachorz, R. A.; Bischoff, F. A.; Glöß, A.; Hättig, C.; Höfener, S.; Klopper, W.; Tew, D. P. The MP2-F12 Method in the Turbomole Program Package. *J. Comput. Chem.* **2011**, *32*, 2492−2513.
(50) Adler, T. B.; Knizia, G.; Werner, H.-J. A simple and efficient CCSD(T)-F12 approximation. *J. Chem. Phys.* **2007**, *127*, 221106.
(51) Werner, H.-J.; Adler, T. B.; Manby, F. R. General orbital invariant MP2-F12 theory. *J. Chem. Phys.* **2007**, *126*, 164102.
(52) Werner, H.-J. Eliminating the domain error in local explicitly correlated second-order Møller−Plesset perturbation theory. *J. Chem. Phys.* **2008**, *129*, 101103.
(53) Höfener, S.; Klopper, W. Analytical nuclear gradients of the explicitly correlated Møller−Plesset second-order energy. *Mol. Phys.* **2010**, *108*, 1783−1796.
(54) Ma, Q.; Werner, H.-J. Scalable Electron Correlation Methods. 2. Parallel PNO-LMP2-F12 with Near Linear Scaling in the Molecular Size. *J. Chem. Theory Comput.* **2015**, *11*, 5291−5304.
(55) Wang, Y. M.; Hättig, C.; Reine, S.; Valeev, E.; Kjærgaard, T.; Kristensen, K. Explicitly correlated second-order Møller-Plesset perturbation theory in a Divide-Expand-Consolidate (DEC) context. *J. Chem. Phys.* **2016**, *144*, 204112.
(56) Győrffy, W.; Knizia, G.; Werner, H.-J. Analytical energy gradients for explicitly correlated wave functions. I. Explicitly correlated second-order Møller-Plesset perturbation theory. *J. Chem. Phys.* **2017**, *147*, 214101.
(57) Urban, L.; Thompson, T. H.; Ochsenfeld, C. A scaled explicitly correlated F12 correction to second-order Møller-Plesset perturbation theory. *J. Chem. Phys.* **2021**, *154*, 044101.
(58) Valeev, E. F. Coupled-cluster methods with perturbative inclusion of explicitly correlated terms: a preliminary investigation. *Phys. Chem. Chem. Phys.* **2008**, *10*, 106−113.
(59) Noga, J.; Kedžuch, S.; Šimunek, J.; Ten-no, S. Explicitly correlated coupled cluster F12 theory with single and double excitations. *J. Chem. Phys.* **2008**, *128*, 174103.
(60) Torheyden, M.; Valeev, E. F. Variational formulation of perturbative explicitly-correlated coupled-cluster methods. *Phys. Chem. Chem. Phys.* **2008**, *10*, 3410−3420.
(61) Valeev, E. F.; Crawford, T. D. Simple coupled-cluster singles and doubles method with perturbative inclusion of triples and explicitly correlated geminals: The CCSD(T)$_{\overline{R12}}$ Model. *J. Chem. Phys.* **2008**, *128*, 244113.
(62) Hättig, C.; Tew, D. P.; Köhn, A. Communications: Accurate and efficient approximations to explicitly correlated coupled-cluster singles and doubles, CCSD-F12. *J. Chem. Phys.* **2010**, *132*, 231102.
(63) Schmitz, G.; Hättig, C.; Tew, D. P. Explicitly correlated PNO-MP2 and PNO-CCSD and their application to the S66 set and large molecular systems. *Phys. Chem. Chem. Phys.* **2014**, *16*, 22167−22178.
(64) Győrffy, W.; Werner, H.-J. Analytical energy gradients for explicitly correlated wave functions. II. Explicitly correlated coupled cluster singles and doubles with perturbative triples corrections: CCSD(T)-F12. *J. Chem. Phys.* **2018**, *148*, 114104.
(65) Ten-no, S. A simple F12 geminal correction in multi-reference perturbation theory. *Chem. Phys. Lett.* **2007**, *447*, 175−179.
(66) Shiozaki, T.; Werner, H.-J. Communication: Second-order multireference perturbation theory with explicit correlation: CASPT2-F12. *J. Chem. Phys.* **2010**, *133*, 141103.
(67) Shiozaki, T.; Knizia, G.; Werner, H.-J. Explicitly correlated multireference configuration interaction: MRCI-F12. *J. Chem. Phys.* **2011**, *134*, 034113.
(68) Shiozaki, T.; Werner, H.-J. Multireference explicitly correlated F12 theories. *Mol. Phys.* **2013**, *111*, 607−630.
(69) Haunschild, R.; Mao, S.; Mukherjee, D.; Klopper, W. A universal explicit electron correlation correction applied to Mukherjee's multi-reference perturbation theory. *Chem. Phys. Lett.* **2012**, *531*, 247−251.
(70) Liu, W.; Hanauer, M.; Köhn, A. Explicitly correlated internally contracted multireference coupled-cluster singles and doubles theory: ic-MRCCSD(F12*). *Chem. Phys. Lett.* **2013**, *565*, 122−127.
(71) Roskop, L. B.; Kong, L.; Valeev, E. F.; Gordon, M. S.; Windus, T. L. Assessment of Perturbative Explicitly Correlated Methods for Prototypes of Multiconfiguration Electronic Structure. *J. Chem. Theory Comput.* **2014**, *10*, 90−101.
(72) Guo, Y.; Sivalingam, K.; Valeev, E. F.; Neese, F. Explicitly correlated N-electron valence state perturbation theory (NEVPT2-F12). *J. Chem. Phys.* **2017**, *147*, 064110.
(73) Hehn, A.-S.; Klopper, W. Communication: Explicitly-correlated second-order correction to the correlation energy in the random-phase approximation. *J. Chem. Phys.* **2013**, *138*, 181104.
(74) Sylvetsky, N.; Peterson, K. A.; Karton, A.; Martin, J. M. L. Toward a W4-F12 approach: Can explicitly correlated and orbital-based ab initio CCSD(T) limits be reconciled? *J. Chem. Phys.* **2016**, *144*, 214101.
(75) Kodrycka, M.; Holzer, C.; Klopper, W.; Patkowski, K. Explicitly Correlated Dispersion and Exchange Dispersion Energies in Symmetry-Adapted Perturbation Theory. *J. Chem. Theory Comput.* **2019**, *15*, 5965−5986.
(76) Liakos, D. G.; Izsák, R.; Valeev, E. F.; Neese, F. What is the most efficient way to reach the canonical MP2 basis set limit? *Mol. Phys.* **2013**, *111*, 2653−2662.
(77) Mintmire, J. W.; Dunlap, B. I. Fitting the Coulomb potential variationally in linear-combination-of- atomic-orbitals density-functional calculations. *Phys. Rev. A* **1982**, *25*, 88−95.
(78) Laqua, H.; Kussmann, J.; Ochsenfeld, C. Accelerating seminumerical Fock-exchange calculations using mixed single- and double-precision arithmethic. *J. Chem. Phys.* **2021**, *154*, 214116.
(79) Kussmann, J.; Ochsenfeld, C. Pre-selective screening for matrix elements in linear-scaling exact exchange calculations. *J. Chem. Phys.* **2013**, *138*, 134114.
(80) Kussmann, J.; Ochsenfeld, C. Preselective screening for linear-scaling exact exchange-gradient calculations for graphics processing units and general strong-scaling massively parallel calculations. *J. Chem. Theory Comput.* **2015**, *11*, 918−922.
(81) Kussmann, J.; Ochsenfeld, C. Employing OpenCL to Accelerate Ab Initio Calculations on Graphics Processing Units. *J. Chem. Theory Comput.* **2017**, *13*, 2712−2716.
(82) Kussmann, J.; Ochsenfeld, C. Hybrid CPU/GPU Integral Engine for Strong-Scaling Ab Initio Methods. *J. Chem. Theory Comput.* **2017**, *13*, 3153−3159.
(83) Obara, S.; Saika, A. Efficient recursive computation of molecular integrals over Cartesian Gaussian functions. *J. Chem. Phys.* **1986**, *84*, 3963−3974.
(84) Ten-no, S. Explicitly correlated second order perturbation theory: Introduction of a rational generator and numerical quadratures. *J. Chem. Phys.* **2004**, *121*, 117−129.
(85) Peterson, K. A.; Adler, T. B.; Werner, H.-J. Systematically convergent basis sets for explicitly correlated wavefunctions: The atoms H, He, B-Ne, and Al-Ar. *J. Chem. Phys.* **2008**, *128*, 084102.
(86) Hill, J. G.; Peterson, K. A. Correlation consistent basis sets for explicitly correlated wavefunctions: Valence and core-valence basis sets for Li, Be, Na, and Mg. *Phys. Chem. Chem. Phys.* **2010**, *12*, 10460−10468.

https://doi.org/10.1021/acs.jctc.2c00215
J. Chem. Theory Comput. 2022, 18, 4218−4228

(87) Hill, J. G.; Peterson, K. A. Correlation consistent basis sets for explicitly correlated wavefunctions: Pseudopotential-based basis sets for the post-*d* main group elements Ga-Rn. *J. Chem. Phys.* **2014**, *141*, 094106.
(88) Shaw, R. A.; Hill, J. G. Approaching the Hartree-Fock Limit through the Complementary Auxiliary Basis Set Singles Correction and Auxiliary Basis Sets. *J. Chem. Theory Comput.* **2017**, *13*, 1691−1698.
(89) Kritikou, S.; Hill, J. G. Auxiliary Basis Sets for Density Fitting in Explicitly Correlated Calculations: The Atoms H-Ar. *J. Chem. Theory Comput.* **2015**, *11*, 5269−5276.
(90) *Intel C++ Compiler*, ver. 19.1.0.166, 2019. https://software.intel.com/c-compilers.
(91) ROCm 3.8.0, 2021. https://www.amd.com/en/graphics/servers-solutions-rocm.
(92) Pulay, P. Convergence acceleration of iterative sequences. The case of SCF iteration. *Chem. Phys. Lett.* **1980**, *73*, 393−398.
(93) Pulay, P. Improved SCF Convergence Acceleration. *J. Comput. Chem.* **1982**, *3*, 556−560.
(94) Boys, S. F.; Bernardi, F. The calculation of small molecular interactions by the differences of separate total energies. Some procedures with reduced errors. *Mol. Phys.* **1970**, *19*, 553−566.
(95) Jurečka, P.; Šponer, J.; Černy, J.; Hobza, P. Benchmark database of accurate (MP2 and CCSD(T) complete basis set limit) interaction energies of small model complexes, DNA base pairs, and amino acid pairs. *Phys. Chem. Chem. Phys.* **2006**, *8*, 1985−1993.
(96) Řezáč, J.; Riley, K. E.; Hobza, P. S66: A well-balanced database of benchmark interaction energies relevant to biomolecular structures. *J. Chem. Theory Comput.* **2011**, *7*, 2427−2438.
(97) Grimme, S.; Steinmetz, M.; Korth, M. How to compute isomerization energies of organic molecules with quantum chemical methods. *J. Org. Chem.* **2007**, *72*, 2118−2126.
(98) Sedlak, R.; Janowski, T.; Pitoňák, M.; Řezáč, J.; Pulay, P.; Hobza, P. Accuracy of quantum chemical methods for large noncovalent complexes. *J. Chem. Theory Comput.* **2013**, *9*, 3364−3374.
(99) Kussmann, J.; Ochsenfeld, C. Linear-scaling method for calculating nuclear magnetic resonance chemical shifts using gauge-including atomic orbitals within Hartree-Fock and density-functional theory. *J. Chem. Phys.* **2007**, *127*, 054103.

https://doi.org/10.1021/acs.jctc.2c00215
J. Chem. Theory Comput. 2022, 18, 4218−4228

Highly Efficient and Accurate Computation of Multiple Orbital Spaces Spanning Fock Matrix Elements on Central and Graphics Processing Units for Application in F12 Theory:

Supporting Information

Lars Urban,[†,‡] Henryk Laqua,[†] and Christian Ochsenfeld[*,†,‡]

†*Chair of Theoretical Chemistry, Department of Chemistry, University of Munich (LMU), D-81377 Munich, Germany*

‡*Max Planck Institute for Solid State Research, D-70569 Stuttgart, Germany*

E-mail: christian.ochsenfeld@uni-muenchen.de

1 Non-Covalent Interaction Energy MAEs/ Isomerization Energy MAEs

Table 1: Detailed MAEs of the HF, CABS singles, MP2, F12, and total non-covalent interaction energies for the S22+S66 test set using our sn-LinK, RI-J, and RI-K methods with different grid combinations and RI basis sets. *1RI-J values. *2RI-JK values.

Test Set(s)	Basis Set(s)	Grid	SCF [μH]	CABS [μH]	MP2 [μH]	F12 [μH]	tot. MAE [μH]	tot. MAE [kJ·mol^{-1}]
S22 + S66 (NCI)	cc-pVDZ-F12	gm[2/0]	1.06	4.47	9.09	0.76	9.61	0.0252
		gm[3/1]	0.19	0.65	2.30	0.22	2.56	0.0067
		gm[4/2]	0.08	0.14	0.45	0.04	0.55	0.0014
		gm[5/3]	0.03	0.03	0.14	0.01	0.16	0.0004
		gm[6/4]	0.01	0.01	0.05	0.01	0.05	0.0001
		gm[7/5]	0.00	0.00	0.03	0.00	0.03	0.0001
	+ cc-pVDZ-JKfit*1	-	0.88	0.57	0.75	0.06	1.09	0.0029
	+ cc-pVTZ-JKfit*1	-	0.45	0.36	0.37	0.04	0.74	0.0019
	+ cc-pVDZ-JKfit*2	-	11.42	2.40	2.47	1.30	13.85	0.0364
	+ cc-pVTZ-JKfit*2	-	9.89	0.73	1.82	0.45	12.04	0.0316
	+ cc-pVDZ-JKfit	gm[5/3]	0.89	0.57	0.76	0.06	1.12	0.0029
	+ cc-pVTZ-JKfit	gm[5/3]	0.44	0.36	0.43	0.04	0.79	0.0021
	cc-pVDTZ-F12	gm[2/0]	1.44	3.87	10.87	0.40	12.09	0.0317
		gm[3/1]	0.21	0.34	2.59	0.12	2.66	0.0070
		gm[4/2]	0.08	0.07	0.52	0.02	0.58	0.0015
		gm[5/3]	0.03	0.01	0.16	0.01	0.17	0.0004
		gm[6/4]	0.01	0.00	0.05	0.00	0.06	0.0001
		gm[7/5]	0.00	0.00	0.03	0.00	0.03	0.0001
	+ cc-pVTZ-JKfit*1	-	0.72	0.11	0.45	0.03	0.79	0.0021
	+ cc-pVQZ-JKfit*1	-	0.21	0.04	0.23	0.02	0.37	0.0009
	+ cc-pVTZ-JKfit*2	-	9.97	0.33	2.27	0.34	12.64	0.0332
	+ cc-pVQZ-JKfit*2	-	2.97	0.14	0.50	0.11	3.56	0.0093
	+ cc-pVTZ-JKfit	gm[5/3]	0.73	0.11	0.50	0.03	0.84	0.0022
	+ cc-pVQZ-JKfit	gm[5/3]	0.22	0.05	0.31	0.02	0.44	0.0011
	cc-pVQZ-F12	gm[2/0]	2.63	7.12	11.13	0.17	12.56	0.0330
		gm[3/1]	0.22	0.40	2.72	0.05	2.69	0.0071
		gm[4/2]	0.09	0.07	0.56	0.01	0.57	0.0015
		gm[5/3]	0.03	0.01	0.17	0.00	0.18	0.0004
		gm[6/4]	0.00	0.01	0.06	0.00	0.06	0.0002
		gm[7/5]	0.00	0.00	0.03	0.00	0.03	0.0001
	+ cc-pVQZ-JKfit*1	-	0.23	0.43	0.26	0.02	0.81	0.0021
	+ cc-pV5Z-JKfit*1	-	0.15	0.37	0.14	0.02	0.60	0.0015
	+ cc-pVQZ-JKfit*2	-	2.91	0.14	0.57	0.10	3.56	0.0093
	+ cc-pV5Z-JKfit*2	-	6.66	0.01	0.07	0.07	6.66	0.0175
	+ cc-pVQZ-JKfit	gm[5/3]	0.21	0.29	0.33	0.02	0.68	0.0018
	+ cc-pV5Z-JKfit	gm[5/3]	0.12	0.23	0.24	0.02	0.47	0.0012

Table 2: Detailed MAEs of the HF, CABS singles, MP2, F12, and total non-covalent interaction energies for the L7 test set using our sn-LinK, RI-J, and RI-K methods with different grid combinations. *1RI-J values. *2RI-JK values.

Test Set(s)	Basis Set(s)	Grid	SCF [μH]	CABS [μH]	MP2 [μH]	F12 [μH]	tot. MAE [μH]	tot. MAE [kJ·mol^{-1}]
L7 (NCI)	cc-pVDZ-F12	gm[2/0]	8.47	12.53	88.78	3.36	98.65	0.2590
		gm[3/1]	1.76	2.83	49.87	1.87	47.96	0.1259
		gm[4/2]	0.58	0.23	8.21	0.35	8.75	0.0230
		gm[5/3]	0.15	0.10	1.98	0.05	1.87	0.0049
		gm[6/4]	0.05	0.06	0.70	0.03	0.70	0.0018
		gm[7/5]	0.01	0.01	0.13	0.06	0.20	0.0005
	+ cc-pVDZ-JKfit*1	-	6.37	3.10	5.03	0.39	4.11	0.0108
	+ cc-pVTZ-JKfit*1	-	1.64	0.70	0.88	0.09	2.15	0.0056
	+ cc-pVDZ-JKfit*2	-	129.27	6.61	10.88	4.78	136.03	0.3571
	+ cc-pVTZ-JKfit*2	-	187.68	3.41	8.41	1.73	196.05	0.5147
	+ cc-pVDZ-JKfit	gm[5/3]	6.23	3.11	5.89	0.44	4.08	0.0100
	+ cc-pVTZ-JKfit	gm[5/3]	1.69	0.66	2.27	0.12	3.28	0.0086

Table 3: Detailed MAEs of the HF, CABS singles, MP2, F12, and total isomerization energies for the ISO34 test set using our sn-LinK, RI-J, and RI-K methods with different grid combinations. *1RI-J values. *2RI-JK values.

Test Set(s)	Basis Set(s)	Grid	SCF [μH]	CABS [μH]	MP2 [μH]	F12 [μH]	tot. MAE [μH]	tot. MAE [kJ·mol^{-1}]
ISO34 (Isomerization)	cc-pVDZ-F12	gm[2/0]	52.93	357.44	157.42	13.64	424.36	1.1138
		gm[3/1]	14.45	33.36	31.50	2.45	57.11	0.1499
		gm[4/2]	5.08	8.94	5.58	0.65	12.31	0.0323
		gm[5/3]	1.27	1.59	1.53	0.18	2.91	0.0076
		gm[6/4]	0.23	0.32	0.33	0.04	0.70	0.0018
		gm[7/5]	0.03	0.08	0.11	0.01	0.18	0.0004
	+ cc-pVDZ-JKfit*1	-	38.88	14.78	9.03	0.60	44.82	0.1177
	+ cc-pVTZ-JKfit*1	-	5.08	2.84	1.45	0.16	6.48	0.0170
	+ cc-pVDZ-JKfit*2	-	28.53	21.08	11.03	2.68	45.97	0.1207
	+ cc-pVTZ-JKfit*2	-	8.43	4.56	1.27	0.77	12.98	0.0341
	+ cc-pVDZ-JKfit	gm[5/3]	38.63	14.98	9.65	0.65	45.62	0.1198
	+ cc-pVTZ-JKfit	gm[5/3]	5.47	3.27	2.51	0.28	7.53	0.0198
	cc-pVDTZ-F12	gm[2/0]	71.97	38.24	148.44	8.10	156.11	0.4099
		gm[3/1]	15.61	1.20	32.72	1.39	36.43	0.0956
		gm[4/2]	5.21	0.25	5.57	0.33	7.05	0.0185
		gm[5/3]	1.31	0.09	1.52	0.09	2.11	0.0055
		gm[6/4]	0.24	0.10	0.32	0.03	0.57	0.0015
		gm[7/5]	0.03	0.11	0.11	0.01	0.20	0.0005
	+ cc-pVTZ-JKfit*1	-	7.23	1.03	1.75	0.10	6.82	0.0179
	+ cc-pVQZ-JKfit*1	-	0.69	0.22	0.25	0.02	0.75	0.0020
	+ cc-pVTZ-JKfit*2	-	11.77	1.58	1.90	0.55	13.95	0.0366
	+ cc-pVQZ-JKfit*2	-	1.62	0.26	0.39	0.15	1.91	0.0050
	+ cc-pVTZ-JKfit	gm[5/3]	7.51	1.23	2.71	0.16	7.31	0.0192
	+ cc-pVQZ-JKfit	gm[5/3]	1.76	0.55	1.59	0.10	2.44	0.0064
	cc-pVQZ-F12	gm[2/0]	105.84	207.81	153.53	4.60	277.10	0.7275
		gm[3/1]	15.31	28.48	31.10	0.73	44.38	0.1165
		gm[4/2]	5.15	3.79	5.26	0.16	9.17	0.0241
		gm[5/3]	1.29	0.96	1.46	0.04	2.37	0.0062
		gm[6/4]	0.24	0.53	0.31	0.01	0.80	0.0021
		gm[7/5]	0.00	0.45	0.11	0.00	0.47	0.0012
	+ cc-pVQZ-JKfit*1	-	0.69	0.55	0.27	0.01	0.79	0.0021
	+ cc-pV5Z-JKfit*1	-	0.21	0.25	0.12	0.01	0.31	0.0008
	+ cc-pVQZ-JKfit*2	-	1.58	0.09	0.49	0.17	1.73	0.0046
	+ cc-pV5Z-JKfit*2	-	2.36	0.05	0.32	0.08	2.47	0.0065
	+ cc-pVQZ-JKfit	gm[5/3]	1.80	1.04	1.53	0.05	2.78	0.0072
	+ cc-pV5Z-JKfit	gm[5/3]	1.45	0.93	1.48	0.05	2.41	0.0063

2 Absolute Energy MAEs

Table 4: Detailed MAEs of the HF, CABS singles, MP2, F12, and total absolute energies for the S22+S66 test set using our sn-LinK, RI-J, and RI-K methods with different grid combinations and RI basis sets. *1RI-J values. *2RI-JK values.

Test Set(s)	Basis Set(s)	Grid	SCF [μH]	CABS [μH]	MP2 [μH]	F12 [μH]	tot. MAE [μH]	tot. MAE [kJ·mol^{-1}]
S22 + S66 (Absolute)	cc-pVDZ-F12	gm[2/0]	89.51	735.12	147.07	17.83	735.35	1.9307
		gm[3/1]	10.17	22.05	22.08	3.06	39.86	0.1047
		gm[4/2]	3.15	6.37	5.81	0.53	11.04	0.0290
		gm[5/3]	1.01	1.08	0.74	0.14	1.83	0.0048
		gm[6/4]	0.12	0.25	0.26	0.04	0.44	0.0011
		gm[7/5]	0.03	0.09	0.07	0.02	0.13	0.0004
	+ cc-pVDZ-JKfit*1	-	218.57	62.03	34.70	2.24	247.67	0.6503
	+ cc-pVTZ-JKfit*1	-	108.12	29.57	15.42	0.73	122.56	0.3218
	+ cc-pVDZ-JKfit*2	-	561.69	364.40	188.87	398.08	1511.93	3.9696
	+ cc-pVTZ-JKfit*2	-	138.20	72.02	88.84	177.73	476.20	1.2503
	+ cc-pVDZ-JKfit	gm[5/3]	218.71	61.79	34.96	2.24	247.29	0.6493
	+ cc-pVTZ-JKfit	gm[5/3]	108.26	29.37	15.67	0.73	122.18	0.3208
	cc-pVDTZ-F12	gm[2/0]	210.78	1327.61	147.08	8.91	1185.88	3.1135
		gm[3/1]	11.42	28.67	22.90	1.54	34.21	0.0898
		gm[4/2]	3.29	2.76	5.88	0.27	6.13	0.0161
		gm[5/3]	1.06	0.51	0.79	0.07	1.53	0.0040
		gm[6/4]	0.12	0.10	0.26	0.02	0.27	0.0007
		gm[7/5]	0.03	0.03	0.08	0.01	0.09	0.0002
	+ cc-pVTZ-JKfit*1	-	156.26	3.44	23.75	0.78	136.60	0.3586
	+ cc-pVQZ-JKfit*1	-	32.44	4.03	1.12	0.06	27.75	0.0729
	+ cc-pVTZ-JKfit*2	-	174.18	33.96	245.93	110.17	563.92	1.4806
	+ cc-pVQZ-JKfit*2	-	26.04	8.55	28.36	32.25	95.20	0.2499
	+ cc-pVTZ-JKfit	gm[5/3]	156.34	3.61	24.02	0.78	136.56	0.3585
	+ cc-pVQZ-JKfit	gm[5/3]	32.52	3.88	1.54	0.10	27.72	0.0728
	cc-pVQZ-F12	gm[2/0]	523.49	2631.00	141.18	5.16	2157.07	5.6634
		gm[3/1]	14.93	59.18	22.55	0.78	52.78	0.1386
		gm[4/2]	3.25	3.58	5.67	0.14	5.82	0.0153
		gm[5/3]	1.07	0.58	0.80	0.04	1.59	0.0042
		gm[6/4]	0.13	0.23	0.26	0.01	0.32	0.0008
		gm[7/5]	0.00	0.07	0.08	0.00	0.11	0.0003
	+ cc-pVQZ-JKfit*1	-	29.94	2.88	1.51	0.06	31.70	0.0832
	+ cc-pV5Z-JKfit*1	-	21.23	1.79	0.63	0.03	23.53	0.0618
	+ cc-pVQZ-JKfit*2	-	32.95	1.22	49.60	16.88	100.66	0.2643
	+ cc-pV5Z-JKfit*2	-	11.71	0.97	13.14	8.96	33.47	0.0879
	+ cc-pVQZ-JKfit	gm[5/3]	30.04	1.73	1.88	0.06	30.29	0.0795
	+ cc-pV5Z-JKfit	gm[5/3]	21.33	0.82	1.07	0.05	22.13	0.0581

Table 5: Detailed MAEs of the HF, CABS singles, MP2, F12, and total absolute energies for the L7 test set using our sn-LinK, RI-J, and RI-K methods with different grid combinations. *1RI-J values. *2RI-JK values.

Test Set(s)	Basis Set(s)	Grid	SCF [μH]	CABS [μH]	MP2 [μH]	F12 [μH]	tot. MAE [μH]	tot. MAE [kJ·mol^{-1}]
L7 (Absolute)	cc-pVDZ-F12	gm[2/0]	706.17	4519.68	1440.70	187.91	5558.74	14.5945
		gm[3/1]	99.35	94.74	137.98	40.27	297.76	0.7818
		gm[4/2]	32.90	52.02	66.39	5.81	126.71	0.3327
		gm[5/3]	6.53	11.55	10.07	1.91	18.13	0.0476
		gm[6/4]	1.55	2.10	2.65	0.48	5.29	0.0139
		gm[7/5]	0.30	0.82	0.85	0.13	1.83	0.0048
	+ cc-pVDZ-JKfit*1	-	962.58	315.08	183.61	7.80	1101.85	2.8929
	+ cc-pVTZ-JKfit*1	-	539.44	146.05	90.33	3.19	598.34	1.5710
	+ cc-pVDZ-JKfit*2	-	3414.55	2193.01	1076.44	1901.82	8585.82	22.5421
	+ cc-pVTZ-JKfit*2	-	1070.82	434.30	491.17	842.63	2838.92	7.4536
	+ cc-pVDZ-JKfit	gm[5/3]	968.18	322.63	178.57	7.99	1119.24	2.9386
	+ cc-pVTZ-JKfit	gm[5/3]	545.03	153.59	85.29	3.35	615.72	1.6166

Table 6: Detailed MAEs of the HF, CABS singles, MP2, F12, and total absolute energies for the ISO34 test set using our sn-LinK, RI-J, and RI-K methods with different grid combinations. *1RI-J values. *2RI-JK values.

Test Set(s)	Basis Set(s)	Grid	SCF [μH]	CABS [μH]	MP2 [μH]	F12 [μH]	tot. MAE [μH]	tot. MAE [kJ·mol^{-1}]
ISO34 (Absolute)	cc-pVDZ-F12	gm[2/0]	68.75	483.70	146.12	13.75	481.03	1.2629
		gm[3/1]	9.48	25.01	21.57	2.36	39.66	0.1041
		gm[4/2]	2.90	6.83	4.63	0.43	10.45	0.0274
		gm[5/3]	0.73	0.98	0.87	0.11	1.69	0.0044
		gm[6/4]	0.12	0.22	0.22	0.03	0.44	0.0012
		gm[7/5]	0.02	0.06	0.07	0.01	0.11	0.0003
	+ cc-pVDZ-JKfit*1	-	175.58	55.91	30.90	2.26	202.85	0.5326
	+ cc-pVTZ-JKfit*1	-	66.61	21.87	10.24	0.68	78.92	0.2072
	+ cc-pVDZ-JKfit*2	-	226.04	147.22	115.97	199.94	689.17	1.8094
	+ cc-pVTZ-JKfit*2	-	61.81	27.01	49.09	88.92	226.76	0.5954
	+ cc-pVDZ-JKfit	gm[5/3]	175.81	56.09	30.74	2.21	203.37	0.5339
	+ cc-pVTZ-JKfit	gm[5/3]	66.84	22.06	10.13	0.65	79.44	0.2086
	cc-pVDTZ-F12	gm[2/0]	139.56	717.20	141.14	8.02	653.14	1.7148
		gm[3/1]	9.73	20.49	23.14	1.29	28.36	0.0745
		gm[4/2]	2.90	2.50	4.61	0.22	6.22	0.0163
		gm[5/3]	0.73	0.40	0.85	0.06	1.27	0.0033
		gm[6/4]	0.13	0.11	0.22	0.02	0.34	0.0009
		gm[7/5]	0.02	0.02	0.07	0.00	0.07	0.0002
	+ cc-pVTZ-JKfit*1	-	98.99	3.18	15.10	0.58	87.58	0.2299
	+ cc-pVQZ-JKfit*1	-	19.56	2.18	0.64	0.04	16.91	0.0444
	+ cc-pVTZ-JKfit*2	-	69.17	15.86	129.67	55.81	270.52	0.7102
	+ cc-pVQZ-JKfit*2	-	12.14	4.63	14.85	16.27	47.89	0.1257
	+ cc-pVTZ-JKfit	gm[5/3]	99.15	3.33	14.95	0.56	88.01	0.2311
	+ cc-pVQZ-JKfit	gm[5/3]	19.72	2.04	1.07	0.07	17.33	0.0455
	cc-pVQZ-F12	gm[2/0]	325.47	1386.96	140.29	4.87	1128.47	2.9628
		gm[3/1]	10.47	37.83	22.00	0.67	34.73	0.0912
		gm[4/2]	2.86	2.50	4.33	0.11	6.39	0.0168
		gm[5/3]	0.73	0.42	0.82	0.03	1.37	0.0036
		gm[6/4]	0.13	0.11	0.21	0.01	0.36	0.0010
		gm[7/5]	0.00	0.04	0.06	0.00	0.08	0.0002
	+ cc-pVQZ-JKfit*1	-	18.06	1.47	0.89	0.04	18.71	0.0491
	+ cc-pV5Z-JKfit*1	-	13.18	1.04	0.22	0.01	14.33	0.0376
	+ cc-pVQZ-JKfit*2	-	16.10	0.56	25.61	8.88	51.16	0.1343
	+ cc-pV5Z-JKfit*2	-	5.43	0.47	6.73	4.73	17.28	0.0454
	+ cc-pVQZ-JKfit	gm[5/3]	18.24	0.87	1.20	0.05	18.32	0.0481
	+ cc-pV5Z-JKfit	gm[5/3]	13.36	0.51	0.89	0.03	13.94	0.0366

3 RI-J/sn-LinK Speedups

Table 7: RI-J/sn-LinK (cc-pVYZ-JKfit/gm[X+2/X]; Y = D, T Q) speedups on CPUs (S_{CPU}) and GPUs (S_{GPU}) for the full F12-type Fock build for each member of the L7 test (cc-pVXZ-F12; X = D, T, Q).*[1] Reference extrapolated from double- and triple-zeta F12 timings.

				gm[2/0]		gm[3/1]		gm[4/2]		gm[5/3]		gm[6/4]		gm[7/5]	
Basis Set	L7 Structure	N_{bas}	N_{CABS}	S_{CPU}	S_{GPU}	S_{CPU}	S_{GPU}	S_{CPU}	S_{GPU}	S_{CPU}	S_{GPU}	S_{CPU}	S_{GPU}	S_{CPU}	S_{GPU}
	L1	1836	5288	209	528	153	442	89	339	52	246	34	184	25	148
	L2	1191	3426	251	469	196	454	123	357	72	284	48	226	35	182
	L3	2255	6486	517	1340	367	1071	214	877	123	627	82	458	60	358
cc-pVDZ-F12	L4	2588	7444	584	1635	419	1311	240	1060	138	715	91	535	67	422
+ cc-pVDZ-JKfit	L5	1818	5232	316	742	232	723	134	530	79	382	52	294	38	233
	L6	1752	5044	446	1072	327	1037	190	778	109	561	72	409	53	323
	L7	1396	4016	311	682	228	630	137	495	82	371	53	281	39	224
	L1	3676	7804	693	1627	496	1353	289	963	169	623	111	475	82	363
	L2	2331	4311	733	1550	554	1295	351	955	208	668	138	502	102	382
	L3	4405	8044	1423	3403	1007	2718	589	2050	342	1345	223	949	154	706
cc-pVTZ-F12	L4	5058	9267	1575	4155	1137	3318	645	2276	346	1551	212	1058	172	795
+ cc-pVTZ-JKfit	L5	3588	6999	976	2017	695	1845	410	1334	240	928	157	646	116	507
	L6	3432	6384	1308	2884	971	2715	554	1811	322	1192	211	864	154	650
	L7	2736	5106	939	1880	686	1688	412	1237	239	847	156	637	117	491
	L1	6996	9700	1551	-	1113	-	637	-	325	-	229	-	163	-
	L2	4281	5229	1488	-	1140	-	668	-	358	-	247	-	185	-
	L3	8065	9733	2761	-	1978	-	1045	-	613	-	413	-	297	-
cc-pVQZ-F12*[1]	L4	9268	11220	2710	-	2053	-	1230	-	704	-	449	-	333	-
+ cc-pVQZ-JKfit	L5	6678	8574	2024	-	1497	-	787	-	453	-	300	-	221	-
	L6	6312	7752	2548	-	1897	-	986	-	578	-	374	-	268	-
	L7	5036	6204	1918	-	1404	-	731	-	442	-	288	-	207	-

4 RI-K

Following the approach of Weigend in Ref 1 (reference 12 in article), the 4-center-2-electron repulsion integral tensor is approximated as

$$(\mu\nu|\lambda\sigma) \approx \sum_{PQ} (\mu\nu|P)(P|Q)^{-1}(Q|\lambda\sigma), \tag{1}$$

where $(P|Q)^{-1}$ denotes the matrix inverse of the auxiliary basis 2-center-2-electron repulsion integrals $(P|Q)$, and which becomes exact in the limit of complete auxiliary basis sets. Inserting Eq. 1 into the atomic orbital expression for the exchange matrix

$$K_{\mu\nu} = \sum_{\lambda\sigma} (\mu\sigma|\lambda\nu) P_{\lambda\sigma}, \tag{2}$$

decomposing

$$(P|Q)^{-1} = \sum_{R} (P|R)^{-\frac{1}{2}} (R|Q)^{-\frac{1}{2}}, \tag{3}$$

and the density matrix

$$P_{\lambda\sigma} = \sum_{i} C_{\lambda i} C_{\sigma i}, \tag{4}$$

where $C_{\lambda i}$ denotes occupied MO coefficients (or, equivalently, Cholesky factors of $\mathbf{P}$), leads to the RI-K expression (cf. Eq. 4 of ref. 1)

$$K_{\mu\nu} = \sum_{\lambda\sigma i PQR} (\mu\sigma|P)(P|R)^{-\frac{1}{2}} (R|Q)^{-\frac{1}{2}} (Q|\lambda\nu) C_{\lambda i} C_{\sigma i}\,. \tag{5}$$

There are multiple viable approaches to evaluate Eq. 5: In the original implementation of Weigend, only $(P|Q)^{-\frac{1}{2}}$ is initially precomputed and the exchange matrix is then formed in each self-consistent field (SCF) iteration as:

$$(i\mu|P) = \sum_{\nu} C_{\nu i}(\nu\mu|P) \tag{6}$$

$$B^Q_{i\mu} = \sum_{P} (i\mu|P)(P|Q)^{-\frac{1}{2}} \tag{7}$$

$$K_{\mu\nu} = \sum_{iQ} B^Q_{i\mu} B^Q_{i\nu}\,. \tag{8}$$

In an alternative approach, the untransformed 3-center-1-electron integrals $(\mu\nu|P)$ are transformed with $(P|Q)^{-\frac{1}{2}}$ in an additional precomputation step

$$B^Q_{\nu\mu} = \sum_{P} (\nu\mu|P)(P|Q)^{-\frac{1}{2}} \tag{9}$$

and the exchange matrix is then obtained in each SCF iteration as

$$B^Q_{i\mu} = \sum_{\nu} C_{\nu i} B^Q_{\nu\mu} \tag{10}$$

$$K_{\mu\nu} = \sum_{iQ} B^Q_{i\mu} B^Q_{i\nu} \qquad \text{(same as Eq. 8).} \tag{11}$$

This approach avoids the second transformation step (Eq. 7) within each SCF cycle at the cost of an additional preparatory step and a higher memory demand (storage of $B^Q_{\nu\mu}$).
In practice, the second approach is highly beneficial for iterative procedures like the SCF method, where the cost of the preparation is overall less significant. For F12-type-Fock builds, however, only a single K-build needs to be performed, so the cost of the precomputation in Eq. 9 outweighs the savings from avoiding the evaluation of Eq. 7. Therefore, we decided to use the precomputation RI-K method (second approach) for the SCF calculation and the integral-direct variant (first approach) for the F12-type Fock build.

References

(1) Weigend, F. A fully direct RI-HF algorithm: Implementation, optimised auxiliary basis sets, demonstration of accuracy and efficiency. *Phys. Chem. Chem. Phys.* **2002**, *4*, 4285–4291.

4.3 Publication III

Efficient Exploitation of Numerical Quadrature with Distance-Dependent Integral Screening in Explicitly Correlated F12 Theory: Linear Scaling Evaluation of the Most Expensive RI-MP2-F12 Term

L. Urban, H. Laqua, T. H. Thompson, and C. Ochsenfeld,
J. Chem. Theory Comput. **2024**, *20*, 3706

Abstract:

We present a linear scaling atomic orbital based algorithm for the computation of the most expensive exchange-type RI-MP2-F12 term by employing numerical quadrature in combination with CABS-RI to avoid six-center-three-electron integrals. Furthermore, a robust distance-dependent integral screening scheme, based on integral partition bounds [Thompson, T. H.; Ochsenfeld, C. *J. Chem. Phys.* **2019**, *150*, 044101], is used to drastically reduce the number of the required three-center-one-electron integrals substantially. The accuracy of our numerical quadrature/CABS-RI approach and the corresponding integral screening is thoroughly assessed for interaction and isomerization energies across a variety of numerical integration grids. Our method outperforms the standard density fitting/CABS-RI approach with errors below 1 μEh even for small grid sizes and moderate screening thresholds. The choice of the grid size and screening threshold allows us to tailor our ansatz to a desired accuracy and computational efficiency. We showcase the approach's effectiveness for the chemically relevant system valinomycin, employing a triple-ζ F12 basis set combination ($C_{54}H_{90}N_6O_{18}$, 5757 AO basis functions, 10,266 CABS basis functions, 735,783 grid points). In this context, our ansatz achieves higher accuracy combined with a 135$\times$ speedup compared to the classical density fitting based variant, requiring notably less computation time than the corresponding RI-MP2 calculation. Additionally, we demonstrate near-linear scaling through calculations on linear alkanes. We achieved an 817-fold acceleration for $C_{80}H_{162}$ and an extrapolated 28,765-fold acceleration for $C_{200}H_{402}$, resulting in a substantially reduced computational time for the latter – from 229 days to just 11.5 min. Our ansatz may also be adapted to the remaining MP2-F12 terms, which will be the subject of future work.

JCTC Journal of Chemical Theory and Computation

pubs.acs.org/JCTC Article

Efficient Exploitation of Numerical Quadrature with Distance-Dependent Integral Screening in Explicitly Correlated F12 Theory: Linear Scaling Evaluation of the Most Expensive RI-MP2-F12 Term

Lars Urban, Henryk Laqua, Travis H. Thompson, and Christian Ochsenfeld*

Cite This: J. Chem. Theory Comput. 2024, 20, 3706−3718

ABSTRACT: We present a linear scaling atomic orbital based algorithm for the computation of the most expensive exchange-type RI-MP2-F12 term by employing numerical quadrature in combination with CABS-RI to avoid six-center-three-electron integrals. Furthermore, a robust distance-dependent integral screening scheme, based on integral partition bounds [Thompson, T. H.; Ochsenfeld, C. *J. Chem. Phys.* **2019**, *150*, 044101], is used to drastically reduce the number of the required three-center-one-electron integrals substantially. The accuracy of our numerical quadrature/CABS-RI approach and the corresponding integral screening is thoroughly assessed for interaction and isomerization energies across a variety of numerical integration grids. Our method outperforms the standard density fitting/CABS-RI approach with errors below 1 μE_h even for small grid sizes and moderate screening thresholds. The choice of the grid size and screening threshold allows us to tailor our ansatz to a desired accuracy and computational efficiency. We showcase the approach's effectiveness for the chemically relevant system valinomycin, employing a triple-ζ F12 basis set combination ($C_{54}H_{90}N_6O_{18}$, 5757 AO basis functions, 10,266 CABS basis functions, 735,783 grid points). In this context, our ansatz achieves higher accuracy combined with a 135× speedup compared to the classical density fitting based variant, requiring notably less computation time than the corresponding RI-MP2 calculation. Additionally, we demonstrate near-linear scaling through calculations on linear alkanes. We achieved an 817-fold acceleration for $C_{80}H_{162}$ and an extrapolated 28,765-fold acceleration for $C_{200}H_{402}$, resulting in a substantially reduced computational time for the latter—from 229 days to just 11.5 min. Our ansatz may also be adapted to the remaining MP2-F12 terms, which will be the subject of future work.

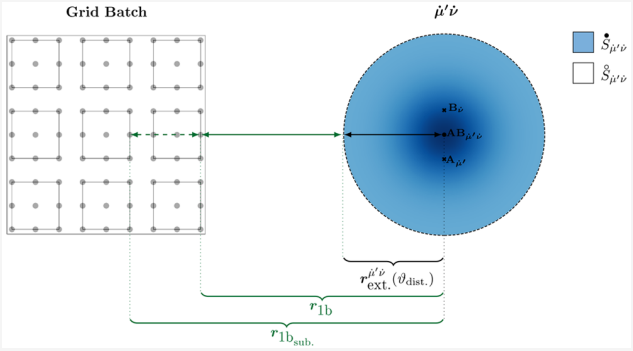

1. INTRODUCTION

The concept of explicitly including the interelectronic distance r_{12} in the electronic wave function description is almost as old as quantum mechanics. It was first proposed for practical calculations in 1929 by Hylleraas in his pioneering study of the helium atom.[1] By incorporating six very compact polynomial terms of r_{12}, he achieved a remarkably accurate ground-state energy, deviating from experimental values by only 0.01 eV. Thus, he explicitly described the electronic cusp, although its theoretical foundation was not established until decades later, as revealed by Kato's study[2] on wave function properties. While extremely potent for dielectronic systems, a direct extension to many electron systems results in high-dimensional integrals that become infeasible to compute. Motivated by the inherent advantages of such an approach, including the precise description of dynamic correlation and the consequential ability to employ a significantly reduced one-electron basis set size for accurate calculations, various strategies have been proposed to mitigate the complexity of the ansatz while retaining its benefits: examples are variational Hylleraas-configuration interaction (Hylleraas-CI),[3−6] usage of explicitly correlated Gaussian (ECG) wave functions,[7−12] or trans-correlated (TC) approaches.[13−18] These methods are generally linked with significant computational costs, limiting their applicability to small system sizes. Nevertheless, the growing interest in the advancement of TC methods has recently resulted in several promising approaches that enable highly accurate calculations.[19−33]

The most successful and practical approaches, even for larger system sizes, are F12 methods, which are widely used corrections in electronic structure theory.[34−40] These methods are based on the groundbreaking work of Kutzelnigg and Klopper, who introduced the so-called R12 corrections.[41−43]

Received: February 15, 2024
Revised: March 23, 2024
Accepted: March 25, 2024
Published: April 16, 2024

https://doi.org/10.1021/acs.jctc.4c00193
J. Chem. Theory Comput. 2024, 20, 3706−3718

Both ansätze incorporate nonvariational, explicitly coupled two-electron terms (geminals) into the wave function description, thereby directly addressing the basis set incompleteness error (BSIE)[44] and enhancing the convergence concerning the size of the one-electron basis. However, the original R12 approach encountered initial difficulties due to the choice of r_{12} as the correlation factor, which exhibits an unfavorable asymptotic behavior at large electron−electron distances. F12 approaches, as introduced by Ten-no,[34] overcome this limitation by accurately reproducing the electron−electron cusp behavior for all interelectronic distances using a flexible r_{12}-dependent factor, making use of so-called Slater-type geminals (STG). The occurring highly dimensional integrals, such as six-center-three-electron (6c3e) and eight-center-four-electron (4e8c) integrals, are typically decomposed using the Resolution-of-the-Identity (RI) technique into manageable sums of four-center-two-electron (4c2e) integrals. In this process, Valeev's complementary auxiliary basis set (CABS)[45] method leads to an advantageous partitioning of orbital spaces. Usually, density fitting (DF) techniques further improve performance by decomposing 4c2e integrals into three-center-two-electron (3c2e) and two-center-two-electron (2c2e) integrals, thus drastically reducing the prefactor of the evaluation. Nowadays, DF/CABS-RI F12 approaches are well-established and feature a wide range of methods and variations, i.e., in perturbation theory,[36,37,46−52] coupled-cluster theory,[38,53−61] the random-phase-approximation (RPA),[62−64] multireference approaches,[65−72] and even in density functional theory (DFT) design.[73,74]

In addition to the standard DF/CABS-RI routes of handling multielectron integrals, a relatively less common, yet highly effective alternative for evaluating 6c3e and 8c4e integrals was introduced by Ten-no.[35,75] He adapted the concept of numerical quadrature (NQ) from Friesner's pseudospectral method[76−79] and applied it to F12 theory, aiming to improve the accuracy of multielectron integral evaluation and, consequently, correlation energies.

However, the lower formal scaling of the NQ variant, in combination with effective screening techniques, has not been exploited in practice to date. Given recent advancements in highly efficient seminumerical integral evaluation,[80−90] particularly in Hartree−Fock (HF) theory and DFT with accurate molecular grids,[91−93] and screening techniques,[94] along with the possibility of combination with the locality of F12 operators, there is immense potential for improved computational efficiency, especially for exchange-type multielectron integrals. In this study, we revisit the generally applicable concept of NQ and demonstrate its capabilities using the example of the most computationally demanding RI-MP2-F12 exchange term. We employ state-of-the-art integral evaluation and screening techniques to formulate a linear scaling atomic orbital (AO) method, which demonstrates superior accuracy and efficiency compared to the current standard in the field—the DF molecular orbital (MO) approach.[95]

2. THEORY

Since second-order Møller−Plesset perturbation (MP2) theory can be expressed as the sum of electron pair energies $E_{\mathrm{MP2}} = \sum_{ij} e_{ij}^{\mathrm{MP2}}$, the energy contribution for each electron pair e_{ij} can be obtained by minimizing the second-order Hylleraas pair functional

$$J_{ij}^{2}[u_{ij}] = \langle u_{ij}|\hat{f}_1 + \hat{f}_2 - \epsilon_i - \epsilon_j|u_{ij}\rangle + 2\langle u_{ij}|\hat{g}_{12}||ij\rangle \tag{1}$$

Here, $\hat{f}_1$ and $\hat{f}_2$ are Fock operators, ϵ_i and ϵ_j are orbital energies, $\hat{g}_{12}$ is the classical Coulomb operator, and $||ij\rangle$ represents the antisymmetrized two-electron state $||ij\rangle = \frac{1}{\sqrt{2}}(|ij\rangle - |ji\rangle)$. In general, u_{ij} describes an arbitrary two-electron state, which can be variationally minimized toward the exact energy e_{ij}^{exact}. In explicitly correlated MP2-F12 theory, u_{ij} is defined as

$$|u_{ij}^{\mathrm{MP2\text{-}F12}}\rangle = |u_{ij}^{\mathrm{MP2}}\rangle + |u_{ij}^{\mathrm{F12}}\rangle \tag{2}$$

$$= \sum_{a<b} t_{ij}^{ab}||ab\rangle + \sum_{x<y} c_{ij}^{xy}\hat{Q}_{12}\hat{F}_{12}||(\hat{S}_{xy}xy)\rangle \tag{3}$$

with two separate linear ansätze $|u_{ij}^{\mathrm{MP2}}\rangle$ and $|u_{ij}^{\mathrm{F12}}\rangle$. Inserting only $|u_{ij}^{\mathrm{MP2}}\rangle$ in eq 1 and minimizing the corresponding amplitudes t_{ij}^{ab} results in the standard MP2 energy. Explicit correlation is achieved through $|u_{ij}^{\mathrm{F12}}\rangle$, which directly introduces the electron−electron cusp behavior in the wave function description via the interelectronic distance-dependent correlation factor $\hat{F}_{12}$. In this context, Ten-no established the so-called rational generator[35]

$$\hat{S}_{xy} = \frac{3}{8} + \frac{1}{8}\hat{L}_{xy} \tag{4}$$

$$\hat{L}_{xy}\phi_x(\boldsymbol{r}_1, \sigma_1)\phi_y(\boldsymbol{r}_2, \sigma_2) = \phi_x(\boldsymbol{r}_2, \sigma_1)\phi_y(\boldsymbol{r}_1, \sigma_2) \tag{5}$$

where $\phi_x(\boldsymbol{r}_1, \sigma_1)$ and $\phi_y(\boldsymbol{r}_2, \sigma_2)$ denote spin orbitals, each associated with corresponding space and spin coordinates $\boldsymbol{r}$ and σ. By design, this approach simultaneously fulfills the s- and p-wave coalescence conditions for both restricted and unrestricted first-order wave functions.[37] The strong orthogonality operator $\hat{Q}_{12}$ defined as

$$\hat{Q}_{12} = (1 - \hat{o}_1)(1 - \hat{o}_2)(1 - \hat{v}_1\hat{v}_2) \tag{6}$$

with $\hat{o}$ and $\hat{v}$ as projectors onto the occupied and virtual space, respectively, ensures orthogonality concerning the double excitations within $|u_{ij}^{\mathrm{MP2}}\rangle$. Here, c_{ij}^{xy} represents additional amplitudes between the occupied Hartree−Fock (HF) and the geminal-generating space. Commonly, these geminal amplitudes are not optimized; instead, they are set using a fixed amplitude approach

$$c_{ij}^{xy} = \delta_x^i\delta_y^j \tag{7}$$

which restricts the explicitly correlated geminal space to HF-occupied orbitals. This ansatz satisfies the cusp condition and leads to the widely used diagonal orbital-invariant version of MP2-F12, whose closed-shell spatial orbital formalism we are following.[37] All these concepts result in a series of intermediates present in the literature,[36,37] with the most complex and computationally demanding exchange-type intermediate

$$\mathcal{B}_{ji}^{ij} = \langle ij|\hat{F}_{12}\hat{Q}_{12}(\hat{f}_1 + \hat{f}_2)\hat{Q}_{12}\hat{F}_{12}|ji\rangle \tag{8}$$

where we can use the symmetry of $\hat{F}_{12}$ and $\hat{Q}_{12}$ for the treatment of $\hat{f}_1$ and $\hat{f}_2$ in the relation

$$\langle ij|\hat{F}_{12}\hat{Q}_{12}\hat{f}_1\hat{Q}_{12}\hat{F}_{12}|ji\rangle = \langle ji|\hat{F}_{12}\hat{Q}_{12}\hat{f}_2\hat{Q}_{12}\hat{F}_{12}|ij\rangle \tag{9}$$

https://doi.org/10.1021/acs.jctc.4c00193
J. Chem. Theory Comput. 2024, 20, 3706−3718

Following this notation, $\mathcal{B}_{ji}^{ij}$ can be exactly described as

$$\mathcal{B}_{ji}^{ij} = \mathcal{A}_{ji}^{ij} + \mathcal{A}_{ij}^{ji} - \mathcal{Z}_{ji}^{ij} - \mathcal{Z}_{ij}^{ji} - \mathcal{F}_{ab}^{ij}C_{ji}^{ab} - \mathcal{F}_{ab}^{ji}C_{ij}^{ab} \quad (10)$$

with subintermediates

$$\mathcal{A}_{ji}^{ij} = \langle ij|\hat{F}_{12}\,\hat{f}_1\,\hat{Q}_{12}\hat{F}_{12}|ji\rangle \quad (11)$$

$$\mathcal{Z}_{ji}^{ij} = \langle ij|\hat{F}_{12}\hat{v}_1\hat{f}_1\,\hat{Q}_{12}\hat{F}_{12}|ji\rangle \quad (12)$$

$$C_{ji}^{ab} = \langle ab|\hat{f}_1\,(1-\hat{v}_1)\hat{Q}_{12}\hat{F}_{12}|ji\rangle \quad (13)$$

$$\mathcal{F}_{ab}^{ij} = \langle ij|\hat{F}_{12}|ab\rangle \quad (14)$$

Further defining $\hat{P}_{12} = 1 - \hat{Q}_{12}$ allows us to additionally decompose $\mathcal{A}_{ji}^{ij}$ as

$$\mathcal{A}_{ji}^{ij} = \mathcal{M}_{ji}^{ij} - \mathcal{N}_{ji}^{ij} \quad (15)$$

with

$$\mathcal{M}_{ji}^{ij} = \langle ij|\hat{F}_{12}\,\hat{f}_1\,\hat{F}_{12}|ji\rangle \quad (16)$$

$$\mathcal{N}_{ji}^{ij} = \langle ij|\hat{F}_{12}\,\hat{f}_1\,\hat{P}_{12}\hat{F}_{12}|ji\rangle \quad (17)$$

The approximation-free evaluation of most of these subintermediates results in steep scaling expensive three- and four-electron integrals,[43] which led to a series of approaches and simplifications primarily utilizing CABS-RI[45] and robust density-fitting (DF) techniques[96−98] (orbital spaces and indexing conventions are summarized in Table 1) to reduce the computational cost. However, particularly in the context of (RI-)MP2-F12 theory, the effort to compute the explicitly correlated correction remains significant, easily exceeding the cost of the corresponding MP2 calculation several times. The exchange-type $\mathcal{M}_{ji}^{ij}$ subintermediate (eq 16) remains as the most demanding CABS-RI term. Through the definition of the closed-shell Fock-operator

$$\hat{f} = \hat{t} + \hat{v} + 2\hat{j} - \hat{k} \quad (18)$$

an exact evaluation leads to nonstandard Fock matrix elements, resulting in the separate computation of the kinetic energy, nuclear attraction, mean-field Coulomb, and mean-field exchange contributions. Here, the evaluation of the exchange contribution

$$\mathcal{K}_{ji}^{ij} = \langle ij|\hat{F}_{12}\hat{k}_1\hat{F}_{12}|ji\rangle \quad (19)$$

dominates the explicitly correlated computation, requiring a triple CABS-RI insertion (entire HF + CABS space) as the only exchange term in RI-MP2-F12 theory. In the following, we briefly review the literature approach to avoid nonstandard Fock matrix elements using the well-known DF/CABS-RI ansatz (Section 2.1) and present a superior highly efficient low-scaling alternative that utilizes numerical quadrature (Section 2.2−2.4). This ansatz is transferable to other (sub)-intermediates in F12 theory, which will be in the scope of future work.

Table 1. Summary of Orbital Spaces and Indexing Conventions

orbital space	indices
AO Hartree−Fock space	$\mu, \nu, \lambda, \sigma$
AO complementary auxiliary space	$\mu'', \nu'', \lambda'', \sigma''$
combined AO HF/CABS space ($\{\mu\} \cup \{\mu''\}$)	$\mu', \nu', \lambda', \sigma'$
MO geminal-generating space	x, y, w, z
MO occupied space	i, j, k, l
MO virtual space	a, b, c, d
MO occupied + virtual space ($\{i\} \cup \{a\}$)	p, q, r, s
MO complementary auxiliary space	p'', q'', r'', s''
combined MO HF/CABS space ($\{p\} \cup \{p''\}$)	p', q', r', s'
density-fitting space	P, Q, R, S

2.1. CABS-RI and Commutator-Approach. One commonly used ansatz to avoid nonstandard Fock-Matrix elements is the Resolution-of-the-Identity (RI)[45,99] approach

$$\hat{\alpha}_n\, g(..., \boldsymbol{r}_n, ...) = \sum_{\alpha} \alpha(\boldsymbol{r}_n)\left(\int \alpha(\boldsymbol{r}_n) g(..., \boldsymbol{r}_n, ...)\mathrm{d}\boldsymbol{r}_n\right) \quad (20)$$

with $\hat{\alpha}_n$ as the formally exact projector onto the complete orthonormal basis set, approximated in practice via $\hat{\alpha}_n \approx \hat{p}_n'$, the projector onto the combined molecular orbital HF and CABS space. A direct factorization of eq 16 requires a triple-RI insertion, which converges too slowly with the size of the RI basis set to be useful. Thus, one typically leverages the commuting behavior of the nuclear attraction $\hat{v}$ and mean-field Coulomb operator $\hat{j}$ with $\hat{F}_{12}$, allowing the formulation of the commutator relation[36,37]

$$\hat{F}_{12}\,\hat{f}_1\,\hat{F}_{12} = \frac{1}{2}[[\hat{F}_{12}, \hat{t}_1], \hat{F}_{12}] - \hat{F}_{12}\hat{k}_1\hat{F}_{12} + \frac{1}{2}((\hat{f}_1 + \hat{k}_1)\hat{F}_{12}^2 + \hat{F}_{12}^2(\hat{f}_1 + \hat{k}_1)) \quad (21)$$

where a triple-RI insertion is only required for the integrals arising from $\hat{F}_{12}\hat{k}_1\hat{F}_{12}$. The remaining integrals require at most a single RI insertion, leaving

$$\langle ij|\hat{F}_{12}\hat{\alpha}_1\hat{k}_1\hat{\alpha}_1\hat{\alpha}_2\hat{F}_{12}|ji\rangle \overset{\mathrm{RI}}{\approx} \mathcal{F}_{p'r'}^{ij}k_{q'}^{p'}\mathcal{F}_{ji}^{q'r'} \quad (22)$$

$$\overset{\mathrm{DF}}{\approx} \mathcal{F}_{P}^{ip'}\tilde{\mathcal{F}}_{Q}^{P}\mathcal{F}_{jr'}^{Q}k_{q'}^{p'}\mathcal{F}_{R}^{q'j}\tilde{\mathcal{F}}_{S}^{R}\mathcal{F}_{r'i}^{S} \quad (23)$$

as the most expensive expression, which can be evaluated via density fitting:

$$\mathcal{F}_{p'r'}^{ij} \approx \mathcal{F}_{P}^{ip'}\tilde{\mathcal{F}}_{Q}^{P}\mathcal{F}_{jr'}^{Q} \quad (24)$$

$$\mathcal{F}_{P}^{ip'} = (ip'|\hat{F}_{12}|P) \quad (25)$$

$$\tilde{\mathcal{F}}_{Q}^{P} = [\mathcal{F}^{-1}]_{Q}^{P} \quad (26)$$

$$\mathcal{F}_{Q}^{P} = (P|\hat{F}_{12}|Q) \quad (27)$$

thereby reducing the computational prefactor. We note that one can use seminumerical integration to greatly speed up the calculation of multiple-orbital spaces spanning F12-type exchange matrix elements $k_{q'}^{p'}$.[52] Nevertheless, the cost of evaluating the complete term scales unfavorably as $O(M^5)$ with the system size M and represents one of the major bottlenecks in the RI-MP2-F12 theory (see Section 4).

2.2. Numerical Quadrature. Numerical quadrature (NQ)[35,75,100−102] can be employed in various ways to evaluate integrals in F12 theory. We demonstrate its effectiveness for

https://doi.org/10.1021/acs.jctc.4c00193
J. Chem. Theory Comput. 2024, 20, 3706−3718

evaluating the exchange contribution $\mathcal{K}_{ji}^{ij}$ (eq 19), proposing an alternative strategy by combining a double CABS-RI insertion with real-space numerical quadrature to circumvent the use of density-fitting techniques. We can formulate the MO ansatz as

$$\langle ij|\hat{F}_{12}\hat{\alpha}_1\hat{k}_1\hat{\alpha}_1\hat{F}_{12}|ji\rangle \overset{\text{RI}}{\approx} \langle ijp'|\hat{F}_{12}\hat{F}_{23}|q'ij\rangle k_{p'}^{q'} \tag{28}$$

$$\overset{\text{NQ}}{\approx} w_g \phi_i^g \phi_j^g (g|iq')_{\hat{F}_{12}} (g|jp')_{\hat{F}_{12}} k_{p'}^{q'} \tag{29}$$

with g and w_g as discrete grid points and corresponding weights, $k_{p'}^{q'}$ as the HF/CABS space spanning F12-type exchange matrix elements and ϕ_i^g as the i'th MO evaluated at the grid point g. The required MO 3c1e integrals $(g|iq')_{\hat{F}_{12}}$ can be obtained via the AO to MO transformation [at the cost of $O(N_\mu N_{p'} N_g N_i) \sim O(M^4)$] of the corresponding AO quantities

$$(g|\mu\nu')_{\hat{F}_{12}} = \int \chi_\mu(\boldsymbol{r}_1)\chi_{\nu'}(\boldsymbol{r}_1)\hat{F}_{1g}\, \mathrm{d}\boldsymbol{r}_1 \tag{30}$$

with $\hat{F}_{1g}$ as a Slater-type correlation factor[34] evaluated on the grid, given by

$$\hat{F}_{1g} = -\frac{1}{\gamma}\mathrm{e}^{-\gamma(|\boldsymbol{r}_1-\boldsymbol{g}|)} \tag{31}$$

The final energy can then be computed in two low-scaling steps (formal time complexity given in parentheses)

$$\text{step 1:} \quad \mathcal{F}_{q'}^{g} = \phi_i^g (g|iq')_{\hat{F}_{12}} \qquad (N_i N_{p'} N_g) \tag{32}$$

$$\text{step 2:} \quad E_{\mathcal{K}_{ji}^{ij}} = w_g \mathcal{F}_{q'}^{g} \mathcal{F}_{p}^{g} k_{p'}^{q'} \qquad (N_{p'}^2 N_g) \tag{33}$$

However, the expensive AO to MO transformation can be avoided by evaluating eq 28 in the favorable pure AO picture leading to

$$\langle ij|\hat{F}_{12}\hat{\alpha}_1\hat{k}_1\hat{\alpha}_1\hat{F}_{12}|ji\rangle \approx w_g c_{\mu i}\chi_\mu(g) c_{\nu j}\chi_\nu(g) c_{\lambda i} c_{\mu' q'} (g|\lambda\mu')_{\hat{F}_{12}} c_{\sigma j} c_{\nu' p'} (g|\sigma\nu')_{\hat{F}_{12}} c_{\lambda' q'} c_{\sigma' p'} k_{\sigma'}^{\lambda'} \tag{34}$$

$$= w_g P_{\mu\lambda} P_{\nu\sigma} P_{\mu'\lambda} P_{\nu'\sigma} \chi_\mu(g)\chi_\nu(g)(g|\lambda\mu')_{\hat{F}_{12}}(g|\sigma\nu')_{\hat{F}_{12}} k_{\sigma'}^{\lambda'} \tag{35}$$

with MO coefficients c, density(-like) matrices P, and AO F12-type Fock matrix elements f for the HF/CABS orbital spaces, respectively. Again, a stepwise computation allows for an efficient low-scaling evaluation:

$$\text{step 1:} \quad \tilde{k}_{\sigma'}^{\mu'} = P_{\mu'\lambda} k_{\sigma'}^{\lambda'} \qquad (N_{\mu'}^3) \tag{36}$$

$$\mathring{k}_{\nu'}^{\mu'} = \tilde{k}_{\sigma'}^{\mu'} P_{\sigma'\nu'} \qquad (N_{\mu'}^3) \tag{37}$$

$$\text{step 2:} \quad B_{\lambda g} = P_{\mu\lambda}\chi_\mu(g) \qquad (N_\mu^2 N_g) \tag{38}$$

$$\text{step 3:} \quad F_{\mu' g} = \sqrt{w_g}(g|\mu'\lambda)_{\hat{F}_{12}} B_{\lambda g} \qquad (N_\mu N_{\mu'} N_g) \tag{39}$$

$$\text{step 4:} \quad E_{\mathcal{K}_{ji}^{ij}} = \mathrm{Tr}(F_{\mu' g} F_{\nu' g} \mathring{k}_{\nu'}^{\mu'}) \qquad (N_{\mu'}^2 N_g) \tag{40}$$

where the formally most expensive step 4 (eq 40) scales as $O(N_{\mu'}^2 N_g)$, which can be reduced to linear by exploiting the sparsity of $F_{\mu' g}$ using block sparse matrix algebra (BSMA).[103] In practice, for most systems, the evaluation of the $O(N_\mu N_{\mu'} N_g)$ scaling AO 3-center-1-electron integrals (eq 30) constitutes the most demanding step, primarily because of its large prefactor for the evaluation of the Ten-no integrals $[0]_{\hat{F}_{12}}^{(m)}$, the analog to Boys integrals[104] for F12 specific operators.[34] However, 3c1e F12 integrals also offer great screening potential due to the locality of the $\hat{F}_{12}$ operator.[94] In this work, we present the first implementation of screening for grid-based F12-specific integrals, as detailed in the upcoming section.

2.3. Efficient Distance-Dependent Integral Screening.

The idea of leveraging the short-range behavior of F12-specific operators (Table 2 and Figure 1) in the integral screening process was first introduced in the course of developing scaling consistent tight upper bounds for a variety of integrals.[94,105,106] The intrinsic advantage of employing such an interelectronic distance (r_{12})-dependent screening becomes evident for the example of the $\hat{F}_{12}$ operator (γ = 1.3), whose value already falls below 10^{-10} at a distance of 17.51 bohr or 9.27 Å, respectively. As a fundamental component of numerical quadrature, our screening analysis commences with a set of 3c1e integrals for a single shell pair and a single grid point g employing the bounded-type $\hat{F}_{12}$ operator (which is finite for all arguments and monotonically decreasing with an increasing distance). The absolute contribution for each integral $\left|(\mu'\nu|g)_{\hat{F}_{12}}\right|$ within this shell pair $\dot{\mu}'\dot{\nu}$ (dotted indices denote shells instead of individual AO basis functions) can be bound by

Table 2. RI-MP2-F12 Operator Values for Different r_{12} Distances [a_0]

short name	operator	10^{-6}	10^{-8}	10^{-10}	10^{-12}
$\hat{g}_{12}$	$1/r_{12}$	10^6	10^8	10^{10}	10^{12}
$\hat{F}_{12}$	$(1/\gamma)\mathrm{e}^{-\gamma r_{12}}$	10.43	13.97	17.51	21.06
$\hat{F}_{12}\hat{g}_{12}$	$(1/\gamma)\mathrm{e}^{-\gamma r_{12}}/r_{12}$	8.76	12.06	15.41	18.80
$\hat{F}_{12}^2$	$(1/\gamma^2)\mathrm{e}^{-2\gamma r_{12}}$	5.11	6.89	8.66	10.43

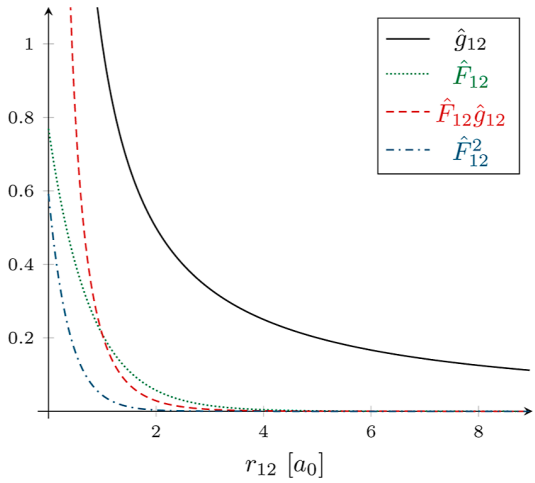

Figure 1. Distance behavior of the operators present in RI-MP2-F12 theory listed in Table 2.

https://doi.org/10.1021/acs.jctc.4c00193
J. Chem. Theory Comput. 2024, 20, 3706−3718

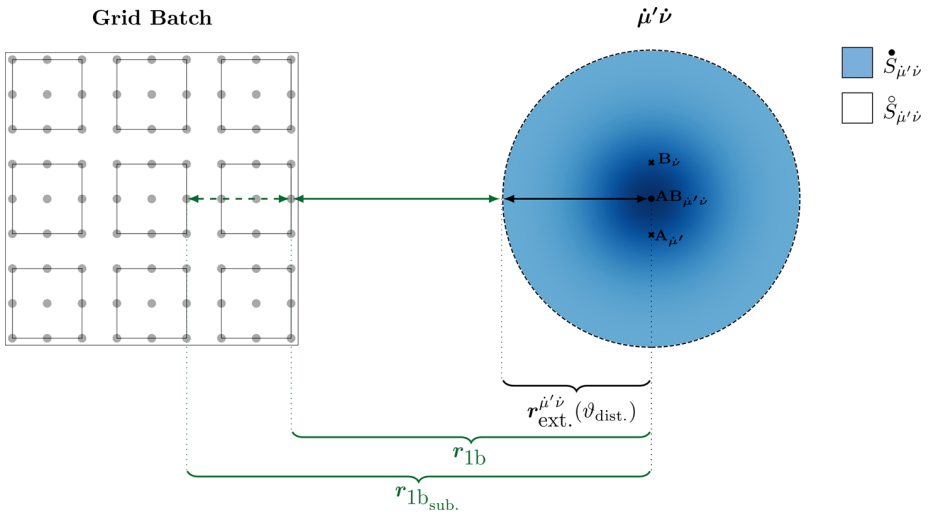

Figure 2. Two-dimensional schematic representation of a batch-wise distance-dependent screening of 3c1e integrals present in F12 theory.

$$\left|(\mu'\nu|g)_{\hat{F}_{12}}\right| \leq \overset{\bullet}{S}_{\dot{\mu}'\dot{\nu}}\hat{F}_{12}(r_{1g} - r^{\dot{\mu}'\dot{\nu}}_{\text{ext.}}(\vartheta_{\text{dist.}})) + \overset{\circ}{S}_{\dot{\mu}'\dot{\nu}}$$
$$\forall\ \mu' \in \dot{\mu}',\ \forall\ \nu \in \dot{\nu} \tag{41}$$

with

$$S_{\dot{\mu}'\dot{\nu}} \geq \int \mathrm{d}\boldsymbol{r}|\Omega_{\mu'\nu}(\boldsymbol{r})| \qquad \forall\ \mu' \in \dot{\mu}',\ \forall\ \nu \in \dot{\nu} \tag{42}$$

$$\overset{\bullet}{S}_{\dot{\mu}'\dot{\nu}} \geq \int_{\bullet} \mathrm{d}\boldsymbol{r}|\Omega_{\mu'\nu}(\boldsymbol{r})| \qquad \forall\ \mu' \in \dot{\mu}',\ \forall\ \nu \in \dot{\nu} \tag{43}$$

$$\overset{\circ}{S}_{\dot{\mu}'\dot{\nu}} \geq \int_{\circ} \mathrm{d}\boldsymbol{r}|\Omega_{\mu'\nu}(\boldsymbol{r})| \qquad \forall\ \mu' \in \dot{\mu}',\ \forall\ \nu \in \dot{\nu} \tag{44}$$

$$\overset{\circ}{S}_{\dot{\mu}'\dot{\nu}} \leq \vartheta_{\text{dist.}} \tag{45}$$

$$\Omega_{\mu'\nu}(\boldsymbol{r}) = \chi_{\mu'}(\boldsymbol{r})\chi_{\nu}(\boldsymbol{r}) \tag{46}$$

$$r_{1g} = |\boldsymbol{r}_{\dot{\mu}'\dot{\nu}} - \boldsymbol{r}_g| \tag{47}$$

where $\boldsymbol{r}_{\dot{\mu}'\dot{\nu}}$ denotes the center of the shell pair $\dot{\mu}'\dot{\nu}$, and $\boldsymbol{r}_g$ represents the coordinates of the grid point g, respectively. For $S_{\dot{\mu}'\dot{\nu}}$, we distinguish integration over the space $\boldsymbol{r}$ inside ($\bullet$) and outside ($\circ$) the shell pair extent $r^{\dot{\mu}'\dot{\nu}}_{\text{ext.}}(\vartheta_{\text{dist.}})$, respectively (cf. Figure 2). Here, $r^{\dot{\mu}'\dot{\nu}}_{\text{ext.}}(\vartheta_{\text{dist.}})$ defines a ball (integration area) around the shell pair center $\boldsymbol{r}_{\dot{\mu}'\dot{\nu}}$, where the contribution from outside $r^{\dot{\mu}'\dot{\nu}}_{\text{ext.}}(\vartheta_{\text{dist.}})$ (bounded by $\overset{\circ}{S}_{\dot{\mu}'\dot{\nu}}$) is smaller than a specified threshold $\vartheta_{\text{dist.}}$. In practice, a set of optimal extents, referred to as integral partition bounds (IPBs), is evaluated via extent equations, as described in Section B of ref 94, and pretabulated for each shell pair across a range of thresholds, covering the entire spectrum of relevant $\vartheta_{\text{dist.}}$. Furthermore, we employ the inequality

$$S_{\dot{\mu}'\dot{\nu}} \geq \overset{\bullet}{S}_{\dot{\mu}'\dot{\nu}} \tag{48}$$

to provide a close estimate of the overlap contribution inside the ball, recognizing that both expressions differ by at most $\vartheta_{\text{dist.}}$.

Expanding this approach beyond a basic 3c1e integral to screen individual equations within F12 theory, we can additionally incorporate all relevant factors that contribute to a given expression. Regarding the case of eq 39, the grid weights $\sqrt{w_g}$, the computational cost associated with evaluating a set of integrals within a shell pair, and the prefactors $B_{\nu g}$ are of relevance. Here, instead of using the absolute grid weight, we have opted for the relative grid weight $\sqrt{\frac{w_g}{w_{\text{avg.}}}}$, where $w_{\text{avg.}}$ represents the average weight across all grid points, leading to a screening approach that is largely independent of grid size. Without this adjustment, the screening gets looser for tighter grids, where individual contributions are comparatively smaller. Further, our objective is to estimate the computational cost associated with computing a set of integrals within a shell pair. This enables us to screen contributions tighter for those that are cheaper to compute and vice versa. To provide a reasonable estimate for the computational cost, we opt for the number of primitive Cartesian basis functions $N^{\text{Cart}}_{\dot{\mu}'\dot{\nu}}$ within the shell pair, as this quantity correlates with the computational workload. Including all of these factors, we arrive at the following estimate for the significance $\varepsilon_{\dot{\mu}'\dot{\nu}g}$ of an individual integral

$$\varepsilon_{\dot{\mu}'\dot{\nu}g} = \frac{1}{N^{\text{Cart}}_{\dot{\mu}'\dot{\nu}}}\sqrt{\frac{w_g}{w_{\text{avg.}}}}B_{\dot{\nu}g}S_{\dot{\mu}'\dot{\nu}}\,\hat{F}_{12}(r_{1g} - r^{\dot{\mu}'\dot{\nu}}_{\text{ext.}}(\vartheta_{\text{dist.}})) \leq \vartheta_{\text{F12}} \tag{49}$$

where ϑ_{F12} is a fixed predefined threshold defining the desired accuracy and

$$B_{\dot{\nu}g} = \sqrt{\sum_{\nu\in\dot{\nu}}|B_{\nu g}|^2} \tag{50}$$

The inequality in eq 49 can also be reformulated to incorporate all prefactors on the right-hand side, resulting in the screening condition

$$S_{\dot{\mu}'\dot{\nu}}\,\hat{F}_{12}(r_{1g} - r^{\dot{\mu}'\dot{\nu}}_{\text{ext.}}) \leq N^{\text{Cart}}_{\dot{\mu}'\dot{\nu}}\sqrt{\frac{w_{\text{avg.}}}{w_g}}\frac{1}{B_{\dot{\nu}g}}\vartheta_{\text{F12}} \equiv \vartheta^{\text{F12}}_{\dot{\mu}'\dot{\nu}g} \tag{51}$$

providing a tighter adjusted threshold $\vartheta^{\text{F12}}_{\dot{\mu}'\dot{\nu}g}$, which is then used in place of $\vartheta_{\text{dist.}}$ to obtain a smaller shell pair extent $r^{\dot{\mu}'\dot{\nu}}_{\text{ext.}}(\vartheta_{\text{dist.}})$.

In order to minimize the screening overhead, the screening is not performed for each grid point individually; instead, it is conducted for entire batches of spatially adjacent grid points (cf. Figure 2). Thus, following the approach in ref 86, we

https://doi.org/10.1021/acs.jctc.4c00193
J. Chem. Theory Comput. 2024, 20, 3706−3718

identify significant batches b under the assumption of their maximal possible contribution, resulting in the batch-wise screening condition

$$S_{\dot{\mu}'\dot{\nu}}\,\hat{F}_{12}(r_{1b} - r_{\text{ext.}}^{\dot{\mu}'\dot{\nu}}(\vartheta_{\text{dist.}})) \leq N_{\dot{\mu}'\dot{\nu}}^{\text{Cart}}\frac{1}{\tilde{B}_{\dot{\nu}b}}\vartheta_{\text{F12}} \equiv \vartheta_{\dot{\mu}'\dot{\nu}b}^{\text{F12}} \tag{52}$$

with

$$r_{1b} \leq \min_{g\in b}(r_{1g}) \tag{53}$$

$$\tilde{B}_{\dot{\nu}b} = \frac{1}{\sqrt{w_{\text{avg.}}}}\max_{g\in b}(\sqrt{w_g}B_{\dot{\nu}g}) \tag{54}$$

In practice, this selection is performed hierarchically, initially employing a coarse preselection on large batches b with 512 points, followed by a final tight selection with smaller sub-batches $b_{\text{sub.}}$ containing 64 points. This approach allows for the estimation of $\varepsilon_{\dot{\mu}'\dot{\nu}b}$ and $\varepsilon_{\dot{\mu}'\dot{\nu}b_{\text{sub.}}}$, also in analogy to the methodology in ref 86. The screening condition in eq 52 ensures asymptotically linear time complexity due to three strong distance decays:

1. $S_{\dot{\mu}'\dot{\nu}}$ decays exponentially with respect to the distance of the centers of shells $\dot{\mu}'$ and $\dot{\nu}$ due to the diminishing basis function overlap (overlap decay).
2. $\hat{F}_{12}(r_{1b} - r_{\text{ext.}}^{\dot{\mu}'\dot{\nu}}(\vartheta_{\text{dist.}}))$ decays exponentially with respect to the distance between the center of the overlap distribution $\Omega_{\dot{\mu}'\nu}$ and the grid batch b (operator decay).
3. $\tilde{B}_{\dot{\nu}b}$ indirectly decays exponentially with respect to the distance between the shell $\dot{\nu}$ and the grid batch b due to the asymptotic sparsity of the density matrix for systems with significant HOMO−LUMO gaps (density decay).

2.4. Implementation. In the following, we discuss every step of an effective AO implementation of eqs 36−40 inspired by existing seminumerical HF/DFT routines[88] summarized in Algorithm 1. We assume MO coefficients,[45] density(-like), and exchange matrices of the HF/CABS space are accessible, and (mixed-)shell pairs are already computed. We commence with step 1, which represents a modified version of the standard F12-type exchange matrix evaluation necessary for various terms in RI-MP2-F12 theory, best evaluated using seminumerical integral evaluation as detailed in ref 52. For contraction of a densely occupied $P_{\dot{\mu}'\dot{\nu}'}$ matrix with $k_{\dot{\sigma}'}^{\dot{\lambda}'}$ we recommend to employ high-performance dense matrix algebra routine (BLAS-3) libraries (i.e., Intel MKL[107]). Conversely, systems featuring a sparsely populated density matrix or an extended size can be more efficiently evaluated by applying block sparse matrix algebra (BSMA) routines, which partition the matrix into blocks of constant size. Each block's significance is determined by examining its Frobenius norm against a specified threshold. Subsequently, the product of two norms decides whether two blocks are multiplied. A more detailed description of the employed BSMA is given in the Supporting Information of ref 103.

Steps 2, 3, and 4 are suitable for optimal batch-independent computation on multicore processors using OpenMP[108] parallelization over grid batches, employing an efficient Hilbert curve-based sub-batching scheme.[86] Here, a maximum of 512 grid points per batch and 64 grid points per sub-batch are used. In step 2, batch-local submatrices of asymptotically constant size, containing only batch-significant elements, are utilized alongside dense BLAS-3 routines for optimal performance with minimal computational effort. For the most expensive step 3, we utilize the screening defined in eq 52 as outlined in Section 2.3. We note that the construction of the primitive $[0]_{\hat{F}_{12}}^{(m)}$ Ten-no integrals is, due to their sheer number, the most computationally expensive step in the entire algorithm for most systems. However, there is potential for significant acceleration by optimizing their evaluation with an efficient interpolation technique. Currently, computing these integrals is roughly five times as costly than the subsequent symbolically optimized Obara−Saika[109] recursion scheme. Finally, step 4 is computed via BLAS-3 routines or BSMA, depending on the system size and the sparsity of $F_{\dot{\mu}'g}$. In total, Algorithm 1 provides a highly efficient evaluation of eq 19, drastically outperforming standard DF/CABS-RI approaches in terms of both accuracy and performance, as demonstrated in Section 4.

Algorithm 1 Algorithmic design for a stepwise evaluation of Eqs. 36-40

Initial Quantities: Shell pairs $\dot{\mu}'\dot{\lambda}$, $c_{\dot{\mu}'\dot{\nu}'}/P_{\dot{\mu}'\dot{\nu}'}$, $k_{\dot{\sigma}'}^{\dot{\lambda}'}$
step 1: evaluate Eqs. 36-37 (BLAS-3/BSMA) → $\hat{k}_{\dot{\nu}'}^{\dot{\mu}'}$
construct molecular grid → batches b
for all batches b **do** ▷ openMP parallel
  step 2:
  compute basis functions $\chi_\mu(\boldsymbol{r}_g)$ on grid
  construct batch-local density $P_{\mu\lambda}$
  evaluate Eq. 38 (BLAS-3) → $B_{\lambda g}$
  precompute $\tilde{B}_{\dot{\nu}b}$ (Eq. 50, 54)
  step 3:
  for all $\dot{\mu}'\dot{\lambda}$ **do**
    evaluate Eq. 52 → $\varepsilon_{\dot{\mu}'\dot{\nu}b}$
    if $\vartheta_{\text{F12}} \leq \varepsilon_{\dot{\mu}'\dot{\nu}b}$ **then**
      for all subbatches $b_{\text{sub.}}$ **do**
        evaluate Eq. 52 → $\varepsilon_{\dot{\mu}'\dot{\nu}b_{\text{sub.}}}$
        if $\vartheta_{\text{F12}} \leq \varepsilon_{\dot{\mu}'\dot{\nu}b_{\text{sub.}}}$ **then**
          for all $g \in b_{\text{sub.}}$ **do**
            for all primitive $\dot{\mu}'\dot{\lambda}$ **do**
              compute primitive integrals $[0]_{\hat{F}_{12}}^{(m)}$ (Ten-no integrals)
              perform optimized Obara-Saika recursions → $(g|\mu'\lambda)_{\hat{F}_{12}}$
            end for
            evaluate Eq. 39 → $F_{\dot{\mu}'g}$
          end for
        end if
      end for
    end if
  end for
  step 4: add batch-local Eq. 40 to global energy (BLAS-3/BSMA) → $E_{K_{ji}^{ij}}$
end for

3. COMPUTATIONAL DETAILS

All calculations presented in this work were conducted using our FermiONs++ program package,[110−113] with optimized DF/CABS-RI F12[94] (Section 2.1) routines serving in a performance benchmark for comparison to our numerical quadrature implementation (Algorithm 1). The SCF convergence criterion was set to within 10^{-7} of the DIIS-commutator norm[114,115] ($\|\mathbf{FPS} - \mathbf{SPF}\|$), and both Hartree−Fock and F12-type Fock-Matrix elements calculations were accelerated using sn-LinK[90] with a gm[5/3] multigrid as well as RI-J[116] in combination with a cc-pVXZ-JKfit[117] (X = D, T, Q) basis.[52] For the F12 correction, we used a fixed Slater-type geminal (STG) correlation factor[34,75] ($\hat{F}_{12} = -\frac{1}{\gamma}\exp(-\gamma r_{12})$ with γ = 1.3) in conjunction with the cc-pVXZ-F12[118−120] basis set family and corresponding CABS cc-pVXZ-F12/OptRI+[121] and density fitting cc-pVXZ-F12/MP2fit[122] basis sets (X = D, T, Q). For numerical quadrature, highly optimized numerical grids[93] (gX) were employed, as summarized in Table 3. All integral kernels have been compiled with the Intel Compiler 19.1.0[123] (flags: -Ofast -march = skylake) to achieve optimal efficiency, and performance was assessed on 2 AMD EPYC 7452 processors (64 cores/128 threads; 2.35 GHz). Basis set superposition errors (BSSE) were corrected via a

https://doi.org/10.1021/acs.jctc.4c00193
J. Chem. Theory Comput. 2024, 20, 3706−3718

Table 3. Summary of Grids Separated into Inner, Medium, and Outer Regions on the Example of the C Atom

grid	n_{rad}	n_{ang} (inner/medium/outer)	$n_{tot,C}$
*g*0	30	14/38/74	1654
*g*1	35	14/50/110	2586
*g*2	40	26/74/194	5056
*g*3	50	38/110/302	9564
*g*4	55	50/194/434	15,526
*g*5	60	50/194/590	21,330
*g*6	70	86/302/974	40,838
*g*7	80	110/434/1454	68,770

mixed scheme employing counterpoise uncorrected and corrected values.[124]

4. RESULTS

The standard DF/CABS-RI approach (Section 2.1) for computing the RI-MP2-F12(3*C) correction incurs significant computational cost, as illustrated in Figure 3. In this graphic, the total time of the F12 correction (61,899 s) and the corresponding percentage cost for evaluating the exchange contribution $\mathcal{K}^{ij}_{ji}$ are shown for the medium-sized circumcoronene-guanine-cytosine trimer ($C_{63}H_{28}N_8O_2$) of the L7 test set,[125] employing a cc-pVDZ-F12 basis set combination (n_{AO} = 2442, $n_{CABS\text{-}RI}$ = 6001, n_{DF} = 8791). In an efficient RI-MP2-F12 implementation, terms and contractions are shared among individual (sub)intermediates to mitigate computational overhead. Our analysis thus distinguishes between costs exclusive to the exchange-type $\mathcal{K}^{ij}_{ji}$ (sub)intermediate, costs shared with other exchange-type intermediates, costs associated with the necessary 4c2e integrals $\mathcal{F}^{ij}_{p'r'}$ (parts also used in other exchange-type intermediates), and costs for all remaining terms. The latter encompasses the construction time for all MO 3c2e- and 2c2e-integrals, all direct-type terms, and all other remaining exchange-type intermediates for every operator present in the MP2-F12 theory (Table 2). The computation of $\mathcal{K}^{ij}_{ji}$ represents the major bottleneck of the F12 correction, with a direct relative contribution of roughly 30% and an indirect contribution of around 80%.

In the following sections, we compare the classical DF/CABS-RI approach to our new NQ/CABS-RI ansatz in terms of accuracy and performance. To assess the accuracy, we compare results to virtually exact reference values employing an extensive *g*7 grid (68,770 grid points per C atom) with no integral screening (ϑ_{F12} = 0). Here, we analyze the precision of our approach by computing noncovalent interaction (NCI) energies and isomerization energies using the cc-pVDZ-F12 basis set combination (AO/CABS-RI/DF) within the L7[125] and ISO34[126] test sets. Comprehensive results, including triple and quadruple-ζ basis sets values as well as results from other commonly used benchmark sets (S22,[127] S66,[128] CARBHB12,[129] PNICO23,[130] and ADIM6[131]), demonstrating similar trends, are included in the Supporting Information.

For performance assessments, we compare the total time required to evaluate $\mathcal{K}^{ij}_{ji}$ using NQ/CABS-RI and DF/CABS-RI, measuring the computational cost for each step in both cases. Only timings required for constructing F12-type exchange matrix elements (step 1, eq 36)[52] are excluded, as they are needed throughout RI-MP2-F12 theory for multiple terms. We focus on the timings of valinomycin[132] to demonstrate real-world performance and evaluate the observed time complexity for linear alkanes.

4.1. Accuracy. Figure 4a,b summarizes the impact of employing NQ/CABS-RI instead of DF/CABS-RI (AO 3c2e IPB[94] screening threshold $\vartheta_{IPB} = 10^{-9}$) on the accuracy of NCI and isomerization energies for the L7 (a) and ISO34 (b) benchmark sets. The figures illustrate mean absolute errors (MAEs) alongside maximum absolute errors (MAXs) and MAEs relative to the average reference energy (MAE/AVG) for different ϑ_{F12}. In line with expectations, the results demonstrate improved accuracy with an increasing grid size, systematically converging toward the numerically exact result, leaving a small constant screening error for $\vartheta_{F12} = 10^{-9}$ and $\vartheta_{F12} = 10^{-10}$. It is important to note that choosing $\vartheta_{F12} = 10^{-8}$ is beneficial primarily for smaller grids up to *g*2, especially for systems made up solely of elements from the first and second periods (see the Supporting Information). However, this choice proves insufficient for systems containing elements from the third period and beyond. Therefore, we conclude that this effect is likely due to a coincidental error cancellation between the grid and the screening error.

For L7 NCI energies, even a small *g*0 grid demonstrates a good level of accuracy, yielding satisfactory MAE and MAE/AVG values of approximately 7 μE_h and 0.07%, respectively.

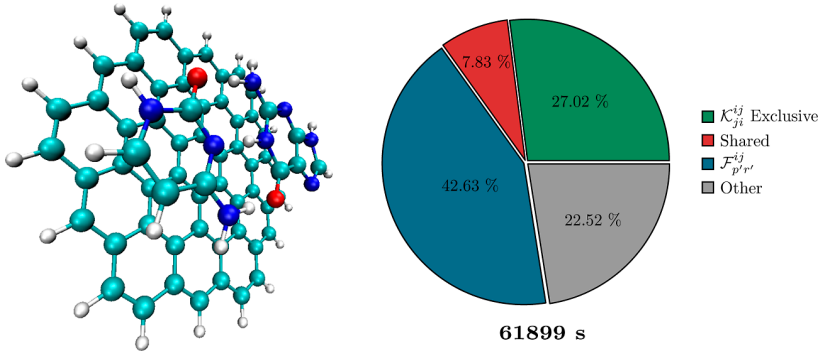

Figure 3. Relative percentage cost for computing individual contributions of the explicitly correlated RI-MP2-F12(3*C) correction (right) for the L7 circumcoronene-guanine-cytosine trimer (left: $C_{63}H_{28}N_8O_2$), utilizing the standard DF/CABS-RI approach (see Section 2.1) with a cc-pVDZ-F12 basis set combination (AO/CABS-RI/DF). Green: percentage cost exclusively for evaluating $\mathcal{K}^{ij}_{ji}$, Red: cost shared with other terms, Blue: cost for constructing $\mathcal{F}^{ij}_{p'r}$ (required for $\mathcal{K}^{ij}_{ji}$), and Gray: cost for all remaining terms.

https://doi.org/10.1021/acs.jctc.4c00193
J. Chem. Theory Comput. 2024, 20, 3706−3718

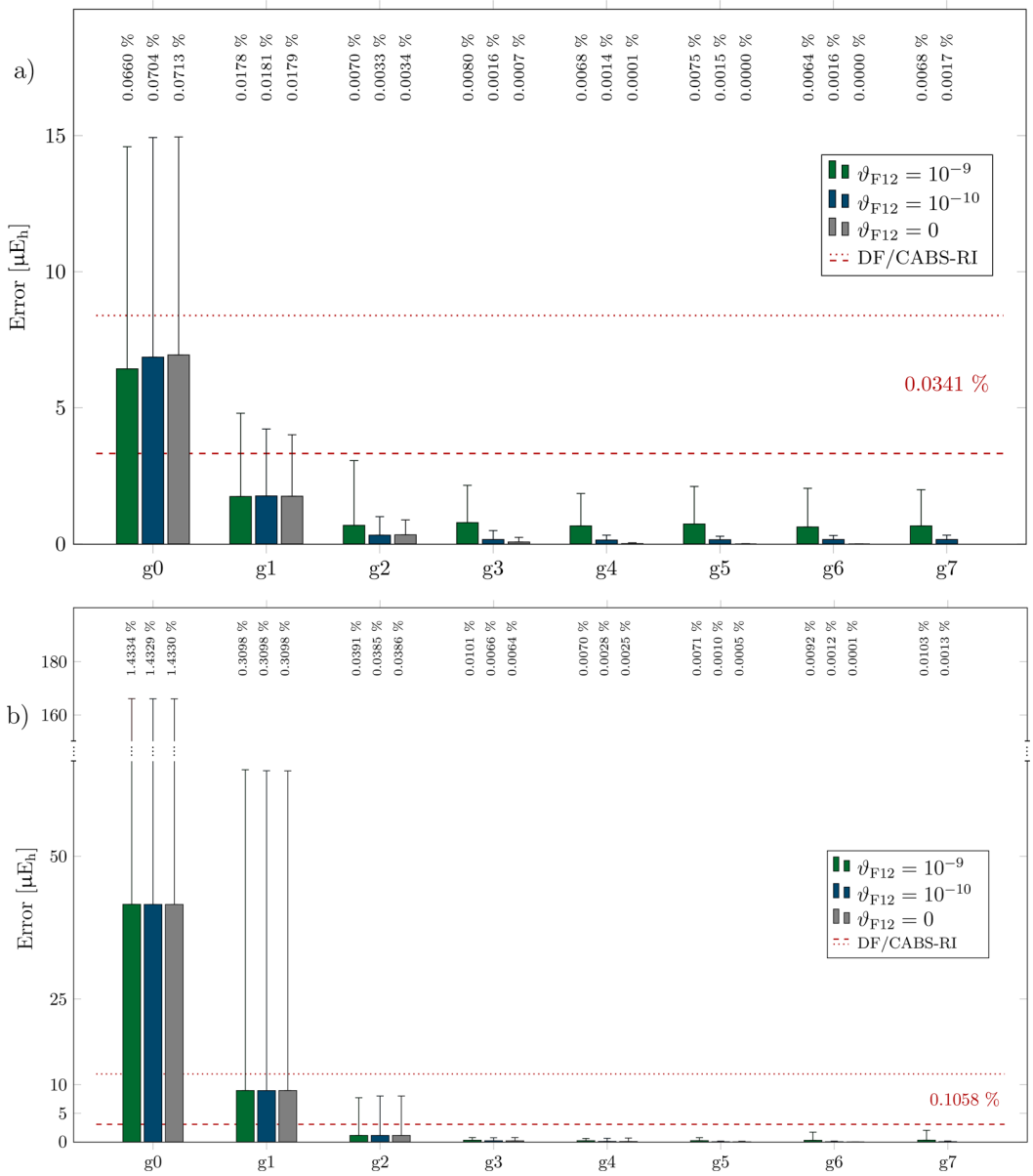

Figure 4. Mean absolute errors (MAEs filled bars), max. absolute errors (MAXs thin error bars), and MAEs relative to the average reference noncovalent-interaction/isomerization energy (MAE/AVG in percent) for the L7 (a) and ISO34 (b) test sets employing NQ/CABS-RI with various grid sizes ($g0$–$g7$)/thresholds ϑ_{F12} and DF/CABS-RI ($\vartheta_{IPB} = 10^{-9}$) for a cc-pVDZ-F12 basis set combination. DF/CABS-RI MAE and MAX values are shown as dashed and dotted lines.

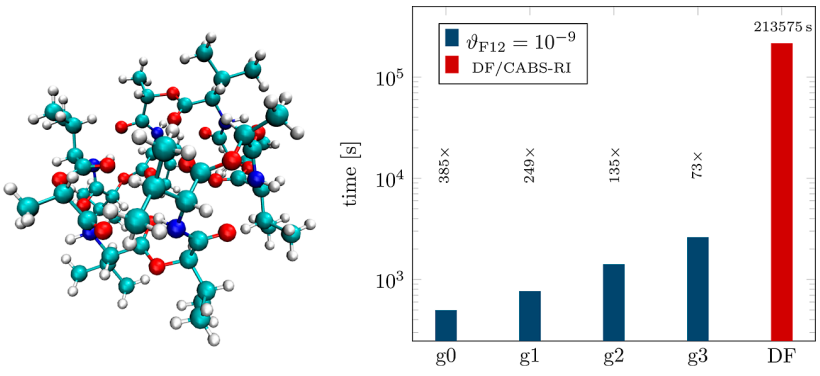

Figure 5. NQ/CABS-RI and DF/CABS-RI timings (log-scale) and corresponding speedups for valinomycin ($C_{54}H_{90}N_6O_{18}$) employing multiple grid sizes and $\vartheta_{F12} = 10^{-9}$, using a cc-pVTZ-F12 basis set combination (AO/CABS-RI/DF; 64 threads).

https://doi.org/10.1021/acs.jctc.4c00193
J. Chem. Theory Comput. 2024, 20, 3706−3718

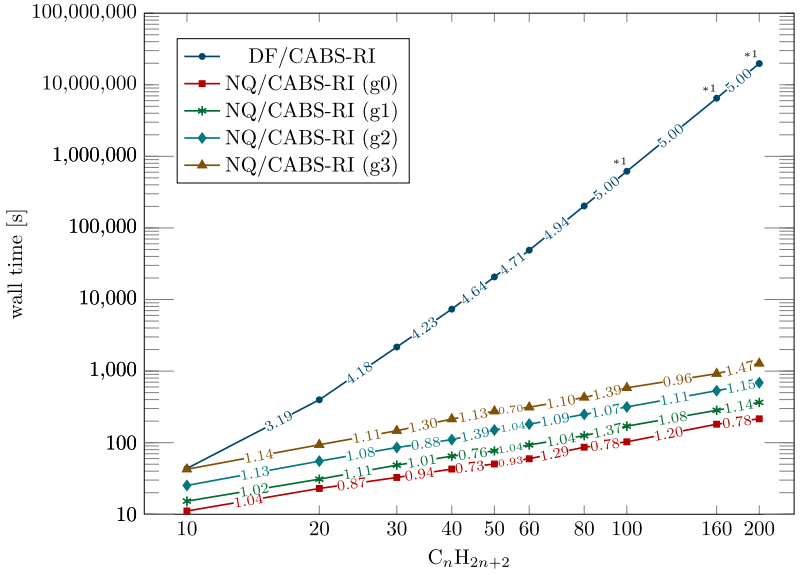

Figure 6. Log−log plot of the wall times and corresponding scaling exponents between two neighboring structures for NQ/CABS-RI ($\vartheta_{F12} = 10^{-9}$) utilizing multiple grid sizes, and DF/CABS-RI of linear *n*-alkanes (C_nH_{2n+2}, $n \in 10, 20, 30, 40, 50, 60, 80, 100, 160, 200$) for a cc-pVDZ-F12 basis set combination (112 threads). *1 Extrapolated according to the theoretical scaling behavior.

Notably, nearly error-free results are already obtained for grids larger than *g*2. In contrast, errors for the ISO34 test set are more sensitive to the choice of the grid. For example, a *g*0 grid yields MAE and MAX values of 44 and 170 μEh (0.12 and 0.45 kJ·mol^{-1}), representing significant discrepancies from the reference. Nevertheless, even moderately larger grids deliver high-quality results, with isomerization energies closely matching the reference.

In summary, the modest *g*2 grid with $\vartheta_{F12} = 10^{-9}$ consistently yields more accurate results than DF/CABS-RI for a double-ζ F12 basis, with MAEs close to 1 μE_h. When examining triple and quadruple-ζ results (cf. Supporting Information), grid errors remain relatively stable, while MAE/AVG values notably increase because the total correction itself decreases. Notably, for triple- and quadruple-ζ basis sets, RI converges toward the exact result due to almost complete RI and DF basis sets, albeit at a significantly higher computational cost. In general, the desired level of accuracy for NQ/CABS-RI calculations can be tailored to the specific application area to achieve the best balance between precision and computational efficiency.

4.2. Performance Comparison. To demonstrate the power of numerical quadrature in the F12 theory, we measured timings for valinomycin using a cc-pVTZ-F12 basis set combination ($C_{54}H_{90}N_6O_{18}$, $n_{AO} = 5754$, $n_{CABS\text{-}RI} = 10{,}266$, $n_{DF} = 18{,}504$) with our NQ/CABS-RI algorithm (Algorithm 1) and compared results to DF/CABS-RI values, as summarized in Figure 5.

With speedups ranging from 73× to 385× faster evaluations, our NQ/CABS-RI algorithm significantly outperforms the DF/CABS-RI reference, additionally providing nearly error-free results for *g*2 and *g*3 grids. Screening of the 3c1e integrals $(g|\mu\nu')_{\hat{F}_{12}}$ is crucial in this process, as their construction represents the most costly step in the computation. The choice of screening threshold ϑ_{F12} only subtly influences performance. For instance, when employing a *g*2 grid in combination with $\vartheta_{F12} = 10^{-9}$, 9.2% of 3c1e integrals need to be calculated. With $\vartheta_{F12} = 10^{-10}$, this number increases only marginally to 12.1% (similar numbers for *g*0, *g*1, and *g*3). Our screened algorithm is roughly ten times faster than an unscreened NQ integral evaluation, eliminating notable overhead.

To contextualize the cost of evaluating the exchange-type $\mathcal{K}^{ij}_{ji}$ intermediate for both approaches, we compare NQ/CABS-RI and DF/CABS-RI results with the computational cost for the corresponding standard RI-MP2 correlation calculation. DF/CABS-RI demands for the evaluation $\mathcal{K}^{ij}_{ji}$ roughly 59.5 h, eight times longer than the corresponding classical RI-MP2 correlation calculation (7.4 h). In contrast, utilizing a *g*2 grid and $\vartheta_{F12} = 10^{-9}$ threshold, NQ/CABS-RI achieves highly precise results, requiring only 26.3 min to compute $\mathcal{K}^{ij}_{ji}$. This makes it 135 times faster than DF/CABS-RI and 17 times faster than RI-MP2. In these calculations, step 3 (eq 39) consumes approximately 75−80% of the computation time, followed by step 4 (eq 40) at approximately 20%, while step 2 (eq 38) requires negligible effort.

In most cases, step 4 is typically the second most computationally intensive in our NQ/CABS-RI algorithm, usually overshadowed by the dominance of step 3. However, as the system size increases and density(-like) matrices become sparser, the number of significant 3c1e integrals in step 3 increases linearly. Consequently, the evaluation of Step 4, scaling as $O(N^2_{\mu'}N_g)$, notably starts to contribute and becomes dominant for extensive system sizes. To address this cubical scaling behavior, we exploit the strong sparsity of the intermediate quantity $F_{\mu' g}$ for these cases, which greatly benefits the use of block sparse matrix algebra (BSMA)[103] (block size = 48 × 48, $\vartheta_{block} = 10^{-8}$, $\vartheta_{mult.} = 10^{-10}$), resulting in a linear scaling evaluation of $\mathcal{K}^{ij}_{ji}$ as demonstrated in Figure 6 for various grid sizes. In practical applications, block sparse matrix algebra introduces a flexible error in the absolute energy for these systems, controllable by adjusting the block size and $\vartheta_{block/mult.}$. Evaluating $C_{160}H_{322}$ using a *g*2 grid ($\vartheta_{F12} = 10^{-9}$) with the previously described BSMA settings introduces an

https://doi.org/10.1021/acs.jctc.4c00193
J. Chem. Theory Comput. 2024, 20, 3706−3718

additional error in the absolute energy of 1.1 mE_h, while drastically reducing the computational cost from 5104 to 532 s.

We achieve astonishing speedups for $C_{80}H_{162}$ and $C_{200}H_{402}$ using a *g*2 grid with a $\vartheta_{F12} = 10^{-9}$ threshold (Note: DF/CABS-RI timings for $C_{200}H_{402}$ are not feasible and were extrapolated according to its theoretical $O(M^5)$ scaling with the system size M): For $C_{80}H_{162}$ NQ/CABS-RI leads to a 817× faster computation requiring 248 s instead of 56.3 h. For $C_{200}H_{402}$ an estimated DF/CABS-RI wall time of 229.23 days is reduced to 11.5 min using NQ/CABS-RI, representing a 28,765× speedup. The presented speedups and timings demonstrate that our NQ/CABS-RI algorithm significantly reduces the cost for the formerly most computationally demanding term in RI-MP2-F12. Both chemically relevant and sparse systems are easily accessible with negligible cost. The evaluation is multiple times faster than the corresponding RI-MP2 calculation, outperforming the current standard DF/CABS-RI approach by several orders of magnitude faster computations while providing higher accuracy since fewer CABS-RI insertions are necessary.

5. CONCLUSIONS

We presented a highly efficient linear scaling AO algorithm based on a combination of numerical quadrature (NQ) with CABS-RI, specifically aimed to reduce the computational cost of the most resource-intensive term in the RI-MP2-F12 theory. In this context, we presented a versatile, robust distance-depending screening scheme for 3c1e integrals employing F12-type operators applicable to all explicitly correlated theories. We tested our approach against a standard DF/CABS-RI method regarding the accuracy of isomerization and interaction energies assessed for different grid sizes and thresholds. Already for a *g*2 grid ($\vartheta_{F12} = 10^{-9}$) NQ/CABS-RI shows consistently higher accuracy and efficiency compared to DF/CABS-RI, further allowing tuning for the best balance between precision and computational efficiency.

Our new approach results in 2 orders of magnitude faster evaluation of the most computationally demanding RI-MP2-F12 term compared to the previous DF/CABS-RI method for medium-sized molecules and basis sets. For example, we achieved a 135× speedup for valinomycin ($C_{54}H_{90}N_6O_{18}$) with a cc-pVTZ-F12 basis set combination, while being more accurate than DF/CABS-RI. The relative cost compared to the corresponding RI-MP2 calculations drops from 800% to only approximately 6% by avoiding DF via our NQ approach, thereby drastically enhancing the practicality of F12 theory. Additionally, we examined the scaling behavior for linear chains of alkanes, demonstrating efficient linear scaling when combined with block sparse matrix algebra. Notably, for the longest chain ($C_{200}H_{402}$), our approach achieves a remarkable acceleration of up to 4 orders of magnitude compared to the standard DF/CABS-RI method.

Future research will focus on further integrating NQ into explicitly correlated F12 theory and implementing our findings into an efficient MO framework. In particular, we plan to merge the strategies presented in this paper to the remaining exchange-type contributions in the (RI-)MP2-F12 theory and investigate for these expressions the most effective interplay between NQ and distance-depending integral screening, CABS-RI, and DF, respectively, to achieve the best performance and accuracy. With these developments, we are optimistic about lowering the cost of the entire F12 correction below the cost of corresponding RI-MP2 calculations, eliminating the need for complete basis set (CBS) extrapolations.

■ ASSOCIATED CONTENT

Supporting Information

The Supporting Information is available free of charge at https://pubs.acs.org/doi/10.1021/acs.jctc.4c00193.

Detailed data on NQ/CABS-RI and DF/CABS-RI NCI and isomerization energies (L7, S22, S66, CARBH12, PNICO23, ADIM6, and ISO34) employing a cc-pVXZ-F12 (X = D, T, Q) basis set combination (PDF)

■ AUTHOR INFORMATION

Corresponding Author

Christian Ochsenfeld − *Chair of Theoretical Chemistry, Department of Chemistry, University of Munich (LMU), D-81377 Munich, Germany; Max Planck Institute for Solid State Research, D-70569 Stuttgart, Germany;* orcid.org/0000-0002-4189-6558; Email: christian.ochsenfeld@uni-muenchen.de

Authors

Lars Urban − *Chair of Theoretical Chemistry, Department of Chemistry, University of Munich (LMU), D-81377 Munich, Germany; Max Planck Institute for Solid State Research, D-70569 Stuttgart, Germany;* orcid.org/0000-0001-9891-3577

Henryk Laqua − *Chair of Theoretical Chemistry, Department of Chemistry, University of Munich (LMU), D-81377 Munich, Germany*

Travis H. Thompson − *Chair of Theoretical Chemistry, Department of Chemistry, University of Munich (LMU), D-81377 Munich, Germany*

Complete contact information is available at: https://pubs.acs.org/10.1021/acs.jctc.4c00193

Funding

Open access funded by Max Planck Society.

Notes

The authors declare no competing financial interest.

■ ACKNOWLEDGMENTS

The authors thank Y. Lemke (LMU Munich) and F. Sacchetta (LMU Munich) for helpful discussions, and Dr. J. Kussmann (LMU Munich) for providing a development version of the FermiONs++[110−113] program package. Financial support was provided by the Excellence Cluster EXC2111-390814868, Munich Center for Quantum Science and Technology (MCQST) by the Deutsche Forschungsgemeinschaft (DFG). C.O. acknowledges, in addition, financial support as Max Planck Fellow of MPI-FKF Stuttgart.

■ REFERENCES

(1) Hylleraas, E. A. Neue Berechnung der Energie des Heliums im Grundzustande. sowie des tiefsten Terms von Ortho-Helium. *Z. Physik* **1929**, *54*, 347−366.

(2) Kato, T. On the eigenfunctions of many-particle systems in quantum mechanics. *Commun. Pure Appl. Math.* **1957**, *10*, 151−177.

(3) Sims, J. S.; Hagstrom, S. Combined Configuration-Interaction—Hylleraas-Type Wave-Function Study of the Ground State of the Beryllium Atom. *Phys. Rev. A* **1971**, *4*, 908−916.

(4) Sims, J. S.; Hagstrom, S. A. Mathematical and computational science issues in high precision Hylleraas-configuration interaction

variational calculations: I. Three-electron integrals. *J. Phys. B: At., Mol. Opt. Phys.* **2004**, *37*, 1519−1540.
(5) Sims, J. S.; Hagstrom, S. A. Mathematical and computational science issues in high precision Hylleraas−configuration interaction variational calculations: II. Kinetic energy and electron−nucleus interaction integrals. *J. Phys. B: At., Mol. Opt. Phys.* **2007**, *40*, 1575−1587.
(6) Sims, J. S.; Hagstrom, S. A. Mathematical and computational science issues in high precision Hylleraas-configuration interaction variational calculations: III. Four-electron integrals. *J. Phys. B: At., Mol. Opt. Phys.* **2015**, *48*, 175003.
(7) Boys, S. F.; Wilkes, M. V. The integral formulae for the variational solution of the molecular many-electron wave equation in terms of Gaussian functions with direct electronic correlation. *Proc. R. Soc. A* **1960**, *258*, 402−411.
(8) Singer, K.; Wilkes, M. V. The use of Gaussian (exponential quadratic) wave functions in molecular problems - I. General formulae for the evaluation of integrals. *Proc. R. Soc. A* **1960**, *258*, 412−420.
(9) Cencek, W.; Rychlewski, J. Many-electron explicitly correlated Gaussian functions. I. General theory and test results. *J. Chem. Phys.* **1993**, *98*, 1252−1261.
(10) Cencek, W.; Komasa, J.; Rychlewski, J. Benchmark calculations for two-electron systems using explicitly correlated Gaussian functions. *Chem. Phys. Lett.* **1995**, *246*, 417−420.
(11) Mitroy, J.; Bubin, S.; Horiuchi, W.; Suzuki, Y.; Adamowicz, L.; Cencek, W.; Szalewicz, K.; Komasa, J.; Blume, D.; Varga, K. Theory and application of explicitly correlated Gaussians. *Rev. Mod. Phys.* **2013**, *85*, 693−749.
(12) Bubin, S.; Pavanello, M.; Tung, W.-C.; Sharkey, K. L.; Adamowicz, L. Born−Oppenheimer and Non-Born−Oppenheimer, Atomic and Molecular Calculations with Explicitly Correlated Gaussians. *Chem. Rev.* **2013**, *113*, 36−79.
(13) Boys, S. F.; Handy, N. C.; Linnett, J. W. A condition to remove the indeterminacy in interelectronic correlation functions. *Proc. R. Soc. A* **1969**, *309*, 209−220.
(14) Boys, S. F.; Handy, N. C.; Linnett, J. W. The determination of energies and wavefunctions with full electronic correlation. *Proc. R. Soc. A* **1969**, *310*, 43−61.
(15) Boys, S. F.; Handy, N. C.; Linnett, J. W. A calculation for the energies and wavefunctions for states of neon with full electronic correlation accuracy. *Proc. R. Soc. A* **1969**, *310*, 63−78.
(16) Boys, S. F.; Handy, N. C.; Linnett, J. W. A first solution, for LiH, of a molecular transcorrelated wave equation by means of restricted numerical integration. *Proc. R. Soc. A* **1969**, *311*, 309−329.
(17) Handy, N. On the minimization of the variance of the transcorrelated hamiltonian. *Mol. Phys.* **1971**, *21*, 817−828.
(18) Handy, N. C. Towards an understanding of the form of correlated wavefunctions for atoms. *J. Chem. Phys.* **1973**, *58*, 279−287.
(19) Ten-no, S. A feasible transcorrelated method for treating electronic cusps using a frozen Gaussian geminal. *Chem. Phys. Lett.* **2000**, *330*, 169−174.
(20) Ten-no, S. Three-electron integral evaluation in the transcorrelated method using a frozen Gaussian geminal. *Chem. Phys. Lett.* **2000**, *330*, 175−179.
(21) Hino, O.; Tanimura, Y.; Ten-no, S. Biorthogonal approach for explicitly correlated calculations using the transcorrelated Hamiltonian. *J. Chem. Phys.* **2001**, *115*, 7865−7871.
(22) Hino, O.; Tanimura, Y.; Ten-no, S. Application of the transcorrelated Hamiltonian to the linearized coupled cluster singles and doubles model. *Chem. Phys. Lett.* **2002**, *353*, 317−323.
(23) Umezawa, N.; Tsuneyuki, S. Transcorrelated method for electronic systems coupled with variational Monte Carlo calculation. *J. Chem. Phys.* **2003**, *119*, 10015−10031.
(24) Luo, H. Variational transcorrelated method. *J. Chem. Phys.* **2010**, *133*, 154109.
(25) Kersten, J. A. F.; Booth, G. H.; Alavi, A. Assessment of multireference approaches to explicitly correlated full configuration interaction quantum Monte Carlo. *J. Chem. Phys.* **2016**, *145*, 054117.
(26) Luo, H.; Alavi, A. Combining the Transcorrelated Method with Full Configuration Interaction Quantum Monte Carlo: Application to the Homogeneous Electron Gas. *J. Chem. Theory Comput.* **2018**, *14*, 1403−1411.
(27) Cohen, A. J.; Luo, H.; Guther, K.; Dobrautz, W.; Tew, D. P.; Alavi, A. Similarity transformation of the electronic Schrödinger equation via Jastrow factorization. *J. Chem. Phys.* **2019**, *151*, 061101.
(28) Baiardi, A.; Reiher, M. Transcorrelated density matrix renormalization group. *J. Chem. Phys.* **2020**, *153*, 164115.
(29) Schraivogel, T.; Cohen, A. J.; Alavi, A.; Kats, D. Transcorrelated coupled cluster methods. *J. Chem. Phys.* **2021**, *155*, 191101.
(30) Baiardi, A.; Lesiuk, M.; Reiher, M. Explicitly Correlated Electronic Structure Calculations with Transcorrelated Matrix Product Operators. *J. Chem. Theory Comput.* **2022**, *18*, 4203−4217.
(31) Ammar, A.; Scemama, A.; Giner, E. Extension of selected configuration interaction for transcorrelated methods. *J. Chem. Phys.* **2022**, *157*, 134107.
(32) Liao, K.; Zhai, H.; Christlmaier, E. M.; Schraivogel, T.; Ríos, P. L.; Kats, D.; Alavi, A. Density Matrix Renormalization Group for Transcorrelated Hamiltonians: Ground and Excited States in Molecules. *J. Chem. Theory Comput.* **2023**, *19*, 1734−1743.
(33) Schraivogel, T.; Christlmaier, E. M.; López Ríos, P.; Alavi, A.; Kats, D. Transcorrelated coupled cluster methods. II. Molecular systems. *J. Chem. Phys.* **2023**, *158*, 214106.
(34) Ten-no, S. Initiation of explicitly correlated Slater-type geminal theory. *Chem. Phys. Lett.* **2004**, *398*, 56−61.
(35) Ten-no, S. Explicitly correlated second order perturbation theory: Introduction of a rational generator and numerical quadratures. *J. Chem. Phys.* **2004**, *121*, 117−129.
(36) Werner, H.-J.; Adler, T. B.; Manby, F. R. General orbital invariant MP2-F12 theory. *J. Chem. Phys.* **2007**, *126*, 164102.
(37) Bachorz, R. A.; Bischoff, F. A.; Glöß, A.; Hättig, C.; Höfener, S.; Klopper, W.; Tew, D. P. The MP2-F12 Method in the Turbomole Program Package. *J. Comput. Chem.* **2011**, *32*, 2492−2513.
(38) Noga, J.; Kedžuch, S.; Šimunek, J.; Ten-no, S. Explicitly correlated coupled cluster F12 theory with single and double excitations. *J. Chem. Phys.* **2008**, *128*, 174103.
(39) Kong, L.; Bischoff, F. A.; Valeev, E. F. Explicitly Correlated R12/F12 Methods for Electronic Structure. *Chem. Rev.* **2012**, *112*, 75−107.
(40) Ten-no, S.; Noga, J. Explicitly correlated electronic structure theory from R12/F12 ansätze. *Wiley Interdiscip. Rev.: Comput. Mol. Sci.* **2012**, *2*, 114−125.
(41) Kutzelnigg, W. r12-Dependent terms in the wave function as closed sums of partial wave amplitudes for large l. *Theor. Chim. Acta* **1985**, *68*, 445−469.
(42) Klopper, W.; Kutzelnigg, W. Møller-plesset calculations taking care of the correlation CUSP. *Chem. Phys. Lett.* **1987**, *134*, 17−22.
(43) Kutzelnigg, W.; Klopper, W. Wave functions with terms linear in the interelectronic coordinates to take care of the correlation cusp. I. General theory. *J. Chem. Phys.* **1991**, *94*, 1985−2001.
(44) Klopper, W. Highly accurate coupled-cluster singlet and triplet pair energies from explicitly correlated calculations in comparison with extrapolation techniques. *Mol. Phys.* **2001**, *99*, 481−507.
(45) Valeev, E. F. Improving on the resolution of the identity in linear R12 ab initio theories. *Chem. Phys. Lett.* **2004**, *395*, 190−195.
(46) Werner, H.-J. Eliminating the domain error in local explicitly correlated second-order Møller−Plesset perturbation theory. *J. Chem. Phys.* **2008**, *129*, 101103.
(47) Höfener, S.; Klopper, W. Analytical nuclear gradients of the explicitly correlated Møller−Plesset second-order energy. *Mol. Phys.* **2010**, *108*, 1783−1796.
(48) Ma, Q.; Werner, H.-J. Scalable Electron Correlation Methods. 2. Parallel PNO-LMP2-F12 with Near Linear Scaling in the Molecular Size. *J. Chem. Theory Comput.* **2015**, *11*, 5291−5304.

https://doi.org/10.1021/acs.jctc.4c00193
J. Chem. Theory Comput. 2024, 20, 3706−3718

(49) Wang, Y. M.; Hättig, C.; Reine, S.; Valeev, E.; Kjærgaard, T.; Kristensen, K. Explicitly correlated second-order Møller-Plesset perturbation theory in a Divide-Expand-Consolidate (DEC) context. *J. Chem. Phys.* **2016**, *144*, 204112.
(50) Győrffy, W.; Knizia, G.; Werner, H.-J. Analytical energy gradients for explicitly correlated wave functions. I. Explicitly correlated second-order Møller-Plesset perturbation theory. *J. Chem. Phys.* **2017**, *147*, 214101.
(51) Urban, L.; Thompson, T. H.; Ochsenfeld, C. A scaled explicitly correlated F12 correction to second-order Møller−Plesset perturbation theory. *J. Chem. Phys.* **2021**, *154*, 044101.
(52) Urban, L.; Laqua, H.; Ochsenfeld, C. Highly Efficient and Accurate Computation of Multiple Orbital Spaces Spanning Fock Matrix Elements on Central and Graphics Processing Units for Application in F12 Theory. *J. Chem. Theory Comput.* **2022**, *18*, 4218−4228.
(53) Adler, T. B.; Knizia, G.; Werner, H.-J. A simple and efficient CCSD(T)-F12 approximation. *J. Chem. Phys.* **2007**, *127*, 221106.
(54) Valeev, E. F. Coupled-cluster methods with perturbative inclusion of explicitly correlated terms: a preliminary investigation. *Phys. Chem. Chem. Phys.* **2008**, *10*, 106−113.
(55) Torheyden, M.; Valeev, E. F. Variational formulation of perturbative explicitly-correlated coupled-cluster methods. *Phys. Chem. Chem. Phys.* **2008**, *10*, 3410−3420.
(56) Shiozaki, T.; Kamiya, M.; Hirata, S.; Valeev, E. F. Explicitly correlated coupled-cluster singles and doubles method based on complete diagrammatic equations. *J. Chem. Phys.* **2008**, *129*, 071101.
(57) Valeev, E. F.; Daniel Crawford, T. Simple coupled-cluster singles and doubles method with perturbative inclusion of triples and explicitly correlated geminals: The CCSD(T)R12^{-} model. *J. Chem. Phys.* **2008**, *128*, 244113.
(58) Noga, J.; Šimunek, J. On the one-particle basis set relaxation in R12 based theories. *Chem. Phys.* **2009**, *356*, 1−6.
(59) Hättig, C.; Tew, D. P.; Köhn, A. Communications: Accurate and efficient approximations to explicitly correlated coupled-cluster singles and doubles, CCSD-F12. *J. Chem. Phys.* **2010**, *132*, 231102.
(60) Schmitz, G.; Hättig, C.; Tew, D. P. Explicitly correlated PNO-MP2 and PNO-CCSD and their application to the S66 set and large molecular systems. *Phys. Chem. Chem. Phys.* **2014**, *16*, 22167−22178.
(61) Győrffy, W.; Werner, H.-J. Analytical energy gradients for explicitly correlated wave functions. II. Explicitly correlated coupled cluster singles and doubles with perturbative triples corrections: CCSD(T)-F12. *J. Chem. Phys.* **2018**, *148*, 114104.
(62) Hehn, A.-S.; Klopper, W. Communication: Explicitly-correlated second-order correction to the correlation energy in the random-phase approximation. *J. Chem. Phys.* **2013**, *138*, 181104.
(63) Hehn, A.-S.; Tew, D. P.; Klopper, W. Explicitly correlated ring-coupled-cluster-doubles theory. *J. Chem. Phys.* **2015**, *142*, 194106.
(64) Hehn, A.-S.; Holzer, C.; Klopper, W. Explicitly-correlated ring-coupled-cluster-doubles theory: Including exchange for computations on closed-shell systems. *Chem. Phys.* **2016**, *479*, 160−169.
(65) Ten-no, S. A simple F12 geminal correction in multi-reference perturbation theory. *Chem. Phys. Lett.* **2007**, *447*, 175−179.
(66) Shiozaki, T.; Werner, H.-J. Communication: Second-order multireference perturbation theory with explicit correlation: CASPT2-F12. *J. Chem. Phys.* **2010**, *133*, 141103.
(67) Shiozaki, T.; Knizia, G.; Werner, H.-J. Explicitly correlated multireference configuration interaction: MRCI-F12. *J. Chem. Phys.* **2011**, *134*, 034113.
(68) Haunschild, R.; Mao, S.; Mukherjee, D.; Klopper, W. A universal explicit electron correlation correction applied to Mukherjee's multi-reference perturbation theory. *Chem. Phys. Lett.* **2012**, *531*, 247−251.
(69) Shiozaki, T.; Werner, H.-J. Multireference explicitly correlated F12 theories. *Mol. Phys.* **2013**, *111*, 607−630.
(70) Liu, W.; Hanauer, M.; Köhn, A. Explicitly correlated internally contracted multireference coupled-cluster singles and doubles theory: Ic-MRCCSD(F12*). *Chem. Phys. Lett.* **2013**, *565*, 122−127.
(71) Roskop, L. B.; Kong, L.; Valeev, E. F.; Gordon, M. S.; Windus, T. L. Assessment of Perturbative Explicitly Correlated Methods for Prototypes of Multiconfiguration Electronic Structure. *J. Chem. Theory Comput.* **2014**, *10*, 90−101.
(72) Guo, Y.; Sivalingam, K.; Valeev, E. F.; Neese, F. Explicitly correlated N-electron valence state perturbation theory (NEVPT2-F12). *J. Chem. Phys.* **2017**, *147*, 064110.
(73) Mehta, N.; Martin, J. M. L. Explicitly Correlated Double-Hybrid DFT: A Comprehensive Analysis of the Basis Set Convergence on the GMTKN55 Database. *J. Chem. Theory Comput.* **2022**, *18*, 5978−5991.
(74) Mehta, N.; Martin, J. M. L. Reduced-Scaling Double Hybrid Density Functional Theory with Rapid Basis Set Convergence through Localized Pair Natural Orbital F12. *J. Phys. Chem. Lett.* **2022**, *13*, 9332−9338.
(75) Ten-no, S. New implementation of second-order Møller-Plesset perturbation theory with an analytic Slater-type geminal. *J. Chem. Phys.* **2007**, *126*, 014108.
(76) Friesner, R. A. Solution of self-consistent field electronic structure equations by a pseudospectral method. *Chem. Phys. Lett.* **1985**, *116*, 39−43.
(77) Friesner, R. A. Solution of the Hartree-Fock equations by a pseudospectral method: Application to diatomic molecules. *J. Chem. Phys.* **1986**, *85*, 1462−1468.
(78) Friesner, R. A. Solution of the Hartree-Fock equations for polyatomic molecules by a pseudospectral method. *J. Chem. Phys.* **1987**, *86*, 3522−3531.
(79) Ringnalda, M. N.; Belhadj, M.; Friesner, R. A. Pseudospectral Hartree-Fock theory: Applications and algorithmic improvements. *J. Chem. Phys.* **1990**, *93*, 3397−3407.
(80) Neese, F.; Wennmohs, F.; Hansen, A.; Becker, U. Efficient, approximate and parallel Hartree-Fock and hybrid DFT calculations. A 'chain-of-spheres' algorithm for the Hartree-Fock exchange. *Chem. Phys.* **2009**, *356*, 98−109.
(81) Plessow, P.; Weigend, F. Seminumerical calculation of the Hartree-Fock exchange matrix: Application to two-component procedures and efficient evaluation of local hybrid density functionals. *J. Comput. Chem.* **2012**, *33*, 810−816.
(82) Bahmann, H.; Kaupp, M. Efficient self-consistent implementation of local hybrid functionals. *J. Chem. Theory Comput.* **2015**, *11*, 1540−1548.
(83) Maier, T. M.; Bahmann, H.; Kaupp, M. Efficient Seminumerical Implementation of Global and Local Hybrid Functionals for Time-Dependent Density Functional Theory. *J. Chem. Theory Comput.* **2015**, *11*, 4226−4237.
(84) Klawohn, S.; Bahmann, H.; Kaupp, M. Implementation of Molecular Gradients for Local Hybrid Density Functionals Using Seminumerical Integration Techniques. *J. Chem. Theory Comput.* **2016**, *12*, 4254−4262.
(85) Liu, F.; Kong, J. Efficient Computation of Exchange Energy Density with Gaussian Basis Functions. *J. Chem. Theory Comput.* **2017**, *13*, 2571−2580.
(86) Laqua, H.; Kussmann, J.; Ochsenfeld, C. Efficient and Linear-Scaling Seminumerical Method for Local Hybrid Density Functionals. *J. Chem. Theory Comput.* **2018**, *14*, 3451−3458.
(87) Holzer, C. An improved seminumerical Coulomb and exchange algorithm for properties and excited states in modern density functional theory. *J. Chem. Phys.* **2020**, *153*, 184115.
(88) Laqua, H.; Thompson, T. H.; Kussmann, J.; Ochsenfeld, C. Highly Efficient, Linear-Scaling Seminumerical Exact-Exchange Method for Graphic Processing Units. *J. Chem. Theory Comput.* **2020**, *16*, 1456−1468.
(89) Helmich-Paris, B.; de Souza, B.; Neese, F.; Izsák, R. An improved chain of spheres for exchange algorithm. *J. Chem. Phys.* **2021**, *155*, 104109.
(90) Laqua, H.; Kussmann, J.; Ochsenfeld, C. Accelerating seminumerical Fock-exchange calculations using mixed single- and double-precision arithmethic. *J. Chem. Phys.* **2021**, *154*, 214116.

https://doi.org/10.1021/acs.jctc.4c00193
J. Chem. Theory Comput. 2024, 20, 3706−3718

(91) Becke, A. D. A multicenter numerical integration scheme for polyatomic molecules. *J. Chem. Phys.* **1988**, *88*, 2547−2553.
(92) Treutler, O.; Ahlrichs, R. Efficient molecular numerical integration schemes. *J. Chem. Phys.* **1995**, *102*, 346−354.
(93) Laqua, H.; Kussmann, J.; Ochsenfeld, C. An improved molecular partitioning scheme for numerical quadratures in density functional theory. *J. Chem. Phys.* **2018**, *149*, 204111.
(94) Thompson, T. H.; Ochsenfeld, C. Integral partition bounds for fast and effective screening of general one-two-and many-electron integrals. *J. Chem. Phys.* **2019**, *150*, 044101.
(95) Liakos, D. G.; Izsák, R.; Valeev, E. F.; Neese, F. What is the most efficient way to reach the canonical MP2 basis set limit? *Mol. Phys.* **2013**, *111*, 2653−2662.
(96) Manby, F. R. Density fitting in second-order linear-r12 Møller−Plesset perturbation theory. *J. Chem. Phys.* **2003**, *119*, 4607−4613.
(97) Ten-no, S.; Manby, F. R. Density fitting for the decomposition of three-electron integrals in explicitly correlated electronic structure theory. *J. Chem. Phys.* **2003**, *119*, 5358−5363.
(98) May, A. J.; Manby, F. R. An explicitly correlated second order Møller-Plesset theory using a frozen Gaussian geminal. *J. Chem. Phys.* **2004**, *121*, 4479−4485.
(99) Klopper, W.; Samson, C. C. M. Explicitly correlated second-order Møller−Plesset methods with auxiliary basis sets. *J. Chem. Phys.* **2002**, *116*, 6397−6410.
(100) Bokhan, D.; Bernadotte, S.; Ten-no, S. Implementation of the CCSD(T)(F12) method using numerical quadratures. *Chem. Phys. Lett.* **2009**, *469*, 214−218.
(101) Bokhan, D.; Trubnikov, D. N. Explicitly correlated second-order Møller-Plesset perturbation theory employing pseudospectral numerical quadratures. *J. Chem. Phys.* **2012**, *136*, 204110.
(102) Thompson, T. H. Integral Bounds and Rigorous Screening Algorithms for Reduced Scaling in Explicitly Correlated, Semi-Numerical, and Non-Hermitian Quantum Chemistry. Ph.D. Thesis, University of Munich (LMU), 2020.
(103) Sacchetta, F.; Graf, D.; Laqua, H.; Ambroise, M. A.; Kussmann, J.; Dreuw, A.; Ochsenfeld, C. An effective sub-quadratic scaling atomic-orbital reformulation of the scaled opposite-spin RI-CC2 ground-state model using Cholesky-decomposed densities and an attenuated Coulomb metric. *J. Chem. Phys.* **2022**, *157*, 104104.
(104) Boys, S. F.; Egerton, A. C. Electronic wave functions - I. A general method of calculation for the stationary states of any molecular system. *Proc. R. Soc. A* **1950**, *200*, 542−554.
(105) Barca, G. M. J.; Gill, P. M. W. Two-Electron Integrals over Gaussian Geminals. *J. Chem. Theory Comput.* **2016**, *12*, 4915−4924.
(106) Barca, G. M. J.; Loos, P.-F. Three- and four-electron integrals involving Gaussian geminals: Fundamental integrals, upper bounds, and recurrence relations. *J. Chem. Phys.* **2017**, *147*, 024103.
(107) Intel Corporation. *Intel Math Kernel Library*, version 2023.4.0, 2023. https://software.intel.com/en-us/mkl.
(108) OpenMP Architecture Review Board (ARB). *OpenMP Application Program Interface*, version 5.1.0, 2023. https://www.openmp.org/.
(109) Obara, S.; Saika, A. Efficient recursive computation of molecular integrals over Cartesian Gaussian functions. *J. Chem. Phys.* **1986**, *84*, 3963−3974.
(110) Kussmann, J.; Ochsenfeld, C. Pre-selective screening for matrix elements in linear-scaling exact exchange calculations. *J. Chem. Phys.* **2013**, *138*, 134114.
(111) Kussmann, J.; Ochsenfeld, C. Preselective screening for linear-scaling exact exchange-gradient calculations for graphics processing units and general strong-scaling massively parallel calculations. *J. Chem. Theory Comput.* **2015**, *11*, 918−922.
(112) Kussmann, J.; Ochsenfeld, C. Employing OpenCL to Accelerate Ab Initio Calculations on Graphics Processing Units. *J. Chem. Theory Comput.* **2017**, *13*, 2712−2716.
(113) Kussmann, J.; Ochsenfeld, C. Hybrid CPU/GPU Integral Engine for Strong-Scaling Ab Initio Methods. *J. Chem. Theory Comput.* **2017**, *13*, 3153−3159.
(114) Pulay, P. Convergence acceleration of iterative sequences. The case of SCF iteration. *Chem. Phys. Lett.* **1980**, *73*, 393−398.
(115) Pulay, P. Improved SCF Convergence Acceleration. *J. Comput. Chem.* **1982**, *3*, 556−560.
(116) Kussmann, J.; Laqua, H.; Ochsenfeld, C. Highly Efficient Resolution-of-Identity Density Functional Theory Calculations on Central and Graphics Processing Units. *J. Chem. Theory Comput.* **2021**, *17*, 1512−1521.
(117) Weigend, F. A fully direct RI-HF algorithm: Implementation, optimised auxiliary basis sets, demonstration of accuracy and efficiency. *Phys. Chem. Chem. Phys.* **2002**, *4*, 4285−4291.
(118) Peterson, K. A.; Adler, T. B.; Werner, H.-J. Systematically convergent basis sets for explicitly correlated wavefunctions: The atoms H, He, B-Ne, and Al-Ar. *J. Chem. Phys.* **2008**, *128*, 084102.
(119) Hill, J. G.; Peterson, K. A. Correlation consistent basis sets for explicitly correlated wavefunctions: Valence and core-valence basis sets for Li, Be, Na, and Mg. *Phys. Chem. Chem. Phys.* **2010**, *12*, 10460−10468.
(120) Hill, J. G.; Peterson, K. A. Correlation consistent basis sets for explicitly correlated wavefunctions: Pseudopotential-based basis sets for the post-*d* main group elements Ga-Rn. *J. Chem. Phys.* **2014**, *141*, 094106.
(121) Shaw, R. A.; Hill, J. G. Approaching the Hartree-Fock Limit through the Complementary Auxiliary Basis Set Singles Correction and Auxiliary Basis Sets. *J. Chem. Theory Comput.* **2017**, *13*, 1691−1698.
(122) Kritikou, S.; Hill, J. G. Auxiliary Basis Sets for Density Fitting in Explicitly Correlated Calculations: The Atoms H-Ar. *J. Chem. Theory Comput.* **2015**, *11*, 5269−5276.
(123) *Intel C++ Compiler*, version 19.1.0.166. https://software.intel.com/c-compilers, 2019.
(124) Boys, S. F.; Bernardi, F. The calculation of small molecular interactions by the differences of separate total energies. Some procedures with reduced errors. *Mol. Phys.* **1970**, *19*, 553−566.
(125) Sedlak, R.; Janowski, T.; Pitoňák, M.; Řezáč, J.; Pulay, P.; Hobza, P. Accuracy of quantum chemical methods for large noncovalent complexes. *J. Chem. Theory Comput.* **2013**, *9*, 3364−3374.
(126) Grimme, S.; Steinmetz, M.; Korth, M. How to compute isomerization energies of organic molecules with quantum chemical methods. *J. Org. Chem.* **2007**, *72*, 2118−2126.
(127) Jurečka, P.; Šponer, J.; Černý, J.; Hobza, P. Benchmark database of accurate (MP2 and CCSD(T) complete basis set limit) interaction energies of small model complexes, DNA base pairs, and amino acid pairs. *Phys. Chem. Chem. Phys.* **2006**, *8*, 1985−1993.
(128) Řezáč, J.; Riley, K. E.; Hobza, P. S66: A well-balanced database of benchmark interaction energies relevant to biomolecular structures. *J. Chem. Theory Comput.* **2011**, *7*, 2427−2438.
(129) Goerigk, L.; Hansen, A.; Bauer, C.; Ehrlich, S.; Najibi, A.; Grimme, S. A look at the density functional theory zoo with the advanced GMTKN55 database for general main group thermochemistry, kinetics and noncovalent interactions. *Phys. Chem. Chem. Phys.* **2017**, *19*, 32184−32215.
(130) Setiawan, D.; Kraka, E.; Cremer, D. Strength of the Pnicogen Bond in Complexes Involving Group Va Elements N, P, and As. *J. Phys. Chem. A* **2015**, *119*, 1642−1656.
(131) Grimme, S.; Antony, J.; Ehrlich, S.; Krieg, H. A consistent and accurate ab initio parametrization of density functional dispersion correction (DFT-D) for the 94 elements H-Pu. *J. Chem. Phys.* **2010**, *132*, 154104.
(132) Tornai, G. J.; Ladjánszki, I.; Rák, Á.; Kis, G.; Cserey, G. Calculation of Quantum Chemical Two-Electron Integrals by Applying Compiler Technology on GPU. *J. Chem. Theory Comput.* **2019**, *15*, 5319−5331.

https://doi.org/10.1021/acs.jctc.4c00193
J. Chem. Theory Comput. 2024, 20, 3706−3718

Efficient Exploitation of Numerical Quadrature with Distance-Dependent Integral Screening in Explicitly Correlated F12 Theory: Linear Scaling Evaluation of the Most Expensive RI-MP2-F12 Term

Supporting Information

Lars Urban,[†,‡] Henryk Laqua,[†] Travis H. Thompson,[†] and Christian Ochsenfeld[*,†,‡]

†*Chair of Theoretical Chemistry, Department of Chemistry, University of Munich (LMU), D-81377 Munich, Germany*

‡*Max Planck Institute for Solid State Research, D-70569 Stuttgart, Germany*

E-mail: christian.ochsenfeld@uni-muenchen.de

1 Isomerization and Non-Covalent Interaction Energies

Table 1: Mean absolute errors [μE_h] (MAEs), max. absolute errors [μE_h] (MAX), and MAEs relative to the average reference isomerization energy [%] for the ISO34 test set employing NQ/CABS-RI with various grid sizes ($g0$-$g7$) and thresholds ϑ_{F12} and DF/CABS-RI ($\vartheta_{IPB} = 10^{-9}$) for different cc-pVXZ-F12 (X = D, T, Q) basis set combinations.

Method		cc-pVDZ-F12			cc-pVTZ-F12			cc-pVQZ-F12		
Grid/DF	ϑ	MAE	MAX	$\frac{MAE}{AVG}$	MAE	MAX	$\frac{MAE}{AVG}$	MAE	MAX	$\frac{MAE}{AVG}$
g0	10^{-8}	44.05	173.19	1.5188	37.77	155.99	1.2580	42.44	154.11	1.4114
	10^{-9}	41.58	166.13	1.4334	39.23	158.92	1.3066	35.22	146.54	1.1712
	10^{-10}	41.56	166.10	1.4329	39.15	159.19	1.3037	35.87	150.54	1.1929
	0	41.56	166.08	1.4330	39.13	159.10	1.3032	35.85	150.66	1.1922
g1	10^{-8}	11.60	65.71	0.3998	16.37	67.57	0.5450	19.98	70.02	0.6644
	10^{-9}	8.99	65.15	0.3098	9.25	65.45	0.3081	8.58	65.90	0.2852
	10^{-10}	8.98	64.99	0.3098	9.12	65.51	0.3036	8.83	65.34	0.2936
	0	8.99	64.95	0.3098	9.14	65.56	0.3043	8.85	65.23	0.2942
g2	10^{-8}	5.89	45.65	0.2032	9.78	40.65	0.3257	15.94	82.10	0.5302
	10^{-9}	1.13	7.72	0.0391	1.37	7.12	0.0456	1.78	7.36	0.0593
	10^{-10}	1.12	7.93	0.0385	1.06	8.12	0.0354	0.97	7.90	0.0322
	0	1.12	8.03	0.0386	1.07	8.05	0.0357	0.98	7.96	0.0328
g3	10^{-8}	7.51	62.78	0.2588	13.11	52.91	0.4365	22.81	96.32	0.7585
	10^{-9}	0.29	0.74	0.0101	1.01	3.44	0.0337	1.63	5.86	0.0542
	10^{-10}	0.19	0.72	0.0066	0.15	0.69	0.0051	0.22	0.61	0.0073
	0	0.18	0.74	0.0064	0.18	0.69	0.0059	0.16	0.70	0.0052
g4	10^{-8}	8.23	62.52	0.2837	13.32	53.54	0.4437	25.91	119.56	0.8616
	10^{-9}	0.20	0.60	0.0070	1.15	3.89	0.0382	1.74	5.00	0.0579
	10^{-10}	0.08	0.63	0.0028	0.11	0.71	0.0035	0.13	0.52	0.0045
	0	0.07	0.67	0.0025	0.07	0.65	0.0023	0.06	0.65	0.0021
g5	10^{-8}	9.38	77.41	0.3234	16.40	61.02	0.5461	27.40	113.10	0.9114
	10^{-9}	0.21	0.73	0.0071	1.17	3.61	0.0391	1.95	5.66	0.0647
	10^{-10}	0.03	0.13	0.0010	0.06	0.20	0.0022	0.11	0.41	0.0035
	0	0.01	0.14	0.0005	0.01	0.13	0.0005	0.02	0.13	0.0005
g6	10^{-8}	13.05	85.58	0.4500	17.99	65.94	0.5993	30.86	116.62	1.0264
	10^{-9}	0.27	1.70	0.0092	1.22	3.84	0.0407	2.11	6.89	0.0703
	10^{-10}	0.03	0.13	0.0012	0.07	0.21	0.0023	0.13	0.38	0.0043
	0	0.00	0.01	0.0001	0.00	0.01	0.0001	0.00	0.01	0.0001
g7	10^{-8}	16.93	125.60	0.5838	17.65	75.28	0.5878	38.64	149.75	1.2851
	10^{-9}	0.30	2.03	0.0103	1.25	4.01	0.0417	2.19	7.65	0.0729
	10^{-10}	0.04	0.13	0.0013	0.08	0.25	0.0028	0.13	0.39	0.0044
DF		3.07	11.89	0.1058	2.20	9.34	0.0734	0.61	2.70	0.0203

Table 2: Mean absolute errors [μE_h] (MAEs), max. absolute errors [μE_h] (MAX), and MAEs relative to the average reference non-covalent interaction energy [%] for the L7 test set employing NQ/CABS-RI with various grid sizes ($g0$-$g7$) and thresholds ϑ_{F12} and DF/CABS-RI ($\vartheta_{IPB} = 10^{-9}$) for different cc-pVXZ-F12 (X = D, T, Q) basis set combinations.

Method		cc-pVDZ-F12			cc-pVTZ-F12			cc-pVQZ-F12		
Grid/DF	ϑ	MAE	MAX	$\frac{MAE}{AVG}$	MAE	MAX	$\frac{MAE}{AVG}$	MAE	MAX	$\frac{MAE}{AVG}$
g0	10^{-8}	4.84	9.81	0.0497	20.76	59.19	0.2165	22.23	40.61	0.2321
	10^{-9}	6.43	14.59	0.0660	9.69	17.92	0.1011	8.64	20.29	0.0902
	10^{-10}	6.86	14.93	0.0704	7.38	17.67	0.0769	7.13	16.95	0.0744
	0	6.94	14.96	0.0713	7.20	16.92	0.0751	7.16	16.90	0.0748
g1	10^{-8}	5.58	10.27	0.0573	25.67	61.88	0.2677	30.38	72.88	0.3172
	10^{-9}	1.74	4.80	0.0178	5.09	12.49	0.0531	4.42	12.78	0.0462
	10^{-10}	1.76	4.22	0.0181	1.97	5.09	0.0206	2.00	3.76	0.0208
	0	1.75	4.00	0.0179	2.01	4.56	0.0210	1.92	3.93	0.0201
g2	10^{-8}	3.49	5.98	0.0358	17.40	54.57	0.1814	23.33	67.22	0.2436
	10^{-9}	0.68	3.06	0.0070	3.61	8.02	0.0376	4.77	9.51	0.0499
	10^{-10}	0.32	1.00	0.0033	0.50	1.20	0.0052	0.47	0.95	0.0049
	0	0.33	0.88	0.0034	0.34	1.01	0.0035	0.34	1.00	0.0036
g3	10^{-8}	8.06	10.66	0.0828	26.37	67.31	0.2750	37.64	74.21	0.3931
	10^{-9}	0.78	2.15	0.0080	4.92	11.10	0.0513	5.73	14.03	0.0598
	10^{-10}	0.16	0.49	0.0016	0.27	0.92	0.0028	0.31	0.49	0.0032
	0	0.07	0.24	0.0007	0.06	0.24	0.0006	0.06	0.25	0.0006
g4	10^{-8}	8.58	14.46	0.0881	35.19	79.47	0.3670	30.59	69.70	0.3195
	10^{-9}	0.66	1.85	0.0068	5.45	11.52	0.0569	7.92	18.46	0.0827
	10^{-10}	0.14	0.32	0.0014	0.32	0.89	0.0033	0.39	0.59	0.0040
	0	0.01	0.04	0.0001	0.01	0.04	0.0001	0.01	0.05	0.0001
g5	10^{-8}	10.09	16.22	0.1036	33.45	70.60	0.3489	43.11	103.33	0.4502
	10^{-9}	0.73	2.11	0.0075	5.57	12.01	0.0580	7.06	16.85	0.0737
	10^{-10}	0.15	0.28	0.0015	0.31	0.93	0.0032	0.39	0.74	0.0041
	0	0.00	0.01	0.0000	0.00	0.01	0.0000	0.00	0.01	0.0000
g6	10^{-8}	11.86	23.33	0.1217	33.95	67.15	0.3540	51.38	103.05	0.5365
	10^{-9}	0.62	2.04	0.0064	5.79	13.48	0.0604	9.08	21.20	0.0949
	10^{-10}	0.16	0.31	0.0016	0.32	1.02	0.0034	0.46	0.82	0.0048
	0	0.00	0.00	0.0000	0.00	0.00	0.0000	0.00	0.00	0.0000
g7	10^{-8}	17.56	35.99	0.1803	34.25	53.10	0.3572	64.07	113.13	0.6690
	10^{-9}	0.66	1.99	0.0068	6.02	14.07	0.0628	10.83	24.12	0.1131
	10^{-10}	0.16	0.32	0.0017	0.34	0.97	0.0036	0.53	0.94	0.0056
DF	10^{-9}	3.32	8.39	0.0341	1.70	2.85	0.0177	0.79	1.69	0.0082

Table 3: Mean absolute errors [μE_h] (MAEs), max. absolute errors [μE_h] (MAX), and MAEs relative to the average reference non-covalent interaction energy [%] for the S22 test set employing NQ/CABS-RI with various grid sizes ($g0$-$g7$) and thresholds ϑ_{F12} and DF/CABS-RI ($\vartheta_{IPB} = 10^{-9}$) for different cc-pVXZ-F12 (X = D, T, Q) basis set combinations.

Method		cc-pVDZ-F12			cc-pVTZ-F12			cc-pVQZ-F12		
Grid/DF	ϑ	MAE	MAX	$\frac{MAE}{AVG}$	MAE	MAX	$\frac{MAE}{AVG}$	MAE	MAX	$\frac{MAE}{AVG}$
g0	10^{-8}	6.60	30.18	0.2120	6.04	27.69	0.1956	9.59	54.48	0.3105
	10^{-9}	5.24	27.05	0.1683	5.85	33.13	0.1895	5.39	31.00	0.1747
	10^{-10}	5.32	27.61	0.1708	6.03	33.94	0.1951	5.90	33.12	0.1910
	0	5.31	27.63	0.1706	6.02	33.71	0.1948	5.93	33.13	0.1921
g1	10^{-8}	4.03	53.86	0.1294	3.85	17.98	0.1247	10.41	34.47	0.3373
	10^{-9}	0.75	2.88	0.0242	1.11	3.91	0.0358	1.42	8.42	0.0458
	10^{-10}	0.66	2.67	0.0212	0.64	2.96	0.0208	0.62	2.87	0.0200
	0	0.66	2.61	0.0211	0.64	3.16	0.0206	0.61	2.86	0.0198
g2	10^{-8}	4.87	79.28	0.1565	3.17	22.82	0.1025	11.23	33.14	0.3637
	10^{-9}	0.30	1.51	0.0096	0.62	2.58	0.0199	1.51	8.65	0.0488
	10^{-10}	0.09	0.32	0.0030	0.10	0.23	0.0033	0.11	0.45	0.0036
	0	0.08	0.27	0.0025	0.09	0.25	0.0029	0.09	0.24	0.0028
g3	10^{-8}	6.46	103.53	0.2075	7.30	30.42	0.2363	15.62	46.36	0.5060
	10^{-9}	0.36	2.86	0.0117	0.92	4.72	0.0298	2.08	10.54	0.0672
	10^{-10}	0.04	0.18	0.0014	0.09	0.34	0.0029	0.06	0.29	0.0020
	0	0.02	0.08	0.0006	0.02	0.08	0.0006	0.02	0.08	0.0006
g4	10^{-8}	6.84	100.68	0.2198	7.80	22.00	0.2524	19.35	56.33	0.6267
	10^{-9}	0.41	3.30	0.0133	1.09	5.95	0.0354	2.35	10.87	0.0763
	10^{-10}	0.04	0.16	0.0013	0.09	0.44	0.0028	0.07	0.30	0.0023
	0	0.00	0.01	0.0001	0.00	0.02	0.0001	0.00	0.02	0.0001
g5	10^{-8}	7.55	122.20	0.2427	6.30	21.95	0.2040	19.83	56.19	0.6424
	10^{-9}	0.43	3.58	0.0137	1.07	4.44	0.0345	2.42	11.40	0.0785
	10^{-10}	0.04	0.16	0.0012	0.10	0.46	0.0032	0.07	0.32	0.0024
	0	0.00	0.01	0.0000	0.00	0.01	0.0001	0.00	0.01	0.0001
g6	10^{-8}	11.39	198.86	0.3661	8.12	24.81	0.2630	21.47	57.41	0.6953
	10^{-9}	0.49	4.70	0.0159	1.08	4.82	0.0350	2.76	10.97	0.0894
	10^{-10}	0.04	0.19	0.0014	0.10	0.43	0.0031	0.09	0.48	0.0029
	0	0.00	0.00	0.0000	0.00	0.00	0.0000	0.00	0.00	0.0000
g7	10^{-8}	14.11	249.11	0.4534	13.29	48.89	0.4304	22.68	58.70	0.7346
	10^{-9}	0.54	5.34	0.0173	1.29	5.62	0.0417	3.19	12.05	0.1032
	10^{-10}	0.04	0.20	0.0014	0.10	0.37	0.0031	0.11	0.59	0.0034
DF	10^{-9}	1.14	4.91	0.0365	0.26	0.92	0.0085	0.28	0.61	0.0090

Table 4: Mean absolute errors [μE_h] (MAEs), max. absolute errors [μE_h] (MAX), and MAEs relative to the average reference non-covalent interaction energy [%] for the S66 test set employing NQ/CABS-RI with various grid sizes ($g0$-$g7$) and thresholds ϑ_{F12} and DF/CABS-RI ($\vartheta_{IPB} = 10^{-9}$) for different cc-pVXZ-F12 (X = D, T, Q) basis set combinations.

Method		cc-pVDZ-F12			cc-pVTZ-F12			cc-pVQZ-F12		
Grid/DF	ϑ	MAE	MAX	$\frac{MAE}{AVG}$	MAE	MAX	$\frac{MAE}{AVG}$	MAE	MAX	$\frac{MAE}{AVG}$
g0	10^{-8}	4.26	30.70	0.1965	6.44	71.99	0.2983	8.05	42.23	0.3729
	10^{-9}	3.92	27.11	0.1810	4.56	29.17	0.2111	4.52	31.63	0.2095
	10^{-10}	3.97	27.11	0.1833	4.50	29.30	0.2083	4.46	30.05	0.2064
	0	3.97	27.10	0.1834	4.52	29.84	0.2092	4.46	30.03	0.2064
g1	10^{-8}	1.56	26.46	0.0720	4.01	33.37	0.1854	9.46	51.85	0.4382
	10^{-9}	0.41	2.80	0.0190	0.56	2.80	0.0257	1.09	9.19	0.0504
	10^{-10}	0.34	2.26	0.0155	0.33	2.02	0.0152	0.31	2.16	0.0144
	0	0.34	2.22	0.0155	0.33	2.50	0.0154	0.32	2.21	0.0146
g2	10^{-8}	1.52	19.47	0.0699	4.34	23.13	0.2007	10.90	57.25	0.5048
	10^{-9}	0.21	1.19	0.0097	0.31	1.66	0.0141	1.01	9.31	0.0468
	10^{-10}	0.06	0.26	0.0029	0.08	0.38	0.0038	0.07	0.39	0.0034
	0	0.06	0.25	0.0026	0.06	0.22	0.0028	0.06	0.23	0.0026
g3	10^{-8}	2.43	36.00	0.1120	4.42	21.55	0.2047	14.80	58.33	0.6856
	10^{-9}	0.21	1.16	0.0096	0.37	2.98	0.0171	1.28	11.66	0.0594
	10^{-10}	0.04	0.13	0.0017	0.06	0.50	0.0030	0.05	0.29	0.0022
	0	0.01	0.04	0.0005	0.01	0.04	0.0005	0.01	0.04	0.0005
g4	10^{-8}	2.99	48.23	0.1379	5.93	38.88	0.2744	17.58	62.46	0.8142
	10^{-9}	0.22	1.30	0.0103	0.46	3.00	0.0215	1.34	12.52	0.0620
	10^{-10}	0.04	0.15	0.0017	0.07	0.46	0.0032	0.04	0.34	0.0021
	0	0.00	0.02	0.0002	0.00	0.02	0.0002	0.00	0.02	0.0002
g5	10^{-8}	3.43	70.91	0.1582	4.61	20.20	0.2136	17.74	62.31	0.8213
	10^{-9}	0.23	1.41	0.0106	0.42	3.27	0.0194	1.43	12.55	0.0661
	10^{-10}	0.04	0.16	0.0018	0.07	0.51	0.0033	0.05	0.37	0.0022
	0	0.00	0.01	0.0001	0.00	0.01	0.0001	0.00	0.01	0.0001
g6	10^{-8}	4.44	95.62	0.2050	6.59	20.26	0.3051	20.76	62.40	0.9613
	10^{-9}	0.23	1.47	0.0106	0.49	3.15	0.0226	1.58	12.27	0.0730
	10^{-10}	0.04	0.20	0.0020	0.07	0.51	0.0032	0.05	0.49	0.0025
	0	0.00	0.00	0.0000	0.00	0.00	0.0000	0.00	0.00	0.0000
g7	10^{-8}	5.45	127.87	0.2515	9.22	47.18	0.4266	23.91	78.25	1.1073
	10^{-9}	0.25	1.52	0.0117	0.52	3.82	0.0242	1.81	13.78	0.0837
	10^{-10}	0.05	0.23	0.0022	0.07	0.51	0.0033	0.06	0.56	0.0029
DF	10^{-9}	0.75	4.79	0.0346	0.29	0.89	0.0132	0.21	0.62	0.0097

Table 5: Mean absolute errors [μE_h] (MAEs), max. absolute errors [μE_h] (MAX), and MAEs relative to the average reference non-covalent interaction energy [%] for the CARBHB12 test set employing NQ/CABS-RI with various grid sizes ($g0$-$g7$) and thresholds ϑ_{F12} and DF/CABS-RI ($\vartheta_{IPB} = 10^{-9}$) for different cc-pVXZ-F12 (X = D, T, Q) basis set combinations.

Method		cc-pVDZ-F12			cc-pVTZ-F12			cc-pVQZ-F12		
Grid/DF	ϑ	MAE	MAX	$\frac{MAE}{AVG}$	MAE	MAX	$\frac{MAE}{AVG}$	MAE	MAX	$\frac{MAE}{AVG}$
g0	10^{-8}	1093.26	3884.24	6.6866	471.79	1161.50	2.8776	33.80	143.46	0.2060
	10^{-9}	14.87	28.12	0.0909	14.10	52.20	0.0860	8.07	26.48	0.0492
	10^{-10}	11.75	28.19	0.0719	6.23	30.79	0.0380	7.45	28.50	0.0454
	0	11.74	28.19	0.0718	6.18	30.81	0.0377	7.57	28.73	0.0461
g1	10^{-8}	770.62	2601.54	4.7133	488.61	1746.09	2.9801	48.30	157.73	0.2943
	10^{-9}	4.48	17.73	0.0274	14.73	67.86	0.0898	3.68	9.33	0.0224
	10^{-10}	1.99	4.02	0.0121	1.64	3.80	0.0100	1.55	3.31	0.0095
	0	1.97	3.95	0.0120	1.24	3.45	0.0076	1.41	3.24	0.0086
g2	10^{-8}	424.03	1987.49	2.5935	479.08	2299.27	2.9220	29.78	91.05	0.1815
	10^{-9}	2.41	9.27	0.0148	27.40	212.38	0.1671	2.36	7.61	0.0144
	10^{-10}	0.13	0.33	0.0008	0.33	1.00	0.0020	0.22	0.45	0.0013
	0	0.08	0.33	0.0005	0.11	0.34	0.0007	0.10	0.28	0.0006
g3	10^{-8}	832.58	3139.83	5.0923	370.20	1617.29	2.2579	30.93	108.70	0.1885
	10^{-9}	3.91	14.00	0.0239	53.30	399.26	0.3251	4.57	11.97	0.0279
	10^{-10}	0.05	0.14	0.0003	0.91	4.78	0.0055	0.20	0.53	0.0012
	0	0.02	0.05	0.0001	0.02	0.04	0.0001	0.01	0.03	0.0001
g4	10^{-8}	677.93	2709.62	4.1464	311.30	1352.12	1.8987	32.70	86.32	0.1993
	10^{-9}	5.59	20.58	0.0342	65.82	407.39	0.4015	5.97	15.62	0.0364
	10^{-10}	0.06	0.24	0.0004	1.10	4.21	0.0067	0.36	1.11	0.0022
	0	0.00	0.01	0.0000	0.00	0.00	0.0000	0.00	0.00	0.0000
g5	10^{-8}	949.09	2869.17	5.8048	310.10	1522.83	1.8913	31.50	85.09	0.1920
	10^{-9}	4.38	15.69	0.0268	44.94	209.96	0.2741	5.92	18.46	0.0361
	10^{-10}	0.07	0.21	0.0004	0.96	5.42	0.0058	0.23	0.52	0.0014
	0	0.00	0.00	0.0000	0.00	0.00	0.0000	0.00	0.00	0.0000
g6	10^{-8}	986.96	3973.40	6.0364	283.87	1212.63	1.7314	32.68	71.04	0.1992
	10^{-9}	3.35	17.96	0.0205	74.86	443.69	0.4566	6.69	17.08	0.0408
	10^{-10}	0.05	0.22	0.0003	1.30	6.06	0.0079	0.27	0.72	0.0016
	0	0.00	0.00	0.0000	0.00	0.00	0.0000	0.00	0.00	0.0000
g7	10^{-8}	904.82	3964.77	5.5341	299.55	1315.03	1.8270	33.30	115.35	0.2030
	10^{-9}	8.08	60.23	0.0494	53.73	454.92	0.3277	6.46	15.50	0.0394
	10^{-10}	0.06	0.24	0.0003	1.23	5.51	0.0075	0.28	0.61	0.0017
DF	10^{-9}	7.49	62.88	0.0458	3.06	28.20	0.0187	1.03	7.90	0.0063

Table 6: Mean absolute errors [μE_h] (MAEs), max. absolute errors [μE_h] (MAX), and MAEs relative to the average reference non-covalent interaction energy [%] for the PNICO23 test set employing NQ/CABS-RI with various grid sizes ($g0$-$g7$) and thresholds ϑ_{F12} and DF/CABS-RI ($\vartheta_{IPB} = 10^{-9}$) for different cc-pVXZ-F12 (X = D, T, Q) basis set combinations.

Method		cc-pVDZ-F12			cc-pVTZ-F12			cc-pVQZ-F12		
Grid/DF	ϑ	MAE	MAX	$\frac{\text{MAE}}{\text{AVG}}$	MAE	MAX	$\frac{\text{MAE}}{\text{AVG}}$	MAE	MAX	$\frac{\text{MAE}}{\text{AVG}}$
g0	10^{-8}	540.48	6345.92	42.8457	388.20	4913.46	30.2768	32.15	167.75	2.5037
	10^{-9}	20.85	280.35	1.6527	3.93	22.28	0.3064	4.47	17.00	0.3481
	10^{-10}	2.37	8.86	0.1879	2.23	8.75	0.1740	2.58	9.00	0.2005
	0	2.36	9.16	0.1871	2.46	9.15	0.1918	2.51	9.19	0.1955
g1	10^{-8}	658.82	9624.31	52.2274	277.61	2130.56	21.6519	38.41	585.87	2.9915
	10^{-9}	14.10	90.78	1.1177	3.06	13.79	0.2389	5.28	41.43	0.4109
	10^{-10}	0.72	2.81	0.0571	0.37	1.09	0.0288	0.42	1.49	0.0324
	0	0.32	1.17	0.0254	0.30	1.13	0.0233	0.31	1.15	0.0240
g2	10^{-8}	523.69	6531.29	41.5152	238.68	2523.47	18.6156	62.98	814.42	4.9046
	10^{-9}	25.54	362.79	2.0246	5.60	27.73	0.4371	5.86	51.31	0.4560
	10^{-10}	0.69	4.63	0.0547	0.36	2.21	0.0277	0.13	0.44	0.0104
	0	0.05	0.20	0.0041	0.05	0.19	0.0038	0.05	0.19	0.0039
g3	10^{-8}	542.59	6809.78	43.0128	401.50	2974.28	31.3141	37.00	388.55	2.8817
	10^{-9}	20.23	200.28	1.6035	10.25	81.23	0.7996	6.53	69.05	0.5088
	10^{-10}	0.62	2.42	0.0495	0.30	1.17	0.0233	0.22	1.84	0.0170
	0	0.01	0.05	0.0005	0.01	0.05	0.0004	0.01	0.05	0.0004
g4	10^{-8}	514.58	6370.00	40.7928	639.55	4164.29	49.8802	114.01	996.04	8.8788
	10^{-9}	32.47	321.47	2.5736	12.86	109.33	1.0028	10.34	85.32	0.8053
	10^{-10}	0.92	4.22	0.0729	0.41	1.86	0.0319	0.31	2.84	0.0238
	0	0.00	0.01	0.0001	0.00	0.01	0.0001	0.00	0.01	0.0001
g5	10^{-8}	554.13	7282.93	43.9279	391.35	3279.11	30.5226	220.66	2468.50	17.1841
	10^{-9}	44.22	426.92	3.5055	10.19	98.36	0.7946	11.46	106.12	0.8927
	10^{-10}	0.73	5.62	0.0576	0.37	1.41	0.0287	0.24	2.02	0.0190
	0	0.00	0.00	0.0000	0.00	0.01	0.0000	0.00	0.01	0.0000
g6	10^{-8}	472.44	5988.03	37.4523	681.09	3363.50	53.1199	229.35	3192.75	17.8607
	10^{-9}	56.51	360.10	4.4800	11.10	78.09	0.8653	11.71	154.82	0.9123
	10^{-10}	0.71	3.96	0.0563	0.52	3.32	0.0406	0.29	2.40	0.0229
	0	0.00	0.00	0.0000	0.00	0.00	0.0000	0.00	0.00	0.0000
g7	10^{-8}	470.44	6042.15	37.2938	1125.80	5879.79	87.8039	359.84	4183.55	28.0231
	10^{-9}	67.23	429.37	5.3296	12.75	117.54	0.9944	18.64	182.39	1.4516
	10^{-10}	0.90	5.34	0.0715	0.54	3.41	0.0418	0.32	2.66	0.0249
DF	10^{-9}	2.32	13.12	0.1837	1.03	5.99	0.0805	0.48	1.92	0.0377

Table 7: Mean absolute errors [μE_h] (MAEs), max. absolute errors [μE_h] (MAX), and MAEs relative to the average reference non-covalent interaction energy [%] for the ADIM6 test set employing NQ/CABS-RI with various grid sizes ($g0$-$g7$) and thresholds ϑ_{F12} and DF/CABS-RI ($\vartheta_{IPB} = 10^{-9}$) for different cc-pVXZ-F12 (X = D, T, Q) basis set combinations.

Method		cc-pVDZ-F12			cc-pVTZ-F12			cc-pVQZ-F12		
Grid/DF	ϑ	MAE	MAX	$\frac{MAE}{AVG}$	MAE	MAX	$\frac{MAE}{AVG}$	MAE	MAX	$\frac{MAE}{AVG}$
g0	10^{-8}	14.82	58.85	1.8577	15.01	64.22	1.8670	21.78	69.49	2.7157
	10^{-9}	14.32	58.44	1.7961	13.79	63.63	1.7143	14.08	64.35	1.7556
	10^{-10}	14.32	58.38	1.7958	13.79	63.48	1.7153	14.02	64.38	1.7482
	0	14.35	58.39	1.7999	13.80	63.48	1.7156	14.10	64.39	1.7579
g1	10^{-8}	3.70	11.65	0.4641	4.46	13.08	0.5552	10.88	18.44	1.3562
	10^{-9}	2.90	12.08	0.3635	2.86	12.36	0.3552	3.22	12.20	0.4018
	10^{-10}	2.82	12.21	0.3538	2.78	12.17	0.3458	2.66	12.07	0.3315
	0	2.84	12.26	0.3567	2.78	12.16	0.3462	2.72	12.08	0.3385
g2	10^{-8}	1.49	3.28	0.1869	0.80	1.67	0.0999	6.55	8.68	0.8167
	10^{-9}	0.78	2.88	0.0982	1.58	2.19	0.1959	1.00	2.45	0.1244
	10^{-10}	0.73	2.76	0.0916	0.68	2.32	0.0848	0.72	2.50	0.0893
	0	0.69	2.70	0.0870	0.68	2.32	0.0849	0.69	2.52	0.0866
g3	10^{-8}	1.30	2.47	0.1627	2.82	3.82	0.3512	13.28	16.92	1.6548
	10^{-9}	0.19	0.27	0.0244	0.26	0.69	0.0323	0.84	1.69	0.1051
	10^{-10}	0.10	0.42	0.0131	0.11	0.48	0.0138	0.10	0.43	0.0130
	0	0.12	0.49	0.0154	0.12	0.47	0.0145	0.11	0.44	0.0142
g4	10^{-8}	1.43	2.68	0.1797	2.97	4.28	0.3687	16.62	21.79	2.0723
	10^{-9}	0.21	0.36	0.0269	0.28	0.49	0.0354	0.88	2.11	0.1093
	10^{-10}	0.07	0.19	0.0085	0.03	0.09	0.0038	0.04	0.12	0.0053
	0	0.03	0.11	0.0036	0.02	0.10	0.0031	0.03	0.10	0.0032
g5	10^{-8}	1.42	2.62	0.1783	3.04	4.30	0.3782	14.27	18.41	1.7794
	10^{-9}	0.20	0.34	0.0247	0.26	0.40	0.0327	1.04	2.30	0.1295
	10^{-10}	0.04	0.08	0.0044	0.01	0.03	0.0015	0.04	0.13	0.0050
	0	0.01	0.02	0.0007	0.01	0.02	0.0006	0.01	0.02	0.0007
g6	10^{-8}	1.63	3.39	0.2048	3.25	4.84	0.4035	18.26	23.45	2.2758
	10^{-9}	0.22	0.36	0.0276	0.29	0.42	0.0364	1.08	2.26	0.1346
	10^{-10}	0.04	0.09	0.0054	0.02	0.03	0.0021	0.04	0.11	0.0046
	0	0.00	0.00	0.0000	0.00	0.00	0.0000	0.00	0.00	0.0000
g7	10^{-8}	1.82	3.97	0.2280	3.40	4.71	0.4232	17.64	25.00	2.1989
	10^{-9}	0.24	0.38	0.0301	0.37	0.51	0.0456	1.36	2.85	0.1693
	10^{-10}	0.05	0.10	0.0057	0.02	0.03	0.0024	0.03	0.08	0.0041
DF	10^{-9}	0.29	0.35	0.0358	0.51	0.77	0.0639	0.15	0.29	0.0185

4.4 Publication IV

Formulation of an Efficient $\mathcal{O}(M^4)$-Scaling Explicitly Correlated MP2-F12 Correction by Combining Numerical Quadrature with Density Fitting and CABS-RI

L. Urban, H. Laqua, T. H. Thompson, and C. Ochsenfeld,
J. Chem. Theory Comput. **2026**, DOI: https://doi.org/10.1021/acs.jctc.5c01874

Abstract:

We present a novel approach that combines numerical quadrature with density fitting and CABS-RI for the evaluation of exchange-type intermediates in RI-MP2-F12 theory, rigorously reducing the formal and practical scaling of the total correction from $\mathcal{O}(M^5)$ to $\mathcal{O}(M^4)$. Our new hybrid NQ/DF/CABS-RI ansatz is based directly on our previously developed NQ/CABS-RI method for the efficient evaluation of 6c3e integrals [Urban, L.; Laqua, H; Thompson, T. H.; Ochsenfeld, C. *J. Chem. Theory Comput.* 2024, *20*, 3706-3718] and extends this approach to the optimized computation of products of 4c2e integrals. In this framework, the main exchange-type intermediates $\mathcal{V}$, $\mathcal{X}$, and $\mathcal{B}$ are reformulated, resulting in more compact expressions, increased shared computations, and fewer CABS-RI insertions. We introduce efficient algorithms that cover all exchange-type contributions, including advantageous batching of integrals. Benchmarks show that NQ/DF/CABS-RI achieves mean errors below 0.01 kcal/mol for non-covalent interaction and isomerization energies already with small to modest grid sizes, while the numerical precision can be adjusted to balance computational cost. Empirical scaling was determined using linear glycine chains, demonstrating the expected $\mathcal{O}(M^4)$ behavior for the rate-determining steps, with the remaining exchange-type expressions scaling nearly linearly. Compared with an idealized DF/CABS-RI implementation, our approach achieves speedups of roughly one order of magnitude for the most expensive steps with virtually no loss of numerical accuracy. Systems with strongly delocalized electronic structures benefit particularly. For example, in a nanotube with 168 carbon atoms, the computational time for the most demanding expressions is reduced from 9.97 to 1.25 days, bringing the cost much closer to that of conventional DF-MP2. At present, NQ/DF/CABS-RI achieves efficient $\mathcal{O}(M^4)$ scaling, and further cost reductions are anticipated through the introduction of integral screening based on Cholesky orbitals, which will be explored in future work.

Formulation of an Efficient $\mathcal{O}(M^4)$-Scaling Explicitly Correlated MP2-F12 Correction by Combining Numerical Quadrature with Density Fitting and CABS-RI

Lars Urban,[†,‡] Henryk Laqua,[†] Travis H. Thompson,[†] and Christian Ochsenfeld[*,†,‡]

†*Chair of Theoretical Chemistry, Department of Chemistry, University of Munich (LMU), D-81377 Munich, Germany*

‡*Max Planck Institute for Solid State Research, D-70569 Stuttgart, Germany*

E-mail: christian.ochsenfeld@uni-muenchen.de

Abstract

We present a novel approach that combines numerical quadrature with density fitting and CABS-RI for the evaluation of exchange-type intermediates in RI-MP2-F12 theory, rigorously reducing the formal and practical scaling of the total correction from $\mathcal{O}(M^5)$ to $\mathcal{O}(M^4)$. Our new hybrid NQ/DF/CABS-RI ansatz is based directly on our previously developed NQ/CABS-RI method for the efficient evaluation of 6c3e integrals [Urban, L.; Laqua, H; Thompson, T. H.; Ochsenfeld, C. *J. Chem. Theory Comput.* 2024, *20*, 3706-3718] and extends this approach to the optimized computation of products of 4c2e integrals. In this framework, the main exchange-type intermediates $\mathcal{V}$, $\mathcal{X}$, and $\mathcal{B}$ are reformulated, resulting in more compact expressions, increased shared computations, and fewer CABS-RI insertions. We introduce efficient algorithms that cover

all exchange-type contributions, including advantageous batching of integrals. Benchmarks show that NQ/DF/CABS-RI achieves mean errors below 0.01 kcal/mol for non-covalent interaction and isomerization energies already with small to modest grid sizes, while the numerical precision can be adjusted to balance computational cost. Empirical scaling was determined using linear glycine chains, demonstrating the expected $\mathcal{O}(M^4)$ behavior for the rate-determining steps, with the remaining exchange-type expressions scaling nearly linearly. Compared with an idealized DF/CABS-RI implementation, our approach achieves speedups of roughly one order of magnitude for the most expensive steps with virtually no loss of numerical accuracy. Systems with strongly delocalized electronic structures benefit particularly. For example, in a nanotube with 168 carbon atoms, the computational time for the most demanding expressions is reduced from 9.97 to 1.25 days, bringing the cost much closer to that of conventional DF-MP2. At present, NQ/DF/CABS-RI achieves efficient $\mathcal{O}(M^4)$ scaling, and further cost reductions are anticipated through the introduction of integral screening based on Cholesky orbitals, which will be explored in future work.

1 Introduction

To this day, the highly accurate and efficient computation of electronic structures of many-body systems remains one of the central challenges in quantum chemistry and physics. While the number of correlated electrons and their corresponding orbitals in small systems remains manageable for steep-scaling high-level methods, their practical applicability to larger systems is severely limited. In particular, accurately describing short-range dynamic correlation significantly increases the computational cost. Conventional correlation methods require a prohibitively large set of basis functions to properly capture the cusp behavior of the exact wave function near the coalescence of two electrons due to the $\frac{1}{\boldsymbol{r}_{12}}$ singularity of the Coulomb operator.[1] Alternatively, ansätze that explicitly incorporate the interelectronic distance r_{12} into their wavefunction description overcome this issue, allowing for a significantly reduced

orbital space. First introduced for practical calculations by Hylleraas in 1929 with his pioneering study of the helium atom,[2] the general idea of including terms explicitly depending on r_{12} has led to various approaches, e.g., variational Hylleraas-configuration interaction (Hylleraas-CI),[3–6] explicitly correlated Gaussian (ECG) wavefunction approaches,[7–12] or transcorrelated (TC) methods.[13–34]

Among these methods, the family of explicitly correlated F12 corrections has emerged as the most popular and widely applied, being typically suited for larger systems than most alternative approaches while significantly accelerating the convergence with respect to the size of the one-electron basis. Its success traces back to the seminal work of Kutzelnigg and Klopper on so-called R12 corrections,[35–37] which introduced explicitly coupled two-electron terms (geminals) into the wave function description. To handle the resulting high-dimensional integrals, such as six-center three-electron (6c3e) and eight-center four-electron (8c4e) integrals, they proposed applying the Resolution-of-the-Identity (RI) technique to decompose them into tractable sums of four-center two-electron (4c2e) integrals. While the original R12 ansatz exhibited intrinsic limitations due to the use of a linear r_{12} correlation factor, which is not optimally suited to describe short-range electron–electron correlation, Ten-no[38] succeeded in reproducing the correct electron–electron cusp behavior by introducing a flexible exponentially-decaying correlation factor, giving rise to what is today known as F12 theory. Following this development, F12 approaches continued to evolve, incorporating several key improvements, most notably Valeev's complementary auxiliary basis set (CABS)[39] method for an advantageous partitioning of orbital spaces, as well as the efficient use of density fitting (DF) techniques[40,41] to drastically reduce the computational prefactor by decomposing 4c2e integrals into three-center-two-electron (3c2e) and two-center-two-electron (2c2e) integrals. Today, DF/CABS-RI F12 approaches are well-established tools, offering an accurate and robust treatment of complex systems with a wide range of corrections for different quantum-chemical methods, such as in perturbation theory,[42–49] coupled-cluster theory,[50–58] the random-phase-approximation (RPA),[59–61] multireference methods,[62–69] in density func-

tional theory (DFT) design,[70,71] and corresponding gradients.[72–75]

Most of these approaches rely on the standard DF/CABS-RI framework to evaluate the required integrals, which often remains computationally demanding. In fact, for explicitly correlated corrections to second-order Møller–Plesset perturbation theory (MP2-F12), the cost of the F12 correction can significantly exceed that of the underlying MP2 calculation. A less common alternative in this regard is three-dimensional numerical quadrature (NQ),[76–79] which was originally introduced to F12 theory for the accurate evaluation of multielectron integrals.[80,81]

We have recently proposed a novel and highly efficient atomic orbital-based ansatz for exchange-type six-center three-electron (6c3e) F12 integrals, combining numerical quadrature (NQ) with CABS-RI and distance-dependent integral screening.[82] By expressing the most computationally demanding term in RI-MP2-F12 theory in the form of such a 6c3e integral, this approach enables substantial reductions in computational effort, yielding significant speedups and a linear-scaling evaluation. However, only certain exchange-type terms in RI-MP2-F12 theory can be efficiently transformed into 6c3e integrals, while the remaining contributions must still be treated as products of four-center two-electron (4c2e) integrals. For direct-type terms, the standard DF/CABS-RI framework remains the most efficient choice, offering an asymptotic $\mathcal{O}(M^4)$ scaling with respect to the system size M. In contrast, exchange-type terms evaluated using DF/CABS-RI alone retain a steeper $\mathcal{O}(M^5)$ scaling.

In the following, we introduce a new approach that combines density fitting and CABS-RI with numerical quadrature to efficiently reduce the computational cost and rigorously lower the formal scaling of the exchange-type product of two 4c2e integrals to $\mathcal{O}(M^4)$. For each major exchange-type intermediate, we identify the most efficient evaluation strategy, employing fewer CABS-RI insertions and reformulated terms. Furthermore, we present efficient algorithms with optimized memory demand for computing exchange-type contributions for all operators involved in RI-MP2-F12 theory, ultimately lowering the overall scaling of the F12 correction to $\mathcal{O}(M^4)$—below the standard $\mathcal{O}(M^5)$ scaling of DF-MP2.

2 Theory

Throughout this work, we use the orbital spaces defined in Table 1.

Table 1: Summary of orbital spaces and indexing conventions.

Orbital space	Indices
AO Hartree–Fock space	$\mu, \nu, \lambda, \sigma, ...$
AO complementary auxiliary space	$\mu'', \nu'', \lambda'', \sigma'', ...$
Combined AO HF/CABS space ($\{\mu\} \cup \{\mu''\}$)	$\mu', \nu', \lambda', \sigma', ...$
geminal space	x, y, w, z
MO active occupied space	i, j
MO occupied space	k, l
MO virtual space	a, b, c, d
MO occupied + virtual space ($\{i\} \cup \{a\}$)	p, q, r, s
MO complementary auxiliary space	p'', q'', r'', s''
Combined MO HF/CABS space ($\{p\} \cup \{p''\}$)	p', q', r', s'
Density-Fitting space	P, Q, R, S

To maintain the readability of the occurring F12 intermediates, we employ an implicit summation convention for indices that appear repeatedly and exclusively within a single expression on one side of an equation (e.g., in energy expressions or AO basis contractions). Explicit summation signs are only included where they are necessary for clarity or to emphasize a specific transformation. Conversely, equations defining the individual elements of a tensor or operator (such as the definitions of the major F12 intermediates) are to be understood such that indices appearing on both sides of the equation are fixed and do not imply summation. To represent the various types of electronic integrals, we employ both Dirac and Mulliken (chemical) notations. For a general two-body operator $\hat{O}_{12}$, a four-center two-electron (4c2e) integral over spatial orbitals can be written in either form:

$$\underbrace{\langle ij|\, \hat{O}_{12}\, |kl\rangle}_{\text{Dirac}} = \underbrace{(ik|\hat{O}_{12}|jl)}_{\text{Mulliken}} = \iint \phi_i^*(\boldsymbol{r}_1)\phi_j^*(\boldsymbol{r}_2)\hat{O}_{12}\phi_k(\boldsymbol{r}_1)\phi_l(\boldsymbol{r}_2)d\boldsymbol{r}_1 d\boldsymbol{r}_2\,. \tag{1}$$

In the following, we discuss the efficient use of numerical quadrature (NQ)[80–84] and its combination with density fitting (DF) techniques[40,41] and CABS-RI[39] for the evaluation of exchange-type intermediates in F12 theory, with particular emphasis on their application within a modified version of the closed-shell MP2-F12(3*C) correction.[43] In this context, the acronym RI (as in RI-MP2-F12) explicitly denotes the use of a MO completeness insertion via CABS-RI, while DF is used exclusively for the approximation of two-electron integrals. We begin with a brief review of the standard 3*C correction, also referred to as 3C(FIX). The correction employs the correlation factor $\hat{F}_{12}$, the Coulomb operator $\hat{g}_{12}$, and corresponding products, defined as

$$\hat{F}_{12} = \frac{1}{\gamma} e^{-\gamma r_{12}} \,, \tag{2}$$

$$\hat{g}_{12} = \frac{1}{r_{12}} \,, \tag{3}$$

$$\hat{F}_{12}\hat{g}_{12} = \frac{1}{\gamma} e^{-\gamma r_{12}} \cdot \frac{1}{r_{12}} \,, \tag{4}$$

$$\hat{F}_{12}^2 = \frac{1}{\gamma^2} e^{-2\gamma r_{12}} \,, \tag{5}$$

where r_{12} is the interelectronic distance. In the 3*C ansatz, the strong orthogonality projector $\hat{Q}_{12}$ takes the form

$$\hat{Q}_{12} = (1 - \hat{\mathrm{o}}_1)(1 - \hat{\mathrm{o}}_2)(1 - \hat{\mathrm{v}}_1\hat{\mathrm{v}}_2) \,, \tag{6}$$

where $\hat{\mathrm{o}}_n$ and $\hat{\mathrm{v}}_n$ are projectors onto the occupied and virtual orbital spaces for electron n, respectively, enforcing orthogonality with respect to double excitations within the explicitly correlated geminal space. Furthermore, the rational generator $\hat{S}_{xy}$[80] ensures the simultaneous fulfillment of the s- and p-wave coalescence conditions, given by

$$\hat{S}_{xy} = \frac{3}{8} + \frac{1}{8}\hat{L}_{xy} \,, \tag{7}$$

where the permutation operator $\hat{L}_{xy}$ exchanges the spatial coordinates $\boldsymbol{r}$ while preserving the spin coordinates σ of two electrons:

$$\hat{L}_{xy}\phi_x(\boldsymbol{r}_1,\sigma_1)\phi_y(\boldsymbol{r}_2,\sigma_2) = \phi_x(\boldsymbol{r}_2,\sigma_1)\phi_y(\boldsymbol{r}_1,\sigma_2)\,. \tag{8}$$

The computationally demanding $\mathcal{O}(M^6)$ variational optimization of geminal amplitudes is avoided by employing the fixed-amplitude ansatz

$$c_{ij}^{xy} = \delta_x^i \delta_y^j\,, \tag{9}$$

which restricts the explicitly correlated geminal space to the Hartree–Fock occupied orbitals, leading to the widely used diagonal, orbital-invariant formulation. In combination with the generalized Brillouin condition (GBC) and the extended Brillouin condition (EBC), which neglect Fock matrix elements between the virtual/occupied and RI auxiliary orbital spaces, the explicitly correlated F12 correction to the MP2 energy in the 3*C approximation takes the form[47]

$$E_{\mathrm{F12}}^{3^*\mathrm{C}} = \frac{5}{4}\mathcal{V}_{ij}^{ij} - \frac{1}{4}\mathcal{V}_{ji}^{ij} + \frac{7}{32}\mathcal{B}_{ji}^{ij} + \frac{1}{32}\mathcal{B}_{ji}^{ij} - \frac{7}{32}(\mathcal{X}_{il}^{ij} f_j^l + \mathcal{X}_{kj}^{ij} f_i^k) - \frac{1}{32}(\mathcal{X}_{li}^{ij} f_j^l + \mathcal{X}_{jk}^{ij} f_i^k)\,. \tag{10}$$

The evaluation of the three primary exchange-type intermediates $\mathcal{V}_{ji}^{ij}$, $\mathcal{X}_{ji}^{ij}$, and $\mathcal{B}_{ji}^{ij}$ clearly dominates the overall computational cost (see section 4.2) and thus, their efficient evaluation is of central importance for a high-performance implementation. These intermediates are defined as

$$\mathcal{V}_{ji}^{ij} = \langle ij|\, \hat{F}_{12}\hat{Q}_{12}\hat{g}_{12}\,|ji\rangle\ , \tag{11}$$

$$\mathcal{X}_{ji}^{ij} = \langle ij|\, \hat{F}_{12}\hat{Q}_{12}\hat{F}_{12}\,|ji\rangle\ , \tag{12}$$

$$\mathcal{B}_{ji}^{ij} = \langle ij|\, \hat{F}_{12}\hat{Q}_{12}(\hat{f}_1 + \hat{f}_2)\hat{Q}_{12}\hat{F}_{12}\,|ji\rangle\ , \tag{13}$$

where $\hat{f}_1$ and $\hat{f}_2$ denote Fock operators, and f_i^k and f_j^l represent Fock matrix elements, which reduce to the orbital energies ϵ_i and ϵ_j when canonical molecular orbitals are used. For further details on the derivation of these intermediates, as well as on other F12 approaches to which the techniques described in the following can be applied, the reader is referred to the literature.[85,86]

The conventional evaluation of $\mathcal{V}_{ji}^{ij}$, $\mathcal{X}_{ji}^{ij}$, and $\mathcal{B}_{ji}^{ij}$ using only CABS-RI and density fitting exhibits an unfavorable $\mathcal{O}(M^5)$ scaling,[45] as standard density fitting techniques reduce only the computational prefactor without improving the formal scaling behavior. However, combining these methods with numerical quadrature enables a reduction to $\mathcal{O}(M^4)$ for the arising products of 4c2e integrals, as discussed for a generic case in section 2.1. Subsequently, we present an alternative, CABS-RI free evaluation of the $\mathcal{V}_{ji}^{ij}$ and $\mathcal{X}_{ji}^{ij}$ exchange-type intermediates based on six-center three-electron (6c3e) integrals (section 2.2), and provide a detailed strategy for evaluating the complicated $\mathcal{B}_{ji}^{ij}$ intermediate with fewer approximations, simplified expressions, and a reduced number of CABS-RI insertions (section 2.3). Finally, in section 2.4, we outline efficient implementation strategies for all intermediates, focusing on minimizing computational cost and memory usage through the reuse of sub-intermediates and the consolidation of shared computational steps across different expressions.

2.1 Decomposition Techniques

Several approaches have been introduced to handle the complicated intermediates $\mathcal{V}$, $\mathcal{X}$, and $\mathcal{B}$, whose approximation-free evaluation leads to high-dimensional expressions involving up to eight-center four-electron (8c4e) integrals, which are infeasible to compute in practice. In particular, the efficient use of the Resolution-of-the-Identity (RI) approximation has been key to the success of R12/F12 methods, as it enables the decomposition of high-dimensional

integrals into products of lower-dimensional ones. Here, the identity operator $\hat{1}$ on the one-electron function space can be exactly resolved for electron n as

$$\hat{\alpha}_n g(..., \boldsymbol{r}_n, ...) = \sum_{\alpha} \alpha(\boldsymbol{r}_n) \left(\int \alpha(\boldsymbol{r}_n) g(..., \boldsymbol{r}_n, ...) d\boldsymbol{r}_n \right) , \tag{14}$$

where $\hat{\alpha}_n$ denotes the formally exact projector onto a complete orthonormal basis. To construct an appropriate approximate projector, one can obtain a large orthogonal set of auxiliary basis functions $\{P_o\}$, e.g., via Löwdin orthogonalization

$$P_o(\boldsymbol{r}) = [\boldsymbol{S}^{-\frac{1}{2}}]^P_Q Q(\boldsymbol{r}) \,, \tag{15}$$

with $\boldsymbol{S}$ being the overlap matrix in the auxiliary basis $\{P\}$. The projector $\hat{\alpha}_n$ can then be approximated as

$$\hat{\alpha}_n \approx |P_o)(P_o| = |P)(PQ)^{-1}(Q| \,, \tag{16}$$

where we use the shorthand notation $(PQ)^{-1} = [\boldsymbol{S}^{-1}]^P_Q$. The most widely used RI scheme in F12 theory today is Valeev's complementary auxiliary basis set (CABS) approach,[39] in which the Resolution-of-the-Identity is performed in the combined orbital space p', formed by the union of the Hartree–Fock orbitals p and the CABS basis functions p''. Whereas CABS-RI plays a key role in the evaluation of integrals in most parts of F12 theory, especially for the direct terms in RI-MP2-F12(3*C), we restrict its use for exchange-type contributions to the evaluation of the $\mathcal{B}$ intermediate, as it involves a large orbital space and entails significant computational cost. However, in this context, it can be used efficiently to decompose expressions into exchange-type six-center three-electron (6c3e) integrals. We have recently demonstrated that these 6c3e integrals can be evaluated with high efficiency and accuracy using numerical quadrature in combination with distance-dependent integral screening, leading to a linear scaling computation of the most expensive term in RI-MP2-F12

theory.[82] A typical approach to decomposing an unspecified molecular orbital 6c3e integral using numerical quadrature is given by

$$\mathcal{WY}^{ijk}_{kij} = \langle ijk|\, \hat{W}_{12}\hat{Y}_{23}\, |kij\rangle \approx w_g \phi^g_j \phi^g_i (g|\hat{W}_{1g}|ik)(g|\hat{Y}_{1g}|kj)\,, \tag{17}$$

where $\hat{W}_{12} = W(|\boldsymbol{r}_1 - \boldsymbol{r}_2|)$ and $\hat{Y}_{23} = Y(|\boldsymbol{r}_2 - \boldsymbol{r}_3|)$ represent generic distance-dependent operators occurring in F12 theory, g and w_g denote discrete grid points and their corresponding weights, and ϕ^g_i describes the i-th molecular orbital evaluated at grid point g. The 3c1e MO integrals $(g|\hat{W}_{1g}|ik)$ with $\hat{W}_{1g} = W(|\boldsymbol{r}_1 - \boldsymbol{r}_g|)$, are computed via an $\mathcal{O}(M^4)$ scaling AO to MO transformation of the 3c1e AO integrals

$$(g|\hat{W}_{1g}|\mu\nu) = \int \chi_\mu(\boldsymbol{r}_1)\chi_\nu(\boldsymbol{r}_1)\hat{W}_{1g}\, d\boldsymbol{r}_1\,. \tag{18}$$

The energy contribution of the 6c3e integral is then obtained via three at most formally $\mathcal{O}(M^3)$ scaling steps

$$\text{step 1:} \qquad \mathcal{W}^g_k \quad = \phi^g_i (g|\hat{W}_{1g}|ik) \qquad (N_g N_k N_i) \tag{19}$$

$$\text{step 2:} \qquad \mathcal{Y}^g_k \quad = \phi^g_j (g|\hat{Y}_{1g}|kj) \qquad (N_g N_k N_i) \tag{20}$$

$$\text{step 3:} \qquad E_{\{\mathcal{WY}^{ijk}_{kij}\}} = w_g \mathcal{W}^g_k \mathcal{Y}^g_k\,, \qquad (N_g N_k) \tag{21}$$

with the formal time complexity for the steepest scaling step given in parentheses. Although the AO to MO transformation of some of the 3c1e AO integrals can not be avoided for an efficient computation of $\mathcal{B}^{ij}_{ji}$, the evaluation of 6c3e exchange-type integrals in the pure AO regime can still be beneficial, as shown in the upcoming sections, resulting in

$$\langle ijk|\, \hat{W}_{12}\hat{Y}_{23}\, |kij\rangle \approx w_g\, c_{\mu j}\chi^g_\mu\, c_{\nu i}\chi^g_\nu\, c_{\lambda i}c_{\sigma k}(g|\hat{W}_{1g}|\lambda\sigma)\, c_{\delta k}c_{\varepsilon j}(g|\hat{Y}_{1g}|\delta\varepsilon) \tag{22}$$

$$= w_g P_{\mu\varepsilon}P_{\nu\lambda}P_{\sigma\delta}\, \chi^g_\mu\chi^g_\nu\, (g|\hat{W}_{1g}|\lambda\sigma)\, (g|\hat{Y}_{1g}|\delta\varepsilon), \tag{23}$$

with MO coefficients c, density matrix elements $P_{\mu\nu} = \sum_i c_{\mu i} c_{\nu i}$ for closed-shell systems, and χ_μ^g denoting the μ-th atomic orbital evaluated at grid point g, respectively. Here, eq. (23) is best computed via a stepwise $\mathcal{O}(M^3)$ scaling evaluation

$$\text{step 1:} \quad \bar{\chi}_\varepsilon^g = P_{\mu\varepsilon}\chi_\mu^g \qquad (N_g N_\mu^2) \tag{24}$$

$$\text{step 2:} \quad \mathcal{W}_\sigma^g = \bar{\chi}_\lambda^g (g|\hat{W}_{1g}|\lambda\sigma) \qquad (N_g N_\mu^2) \tag{25}$$

$$\text{step 3:} \quad \mathcal{Y}_\delta^g = \bar{\chi}_\varepsilon^g (g|\hat{Y}_{1g}|\delta\varepsilon) \qquad (N_g N_\mu^2) \tag{26}$$

$$\text{step 4:} \quad E_{\{\mathcal{W}\mathcal{Y}_{kij}^{ijk}\}} = w_g P_{\sigma\delta} \mathcal{W}_\sigma^g \mathcal{Y}_\delta^g \,. \qquad (N_g N_\mu^2) \tag{27}$$

The advantages of an AO-based approach lie in the ability to combine the overlap decay of the basis functions, the sparsity of the density matrix, and the operator decay into an efficient, distance-dependent integral screening for the evaluation of the 3c1e AO integrals, as described in detail in Section 2 of Ref. 82. Moreover, the use of block-sparse matrix algebra (BSMA)[87] in the contractions of eqs. (24) to (27) enables a reduction of computational scaling to linear by leveraging the inherent sparsity of the involved quantities.

Unfortunately, not all exchange-type terms can be expressed in the form of 6c3e integrals but instead decompose into products of two four-center two-electron (4c2e) integrals. In previous work,[43,45] such terms have predominantly been treated using density fitting techniques, as exemplified by

$$\mathcal{W}_{kl}^{ij}\mathcal{Y}_{ji}^{kl} = \langle ij|\,\hat{W}_{12}\,|kl\rangle\,\langle kl|\,\hat{Y}_{12}\,|ji\rangle \approx \mathcal{W}_P^{ik}\tilde{\mathcal{W}}_Q^P\mathcal{W}_{jl}^Q\mathcal{Y}_R^{kj}\tilde{\mathcal{Y}}_S^R\mathcal{Y}_{li}^S \tag{28}$$

with

$$\mathcal{Y}_R^{kj} = (kj|\hat{Y}_{12}|R) \tag{29}$$

$$\tilde{\mathcal{Y}}_S^R = [\mathcal{Y}^{-1}]_S^R \tag{30}$$

$$\mathcal{Y}_S^R = (R|\hat{Y}_{12}|S)\,. \tag{31}$$

While a purely density-fitting-based approach substantially lowers the computational prefactor, the formal scaling of the overall computation remains $\mathcal{O}(M^5)$. Here, we propose an alternative ansatz that combines density fitting with numerical quadrature, thereby reducing the formal scaling to $\mathcal{O}(M^4)$. Specifically, we express the product of two 4c2e integrals as

$$\langle ij|\,\hat{W}_{12}\,|kl\rangle\,\langle kl|\,\hat{Y}_{12}\,|ji\rangle \approx w_g\,\phi_i^g\phi_k^g\,(g|\hat{W}_{1g}|jl)\,\mathcal{Y}_R^{kj}\tilde{\mathcal{Y}}_S^R\mathcal{Y}_{li}^S\,, \tag{32}$$

which can again be stepwise computed via

$$\text{step 1:} \quad \tilde{\mathcal{Y}}_{li}^R = \tilde{\mathcal{Y}}_S^R\mathcal{Y}_{li}^S \qquad (N_P^2N_kN_i) \tag{33}$$

$$\text{step 2:} \quad \tilde{\mathcal{Y}}_{lg}^R = \phi_i^g\,\tilde{\mathcal{Y}}_{li}^R \qquad (N_gN_PN_kN_i) \tag{34}$$

$$\text{step 3:} \quad \mathcal{Y}_R^{gj} = \phi_k^g\,\mathcal{Y}_R^{kj} \qquad (N_gN_PN_kN_i) \tag{35}$$

$$\text{step 4:} \quad \mathcal{Y}_{gjl} = \tilde{\mathcal{Y}}_{lg}^R\,\mathcal{Y}_R^{gj} \qquad (N_gN_PN_kN_i) \tag{36}$$

$$\text{step 5:} \quad E_{\{\mathcal{W}\mathcal{Y}_{ji}^{ij}\}} = w_g(g|\hat{W}_{1g}|jl)\mathcal{Y}_{gjl} \qquad (N_gN_kN_i)\,. \tag{37}$$

The choice of which electron is represented as molecular orbitals on the grid, and consequently the placement of the numerical quadrature within the integral product, is crucial for achieving maximum efficiency in the evaluation, particularly for integrals involving some form of CABS-RI. Optimal performance is typically achieved when the largest orbital space is represented as MO on a grid and an early contraction is performed. This approach is especially advantageous for integrals involving additional multiple orbital spaces spanning Fock or exchange matrix elements,[49] as it allows an early contraction of the largest indices with a formal scaling of $\mathcal{O}(M^3)$.

2.2 $\mathcal{V}_{ji}^{ij}$- and $\mathcal{X}_{ji}^{ij}$-Intermediate

Both intermediates, $\mathcal{V}_{ji}^{ij}$ (eq. (11)) and $\mathcal{X}_{ji}^{ij}$ (eq. (12)), share a similar structure and can be evaluated using the same decomposition scheme. For $\mathcal{X}_{ji}^{ij}$, we assume that canonical

molecular orbitals are used for the Fock matrix elements f_i^k and f_j^l, yielding the corresponding orbital energies ϵ_i and ϵ_j. In contrast to the conventional approach, which relies on an approximate form of the strong orthogonality projector,

$$\hat{Q}_{12}^{\text{approx}} = 1 - \hat{\mathrm{p}}_1\hat{\mathrm{p}}_2 - \hat{\mathrm{o}}_1\hat{\mathrm{p}}_2'' - \hat{\mathrm{p}}_1''\hat{\mathrm{o}}_2\,, \tag{38}$$

we instead employ the exact operator as defined in eq. (6). The exact expression for both exchange-type intermediates is then given by

$$\mathcal{V}_{ji}^{ij} = \mathcal{FG}_{ji}^{ij} + \mathcal{F}_{kl}^{ij}\mathcal{G}_{ji}^{kl} - \mathcal{F}_{ab}^{ij}\mathcal{G}_{ji}^{ab} - \langle ijk|\,\hat{F}_{12}\hat{g}_{23}\,|kij\rangle - \langle jik|\,\hat{F}_{12}\hat{g}_{23}\,|kji\rangle \tag{39}$$

$$\mathcal{X}_{ji}^{ij} = \mathcal{FF}_{ji}^{ij} + \mathcal{F}_{kl}^{ij}\mathcal{F}_{ji}^{kl} - \mathcal{F}_{ab}^{ij}\mathcal{F}_{ji}^{ab} - \langle ijk|\,\hat{F}_{12}\hat{F}_{23}\,|kij\rangle - \langle jik|\,\hat{F}_{12}\hat{F}_{23}\,|kji\rangle\,, \tag{40}$$

leading for each intermediate to a combination of two identical true 6c3e exchange-type integrals, one 4c2e integral, and the products of 4c2e integrals. For $\mathcal{V}_{ji}^{ij}$, the arising integrals are best decomposed as follows:

$$\mathcal{FG}_{ji}^{ij} \approx w_g P_{\mu\sigma} P_{\nu\lambda} \chi_\mu^g \chi_\nu^g (g|\hat{F}_{1g}\hat{g}_{1g}|\lambda\sigma) \quad (N_g N_\mu^2) \tag{41}$$

$$\mathcal{F}_{kl}^{ij}\mathcal{G}_{ji}^{kl} \approx \mathcal{F}_P^{ik}\tilde{\mathcal{F}}_Q^P\mathcal{F}_{jl}^Q w_g \phi_k^g \phi_j^g (g|\hat{g}_{1g}|li) \quad (N_g N_P N_k N_i) \tag{42}$$

$$\mathcal{F}_{ab}^{ij}\mathcal{G}_{ji}^{ab} \approx \mathcal{F}_P^{ia}\tilde{\mathcal{F}}_Q^P\mathcal{F}_{jb}^Q w_g \phi_a^g \phi_j^g (g|\hat{g}_{1g}|bi) \quad (N_g N_P N_a N_i) \tag{43}$$

$$\langle ijk|\,\hat{F}_{12}\hat{g}_{23}\,|kij\rangle \approx w_g P_{\mu\varepsilon} P_{\nu\lambda} P_{\sigma\delta}\, \chi_\mu^g \chi_\nu^g\, (g|\hat{F}_{1g}|\lambda\sigma)\, (g|\hat{g}_{1g}|\delta\varepsilon) \quad (N_g N_\mu^2)\,, \tag{44}$$

where the AO formalism is applied when it is most efficient. $\mathcal{X}_{ji}^{ij}$ decomposes similarly

$$\mathcal{FF}_{ji}^{ij} \approx w_g P_{\mu\sigma} P_{\nu\lambda} \chi_\mu^g \chi_\nu^g (g|\hat{F}_{1g}^2|\lambda\sigma) \quad (N_g N_\mu^2) \tag{45}$$

$$\mathcal{F}_{kl}^{ij}\mathcal{F}_{ji}^{kl} \approx \mathcal{F}_P^{ik}\tilde{\mathcal{F}}_Q^P\mathcal{F}_{jl}^Q w_g \phi_k^g \phi_j^g (g|\hat{F}_{1g}|li) \quad (N_g N_P N_k N_i) \tag{46}$$

$$\mathcal{F}_{ab}^{ij}\mathcal{G}_{ji}^{ab} \approx \mathcal{F}_P^{ia}\tilde{\mathcal{F}}_Q^P\mathcal{F}_{jb}^Q w_g \phi_a^g \phi_j^g (g|\hat{F}_{1g}|bi) \quad (N_g N_P N_a N_i) \tag{47}$$

$$\langle ijk|\,\hat{F}_{12}\hat{F}_{23}\,|kij\rangle \approx w_g P_{\mu\varepsilon} P_{\nu\lambda} P_{\sigma\delta}\, \chi_\mu^g \chi_\nu^g\, (g|\hat{F}_{1g}|\lambda\sigma)\, (g|\hat{F}_{1g}|\delta\varepsilon) \quad (N_g N_\mu^2)\,, \tag{48}$$

where the operators on the grid for both intermediates are defined as

$$\hat{F}_{1g} = \frac{1}{\gamma} e^{-\gamma r_{1g}} \tag{49}$$

$$\hat{g}_{1g} = \frac{1}{r_{1g}} \tag{50}$$

$$\hat{F}_{1g}\hat{g}_{1g} = \frac{1}{\gamma} e^{-\gamma r_{1g}} \cdot \frac{1}{r_{1g}} \tag{51}$$

$$\hat{F}_{1g}^2 = \frac{1}{\gamma^2} e^{-2\gamma r_{1g}}\,, \tag{52}$$

with $r_{1g} = |\boldsymbol{r}_1 - \boldsymbol{r}_g|$. In eq. (42) and (43), the 4c2e integrals involving the classical Coulomb operator $\hat{g}_{12}$ are decomposed via numerical quadrature rather than those involving the correlation factor $\hat{F}_{12}$. This eliminates the need to access additional 3c2e and 2c2e integrals during the computation, as the required 3c1e integrals for $\hat{g}_{12}$ are already used in eq. (44), thereby lowering the memory demand. Beyond the reduction in formal scaling, a key benefit of using the exact form of $\hat{Q}_{12}$ is that the evaluation remains entirely CABS-RI free, eliminating associated errors and overhead.

2.3 $\mathcal{B}_{ji}^{ij}$-Intermediate

Among all intermediates in RI-MP2-F12 theory, $\mathcal{B}_{ji}^{ij}$ (eq. (13)) stands out as the most intricate and computationally intensive, due to the incorporation of Fock operators into the integral expression in conjunction with the projectors in $\hat{Q}_{12}$ (eq. (6)). In this context, the symmetry of $\hat{F}_{12}$ and $\hat{Q}_{12}$ with respect to the electron labels is exploited to treat $\hat{f}_1$ and $\hat{f}_2$ on equal footing, allowing us to write

$$\langle ij|\, \hat{F}_{12}\hat{Q}_{12}\hat{f}_1\hat{Q}_{12}\hat{F}_{12}\, |ji\rangle = \langle ji|\, \hat{F}_{12}\hat{Q}_{12}\hat{f}_2\hat{Q}_{12}\hat{F}_{12}\, |ij\rangle\ , \tag{53}$$

so that only $\hat{Q}_{12}\hat{f}_1\hat{Q}_{12}$ needs to be considered. Inserting the definition of $\hat{Q}_{12}$ leads to the following distinct combinations of operators and projectors:

$$\begin{array}{rrrrr}
\hat{f}_1 & -\hat{f}_1\hat{o}_1 & -\hat{f}_1\hat{o}_2 & \hat{f}_1\hat{o}_1\hat{o}_2 & -\hat{f}_1\hat{v}_1\hat{v}_2 \\
-\hat{o}_1\hat{f}_1 & \hat{o}_1\hat{f}_1\hat{o}_1 & \hat{o}_1\hat{f}_1\hat{o}_2 & -\hat{o}_1\hat{f}_1\hat{o}_1\hat{o}_2 & \hat{o}_1\hat{f}_1\hat{v}_1\hat{v}_2 \\
-\hat{o}_2\hat{f}_1 & \hat{o}_2\hat{f}_1\hat{o}_1 & \hat{o}_2\hat{f}_1\hat{o}_2 & -\hat{o}_2\hat{f}_1\hat{o}_1\hat{o}_2 & \hat{o}_2\hat{f}_1\hat{v}_1\hat{v}_2 \\
\hat{o}_1\hat{o}_2\hat{f}_1 & -\hat{o}_1\hat{o}_2\hat{f}_1\hat{o}_1 & -\hat{o}_1\hat{o}_2\hat{f}_1\hat{o}_2 & \hat{o}_1\hat{o}_2\hat{f}_1\hat{o}_1\hat{o}_2 & -\hat{o}_1\hat{o}_2\hat{f}_1\hat{v}_1\hat{v}_2 \\
-\hat{v}_1\hat{v}_2\hat{f}_1 & \hat{v}_1\hat{v}_2\hat{f}_1\hat{o}_1 & \hat{v}_1\hat{v}_2\hat{f}_1\hat{o}_2 & -\hat{v}_1\hat{v}_2\hat{f}_1\hat{o}_1\hat{o}_2 & \hat{v}_1\hat{v}_2\hat{f}_1\hat{v}_1\hat{v}_2
\end{array} \tag{54}$$

Fortunately, we can leverage the idempotency of projectors, the commuting behavior of operators, and the identities

$$\hat{o}_n\hat{v}_n = \hat{v}_n\hat{o}_n = \hat{o}_n\hat{f}_n\hat{v}_n = \hat{v}_n\hat{f}_n\hat{o}_n = 0\,, \tag{55}$$

which, together with the removal of canceling terms, allows for the reduction of eq. (54) to the following form:

$$\begin{array}{rrrrr}
\hat{f}_1 & -\hat{f}_1\hat{o}_1 & -\hat{f}_1\hat{o}_2 & \hat{f}_1\hat{o}_1\hat{o}_2 & -\hat{f}_1\hat{v}_1\hat{v}_2 \\
-\hat{o}_1\hat{f}_1 & \hat{o}_1\hat{f}_1\hat{o}_1 & \hat{o}_1\hat{o}_2\hat{f}_1 & -\hat{o}_1\hat{f}_1\hat{o}_1\hat{o}_2 & 0 \\
0 & 0 & 0 & 0 & 0 \\
0 & 0 & 0 & 0 & 0 \\
-\hat{v}_1\hat{v}_2\hat{f}_1 & 0 & 0 & 0 & \hat{v}_1\hat{f}_1\hat{v}_1\hat{v}_2
\end{array} \tag{56}$$

Overall, $\hat{Q}_{12}\hat{f}_1\hat{Q}_{12}$ can thus be expressed as

$$\hat{Q}_{12}\hat{f}_1\hat{Q}_{12} = \hat{f}_1 - \hat{f}_1\hat{o}_2 + \hat{T}(-\hat{f}_1\hat{o}_1 + \hat{f}_1\hat{o}_1\hat{o}_2 - \hat{f}_1\hat{v}_1\hat{v}_2) + \hat{o}_1\hat{f}_1\hat{o}_1 - \hat{o}_1\hat{f}_1\hat{o}_1\hat{o}_2 + \hat{v}_1\hat{f}_1\hat{v}_1\hat{v}_2\,, \tag{57}$$

where the linear operator $\hat{T}$ introduces the transpose, e.g., $\hat{T}\hat{f}_1\hat{o}_1\hat{o}_2 = \hat{f}_1\hat{o}_1\hat{o}_2 + \hat{o}_1\hat{o}_2\hat{f}_1$, which combines identical terms due to the symmetry of the resulting integrals. The approximation-free evaluation of the integrals arising from the operator combinations in eq. (57) results in complex multielectron integrals, including up to eight-center four-electron integrals, along

with non-standard Fock matrix elements. Previous work avoided these by applying various CABS-RI insertions, splitting the resulting integrals exclusively into products of 4c2e integrals. This strategy yields a set of (sub-)intermediates, which appears to be the most efficient approach for handling direct-type integrals.

However, for the exchange-type $\mathcal{B}_{ji}^{ij}$ intermediate, we developed a more advanced approach that requires fewer CABS-RI insertions. Our novel formalism decomposes certain operator and projector combinations from eq. (57) into 6c3e integrals that can be highly efficiently evaluated, and moreover, leads to a more efficient use of DF + NQ for the remaining products of 4c2e integrals. In this context, we exploit the fact that, for $\hat{f}_1$, the nuclear attraction $\hat{v}$ and the mean-field Coulomb operator $\hat{j}$ commute with the correlation factor $\hat{F}_{12}$, which enables the formulation of the well-known commutator relation[43,45]

$$\hat{F}_{12}\hat{f}_1\hat{F}_{12} = \frac{1}{2}\big[[\hat{F}_{12},\hat{t}_1],\hat{F}_{12}\big] - \hat{F}_{12}\hat{k}_1\hat{F}_{12} + \frac{1}{2}\big((\hat{f}_1+\hat{k}_1)\hat{F}_{12}^2 + \hat{F}_{12}^2(\hat{f}_1+\hat{k}_1)\big)\,, \tag{58}$$

where the term involving the kinetic energy operator $\hat{t}$ can be further decomposed using the product rules for the Laplacian Δ_1 and the gradient operator ∇_1 as

$$\big[[\hat{F}_{12},\hat{t}_1],\hat{F}_{12}\big] = (\nabla_1\hat{F}_{12}\,\cdot\,\nabla_1\hat{F}_{12})\,. \tag{59}$$

This expression can then be evaluated in the AO picture using NQ as

$$\langle ij|\,(\nabla_1\hat{F}_{12}\,\cdot\,\nabla_1\hat{F}_{12})\,|ji\rangle \approx \gamma^2 w_g P_{\mu\sigma}P_{\nu\lambda}\chi_\mu^g\chi_\nu^g(g|\hat{F}_{1g}^2|\lambda\sigma) \quad (N_gN_\mu^2)\,. \tag{60}$$

The last two terms in eq. (58) are identical and can be transformed using a single full-RI insertion. In combination with NQ, this yields

$$\langle ij|\,(\hat{f}_1+\hat{k}_1)\hat{\alpha}_1\hat{F}_{12}^2\,|ji\rangle \approx w_g P_{\mu\lambda}P_{\nu\sigma}P_{\epsilon'\delta'}\chi_\mu^g\chi_{\epsilon'}^g(g|\hat{F}_{1g}^2|\nu\lambda)(f+k)_\sigma^{\delta'} \quad (N_gN_{\mu'}N_\mu)\,, \tag{61}$$

where most of the computational effort for both eq. (60) and eq. (61) is shared with expressions occurring in the $\mathcal{X}_{ji}^{ij}$ intermediate. The operator combinations $\hat{k}_1$ (result of eq. (58)), $\hat{f}_1\hat{\mathrm{o}}_1$, and $\hat{\mathrm{o}}_1\hat{f}_1\hat{\mathrm{o}}_1$ give rise to integrals that are, or can be, transformed into, 6c3e integrals through full-RI insertions $\hat{\alpha}'$, which are most efficiently evaluated within the AO formalism as follows:

$$\hat{k}_1 \to \hat{\alpha}'_1\hat{k}_1\hat{\alpha}'_1 : \ \langle ijp'|\, \hat{F}_{12}\hat{F}_{23}\, |q'ij\rangle\, k_{q'}^{p'} \approx w_g P_{\mu\lambda}P_{\nu\sigma}P_{\delta'\gamma'}P_{\epsilon'\zeta'}\chi_\mu^g\chi_\nu^g \times (g|\hat{F}_{1g}|\lambda\delta')(g|\hat{F}_{1g}|\sigma\epsilon')k_{\gamma'}^{\zeta'} \tag{62}$$

$$\hat{f}_1\hat{\mathrm{o}}_1 \to \hat{\alpha}'_1\hat{f}_1\hat{\mathrm{o}}_1 : \langle ijp'|\, \hat{F}_{12}\hat{F}_{23}\, |lij\rangle\, f_l^{p'} \approx w_g P_{\mu\lambda}P_{\nu\sigma}P_{\delta\gamma}P_{\epsilon'\zeta'}\chi_\mu^g\chi_\nu^g \times (g|\hat{F}_{1g}|\lambda\delta)(g|\hat{F}_{1g}|\sigma\epsilon')f_\gamma^{\zeta'} \tag{63}$$

$$\hat{\mathrm{o}}_1\hat{f}_1\hat{\mathrm{o}}_1 : \qquad \langle ijk|\, \hat{F}_{12}\hat{F}_{23}\, |lij\rangle\, f_l^{k} \approx w_g P_{\mu\lambda}P_{\nu\sigma}P_{\delta\gamma}P_{\epsilon\zeta}\chi_\mu^g\chi_\nu^g \times (g|\hat{F}_{1g}|\lambda\delta)(g|\hat{F}_{1g}|\sigma\epsilon)f_\gamma^{\zeta} \tag{64}$$

Besides the exchange and Fock matrix elements, which are contracted in a final step, eq. (63) and eq. (64) span only subspaces of eq. (62). Consequently, most parts of these three expressions can be evaluated simultaneously at no additional computational cost, while retaining the overall $\mathcal{O}(N_g N_{\mu'}^2)$ formal scaling, as analyzed and efficiently implemented for eq. (62) in Ref. 82.

The remaining operator combinations $\hat{f}_1\hat{\mathrm{o}}_2$, $\hat{f}_1\hat{\mathrm{o}}_1\hat{\mathrm{o}}_2$, $\hat{\mathrm{o}}_1\hat{f}_1\hat{\mathrm{o}}_1\hat{\mathrm{o}}_2$, $\hat{f}_1\hat{\mathrm{v}}_1\hat{\mathrm{v}}_2$, and $\hat{\mathrm{v}}_1\hat{f}_1\hat{\mathrm{v}}_1\hat{\mathrm{v}}_2$ are evaluated as products of 4c2e integrals in the MO representation, requiring at most a double full-RI insertion in combination with DF and NQ. This yields the following relations:

$$\hat{f}_1\hat{o}_2 \to \hat{\alpha}'_1\hat{f}_1\hat{\alpha}'_1\hat{o}_2: \quad \mathcal{F}^{ij}_{p'm} f^{p'}_{r'} \mathcal{F}^{r'm}_{ji} \approx w_g \phi^g_i \phi^g_{p'} (g|\hat{F}_{1g}|jm)\, \mathcal{F}^{r'j}_R \tilde{\mathcal{F}}^R_S \mathcal{F}^S_{mi} f^{p'}_{r'} \tag{65}$$

$$\hat{f}_1\hat{o}_1\hat{o}_2 \to \hat{\alpha}'_1\hat{f}_1\hat{o}_1\hat{o}_2: \quad \mathcal{F}^{ij}_{p'm} f^{p'}_{l} \mathcal{F}^{lm}_{ji} \approx w_g \phi^g_i \phi^g_{p'} (g|\hat{F}_{1g}|jm)\, \mathcal{F}^{lj}_R \tilde{\mathcal{F}}^R_S \mathcal{F}^S_{mi} f^{p'}_{l} \tag{66}$$

$$\hat{o}_1\hat{f}_1\hat{o}_1\hat{o}_2: \quad \mathcal{F}^{ij}_{km} f^{k}_{l} \mathcal{F}^{lm}_{ji} \approx w_g \phi^g_i \phi^g_{k} (g|\hat{F}_{1g}|jm)\, \mathcal{F}^{lj}_R \tilde{\mathcal{F}}^R_S \mathcal{F}^S_{mi} f^{k}_{l} \tag{67}$$

$$\hat{f}_1\hat{v}_1\hat{v}_2 \to \hat{\alpha}'_1\hat{f}_1\hat{v}_1\hat{v}_2: \quad \mathcal{F}^{ij}_{p'c} f^{p'}_{b} \mathcal{F}^{bc}_{ji} \approx w_g \phi^g_i \phi^g_{p'} (g|\hat{F}_{1g}|jc)\, \mathcal{F}^{bj}_R \tilde{\mathcal{F}}^R_S \mathcal{F}^S_{ci} f^{p'}_{b} \tag{68}$$

$$\hat{v}_1\hat{f}_1\hat{v}_1\hat{v}_2: \quad \mathcal{F}^{ij}_{ac} f^{a}_{b} \mathcal{F}^{bc}_{ji} \approx w_g \phi^g_i \phi^g_{a} (g|\hat{F}_{1g}|jc)\, \mathcal{F}^{bj}_R \tilde{\mathcal{F}}^R_S \mathcal{F}^S_{ci} f^{a}_{b}\,, \tag{69}$$

where eq. (66) and eq. (67) share the same subspaces as eq. (65), and eq. (69) as eq. (68). These terms can be computed simultaneously by scaling the respective subspaces once, which is easily achieved by adjusting the p'-th MO on the grid $\phi^g_{p'}$, accordingly. We can thus formulate the following intermediates

$$\mathcal{U}^{ij}_{ji} = w_g \phi^g_i \phi^g_{p',\{\mathcal{U}\}} (g|\hat{F}_{1g}|jm)\, \mathcal{F}^{r'j}_R \tilde{\mathcal{F}}^R_S \mathcal{F}^S_{mi} f^{p'}_{r'} \qquad (N_g N_P N_{p'} N_i) \tag{70}$$

$$\mathcal{T}^{ij}_{ji} = w_g \phi^g_i \phi^g_{p',\{\mathcal{T}\}} (g|\hat{F}_{1g}|jc)\, \mathcal{F}^{bj}_R \tilde{\mathcal{F}}^R_S \mathcal{F}^S_{ci} f^{p'}_{b} \qquad (N_g N_P N_a N_i) \tag{71}$$

with $\phi^g_{p',\{\mathcal{U}\}}$ and $\phi^g_{p',\{\mathcal{T}\}}$ as scaled MO's on the grid. $\mathcal{U}^{ij}_{ji}$ represents the most computationally demanding intermediate in the total explicitly correlated correction. It is the only exchange-type term for which the approximated complete space p' cannot be contracted in an $\mathcal{O}(M^3)$ evaluation, but instead requires a $\mathcal{O}(N_g N_P N_{p'} N_i)$ scaling contraction. Fortunately, this step can be carried out early in the computation, effectively removing p' from subsequent evaluations. Generally, the structure of $\mathcal{U}^{ij}_{ji}$ and $\mathcal{T}^{ij}_{ji}$ is more naturally suited to a homogeneous evaluation with numerical quadrature and density fitting than the conventional ansatz of separating $\mathcal{B}$ into intermediates optimized for pure density fitting, leading to greater reuse of intermediate computations.

2.4 Implementation

In the following, we present an efficient implementation of the previously derived terms, focusing on computational performance and memory usage. Careful optimization is key to achieving efficiency and avoiding significant computational overhead. We provide a step-by-step breakdown of the implementation, including the formal scaling of all performance-critical operations, with the most expensive step highlighted. For each operator, we present dedicated algorithms yielding the corresponding energy contributions, starting with algorithm 1, which addresses the $\hat{F}_{12}\hat{g}_{12}$ operator and introduces the key concepts. Here, we assume that the density matrix P and a molecular grid (MG)[88] are provided by the underlying code base. Algorithm 1 closely follows the procedure used in seminumerical exact-exchange meth-

Algorithm 1 Efficient stepwise computation of $\hat{F}_{12}\hat{g}_{12}$ integrals.
(*Energy contr. for* $\mathcal{V}_{ji}^{ij}$: eq. 41)

1:	*Initial Quantities:* P, MG	
2:	**for all** batches $b \in$ MG $(\forall g \in b)$:	$\triangleright$ openMP parallel
3:	compute AO basis functions χ_μ^g for batch b	
4:	construct batch-local density matrix $P_{\mu\nu}^b$	
5:	compute $\bar{\chi}_\mu^g$ and $\bar{\chi}_\nu^{wg}$ (with w_g) via eq. (24)	$\mathcal{O}(N_g N_\mu^2)$
6:	construct $(g\|\hat{F}_{1g}\hat{g}_{1g}\|\mu\nu)$ + contraction with $\bar{\chi}_\nu^{wg}$:	
	▸ distance-dependent integral screening	
	▸ computation of $[0]_{\hat{F}_{12}\hat{g}_{12}}^{(m)}$ + Obara-Saika recursions	$\mathcal{O}(N_g N_\mu^2)$
	▸ contract $\mathcal{FG}_\mu^{wg} = \bar{\chi}_\nu^{wg}(g\|\hat{F}_{1g}\hat{g}_{1g}\|\mu\nu)$ (eq. (25))	$\mathcal{O}(N_g N_\mu^2)$
7:	compute $E_{(41)}$ += $\bar{\chi}_\mu^g \mathcal{FG}_\mu^{wg}$	$\mathcal{O}(N_g N_\mu)$

ods within Hartree–Fock and hybrid density functional theory, e.g., sn-LinK,[89] and builds on their underlying infrastructure and conceptual framework. Energy contributions are evaluated in a batch-wise manner by partitioning the molecular grid into suitable subsets b, each containing at most 64 grid points g to maintain consistency with the more memory-intensive evaluations of other operators. For completeness, the formal scaling of the most important steps is explicitly given. Only the significant atomic orbitals χ_μ^g (AOs) are constructed for each batch b and contracted with the corresponding batch-local density matrix $P_{\mu\nu}^b$. We ad-

ditionally exploit operator sparsity and apply a highly efficient distance-dependent integral screening scheme during the construction of the 3c1e integrals $(g|\hat{F}_{1g}\hat{g}_{1g}|\mu\nu)$, as detailed in Ref. 82, Sec. 2.3. Together with the decay of basis function overlaps and the asymptotic sparsity of the batch-local density matrix for systems with a significant HOMO–LUMO gap, this enables an efficient, linear-scaling evaluation of eq. (41). Here, the construction of the primitive $[0]^{(m)}_{\hat{F}_{12}\hat{g}_{12}}$ Ten-no integrals remains the primary bottleneck and is even more expensive than the corresponding Obara–Saika[90] recursion scheme for medium- to large-sized systems.

Algorithm 2 Efficient stepwise computation of $\hat{F}_{12}^2$ integrals.
(*Energy contr. for* $\mathcal{X}_{ji}^{ij}$: eq. 45 *and* $\mathcal{B}_{ji}^{ij}$: eqs. 60/61)

1:	*Initial Quantities:* P, c, ϵ, $(f+k)$, MG	
2:	**for all** batches $b \in$ MG $(\forall g \in b)$:	▷ openMP parallel
3:	compute $\chi^g_{\mu'}$ (AO) and $\phi^g_{p'}$ (MO) basis functions for batch b	
4:	construct batch-local density matrix $P^b_{\mu\nu}$ and $\tilde{P}^b_{\mu\nu}$ (includes ϵ_i)	
5:	compute $\bar{\chi}^g_\mu$, $\tilde{\chi}^g_\mu$ (with $\tilde{P}^b_{\mu\nu}$), and $\bar{\chi}^{wg}_\nu$ (with w_g) via eq. (24)	$\mathcal{O}(N_g N_\mu^2)$
6:	compute $\mathring{\phi}^g_i = \phi^g_{p'}(f+k)^{p'}_i$	$\mathcal{O}(N_g N_{p'} N_i)$
7:	construct $(g\|\hat{F}^2_{1g}\|\mu\nu)$ + contraction with $\bar{\chi}^{wg}_\nu$:	
	▸ distance-dependent integral screening	
	▸ computation of $[0]^{(m)}_{\hat{F}^2_{12}}$ + Obara–Saika recursions	$\underline{\mathcal{O}(N_g N_\mu^2)}$
	▸ contract $\mathcal{FF}^{wg}_\mu = \bar{\chi}^g_\nu (g\|\hat{F}^2_{1g}\|\mu\nu)$ (eq. (25))	$\mathcal{O}(N_g N_\mu^2)$
8:	compute $\mathcal{FF}^{wg}_i = \mathcal{FF}^{wg}_\mu c_{\mu i}$	$\mathcal{O}(N_g N_\mu N_i)$
9:	compute $E_{(45)}$ += $\tilde{\chi}^g_\mu \mathcal{FF}^{wg}_\mu$	$\mathcal{O}(N_g N_\mu)$
10:	compute $E_{(60)}$ += $\gamma^2\, \bar{\chi}^g_\mu \mathcal{FF}^{wg}_\mu$	$\mathcal{O}(N_g N_\mu)$
11:	compute $E_{(61)}$ += $\mathring{\phi}^g_i \mathcal{FF}^{wg}_i$	$\mathcal{O}(N_g N_i)$

The evaluation of terms involving the $\hat{F}_{12}^2$ operator in algorithm 2 closely mirrors that in algorithm 1, with the primary distinction being the incorporation of orbital energies ϵ, which leads to adapted local density matrices $\tilde{P}^b_{\mu\nu}$. Otherwise, the evaluation follows the same general structure. The additional contributions in eq. (60) and eq. (61) arise from the commutator relation in eq. (58) and may be omitted depending on the chosen level of approximation. For eq. (60), the final energy contribution is simply scaled by γ^2, where γ is the exponent

of the correlation factor $\hat{F}_{12}$. The $(f+k)$ matrices are introduced by transforming $\mathcal{FF}_{\mu}^{wg}$ into the molecular orbital basis. Algorithm 2 likewise enables a highly efficient, low-scaling implementation with asymptotically linear computational complexity using only numerical quadrature for the evaluation of the occurring 4c2e integrals.

The efficient evaluation of all integrals involving either one or both of the $\hat{F}_{12}$ and $\hat{g}_{12}$ operators is outlined in algorithm 3, based on a hybrid NQ/DF/CABS-RI scheme that combines atomic and molecular orbital representations. All 6c3e integrals are treated entirely in the AO basis, as exemplified in detail for eq. (62) in Ref. 82, which enables a linear scaling evaluation of these contributions. The remaining products of 4c2e integrals appearing in the intermediates $\mathcal{V}_{ji}^{ij}$, $\mathcal{X}_{ji}^{ij}$, and $\mathcal{B}_{ji}^{ij}$ are handled in the MO basis. While a purely AO-based implementation of these products is in principle possible and would yield asymptotically linear scaling due to the decay of both electron density and operator contributions, this approach suffers from a substantially larger computational overhead. In contrast, any MO-based treatment, including localized approaches, benefits from the reduced dimensionality of the occupied MO space (number of electrons) compared to the HF AO space (number of basis functions) and can further exploit restrictions such as the frozen core approximation, making it more practical for basically all feasible systems. If multiple similar contractions differ only by the orbital space or operator, we report the formal scaling based on the most expensive among them.

The AO part of algorithm 3 largely follows the strategies employed in algorithm 1 and algorithm 2, differing primarily by additional contractions for the 6c3e integrals. The use of the commutator relation only slightly increases the computational cost, as the contraction of the combined 3c1e integrals with the exchange matrix elements $k_{\sigma'}^{\lambda'}$ scales merely as $\mathcal{O}(N_{\mu'}^2 N_b)$, with N_b denoting the number of batches, and represents just one of several contributing terms.

Algorithm 3 Efficient stepwise computation of $\hat{F}_{12}$ and $\hat{g}_{12}$ integrals.
(*Energy contr. for* $\mathcal{V}_{ji}^{ij}$: eqs. 42/43/44, $\mathcal{X}_{ji}^{ij}$: eqs. 46/47/48, *and* $\mathcal{B}_{ji}^{ij}$: eqs. 62/63/64/70/71)

Initial Quantities: P, c, ϵ, f, k, MG, $\mathcal{F}_P^{ip'}$, $\tilde{\mathcal{F}}_P^{ip} = \tilde{\mathcal{F}}_R^P \mathcal{F}_{ip}^R$

▸ stepwise: $x_{\sigma'}^{\lambda'} = P_{\lambda'\kappa'} x_{\epsilon'}^{\kappa'} P_{\sigma'\epsilon'} \rightarrow k_{\sigma'}^{\lambda'}$, $f_\sigma^{\lambda'}$, f_σ^λ $\quad \mathcal{O}(N_{\mu'}^3)$

for all batches $b \in$ MG $(\forall g \in b)$: $\quad \triangleright$ openMP parallel

compute AO basis functions $\chi_{\mu'}^g$ (AO)

construct batch-local density matrix $P_{\mu\nu}^b$ and $\tilde{P}_{\mu\nu}^b$ (includes ϵ_i)

compute $\bar{\chi}_\mu^g$, $\tilde{\chi}_\mu^g$ (with $\tilde{P}_{\mu\nu}^b$), and $\bar{\chi}_\nu^{wg}$ (with w_g) via eq. (24) $\quad \mathcal{O}(N_g N_\mu^2)$

construct $(g|\hat{F}_{1g}|\mu\nu)$, $(g|\hat{F}_{1g}|\mu\nu'')$, $(g|\hat{g}_{1g}|\mu\nu)$ + contraction with $\bar{\chi}_\mu^g/\tilde{\chi}_\mu^g$:

▸ distance-dependent integral screening

▸ computation of $[0]_{\hat{F}_{12}}^{(m)}/[0]_{\hat{g}_{12}}^{(m)}$ + Obara–Saika recursions $\quad \mathcal{O}(N_g N_{\mu'} N_\mu)$

▸ contract $\mathcal{F}_{\nu'}^{(\cdot)} = \chi_\mu^{(\cdot)}(g|\hat{F}_{1g}|\mu\nu')$ (eq. (25)) $\rightarrow \mathcal{F}_{\nu'}^g$, $\mathcal{F}_{\nu'}^{wg} = \mathcal{F}_{\nu'}^g \cdot w_g$, $\mathcal{F}_\nu^g$, $\mathcal{F}_{\tilde{\nu}}^g$ $\quad \mathcal{O}(N_g N_{\mu'} N_\mu)$

▸ contract $\mathcal{G}_\nu^g = \bar{\chi}_\mu^g\,(g|\hat{g}_{1g}|\mu\nu)$ (eq. (25)) $\quad \mathcal{O}(N_g N_\mu^2)$

compute $\square_1 = \mathcal{W}_{(\cdot)}^{wg} \mathcal{Y}_{(\cdot)}^g \rightarrow \square_1 = \mathcal{F}_{\lambda'\sigma'}, \mathcal{F}_{\lambda'\sigma}, \mathcal{F}_{\lambda\sigma}, \mathcal{F}_{\tilde{\lambda}\sigma}, \mathcal{FG}_{\lambda\sigma}$ $\quad \mathcal{O}(N_g N_{\mu'} N_\mu)$

compute $E_{6c3e}^{\square}$ += $\square_1 \cdot \square_2$ with $\square_2 = k_{\sigma'}^{\lambda'}$, $f_\sigma^{\lambda'}$, f_σ^λ, $P_{\lambda\sigma}$ $\quad \mathcal{O}(N_{\mu'}^2)$

▸ $E_{6c3e}^{\square} = E_{(44)}, E_{(48)}, E_{(62)}, E_{(63)}, E_{(64)}$

AO to MO transformation: $(g|\hat{F}_{1g}|\mu\nu)/(g|\hat{g}_{1g}|\mu\nu) \rightarrow (g|\hat{F}_{1g}|ip)/(g|\hat{g}_{1g}|ip)$ $\quad \mathcal{O}(N_g N_\mu^2 N_i)$

compute $\phi_{p'}^g$, $\quad \phi_i^{wg} = w_g \phi_i^g$, $\quad \dot{\phi}_p^g = \phi_i^g \cup \big(-\phi_a^g\big)$, $\quad \tilde{\phi}_{p'}^{\prime g} = \phi_{q'}^g f_{p'}^{q'}$, $\quad \check{\phi}_a^g = \phi_b^g f_a^b$, $\quad \check{\phi}_k^g = \phi_l^g f_k^l$

for all aux batches $P_{\text{aux}} \in P$ $(\forall Q \in P_{\text{aux}})$:

contract $\mathcal{F}_Q^{ix}/\tilde{\mathcal{F}}_{pi}^Q$ with $\{\phi^g\}$:

$$
\begin{array}{lcll}
\mathring{\mathcal{F}}_{pg}^{Q}{}_{[Qp\times g]} & = & \tilde{\mathcal{F}}_{pi}^{Q}{}_{[Qp\times i]}\, \phi_i^{wg}{}_{[i\times g]} & \big[\mathcal{V}_{ji}^{ij}, \mathcal{X}_{ji}^{ij}, \mathcal{B}_{ji}^{ij}\big] \quad \mathcal{O}(N_g N_P N_p N_i) \\
\overset{\bullet}{\mathcal{F}}_{Q}^{ig}{}_{[iQ\times g]} & = & \mathcal{F}_{Q}^{ip}{}_{[iQ\times p]}\, \dot{\phi}_p^g{}_{[p\times g]} & \big[\mathcal{V}_{ji}^{ij}, \mathcal{X}_{ji}^{ij}\big] \quad \mathcal{O}(N_g N_P N_p N_i) \\
\overset{t}{\mathcal{F}}_{Q}^{ig}{}_{[iQ\times g]} & = & \mathcal{F}_{Q}^{ia}{}_{[iQ\times a]}\, \check{\phi}_a^g{}_{[a\times g]} \quad \text{(scale -0.5)} & \big[\mathcal{T}_{ji}^{ij}\big] \quad \mathcal{O}(N_g N_P N_a N_i) \\
\overset{u}{\mathcal{F}}_{Q}^{ig}{}_{[iQ\times g]} & = & \mathcal{F}_{Q}^{ik}{}_{[iQ\times k]}\, \tilde{\phi}_k^{\prime g}{}_{[k\times g]} \quad \text{(scale -1.0)} & \big[\mathcal{U}_{ji}^{ij}\big] \quad \mathcal{O}(N_g N_P N_k N_i) \\
\check{\mathcal{F}}_{Q}^{ig}{}_{[iQ\times g]} & = & \mathcal{F}_{Q}^{ia}{}_{[iQ\times a]}\, \tilde{\phi}_a^{\prime g}{}_{[a\times g]} \quad \text{add to } \overset{u}{\mathcal{F}}_{Q}^{ig}, \overset{t}{\mathcal{F}}_{Q}^{ig} & \big[\mathcal{T}_{ji}^{ij}, \mathcal{U}_{ji}^{ij}\big] \quad \mathcal{O}(N_g N_P N_a N_i) \\
\overset{u}{\mathcal{F}}_{Q}^{ig}{}_{[iQ\times g]} & \mathrel{+}= & \mathcal{F}_{Q}^{ip''}{}_{[iQ\times p'']}\, \tilde{\phi}_{p''}^{\prime g}{}_{[p''\times g]} & \big[\mathcal{U}_{ji}^{ij}\big] \quad \underline{\mathcal{O}(N_g N_P N_{p''} N_i)} \\
\overset{u}{\mathcal{F}}_{Q}^{ig}{}_{[iQ\times g]} & \mathrel{+}= & \mathcal{F}_{Q}^{ik}{}_{[iQ\times k]}\, \check{\phi}_k^g{}_{[k\times g]} & \big[\mathcal{U}_{ji}^{ij}\big] \quad \mathcal{O}(N_g N_P N_k N_i)
\end{array}
$$

for all g $(\forall * \in g)$:

compute $\triangle_1 = \Big[\overset{\bullet}{\mathcal{F}}_{Q}^{i*}, \overset{t}{\mathcal{F}}_{Q}^{i*}, \overset{u}{\mathcal{F}}_{Q}^{i*}\Big]_{[i\times Q]} \mathring{\mathcal{F}}_{(p,a,k)\,*}^{Q}{}_{[Q\times(p,a,k)]} \rightarrow \triangle_1 = \underline{\overset{\bullet}{\mathcal{F}}}_{ip}^{*}, \underline{\overset{t}{\mathcal{F}}}_{ia}^{*}, \underline{\overset{u}{\mathcal{F}}}_{ik}^{*}$ $\mathcal{O}(N_g N_P N_p N_i)$

compute $E_{(42/43)}$ += $(*|\hat{g}_{1*}|ip)\, \underline{\overset{\bullet}{\mathcal{F}}}_{ip}^{*}$ $\quad \mathcal{O}(N_g N_p N_i)$

compute $E_{(46/47)}$ += $\epsilon_i (*|\hat{F}_{1*}|ip)\, \underline{\overset{\bullet}{\mathcal{F}}}_{ip}^{*}$ $\quad \mathcal{O}(N_g N_p N_i)$

compute $E_{(70)}$ += $(*|\hat{F}_{1*}|ik)\, \underline{\overset{u}{\mathcal{F}}}_{ik}^{*}$ $\quad \mathcal{O}(N_g N_k N_i)$

compute $E_{(71)}$ += $(*|\hat{F}_{1*}|ia)\, \underline{\overset{t}{\mathcal{F}}}_{ia}^{*}$ $\quad \mathcal{O}(N_g N_a N_i)$

Regarding the MO part of algorithm 3, the construction of the MO 3c1e integrals is summarized in a single step. However, for a memory-efficient implementation, the different subspaces and operators are treated separately, and the AO to MO transformation is carried out subsequently and in batches of 16 numerical grid points. This approach ensures that only one subset of AO 3c1e integrals needs to be kept in memory at a time. In this context, one major advantage of following our new evaluation through $\mathcal{U}_{ji}^{ij}$ and $\mathcal{T}_{ji}^{ij}$ is that it avoids the use of $(g|\hat{F}_{1g}|ip'')$ integrals, thus bypassing the corresponding $\mathcal{O}(N_g N_{\mu''} N_\mu N_i)$ scaling of the AO to MO transformation and the associated memory requirements. The next step involves constructing molecular orbitals for each batch of grid points, which are scaled by a factor or contracted with multiple orbital spaces spanning Fock matrix elements. This enables an efficient contraction over the approximated complete space index p', incurring a computational cost of only $\mathcal{O}(N_g N_{p'}^2)$.

All subsequent evaluations scale as $\mathcal{O}(M^4)$ and may require up to $N_g N_P N_p$ of memory per batch. To alleviate this demand, we recommend introducing an additional batching scheme for the auxiliary basis functions used in density fitting, with each auxiliary batch P_{aux} comprising 16 auxiliary functions Q. This choice is motivated by the fact that the auxiliary index is the only one shared across all storage-intensive intermediates, as well as both uncontracted and contracted three-center two-electron integrals, thereby avoiding inefficient matrix-vector products during contraction. For the latter, we applied an optimized reordering scheme by organizing the data into auxiliary batches. The recommended storage layout is indicated in square brackets, for example, $[xy \times z]$, with x as the fastest-changing index and z as the leading one. This format ensures that, in column-major storage, the data can be directly interpreted as a $xy \times z$ matrix. Further contraction with transposed molecular orbitals $\{\phi^g\}$ via matrix-matrix multiplication yields the intermediates $\overset{\circ}{\mathcal{F}}{}_{pg}^{Q}$, $\overset{\bullet}{\mathcal{F}}{}_{Q}^{ig}$, $\overset{u}{\mathcal{F}}{}_{Q}^{ig}$, and $\overset{t}{\mathcal{F}}{}_{Q}^{ig}$, all of which have g as their leading index. In this step, the remaining full-RI index p' is contracted out, representing the most computationally demanding operation in the entire explicitly correlated code, with a total formal scaling over all batches of $\mathcal{O}(N_g N_P N_{p'} N_i)$. The resulting

intermediates can then be used to compute the final contributions for each grid point within the batch via additional matrix-matrix multiplications, yielding the desired energies upon contraction with the respective MO 3c1e integrals.

Due to the increased memory requirements of the hybrid AO and MO evaluation in algorithm 3, we generally recommend smaller grid batch sizes of 64 or 128, which only marginally affect the performance of the distance-dependent integral screening.[82,91] With additional batching over the auxiliary basis functions, the memory footprint per grid batch scales only quadratically as $\mathcal{O}(N_{p'}N_i)$, though with a considerable prefactor. For all parts of the algorithm involving densely populated intermediates, we recommend using high-performance matrix algebra routines (BLAS-3), such as Intel MKL.[92] To further reduce the number of significant elements, one possible strategy could be to enhance sparsity in the MO representation by introducing localized orbitals. To preserve the correspondence between the Fock matrix elements f and the orbital energies ϵ, some occupied indices would, however, need to remain in canonical form during contractions. The additional sparsity introduced by localization could potentially be exploited in conjunction with the intrinsic overlap and operator sparsity of the AO 3c1e and 3c2e F12 integrals.

3 Computational Details

All calculations presented in this work were carried out with a development version of our FermiONs++ program package.[93–96] Preliminary SCF calculations were converged to within 10^{-7} in the DIIS commutator norm,[97,98] defined as $||\mathbf{FPS} - \mathbf{SPF}||$. Hartree–Fock and F12-type Fock matrix elements were evaluated using sn-LinK[89,99] with a gm[5/3] multigrid, and RI-J[100] in combination with the cc-pVXZ-JKfit basis[101] (X = D, T, Q), as described in Ref. 49. The explicitly correlated F12 corrections employed a fixed Slater-type geminal (STG) correlation factor,[38,81] defined as $\hat{F}_{12} = \frac{1}{\gamma}\exp(-\gamma r_{12})$ with $\gamma = 1.3$, together with the cc-pVXZ-F12 basis set family.[102–104] The corresponding complementary auxiliary basis sets, cc-pVXZ-F12/OptRI+,[105] and the density-fitting sets, cc-pVXZ-F12/MP2fit,[106] were used accordingly (X = D, T, Q). All numerical quadrature computations employed highly optimized numerical grids[88] (denoted as gX) with a grid point threshold of 10^{-5}, as summarized in Table 2. Integral kernels and the corresponding FermiONs++ binary were compiled with the Intel Compiler 19.1.0[107] using the optimization flags `-Ofast` and `-march=native`, enabling AVX-512 instructions for optimal efficiency. Performance was assessed on two AMD EPYC 9334 processors (64 cores, 2.5 GHz base clock, with a theoretical maximum single-core boost frequency of 3.91 GHz) with SMT disabled to reduce the effective memory footprint per thread. Basis set superposition errors (BSSE) were corrected via a mixed scheme employing counterpoise uncorrected and corrected values.[108]

Table 2: Summary of the grid layout for the carbon atom, separated into inner, medium, and outer regions without grid point screening.

Grid	n_{rad}	$n_{\text{ang}(\text{inner/medium/outer})}$	$n_{\text{tot,C}}$
$g0$	15	14/38/ 74	916
$g1$	20	14/50/110	1646
$g2$	25	26/74/194	3372
$g3$	35	38/110/302	7040
$g4$	45	50/194/434	13012
$g7$	65	110/434/1454	57284

4 Results

In the following section, we compare our novel hybrid NQ/DF/CABS-RI ansatz with the conventional DF/CABS-RI approach in terms of both numerical precision and performance. Precision is assessed against virtually exact reference data obtained with an extensive g7 grid (57 284 points per carbon atom) and without distance-dependent screening of the 3c1e AO integrals ($\vartheta_{\mathrm{NQ}} = 0$) using NQ/DF/CABS-RI. We evaluate non-covalent interaction (NCI) and isomerization energies using cc-pVXZ-F12 (X = D, T, Q) basis-set combinations (HF/CABS-RI/DF) for the S22[109] and ISO34[110] benchmark sets, and provide cc-pVDZ-F12 results for the L7 set,[111] including larger systems (sec. 4.1). Additional results for the S66 set,[112] showing similar trends, as well as a detailed comparison of absolute energies for the L7 set, illustrating the impact of the DF/CABS-RI and NQ/DF/CABS-RI ansatz on the total correlation energy, are provided in the Supporting Information (SI). To investigate efficiency, we separate the performance analysis into the computation of the 4c2e integrals (algorithms 1 and 2) and of the remaining intermediates (algorithm 3), considering different grid sizes and screening thresholds (sec. 4.2). For the first two algorithms, we demonstrate near-linear scaling using glycine chains,[113] in line with previous findings. For algorithm 3, we further report timings for daptomycin and a carbon nanotube to illustrate real-world performance. To ensure fair comparison across program packages, reference DF/CABS-RI timings are based on the FLOP counts of the rate-determining steps divided by peak BLAS matrix–matrix multiplication efficiency (DGEMM), excluding memory allocation and copying. Finally, we emphasize that no form of MO integral screening is applied throughout this analysis.

4.1 Precision

Figures 1a-f illustrate the effect of employing NQ/DF/CABS-RI instead of DF/CABS-RI (AO 3c2e integral screening via IPB[91] with screening threshold $\vartheta_{\mathrm{DF}} = 10^{-9}$) on the precision of DF-MP2 + F12 NCI and isomerization energies for the S22 (a,c,e) and ISO34 (b,d,f)

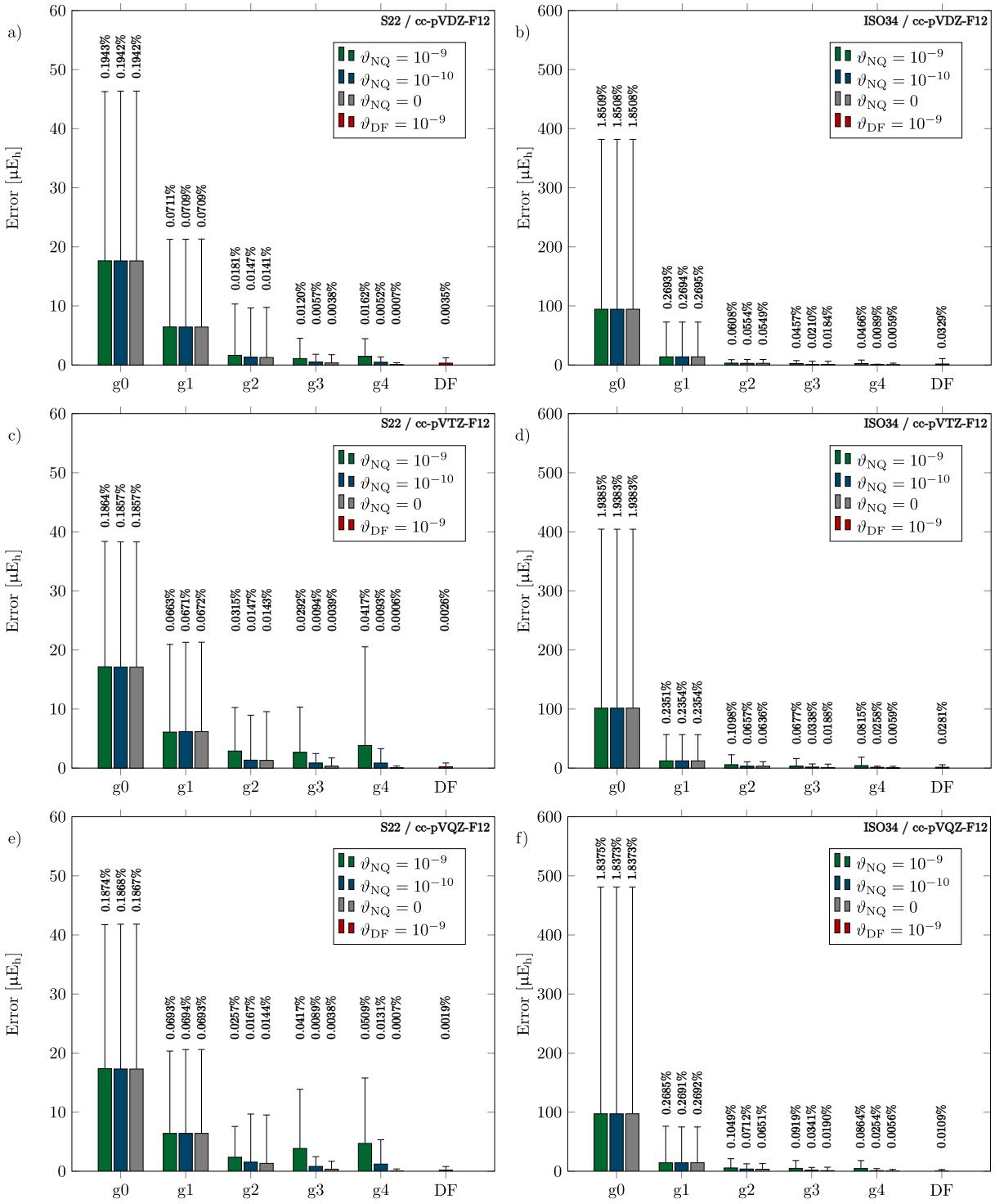

Figure 1: Mean absolute errors (MAE), maximum absolute errors (MAX), and MAEs relative to the average reference DF-MP2 + F12 non-covalent interaction or isomerization energy (MAE/AVG in %) for the S22 (a,c,e) and ISO34 (b,d,f) test sets, respectively. Results are shown for DF/NQ/CABS-RI with various grid sizes (g0–g4) and thresholds ϑ_{NQ}, as well as for DF/CABS-RI with $\vartheta_{\mathrm{DF}} = 10^{-9}$. Data are given for cc-pVDZ-F12 (a,b), cc-pVTZ-F12 (c,d), and cc-pVQZ-F12 (e,f) basis set combinations.

benchmark sets using double-, triple-, and quadruple-ζ basis set combinations. The plots show mean absolute errors (MAE), maximum absolute errors (MAX), and mean absolute errors normalized to the average DF-MP2 + F12 reference energy (MAE/AVG) for different AO 3c1e integral screening thresholds ϑ_{NQ}.

Generally, NQ/DF/CABS-RI delivers high precision already for medium-sized grids. For example, the mean absolute errors for a g2 grid are below 6 μE_h (0.004 kcal/mol) for the S22 and ISO34 test sets. As expected, systematically increasing the grid size further improves precision, with results converging toward the numerically exact limit. Here, we follow our previously developed screening protocol in Ref. 82, designed to avoid under- and overscreening of the AO 3c1e integrals. For larger grids (g3 and g4), a small intentional error persists, increasing slightly from double- to quadruple-ζ basis due to the larger number of screened basis functions per atom. With a screening threshold of $\vartheta_{\mathrm{NQ}} = 10^{-9}$, mean errors range from about 1 to 5 μE_h, with maximum deviations around 20 μE_h (0.013 kcal/mol). For $\vartheta_{\mathrm{NQ}} = 10^{-10}$, mean errors are lower, ranging from 0.5 to 1.5 μE_h, with maximum deviations around 10 μE_h (0.006 kcal/mol).

Our NQ/DF/CABS-RI approach maintains a grid-defined level of precision that is largely independent of basis set size, with consistent mean absolute and percentage errors. While the F12 correction diminishes with increasing basis set size, the absolute grid error remains essentially constant, whereas the contribution of the DF-MP2 correlation energies increases. The conventional DF/CABS-RI approach yields nearly error-free results that converge toward the exact limit as both the basis set and the DF basis set are increased, albeit at substantially higher computational cost. Notably, the finest grids (g3 and g4) match or even exceed the precision of the conventional DF approach, particularly when a sufficiently tight screening threshold is applied. To further investigate the precision for larger molecular systems, Figure 2 presents results for the L7 interaction energy test set, which comprises structures of up to 112 atoms. As expected, errors decrease with increasing grid size, although absolute deviations are somewhat larger than for the smaller S22 set.

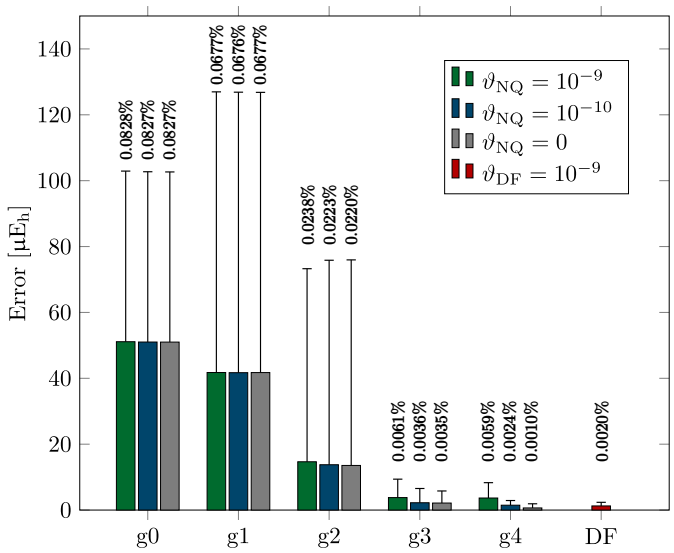

Figure 2: Mean absolute errors (MAE), maximum absolute errors (MAX), and MAEs relative to the average reference DF-MP2 + F12 non-covalent interaction energy (MAE/AVG in %) for the L7 test set. Results are shown for DF/NQ/CABS-RI with various grid sizes (g0–g4) and thresholds ϑ_{NQ}, as well as for DF/CABS-RI with $\vartheta_{\mathrm{DF}} = 10^{-9}$ for a cc-pVDZ-F12 basis set combination.

Across all test sets, the g2 grid serves as our standard choice, yielding negligible errors with maximum deviations below 80 μE_h (0.05 kcal/mol), and often substantially smaller. The g1 grid remains suitable for many applications, with maximum errors below 130 μE_h (0.08 kcal/mol). Even the coarsest g0 grid, while providing less accurate estimates for isomerization energies, remains useful for interaction energies in larger systems with percentage errors around 0.1 %. For comparison, the largest member of the L7 test set, which features the highest number of basis functions, shows an error of 0.11 % with a g0 grid, whereas DF-MP2 without the F12 correction introduces an error of 4.63 %.

In general, the target precision of NQ/DF/CABS-RI calculations can be adjusted to the specific application, enabling an optimal balance between numerical precision and computational efficiency. To avoid introducing additional errors, we chose a $\vartheta_{\mathrm{NQ}} = 10^{-10}$ screening threshold for 3c1e integrals in our performance tests of NQ/DF/CABS-RI.

4.2 Performance Comparison

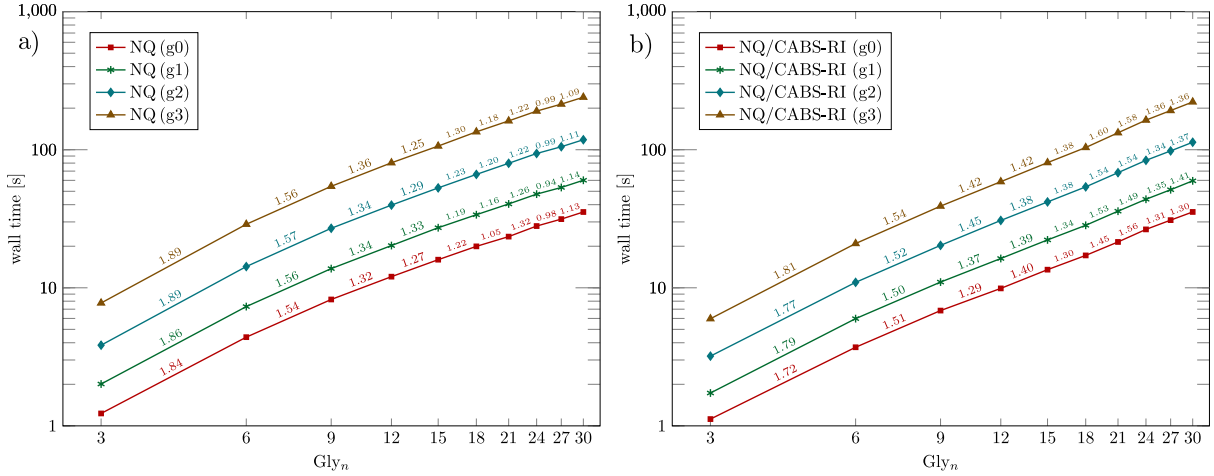

Figure 3: Log-log plot of the wall times and the corresponding scaling exponents between consecutive structures for algorithm 1 (a) and algorithm 2 (b) ($\vartheta_{\mathrm{NQ}} = 10^{-10}$), using multiple grid sizes for linear glycine chains (Gly_n, $n \in \{3, 6, 9, 12, 15, 18, 21, 24, 27, 30\}$) with a cc-pVDZ-F12 basis set combination.

Figures 3a and 3b depict the scaling behavior of algorithm 1 and algorithm 2 for different grid sizes (g0–g3) using linear glycine chains. Algorithm 1 exhibits slightly lower efficiency for small system sizes compared to algorithm 2, which can be attributed to the enhanced locality of the $\hat{F}_{12}^2$ operator. For the largest systems, the scaling exponents of algorithm 2 remain around 1.3–1.4 due to the growing contribution of additional terms arising from the commutator relation. Overall, both algorithms achieve near-linear scaling, with exponents around 1.4 or 1.1, respectively. For the corresponding direct terms, we anticipate that combining RI-J with the J-engine ansatz[100,113] will yield the best performance, which, however, lies beyond the scope of the present work.

Since algorithm 3 encompasses the most computationally demanding part of the whole explicitly correlated F12 correction, we place special emphasis on investigating its scaling behavior and performance relative to the classical DF/CABS-RI approach. To enable a unified comparison across different quantum chemical codes, we report the total number of TFLOPs per structure and per calculation for the rate-determining $\mathcal{O}(M^4)$ steps of our

novel NQ/DF/CABS-RI method, alongside the corresponding timings. For the classical DF/CABS-RI approach, performance is evaluated under the assumption of peak hardware efficiency, counting the total number of TFLOPs for the performance-critical $\mathcal{O}(M^4)$ and $\mathcal{O}(M^5)$ scaling steps. This framework provides a quantitative basis to assess the efficiency and scaling of our new approach relative to established methodologies. The theoretical peak double-precision (FP64) performance of the two AMD EPYC 9334 processors used in this study, with a total of 64 cores and an aggregate theoretical peak parallel clock frequency of 2.7 GHz, can be estimated as follows. Each core supports two FMA units, with each AVX-512 FMA executing eight FP64 operations per instruction. At the maximum boost frequency, the processors lead to a theoretical peak performance of

$$64 \times 2.7\ \text{GHz} \times 2\ \text{FMA/core} \times 8\ \text{FP64/FMA} \approx 2.76\ \text{TFLOPs}. \tag{72}$$

This value represents a theoretical upper bound for the achievable double-precision throughput on this processor. In our CPU benchmarks, we employed matrix–matrix multiplication of $10\,000 \times 10\,000$ matrices using highly optimized BLAS routines (DGEMM). The matrices were allocated once and subsequently reused with random values over multiple iterations, so that no additional costs for memory allocation, data copying, or management occurred during the measurement. This achieved a performance of about 2.35 TFLOPs/s, corresponding to roughly 85% of the theoretical peak performance. Since no practical implementation can surpass the performance of pure DGEMM and most fall noticeably short, we take this value as an idealized reference for all DF/CABS-RI timings. To analyze the performance of algorithm 3 (NQ/DF/CABS-RI) for different grid sizes, we again considered linear glycine chains, with results summarized in Figure 4 for cc-pVDZ-F12 (a, c, e) and cc-pVTZ-F12 (b, d, f) basis set combinations. Panels a) and b) present log–log plots of wall times together with the scaling exponents between consecutive structures.

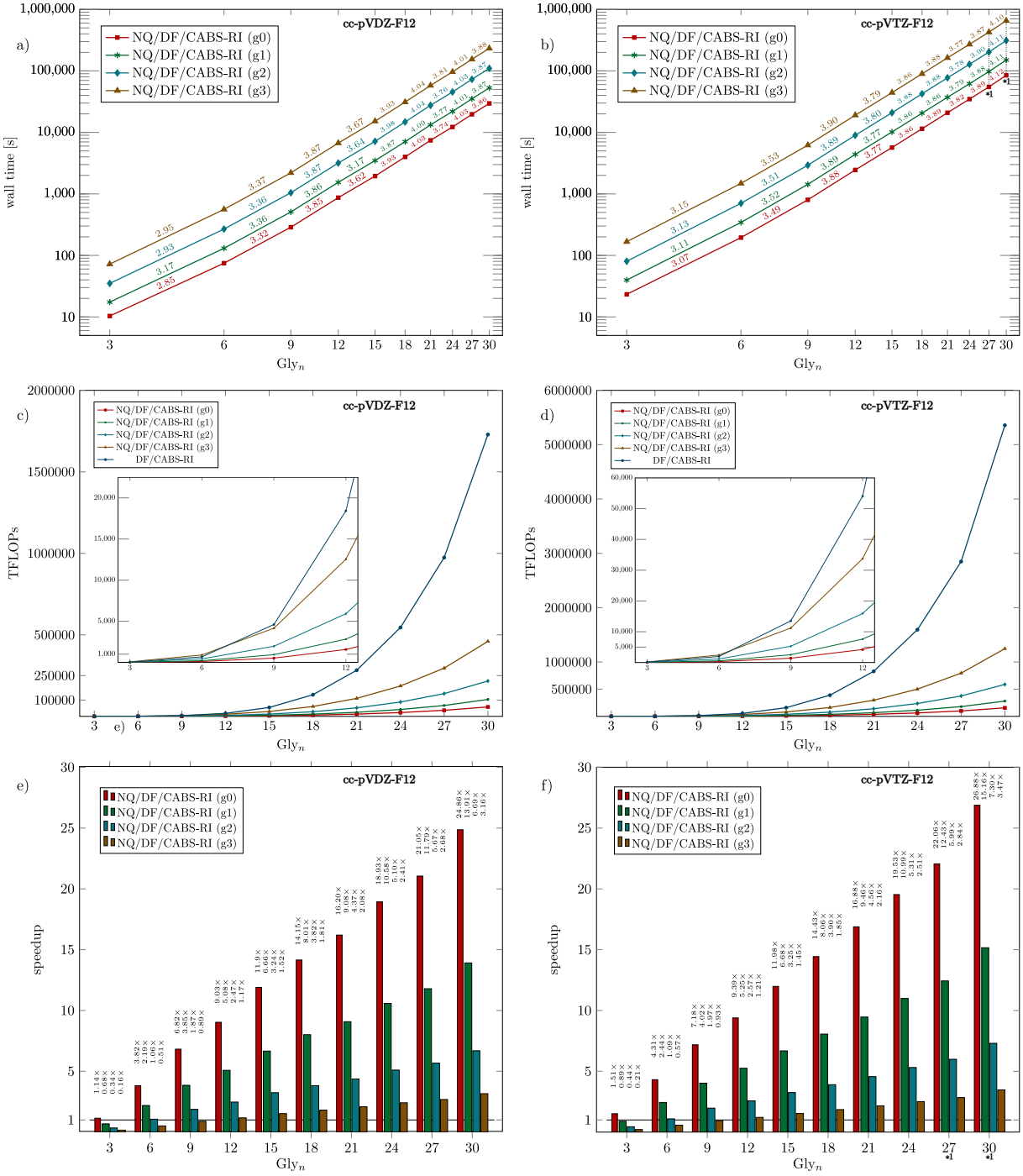

Figure 4: Comparison of algorithm 3 (NQ/DF/CABS-RI with $\vartheta_{\mathrm{NQ}} = 10^{-10}$, using multiple grid sizes) and DF/CABS-RI for linear glycine chains (Gly$_n$, $n \in \{3, 6, 9, 12, 15, 18, 21, 24, 27, 30\}$): Log-log plots of wall times and scaling exponents between consecutive structures (a,b), comparisons of floating point operations for the rate-determining steps per structure (TFLOPs) (c,d), and corresponding speedups for NQ/DF/CABS-RI (e,f) using cc-pVDZ-F12 (a,c,e) and cc-pVTZ-F12 (b,d,f) basis set combinations.

Here, the empirical scaling behavior of algorithm 3 approaches $\mathcal{O}(M^4)$ with system size M, starting from an effective scaling of approximately $\mathcal{O}(M^3)$ for small systems where the construction of the three-center one-electron integrals has a strong influence on performance. Panels c) and d) compare the theoretical floating-point operation counts for the rate-determining steps per structure (TFLOPs) for NQ/DF/CABS-RI as well as DF/CABS-RI. The speedups shown in panels e) and f) are obtained by comparing measured NQ/DF/CABS-RI timings against an idealized perfectly performing DF/CABS-RI implementation (DGEMM efficiency). As expected, smaller grids lead to better performance and an earlier break-even point between DF/CABS-RI and NQ/DF/CABS-RI. Moreover, NQ/DF/CABS-RI gains additional efficiency for larger basis sets, since the number of grid points remains essentially constant and thus scales like a fixed index, which benefits the lower-scaling NQ-based formulation.

Overall, NQ/DF/CABS-RI exhibits clear advantages starting from Gly_9 ($C_{18}H_{29}N_9O_{10}$), achieving roughly twice the speed of DF/CABS-RI. This advantage increases with system size, reaching up to 6.7× speedup for the g2 grid with the double-ζ basis. For the largest triple-ζ calculations (Gly_{27} and Gly_{30}), computational times were carefully estimated based on FLOP counts, as the required RAM exceeded available memory. For Gly_{30}, this results in estimated speedups ranging from 3.5× to 26.9×, depending on grid size. RAM limitations for larger systems can be addressed through extended batching, which entails computing the 3c1e MO integrals $N_{\text{batch}}^{\text{3c1e}}$ times as an additional cost. Further optimization of the batching procedure beyond algorithm 3, such as Lagrangian-based minimal-overhead batching,[114] would be possible but lies outside the scope of the present work.

Figure 5 highlights the performance of NQ/DF/CABS-RI relative to DF/CABS-RI for two representative real-world examples: (a) daptomycin, an antibiotic drug of last resort, and (b) a carbon nanotube with a highly delocalized electronic structure. For daptomycin, speedups ranging from 21.69 to 2.74 are achieved across different grid sizes, where our NQ/DF/CABS-RI code shows around 70 % of the theoretical maximum hardware efficiency

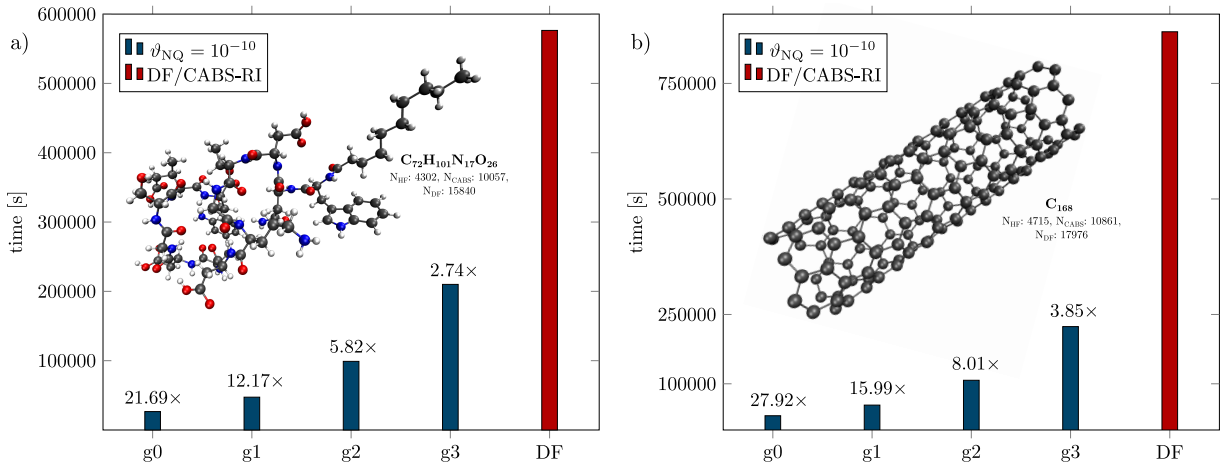

Figure 5: NQ/DF/CABS-RI and DF/CABS-RI timings and corresponding speedups for (a) daptomycin ($C_{72}H_{101}N_{17}O_{26}$) and (b) a C_{168} nanotube, using multiple grid sizes and $\vartheta_{NQ} = 10^{-10}$ with a cc-pVDZ-F12 basis set combination (HF/CABS-RI/DF).

(2.76 TFLOPs/s). Generally, for systems with a significant HOMO-LUMO gap, further performance gains of NQ/DF/CABS-RI appear feasible by introducing some form of localized MOs and corresponding screening, for example, through a pair natural orbital approach,[44,58,115] distance-dependent MO screening via integral partition bounds,[91] or a hybrid strategy. This perspective is motivated by the observation that, for this structure, even in the MO picture roughly 50 % of the 3c1e integral values fall below 10^{-12} for both the $\hat{F}_{12}$ and $\hat{g}_{12}$ operators.

For the computed nanotube, localized MO-based integral screening might compromise accuracy due to the strong delocalization of the electronic structure. In this case, NQ/DF/CABS-RI itself drastically reduces the computational time relative to DF/CABS-RI by factors of 27.92 (g0), 15.99 (g1), 8.01 (g2), and 3.85 (g3). A g2 grid provides a particularly favorable balance, lowering the cost by roughly one order of magnitude while maintaining high precision. Although the nanotube involves a comparable number of basis functions as daptomycin, it achieves better performance because of the more favorable ratio of active orbitals to numerical grid points. This demonstrates the efficiency and robustness of NQ/DF/CABS-RI, especially for systems with strongly delocalized electronic structures.

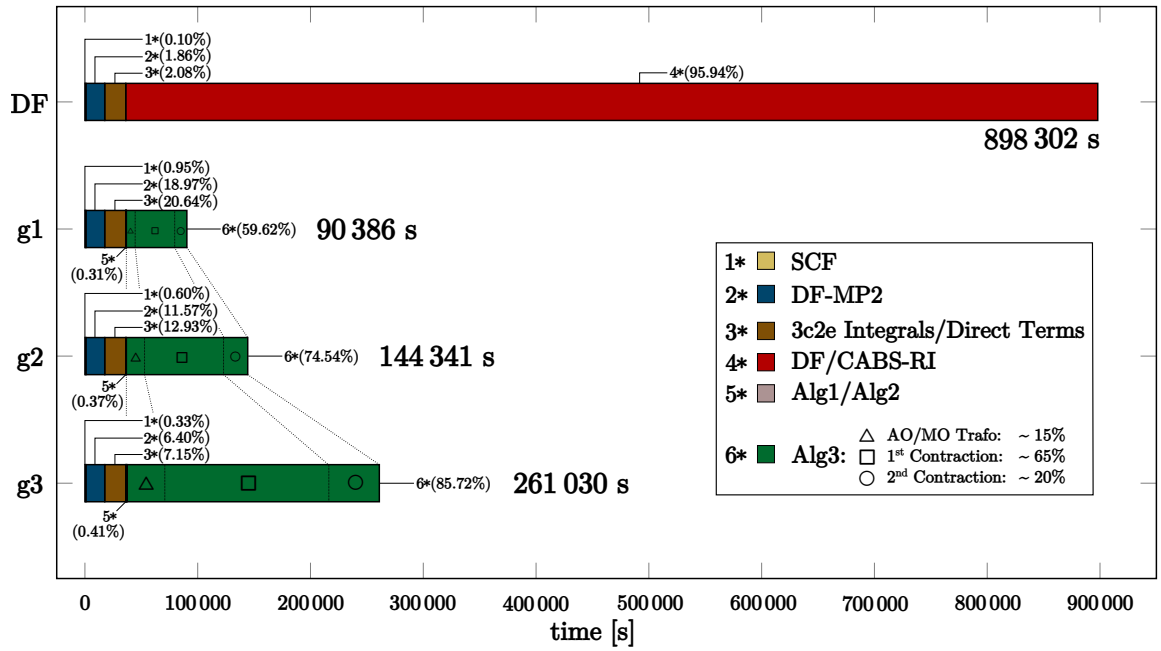

Figure 6: Absolute and relative computational costs for SCF + DF-MP2 + F12 calculations of a C_{168} nanotube, comparing DF/CABS-RI (estimated via DGEMM efficiency) with NQ/DF/CABS-RI using g1, g2, and g3 grids, including a detailed cost breakdown, all computed with the cc-pVDZ-F12 basis set combination.

Figure 6 outlines the relative computational cost for an RI-MP2-F12 calculation of the C_{168} nanotube, including SCF and DF-MP2 steps, using DF/CABS-RI and NQ/DF/CABS-RI with a g1, g2, and g3 grid. While the cost of the SCF (∼15 min) and DF-MP2 (∼4.5 h) calculations remains overall the same, the DF/CABS-RI route requires an additional 9.97 days for the F12 correction, whereas the hybrid NQ/DF/CABS-RI approach requires only approx. 1.25 days for a g2 grid. Considering the full calculation (SCF + DF-MP2 + F12), excluding the exchange-type terms involving $\hat{F}_{12}$ and $\hat{g}_{12}$, both methods require approximately 10 h. The computation of the direct-type intermediates accounts for only a minor fraction of the total cost, typically being significantly less demanding than the construction of the required 3c2e integrals. For our NQ ansatz, the additional cost for these exchange-type terms (algorithm 3) amounts to 14.9 h for g1, 29.9 h for g2, and 62.2 h for g3, respectively. Although algorithm 3 still dominates the computation, its cost is substantially lower than the 239.4 h required by DF/CABS-RI. Regarding the individual steps of algorithm 3, the computational

time for the construction of AO 3c1e integrals becomes negligible for these system sizes due to effective screening, while the AO to MO transformation of the 3c1e integrals accounts for roughly 10–15% (△). The contraction of the 3c2e integrals with the MO quantities on the grid dominates the overall workload, contributing approximately 65–70% (□), including the formally most expensive step, followed by the final contraction with the 3c1e integrals, which contributes around 20% (◯). Following our approach and considering even larger systems, the total cost for the F12 correction will eventually drop below that of the corresponding DF-MP2 calculation when using the same basis set, potentially rendering CBS extrapolation methods unnecessary.

5 Conclusion

We have introduced a novel and efficient framework for treating exchange-type contributions within the explicitly correlated F12 correction to second-order Møller–Plesset perturbation theory. By employing numerical quadrature, both the formal and the observed empirical scaling with respect to the system size M are rigorously reduced from $\mathcal{O}(M^5)$ to $\mathcal{O}(M^4)$. The approach is rooted in an approximation-free formulation of the strong-orthogonality operator $\hat{Q}_{12}$, which enables a fundamentally different treatment of the key exchange-type intermediates $\mathcal{V}$, $\mathcal{X}$, and $\mathcal{B}$. In this reformulation, exchange-type four-center two-electron (4c2e) and six-center three-electron (6c3e) integrals can be evaluated with high efficiency in the AO picture and exhibit linear scaling with the system size by means of the NQ/CABS-RI approach. The remaining products of 4c2e integrals are computed using a novel MO scheme that combines numerical quadrature with density fitting, denoted as NQ/DF/CABS-RI. Moreover, the resulting expressions require fewer CABS-RI insertions, with indices spanning the full orbital space being contracted at an early stage of the evaluation. For both NQ/CABS-RI and NQ/DF/CABS-RI, we have developed efficient algorithms that enable the systematic contraction of all terms while exploiting shared subspaces and intermediate

quantities.

Benchmarks on several representative test sets demonstrate that our approach attains accuracies comparable to the conventional DF/CABS-RI ansatz, with the precision systematically controlled by the quadrature grid size. Even for large molecules, a modest g2 grid yields mean absolute deviations to the explicitly correlated correction below 0.01 kcal/mol and maximum errors under 0.05 kcal/mol, which ensures reliable results for both noncovalent interaction and isomerization energies. Overall, NQ/DF/CABS-RI enables a flexible balance between numerical precision and efficiency.

We further investigated the scaling behavior of the proposed methods using linear glycine chains. The results demonstrate near linear scaling for our NQ/CABS-RI ansatz, resulting in a negligible computational cost even for large systems. Generally, the largest computational effort arises from the products of 4c2e integrals, which can be efficiently evaluated with $\mathcal{O}(M^4)$ scaling using DF/NQ/CABS-RI. To enable a unified comparison across different software packages, we take as reference an idealized DF/CABS-RI implementation achieving the efficiency of highly optimized BLAS-3 matrix–matrix (DGEMM) operations on the target hardware, considering only the number of floating-point operations in the rate-determining contractions and ignoring memory management. This choice is intentionally conservative and likely underestimates the speedups achievable in practice. In this comparison, for a g2 grid and molecules of approximately 40 second-period atoms (C, N, O, F) and corresponding H atoms, the NQ/DF/CABS-RI approach achieves more than twice the computational speed. For larger systems, the speedup increases significantly, e.g., a chain of 30 glycine monomers using a cc-pVTZ-F12 basis set combination exhibits speedups ranging from 3.5× to 26.9×, depending on grid size. For real-world examples, speedups of roughly one order of magnitude are achieved for the rate-determining steps with virtually no loss of numerical precision. This effect is particularly pronounced for systems with strongly delocalized electronic structures, where the computational time for the total F12 correction can be reduced from 10.6 days to 1.5 days. In general, NQ/DF/CABS-RI substantially narrows the gap in

computational cost between the explicitly correlated F12 correction and the corresponding conventional DF-MP2 calculation using the same basis set. Future work will focus on developing an efficient screening strategy based on localized MOs to further reduce computational cost.

Acknowledgement

The authors thank Y. Lemke (LMU Munich) for helpful discussions and Dr. J. Kussmann (LMU Munich) for providing a development version of the FermiONs++[93–96] program package. Financial support was provided by the Excellence Cluster EXC2111-390814868 "Munich Center for Quantum Science and Technology" (MCQST) by the Deutsche Forschungsgemeinschaft (DFG). C.O. acknowledges, in addition, financial support as Max Planck Fellow of MPI-FKF Stuttgart.

Supporting Information Available

Detailed data on NQ/DF/CABS-RI benchmark data (S22, S66, ISO34) are included in the supporting information.

References

(1) Kato, T. On the eigenfunctions of many-particle systems in quantum mechanics. *Commun. Pure Appl. Math.* **1957**, *10*, 151–177.

(2) Hylleraas, E. A. Neue Berechnung der Energie des Heliums im Grundzustande, sowie des tiefsten Terms von Ortho-Helium. *Z. Phys.* **1929**, *54*, 347–366.

(3) Sims, J. S.; Hagstrom, S. Combined Configuration-Interaction—Hylleraas-Type Wave-Function Study of the Ground State of the Beryllium Atom. *Phys. Rev. A* **1971**, *4*, 908.

(4) Sims, J. S.; Hagstrom, S. A. Mathematical and computational science issues in high precision Hylleraas-configuration interaction variational calculations: I. Three-electron integrals. *J. Phys. B At. Mol. Opt. Phys.* **2004**, *37*, 1519.

(5) Sims, J. S.; Hagstrom, S. A. Mathematical and computational science issues in high precision Hylleraas–configuration interaction variational calculations: II. Kinetic energy and electron–nucleus interaction integrals. *J. Phys. B At. Mol. Opt. Phys.* **2007**, *40*, 1575.

(6) Sims, J. S.; Hagstrom, S. A. Mathematical and computational science issues in high precision Hylleraas-configuration interaction variational calculations: III. Four-electron integrals. *J. Phys. B At. Mol. Opt. Phys.* **2015**, *48*, 175003.

(7) Boys S.F; Handy N.C The integral formulae for the variational solution of the molecular many-electron wave equation in terms of Gaussian functions with direct electronic correlation. *Proc. R. Soc. London. Ser. A. Math. Phys. Sci.* **1960**, *258*, 402–411.

(8) Singer, K. The use of Gaussian (exponential quadratic) wave functions in molecular problems - I. General formulae for the evaluation of integrals. *Proc. R. Soc. London. Ser. A. Math. Phys. Sci.* **1960**, *258*, 412–420.

(9) Cencek, W.; Rychlewski, J. Many-electron explicitly correlated Gaussian functions. I. General theory and test results. *J. Chem. Phys.* **1993**, *98*, 1252–1261.

(10) Cencek, W.; Komasa, J.; Rychlewski, J. Benchmark calculations for two-electron systems using explicitly correlated Gaussian functions. *Chem. Phys. Lett.* **1995**, *246*, 417–420.

(11) Mitroy, J.; Bubin, S.; Horiuchi, W.; Suzuki, Y.; Adamowicz, L.; Cencek, W.; Szalewicz, K.; Komasa, J.; Blume, D.; Varga, K. Theory and application of explicitly correlated Gaussians. *Rev. Mod. Phys.* **2013**, *85*, 693–749.

(12) Bubin, S.; Pavanello, M.; Tung, W. C.; Sharkey, K. L.; Adamowicz, L. Born-oppenheimer and non-born-oppenheimer, atomic and molecular calculations with explicitly correlated gaussians. *Chem. Rev.* **2013**, *113*, 36–79.

(13) Boys S.F; Handy N.C A calculation for the energies and wavefunctions for states of neon with full electronic correlation accuracy. *Proc. R. Soc. London. A. Math. Phys. Sci.* **1969**, *310*, 63–78.

(14) Boys S.F; Handy N.C A condition to remove the indeterminacy in interelectronic correlation functions. *Proc. R. Soc. London. A. Math. Phys. Sci.* **1969**, *309*, 209–220.

(15) Boys S.F; Handy N.C The determination of energies and wavefunctions with full electronic correlation. *Proc. R. Soc. London. A. Math. Phys. Sci.* **1969**, *310*, 43–61.

(16) Boys S.F; Handy N.C. A first solution, for LiH, of a molecular transcorrelated wave equation by means of restricted numerical integration. *Proc. R. Soc. London. A. Math. Phys. Sci.* **1969**, *311*, 309–329.

(17) Handy, N. C. On the minimization of the variance of the transcorrelated hamiltonian. *Mol. Phys.* **1971**, *21*, 817–828.

(18) Handy, N. C. Towards an understanding of the form of correlated wavefunctions for atoms. *J. Chem. Phys.* **1973**, *58*, 279–287.

(19) Ten-No, S. A feasible transcorrelated method for treating electronic cusps using a frozen Gaussian geminal. *Chem. Phys. Lett.* **2000**, *330*, 169–174.

(20) Ten-No, S. Three-electron integral evaluation in the transcorrelated method using a frozen Gaussian geminal. *Chem. Phys. Lett.* **2000**, *330*, 175–179.

(21) Hino, O.; Tanimura, Y.; Ten-no, S. Biorthogonal approach for explicitly correlated calculations using the transcorrelated Hamiltonian. *J. Chem. Phys.* **2001**, *115*, 7865–7871.

(22) Hino, O.; Tanimura, Y.; Ten-no, S. Application of the transcorrelated Hamiltonian to the linearized coupled cluster singles and doubles model. *Chem. Phys. Lett.* **2002**, *353*, 317–323.

(23) Umezawa, N.; Tsuneyuki, S. Transcorrelated method for electronic systems coupled with variational Monte Carlo calculation. *J. Chem. Phys.* **2003**, *119*, 10015–10031.

(24) Luo, H. Variational transcorrelated method. *J. Chem. Phys.* **2010**, *133*, 154109.

(25) Kersten, J. A.; Booth, G. H.; Alavi, A. Assessment of multireference approaches to explicitly correlated full configuration interaction quantum Monte Carlo. *J. Chem. Phys.* **2016**, *145*, 54117.

(26) Luo, H.; Alavi, A. Combining the Transcorrelated Method with Full Configuration Interaction Quantum Monte Carlo: Application to the Homogeneous Electron Gas. *J. Chem. Theory Comput.* **2018**, *14*, 1403–1411.

(27) Cohen, A. J.; Luo, H.; Guther, K.; Dobrautz, W.; Tew, D. P.; Alavi, A. Similarity transformation of the electronic Schrödinger equation via Jastrow factorization. *J. Chem. Phys.* **2019**, *151*, 61101.

(28) Baiardi, A.; Reiher, M. Transcorrelated density matrix renormalization group. *J. Chem. Phys.* **2020**, *153*, 164115.

(29) Schraivogel, T.; Cohen, A. J.; Alavi, A.; Kats, D. Transcorrelated coupled cluster methods. *J. Chem. Phys.* **2021**, *155*, 191101.

(30) Baiardi, A.; Lesiuk, M.; Reiher, M. Explicitly Correlated Electronic Structure Calculations with Transcorrelated Matrix Product Operators. *J. Chem. Theory Comput.* **2022**, *18*, 4203–4217.

(31) Ammar, A.; Scemama, A.; Giner, E. Extension of selected configuration interaction for transcorrelated methods. *J. Chem. Phys.* **2022**, *157*, 134107.

(32) Liao, K.; Zhai, H.; Christlmaier, E. M.; Schraivogel, T.; Ríos, P. L.; Kats, D.; Alavi, A. Density Matrix Renormalization Group for Transcorrelated Hamiltonians: Ground and Excited States in Molecules. *J. Chem. Theory Comput.* **2023**, *19*, 1734–1743.

(33) Schraivogel, T.; Christlmaier, E. M.; López Ríos, P.; Alavi, A.; Kats, D. Transcorrelated coupled cluster methods. II. Molecular systems. *J. Chem. Phys.* **2023**, *158*, 214106.

(34) Ten-No, S. L. Nonunitary projective transcorrelation theory inspired by the F12 ansatz. *J. Chem. Phys.* **2023**, *159*.

(35) Kutzelnigg, W. r12-Dependent terms in the wave function as closed sums of partial wave amplitudes for large l. *Theor. Chim. Acta.* **1985**, *68*, 445–469.

(36) Klopper, W.; Kutzelnigg, W. Møller-plesset calculations taking care of the correlation CUSP. *Chem. Phys. Lett.* **1987**, *134*, 17–22.

(37) Kutzelnigg, W.; Klopper, W. Wave functions with terms linear in the interelectronic coordinates to take care of the correlation cusp. I. General theory. *J. Chem. Phys.* **1991**, *94*, 1985–2001.

(38) Ten-no, S. Initiation of explicitly correlated Slater-type geminal theory. *Chem. Phys. Lett.* **2004**, *398*, 56–61.

(39) Valeev, E. F. Improving on the resolution of the identity in linear R12 ab initio theories. *Chem. Phys. Lett.* **2004**, *395*, 190–195.

(40) Manby, F. R. Density fitting in second-order linear-r12 Møller–Plesset perturbation theory. *J. Chem. Phys.* **2003**, *119*, 4607–4613.

(41) Ten-No, S.; Manby, F. R. Density fitting for the decomposition of three-electron integrals in explicitly correlated electronic structure theory. *J. Chem. Phys.* **2003**, *119*, 5358–5363.

(42) Klopper, W.; Samson, C. C. Explicitly correlated second-order Møller–Plesset methods with auxiliary basis sets. *J. Chem. Phys.* **2002**, *116*, 6397–6410.

(43) Werner, H. J.; Adler, T. B.; Manby, F. R. General orbital invariant MP2-F12 theory. *J. Chem. Phys.* **2007**, *126*, 164102.

(44) Werner, H. J. Eliminating the domain error in local explicitly correlated second-order Møller-Plesset perturbation theory. *J. Chem. Phys.* **2008**, *129*, 51.

(45) Bachorz, R. A.; Bischoff, F. A.; Glöß, A.; Hättig, C.; Höfener, S.; Klopper, W.; Tew, D. P. The MP2-F12 method in the TURBOMOLE program package. *J. Comput. Chem.* **2011**, *32*, 2492–2513.

(46) Ma, Q.; Werner, H. J. Scalable Electron Correlation Methods. 2. Parallel PNO-LMP2-F12 with Near Linear Scaling in the Molecular Size. *J. Chem. Theory Comput.* **2015**, *11*, 5291–5304.

(47) Wang, Y. M.; Hättig, C.; Reine, S.; Valeev, E.; Kjærgaard, T.; Kristensen, K. Explicitly correlated second-order Møller-Plesset perturbation theory in a Divide-Expand-Consolidate (DEC) context. *J. Chem. Phys.* **2016**, *144*, 204112.

(48) Urban, L.; Thompson, T. H.; Ochsenfeld, C. A scaled explicitly correlated F12 correction to second-order Møller-Plesset perturbation theory. *J. Chem. Phys.* **2021**, *154*, 44101.

(49) Urban, L.; Laqua, H.; Ochsenfeld, C. Highly Efficient and Accurate Computation of Multiple Orbital Spaces Spanning Fock Matrix Elements on Central and Graphics Processing Units for Application in F12 Theory. *J. Chem. Theory Comput.* **2022**, *18*, 4218–4228.

(50) Klopper, W. Highly accurate coupled-cluster singlet and triplet pair energies from explicitly correlated calculations in comparison with extrapolation techniques. *Mol. Phys.* **2001**, *99*, 481–507.

(51) Valeev, E. F. Coupled-cluster methods with perturbative inclusion of explicitly correlated terms: a preliminary investigation. *Phys. Chem. Chem. Phys.* **2007**, *10*, 106–113.

(52) Noga, J.; Kedžuch, S.; Šimunek, J.; Ten-No, S. Explicitly correlated coupled cluster F12 theory with single and double excitations. *J. Chem. Phys.* **2008**, *128*, 174103.

(53) Torheyden, M.; Valeev, E. F. Variational formulation of perturbative explicitly-correlated coupled-cluster methods. *Phys. Chem. Chem. Phys.* **2008**, *10*, 3410–3420.

(54) Shiozaki, T.; Kamiya, M.; Hirata, S.; Valeev, E. F. Explicitly correlated coupled-cluster singles and doubles method based on complete diagrammatic equations. *J. Chem. Phys.* **2008**, *129*, 71101.

(55) Valeev, E. F.; Daniel Crawford, T. Simple coupled-cluster singles and doubles method with perturbative inclusion of triples and explicitly correlated geminals: The CCSD $(\mathrm{T})_{\overline{\mathrm{R12}}}$ model. *J. Chem. Phys.* **2008**, *128*, 244113.

(56) Noga, J.; Šimunek, J. On the one-particle basis set relaxation in R12 based theories. *Chem. Phys.* **2009**, *356*, 1–6.

(57) Hättig, C.; Tew, D. P.; Köhn, A. Communications: Accurate and efficient approximations to explicitly correlated coupled-cluster singles and doubles, CCSD-F12. *J. Chem. Phys.* **2010**, *132*, 231102.

(58) Schmitz, G.; Hättig, C.; Tew, D. P. Explicitly correlated PNO-MP2 and PNO-CCSD and their application to the S66 set and large molecular systems. *Phys. Chem. Chem. Phys.* **2014**, *16*, 22167–22178.

(59) Hehn, A. S.; Klopper, W. Communication: Explicitly-correlated second-order correction to the correlation energy in the random-phase approximation. *J. Chem. Phys.* **2013**, *138*, 181104.

(60) Hehn, A. S.; Tew, D. P.; Klopper, W. Explicitly correlated ring-coupled-cluster-doubles theory. *J. Chem. Phys.* **2015**, *142*, 194106.

(61) Hehn, A. S.; Holzer, C.; Klopper, W. Explicitly-correlated ring-coupled-cluster-doubles theory: Including exchange for computations on closed-shell systems. *Chem. Phys.* **2016**, *479*, 160–169.

(62) Ten-no, S. A simple F12 geminal correction in multi-reference perturbation theory. *Chem. Phys. Lett.* **2007**, *447*, 175–179.

(63) Shiozaki, T.; Werner, H. J. Communication: Second-order multireference perturbation theory with explicit correlation: CASPT2-F12. *J. Chem. Phys.* **2010**, *133*, 141103.

(64) Shiozaki, T.; Knizia, G.; Werner, H. J. Explicitly correlated multireference configuration interaction: MRCI-F12. *J. Chem. Phys.* **2011**, *134*, 34113.

(65) Haunschild, R.; Mao, S.; Mukherjee, D.; Klopper, W. A universal explicit electron correlation correction applied to Mukherjee's multi-reference perturbation theory. *Chem. Phys. Lett.* **2012**, *531*, 247–251.

(66) Shiozaki, T.; Werner, H. J. Multireference explicitly correlated F12 theories. *Mol. Phys.* **2013**, *111*, 607–630.

(67) Liu, W.; Hanauer, M.; Köhn, A. Explicitly correlated internally contracted multireference coupled-cluster singles and doubles theory: ic-MRCCSD(F12*). *Chem. Phys. Lett.* **2013**, *565*, 122–127.

(68) Roskop, L. B.; Kong, L.; Valeev, E. F.; Gordon, M. S.; Windus, T. L. Assessment of perturbative explicitly correlated methods for prototypes of multiconfiguration electronic structure. *J. Chem. Theory Comput.* **2014**, *10*, 90–101.

(69) Guo, Y.; Sivalingam, K.; Valeev, E. F.; Neese, F. Explicitly correlated N-electron valence state perturbation theory (NEVPT2-F12). *J. Chem. Phys.* **2017**, *147*, 64110.

(70) Mehta, N.; Martin, J. M. Reduced-Scaling Double Hybrid Density Functional Theory with Rapid Basis Set Convergence through Localized Pair Natural Orbital F12. *J. Phys. Chem. Lett.* **2022**, *13*, 9332–9338.

(71) Mehta, N.; Martin, J. M. Explicitly Correlated Double-Hybrid DFT: A Comprehensive Analysis of the Basis Set Convergence on the GMTKN55 Database. *J. Chem. Theory Comput.* **2022**, *18*, 5978–5991.

(72) Hofener, S.; Klopper, W. Analytical nuclear gradients of the explicitly correlated Møller–Plesset second-order energy. *Mol. Phys.* **2010**, *108*, 1783–1796.

(73) Gyorffy, W.; Knizia, G.; Werner, H. J. Analytical energy gradients for explicitly correlated wave functions. I. Explicitly correlated second-order Møller-Plesset perturbation theory. *J. Chem. Phys.* **2017**, *147*, 214101.

(74) Gyorffy, W.; Werner, H. J. Analytical energy gradients for explicitly correlated wave functions. II. Explicitly correlated coupled cluster singles and doubles with perturbative triples corrections: CCSD(T)-F12. *J. Chem. Phys.* **2018**, *148*, 114104.

(75) Mitchell, E. C.; Turney, J. M.; Schaefer, H. F. Automatic Differentiation for Explicitly Correlated MP2. *J. Chem. Theory Comput.* **2024**, *20*, 8538.

(76) Friesner, R. A. Solution of self-consistent field electronic structure equations by a pseudospectral method. *Chem. Phys. Lett.* **1985**, *116*, 39–43.

(77) Friesner, R. A. Solution of the Hartree–Fock equations by a pseudospectral method: Application to diatomic molecules. *J. Chem. Phys.* **1986**, *85*, 1462–1468.

(78) Friesner, R. A.; Friesne, R. A. Solution of the Hartree–Fock equations for polyatomic molecules by a pseudospectral method. *J. Chem. Phys.* **1987**, *86*, 3522–3531.

(79) Ringnalda, M. N.; Belhadj, M.; Friesner, R. A. Pseudospectral Hartree–Fock theory: Applications and algorithmic improvements. *J. Chem. Phys.* **1990**, *93*, 3397–3407.

(80) Ten-No, S. Explicitly correlated second order perturbation theory: Introduction of a rational generator and numerical quadratures. *J. Chem. Phys.* **2004**, *121*, 117–129.

(81) Ten-no, S. New implementation of second-order Møller-Plesset perturbation theory with an analytic Slater-type geminal. *J. Chem. Phys.* **2007**, *126*, 14108.

(82) Urban, L.; Laqua, H.; Thompson, T. H.; Ochsenfeld, C. Efficient Exploitation of Numerical Quadrature with Distance-Dependent Integral Screening in Explicitly Correlated F12 Theory: Linear Scaling Evaluation of the Most Expensive RI-MP2-F12 Term. *J. Chem. Theory Comput.* **2024**, *20*, 3706–3718.

(83) Bokhan, D.; Bernadotte, S.; Ten-no, S. Implementation of the CCSD(T)(F12) method using numerical quadratures. *Chem. Phys. Lett.* **2009**, *469*, 214–218.

(84) Bokhan, D.; Trubnikov, D. N. Explicitly correlated second-order Møller-Plesset perturbation theory employing pseudospectral numerical quadratures. *J. Chem. Phys.* **2012**, *136*, 204110.

(85) Kong, L.; Bischoff, F. A.; Valeev, E. F. Explicitly correlated R12/F12 methods for electronic structure. *Chem. Rev.* **2012**, *112*, 75–107.

(86) Ten-no, S.; Noga, J. Explicitly correlated electronic structure theory from R12/F12 ansätze. *Wiley Interdiscip. Rev. Comput. Mol. Sci.* **2012**, *2*, 114–125.

(87) Sacchetta, F.; Graf, D.; Laqua, H.; Ambroise, M. A.; Kussmann, J.; Dreuw, A.; Ochsenfeld, C. An effective sub-quadratic scaling atomic-orbital reformulation of the scaled opposite-spin RI-CC2 ground-state model using Cholesky-decomposed densities and an attenuated Coulomb metric. *J. Chem. Phys.* **2022**, *157*, 104104.

(88) Laqua, H.; Kussmann, J.; Ochsenfeld, C. An improved molecular partitioning scheme for numerical quadratures in density functional theory. *J. Chem. Phys.* **2018**, *149*, 204111.

(89) Laqua, H.; Thompson, T. H.; Kussmann, J.; Ochsenfeld, C. Highly Efficient, Linear-Scaling Seminumerical Exact-Exchange Method for Graphic Processing Units. *J. Chem. Theory Comput.* **2020**, *16*, 1456–1468.

(90) Obara, S.; Saika, A. Efficient recursive computation of molecular integrals over Cartesian Gaussian functions. *J. Chem. Phys.* **1986**, *84*, 3963–3974.

(91) Thompson, T. H.; Ochsenfeld, C. Integral partition bounds for fast and effective screening of general one-, two-, and many-electron integrals. *J. Chem. Phys.* **2019**, *150*, 44101.

(92) *Intel Corporation: Intel Math Kernel Library*, version 2023.4.0, see. `https://software.intel.com/en-us/mkl`, 2023.

(93) Kussmann, J.; Ochsenfeld, C. Pre-selective screening for matrix elements in linear-scaling exact exchange calculations. *J. Chem. Phys.* **2013**, *138*, 134114.

(94) Kussmann, J.; Ochsenfeld, C. Preselective screening for linear-scaling exact exchange-gradient calculations for graphics processing units and general strong-scaling massively parallel calculations. *J. Chem. Theory Comput.* **2015**, *11*, 918–922.

(95) Kussmann, J.; Ochsenfeld, C. Employing OpenCL to Accelerate Ab Initio Calculations on Graphics Processing Units. *J. Chem. Theory Comput.* **2017**, *13*, 2712–2716.

(96) Kussmann, J.; Ochsenfeld, C. Hybrid CPU/GPU Integral Engine for Strong-Scaling Ab Initio Methods. *J. Chem. Theory Comput.* **2017**, *13*, 3153–3159.

(97) Pulay, P. Convergence acceleration of iterative sequences. the case of scf iteration. *Chem. Phys. Lett.* **1980**, *73*, 393–398.

(98) Pulay, P. Improved SCF convergence acceleration. *J. Comput. Chem.* **1982**, *3*, 556–560.

(99) Laqua, H.; Kussmann, J.; Ochsenfeld, C. Accelerating seminumerical Fock-exchange calculations using mixed single- And double-precision arithmethic. *J. Chem. Phys.* **2021**, *154*, 214116.

(100) Kussmann, J.; Laqua, H.; Ochsenfeld, C. Highly Efficient Resolution-of-Identity Density Functional Theory Calculations on Central and Graphics Processing Units. *J. Chem. Theory Comput.* **2021**, *17*, 1512–1521.

(101) Weigend, F. A fully direct RI-HF algorithm: Implementation, optimised auxiliary basis sets, demonstration of accuracy and efficiency. *Phys. Chem. Chem. Phys.* **2002**, *4*, 4285–4291.

(102) Peterson, K. A.; Adler, T. B.; Werner, H. J. Systematically convergent basis sets for explicitly correlated wavefunctions: The atoms H, He, B-Ne, and Al-Ar. *J. Chem. Phys.* **2008**, *128*, 84102.

(103) Hill, J. G.; Peterson, K. A. Correlation consistent basis sets for explicitly correlated wavefunctions: valence and core–valence basis sets for Li, Be, Na, and Mg. *Phys. Chem. Chem. Phys.* **2010**, *12*, 10460–10468.

(104) Hill, J. G.; Peterson, K. A. Correlation consistent basis sets for explicitly correlated wavefunctions: Pseudopotential-based basis sets for the post- d main group elements Ga-Rn. *J. Chem. Phys.* **2014**, *141*, 94106.

(105) Shaw, R. A.; Hill, J. G. Approaching the Hartree-Fock Limit through the Complementary Auxiliary Basis Set Singles Correction and Auxiliary Basis Sets. *J. Chem. Theory Comput.* **2017**, *13*, 1691–1698.

(106) Kritikou, S.; Hill, J. G. Auxiliary Basis Sets for Density Fitting in Explicitly Correlated Calculations: The Atoms H-Ar. *J. Chem. Theory Comput.* **2015**, *11*, 5269–5276.

(107) *Intel C++ Compiler*, version 19.1.0.166, see. `https://software.intel.com/c-compilers`, 2019.

(108) Boys, S. F.; Bernardi, F. The calculation of small molecular interactions by the differences of separate total energies. Some procedures with reduced errors. *Mol. Phys.* **1970**, *19*, 553–566.

(109) Jurečka, P.; Šponer, J.; Černý, J.; Hobza, P. Benchmark database of accurate (MP2 and CCSD(T) complete basis set limit) interaction energies of small model complexes, DNA base pairs, and amino acid pairs. *Phys. Chem. Chem. Phys.* **2006**, *8*, 1985–1993.

(110) Grimme, S.; Steinmetz, M.; Korth, M. How to compute isomerization energies of organic molecules with quantum chemical methods. *J. Org. Chem.* **2007**, *72*, 2118–2126.

(111) Sedlak, R.; Janowski, T.; Pitoňák, M.; Řezáč, J.; Pulay, P.; Hobza, P. Accuracy of quantum chemical methods for large noncovalent complexes. *J. Chem. Theory Comput.* **2013**, *9*, 3364–3374.

(112) Řezáč, J.; Riley, K. E.; Hobza, P. S66: A well-balanced database of benchmark interaction energies relevant to biomolecular structures. *J. Chem. Theory Comput.* **2011**, *7*, 2427–2438.

(113) Neese, F.; Colinet, P.; DeSouza, B.; Helmich-Paris, B.; Wennmohs, F.; Becker, U. The "Bubblepole" (BUPO) Method for Linear-Scaling Coulomb Matrix Construction with or without Density Fitting. *J. Phys. Chem. A* **2025**, *129*, 2618–2637.

(114) Drontschenko, V.; Graf, D.; Laqua, H.; Ochsenfeld, C. Lagrangian-Based Minimal-Overhead Batching Scheme for the Efficient Integral-Direct Evaluation of the RPA Correlation Energy. *J. Chem. Theory Comput.* **2021**, *17*, 5623–5634.

(115) Werner, H. J.; Hansen, A. Accurate Calculation of Isomerization and Conformational Energies of Larger Molecules Using Explicitly Correlated Local Coupled Cluster Methods in Molpro and ORCA. *J. Chem. Theory Comput.* **2023**, *19*, 7007–7030.

TOC Graphic

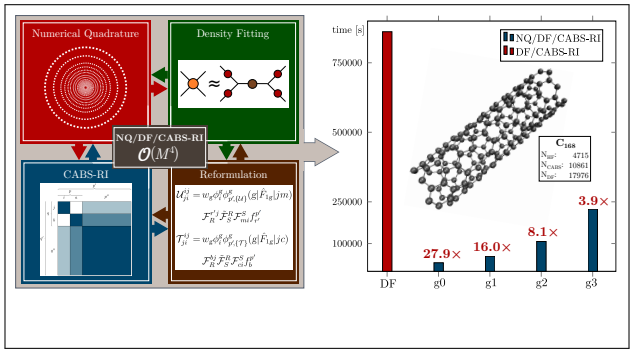
Numerical Quadrature
Density Fitting
NQ/DF/CABS-RI
$\mathcal{O}(M^4)$
CABS-RI
Reformulation
time [s]
NQ/DF/CABS-RI
DF/CABS-RI
750000
500000
250000
100000
C_{168}
N_{BF}: 4715
N_{CABS}: 10861
N_{BF}: 17976
27.9×
16.0×
8.1×
3.9×
DF
g0
g1
g2
g3

Formulation of an Efficient $\mathcal{O}(M^4)$-Scaling Explicitly Correlated MP2-F12 Correction by Combining Numerical Quadrature with Density Fitting and CABS-RI

Supporting Information

Lars Urban,[†,‡] Henryk Laqua,[†] Travis H. Thompson,[†] and Christian Ochsenfeld[*,†,‡]

†*Chair of Theoretical Chemistry, Department of Chemistry, University of Munich (LMU), D-81377 Munich, Germany*

‡*Max Planck Institute for Solid State Research, D-70569 Stuttgart, Germany*

E-mail: christian.ochsenfeld@uni-muenchen.de

1 Absolute Energies

To illustrate the contribution of the exchange-type F12 correction to the overall correlation energy, Table S1 reports the mean exchange energies $E^{3*C}_{F12,exch}$ for DF/NQ/CABS-RI and DF/CABS-RI and their ratios relative to the direct contribution ($E^{3*C}_{F12,direct}$), the total F12 correction (E^{3*C}_{F12}), and the total correlation energy (DF-MP2 + F12) for the L7 benchmark set (Ref. 111 in main text). As expected from perturbation theory, the exchange corrections are positive (destabilizing), partially canceling approximately 26.5% of the negative (stabilizing) direct contributions. The exchange term accounts for roughly 36% of the net F12 correction, while the total F12 correction contributes approximately 16.4% to the overall correlation energy. Notably, these ratios remain virtually constant across all grid sizes, demonstrating the robustness of the NQ/DF/CABS-RI approach.

Table S1: Mean exchange correlation energies [mE_h] and corresponding ratios [%] for the L7 benchmark set employing NQ/DF/CABS-RI with various grid sizes (g0–g4, $\vartheta_{NQ} = 10^{-10}$) and DF/CABS-RI ($\vartheta_{IPB} = 10^{-9}$) for the cc-pVDZ-F12 basis set combination. Reference values (grid-independent): $E_{DF\text{-}MP2} = \mathbf{-7575.729}$ mE_h, $E_{F12,direct} = \mathbf{-2025.493}$ mE_h.

Method	$E^{3*C}_{F12,exch}$	$\left\lvert\frac{Exch}{Direct}\right\rvert$	$\left\lvert\frac{Exch}{F12}\right\rvert$	$\left\lvert\frac{F12}{Corr_{tot}}\right\rvert$
g0	537.486	26.536	36.121	16.417
g1	537.276	26.526	36.102	16.419
g2	537.301	26.527	36.104	16.419
g3	537.259	26.525	36.100	16.419
g4	537.247	26.524	36.099	16.419
DF	537.770	26.550	36.147	16.415

Figure S1 illustrates the effect of employing NQ/DF/CABS-RI and DF/CABS-RI on the precision of DF-MP2 + F12 overall correlation energies for the L7 benchmark set using the cc-pVDZ-F12 basis set combination. The figure shows mean absolute errors (MAE), maximum absolute errors (MAX), and mean absolute errors normalized to the average reference energy (MAE/AVG) for different grid sizes and screening thresholds ϑ_{NQ}.

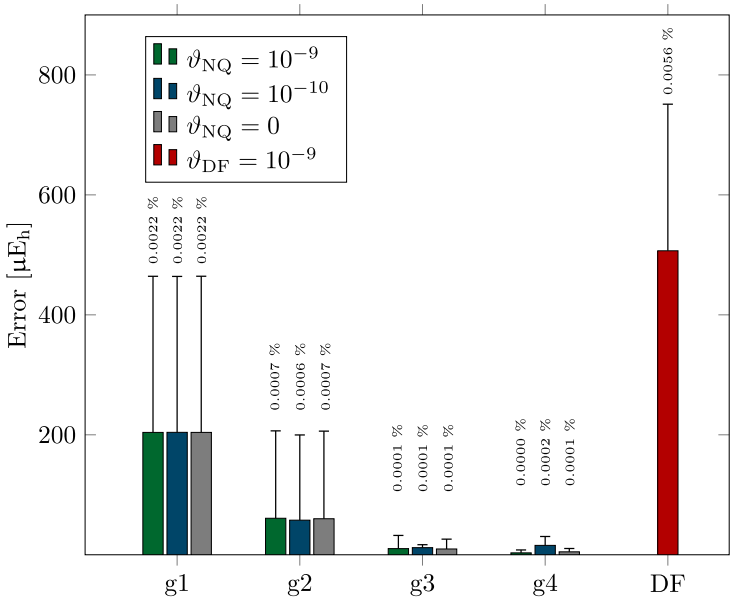

Figure S1: Mean absolute errors (MAE), maximum absolute errors (MAX), and MAEs relative to the average reference absolute energy (MAE/AVG in %) for the L7 test set. Results are shown for NQ/DF/CABS-RI with various grid sizes (g1–g4) and thresholds ϑ_{NQ}, as well as for DF/CABS-RI with $\vartheta_{\mathrm{DF}} = 10^{-9}$. Errors were evaluated against a g7 grid ($\vartheta_{\mathrm{NQ}} = 0$) reference.

As expected, the error decreases with increasing grid size (g0 results were excluded to improve the visualization). Generally, a g2 grid already provides excellent precision with mean errors of roughly 0.04 kcal/mol, delivering reliable results even for the large system sizes considered. The observed differences in overall energies between DF/CABS-RI and the NQ/DF/CABS-RI reference (using a converged g7 grid) stem from the different mathematical approximations inherent to each approach. Density fitting introduces a systematic error through the incompleteness of the auxiliary basis set. While this error is highly consistent and largely cancels in relative energies (such as non-covalent interactions or isomerization energies), it manifests as a constant shift in absolute energies. In contrast, NQ/DF/CABS-RI evaluates certain components of the exchange-type intermediates directly in real space via numerical quadrature, thereby reducing the reliance on auxiliary basis functions for these terms. Consequently, the two methods converge to slightly different absolute energies, though both provide comparable precision for chemically relevant energy differences, as demonstrated by the benchmark results presented in this work.

2 Isomerization and Non-Covalent Interaction Energies

Table S2: Mean absolute errors [μE_h] (MAEs), max. absolute errors [μE_h] (MAX), and MAEs relative to the average reference RI-MP2 + F12 non-covalent isomerization energy [%] for the **ISO34** test set (Ref. 110 in main text) employing NQ/DF/CABS-RI with various grid sizes ($g0$-$g4$) and thresholds ϑ_{NQ} and DF/CABS-RI ($\vartheta_{IPB} = 10^{-9}$) for different cc-pVXZ-F12 (X = D, T, Q) basis set combinations. Errors were evaluated against a g7 grid ($\vartheta = 0$) reference.

Method		cc-pVDZ-F12			cc-pVTZ-F12			cc-pVQZ-F12		
Grid/DF	ϑ	MAE	MAX	$\frac{\text{MAE}}{\text{AVG}}$	MAE	MAX	$\frac{\text{MAE}}{\text{AVG}}$	MAE	MAX	$\frac{\text{MAE}}{\text{AVG}}$
	10^{-9}	94.382	381.816	1.8509	101.543	404.424	1.9385	97.226	481.028	1.8375
g0	10^{-10}	94.380	381.814	1.8508	101.534	404.286	1.9383	97.216	481.098	1.8373
	0	94.379	381.812	1.8508	101.536	404.284	1.9383	97.215	481.080	1.8373
	10^{-9}	13.836	72.728	0.2693	12.363	56.887	0.2351	14.294	76.211	0.2685
g1	10^{-10}	13.841	72.640	0.2694	12.379	56.749	0.2354	14.325	74.959	0.2691
	0	13.842	72.633	0.2695	12.375	56.723	0.2354	14.332	74.966	0.2692
	10^{-9}	3.123	9.025	0.0608	5.769	22.560	0.1098	5.586	21.198	0.1049
g2	10^{-10}	2.845	9.226	0.0554	3.454	10.752	0.0657	3.792	12.587	0.0712
	0	2.821	9.299	0.0549	3.343	10.896	0.0636	3.468	12.912	0.0651
	10^{-9}	2.349	7.448	0.0457	3.560	16.245	0.0677	4.896	18.169	0.0919
g3	10^{-10}	1.078	6.587	0.0210	1.778	7.016	0.0338	1.815	6.471	0.0341
	0	0.947	6.534	0.0184	0.990	6.753	0.0188	1.012	6.834	0.0190
	10^{-9}	2.393	8.389	0.0466	4.287	18.513	0.0815	4.601	18.072	0.0864
g4	10^{-10}	0.459	1.386	0.0089	1.356	3.332	0.0258	1.354	4.767	0.0254
	0	0.305	3.132	0.0059	0.308	3.175	0.0059	0.300	3.155	0.0056
DF	10^{-9}	1.689	10.896	0.0329	1.480	5.709	0.0281	0.580	3.035	0.0109

Table S3: Mean absolute errors [μE_h] (MAEs), max. absolute errors [μE_h] (MAX), and MAEs relative to the average reference RI-MP2 + F12 non-covalent interaction energy [%] for the **S22** test set (Ref. 109 in main text) employing NQ/DF/CABS-RI with various grid sizes ($g0$-$g4$) and thresholds ϑ_{NQ} and DF/CABS-RI ($\vartheta_{IPB} = 10^{-9}$) for different cc-pVXZ-F12 (X = D, T, Q) basis set combinations. Errors were evaluated against a g7 grid ($\vartheta = 0$) reference.

Method		cc-pVDZ-F12			cc-pVTZ-F12			cc-pVQZ-F12		
Grid/DF	ϑ	MAE	MAX	$\frac{\text{MAE}}{\text{AVG}}$	MAE	MAX	$\frac{\text{MAE}}{\text{AVG}}$	MAE	MAX	$\frac{\text{MAE}}{\text{AVG}}$
	10^{-9}	17.628	46.274	0.1943	17.158	38.374	0.1864	17.362	41.734	0.1874
g0	10^{-10}	17.619	46.357	0.1942	17.095	38.298	0.1857	17.305	41.816	0.1868
	0	17.616	46.358	0.1942	17.093	38.303	0.1857	17.299	41.818	0.1867
	10^{-9}	6.436	21.268	0.0711	6.092	20.945	0.0663	6.411	20.335	0.0693
g1	10^{-10}	6.423	21.291	0.0709	6.167	21.293	0.0671	6.413	20.600	0.0694
	0	6.421	21.320	0.0709	6.169	21.283	0.0672	6.411	20.603	0.0693
	10^{-9}	1.636	10.323	0.0181	2.890	10.264	0.0315	2.374	7.594	0.0257
g2	10^{-10}	1.331	9.662	0.0147	1.350	8.959	0.0147	1.546	9.689	0.0167
	0	1.275	9.747	0.0141	1.310	9.566	0.0143	1.330	9.530	0.0144
	10^{-9}	1.087	4.525	0.0120	2.686	10.339	0.0292	3.860	13.872	0.0417
g3	10^{-10}	0.514	1.813	0.0057	0.868	2.468	0.0094	0.821	2.466	0.0089
	0	0.348	1.738	0.0038	0.355	1.722	0.0039	0.353	1.694	0.0038
	10^{-9}	1.469	4.458	0.0162	3.829	20.533	0.0417	4.707	15.781	0.0509
g4	10^{-10}	0.470	1.366	0.0052	0.857	3.292	0.0093	1.212	5.323	0.0131
	0	0.060	0.383	0.0007	0.056	0.371	0.0006	0.060	0.388	0.0007
DF	10^{-9}	0.314	1.214	0.0035	0.238	0.868	0.0026	0.180	0.800	0.0019

Table S4: Mean absolute errors [μE_h] (MAEs), max. absolute errors [μE_h] (MAX), and MAEs relative to the average reference RI-MP2 + F12 non-covalent interaction energy [%] for the **S66** test set (Ref. 112 in main text) employing NQ/DF/CABS-RI with various grid sizes ($g0$-$g4$) and thresholds ϑ_{NQ} and DF/CABS-RI ($\vartheta_{IPB} = 10^{-9}$) for different cc-pVXZ-F12 (X = D, T, Q) basis set combinations. Errors were evaluated against a g7 grid ($\vartheta = 0$) reference.

Method		cc-pVDZ-F12			cc-pVTZ-F12			cc-pVQZ-F12		
Grid/DF	ϑ	MAE	MAX	$\frac{\text{MAE}}{\text{AVG}}$	MAE	MAX	$\frac{\text{MAE}}{\text{AVG}}$	MAE	MAX	$\frac{\text{MAE}}{\text{AVG}}$
	10^{-9}	11.654	40.345	0.1600	10.083	39.472	0.1362	11.541	40.709	0.1547
g0	10^{-10}	11.649	40.262	0.1600	10.073	39.188	0.1360	11.519	40.571	0.1544
	0	11.650	40.270	0.1600	10.075	39.149	0.1360	11.515	40.556	0.1544
	10^{-9}	4.596	22.819	0.0631	4.537	23.084	0.0613	4.595	23.239	0.0616
g1	10^{-10}	4.589	22.629	0.0630	4.527	22.789	0.0611	4.585	23.123	0.0615
	0	4.587	22.587	0.0630	4.523	22.767	0.0611	4.584	23.130	0.0615
	10^{-9}	1.389	8.689	0.0191	2.620	11.173	0.0354	2.618	13.401	0.0351
g2	10^{-10}	1.141	8.425	0.0157	1.256	7.708	0.0170	1.310	7.545	0.0176
	0	1.151	8.495	0.0158	1.137	8.271	0.0154	1.147	7.952	0.0154
	10^{-9}	1.146	5.080	0.0158	2.673	10.359	0.0361	3.495	13.382	0.0469
g3	10^{-10}	0.391	1.479	0.0054	1.046	6.105	0.0141	0.937	5.523	0.0126
	0	0.173	1.341	0.0024	0.172	1.339	0.0023	0.174	1.299	0.0023
	10^{-9}	2.413	18.037	0.0332	4.598	17.132	0.0621	4.805	15.782	0.0645
g4	10^{-10}	0.364	1.246	0.0050	0.860	3.000	0.0116	0.981	2.931	0.0132
	0	0.056	0.466	0.0008	0.056	0.455	0.0008	0.055	0.457	0.0007
DF	10^{-9}	0.315	1.338	0.0043	0.173	0.774	0.0023	0.151	0.581	0.0020

Chapter 5

Conclusion and Outlook

This thesis comprises several novel strategies and methods for accelerating explicitly correlated approaches, employing empirical scaling and decomposition techniques. Focusing on the explicitly correlated F12 ansatz, the corrections arising from this approach effectively account for the basis set incompleteness error by directly introducing terms into the wave function that describe the short-range electron–electron cusp behavior. While the near-universal form of correlation cusps requires only very few or a single parameter for an accurate description, the resulting high-dimensional integrals constitute the major computational challenge. Although these integrals can be factorized using decomposition techniques, significant computational bottlenecks remain, particularly for the treatment of exchange-type corrections.

To circumvent most of these computationally intensive contributions entirely, a scaled variant of explicitly correlated F12 theory is introduced in **Publication I**. By applying an empirically optimized scaling factor to the geminal–geminal component of explicitly correlated second-order Møller–Plesset theory, the corresponding F12 correction to interaction energies can be reproduced with high accuracy. Basis-set-dependent scaling factors compensate for the more rapid convergence of triplet contributions toward the complete basis set limit. This approach yields substantial computational speedups, particularly for medium- to large-sized molecular systems, and can be extended to other forms of F12 pair corrections. The methodologies developed in **Publication II–IV** provide additional acceleration and integrate seamlessly with the scaled F12 framework. For Fock matrix elements spanning multiple orbital spaces, established density fitting procedures are combined with numerical quadrature techniques from HF and DFT theory, as detailed in **Publication II**. These methods achieve substantial accelerations exceeding three orders of magnitude relative to the unapproximated evaluation while remaining highly accurate. As a result, what would otherwise represent a formal bottleneck of the theory becomes computationally negligible. In addition, efficient decomposition strategies are introduced that enable compact factorizations of integrals arising in explicitly correlated theory, focusing on the interplay between numerical quadrature, density fitting techniques, and CABS-RI. In particular, the evaluation of exchange-type six-center three-electron integrals benefits substantially from a

quadrature-based decomposition, which reduces the formal computational scaling to $\mathcal{O}(M^3)$ with system size M, and approaches linear scaling when combined with a novel batch-wise, highly efficient distance-dependent integral screening based on integral partition bounds, as presented in **Publication III**. A reformulation of the relevant expressions, together with a factorization of composite products of exchange-type four-center two-electron integrals arising from the insertion of CABS-RI via numerical quadrature and density fitting, is discussed in **Publication IV**. This approach yields speedups of roughly one order of magnitude for RI-MP2-F12 corrections in large molecular systems with virtually no loss of accuracy. The concepts and techniques presented may be further accelerated by employing localized molecular orbitals and related screening procedures, including pair natural orbitals, distance-dependent screening based on integral partition bounds, and suitable hybrid techniques.

The strategies introduced in this thesis are not restricted to RI-MP2-F12 but can be applied to other F12 corrections, such as those in random phase approximation (RPA), coupled-cluster, multi-reference approaches, and gradient theories. Further, the underlying ideas can also be transferred to other explicitly correlated frameworks, including transcorrelated methods.

Bibliography

[1] E. Schrödinger, *Phys. Rev.* **1926**, *28*, 1049.

[2] D.R. Hartree, *Math. Proc. Camb. Philos. Soc.* **1928**, *24*, 89.

[3] V. Fock, *Z. Phys.* **1930**, *61*, 126.

[4] J.C. Slater, *Phys. Rev.* **1929**, *34*, 1293.

[5] G.W. Kellner, *Z. Phys.* **1927**, *44*, 91.

[6] E.U. Condon, *Phys. Rev.* **1930**, *36*, 1121.

[7] E. Schrödinger, *Ann. Phys.* **1926**, *385*, 437.

[8] L. Euler and L. Courvoisier: *Theoria motuum lunae : nova methodo pertractata.* Orell Füssli, 1958.

[9] J.W.S. Rayleigh: *The theory of sound. Volume 1.* Macmillan and Co., 1877.

[10] C. Møller and M.S. Plesset, *Phys. Rev.* **1934**, *46*, 618.

[11] J. Čížek, *J. Chem. Phys.* **1966**, *45*, 4256.

[12] J. Čížek, *Adv. Chem. Phys.* **1969**, *14*, 35.

[13] J. Čižek and J. Paldus, *Int. J. Quantum Chem.* **1971**, *5*, 359.

[14] K. Raghavachari, G.W. Trucks, J.A. Pople and M. Head-Gordon, *Chem. Phys. Lett.* **1989**, *157*, 479.

[15] S.F. Boys, *Proc. R. Soc. London. A. Math. Phys. Sci.* **1950**, *200*, 542.

[16] T. Kato, *Commun. Pure Appl. Math.* **1957**, *10*, 151.

[17] J.S. Sims and S. Hagstrom, *Phys. Rev. A* **1971**, *4*, 908.

[18] D.C. Clary and N.C. Handy, *Phys. Rev. A* **1976**, *14*, 1607.

[19] Boys S. F., *Proc. R. Soc. London. Ser. A. Math. Phys. Sci.* **1960**, *258*, 402.

[20] K. Singer, *Proc. R. Soc. London. Ser. A. Math. Phys. Sci.* **1960**, *258*, 412.

[21] Boys S. F. and Handy N. C., *Proc. R. Soc. London. A. Math. Phys. Sci.* **1969**, *309*, 209.

[22] Boys S. F. and Handy N. C., *Proc. R. Soc. London. A. Math. Phys. Sci.* **1969**, *310*, 43.

[23] Boys S. F. and Handy N. C., *Proc. R. Soc. London. A. Math. Phys. Sci.* **1969**, *310*, 63.

[24] Boys S. F. and Handy N. C., *Proc. R. Soc. London. A. Math. Phys. Sci.* **1969**, *311*, 309.

[25] W. Kutzelnigg, *Theor. Chim. Acta* **1985**, *68*, 445.

[26] W. Klopper and W. Kutzelnigg, *Chem. Phys. Lett.* **1987**, *134*, 17.

[27] W. Kutzelnigg and W. Klopper, *J. Chem. Phys.* **1991**, *94*, 1985.

[28] S. Ten-no, *Chem. Phys. Lett.* **2004**, *398*, 56.

[29] M.B. Ruiz, *J. Coord. Chem.* **2015**, *68*, 3340.

[30] J. Noga and W. Kutzelnigg, *J. Chem. Phys.* **1994**, *101*, 7738.

[31] H.J. Werner, T.B. Adler and F.R. Manby, *J. Chem. Phys.* **2007**, *126*, 164102.

[32] R.A. Bachorz, F.A. Bischoff, A. Glöß, C. Hättig, S. Höfener, W. Klopper and D.P. Tew, *J. Comput. Chem.* **2011**, *32*, 2492.

[33] E.F. Valeev, *Chem. Phys. Lett.* **2004**, *395*, 190.

[34] F.R. Manby, *J. Chem. Phys.* **2003**, *119*, 4607.

[35] S. Ten-No and F.R. Manby, *J. Chem. Phys.* **2003**, *119*, 5358.

[36] R.A. Friesner, *Chem. Phys. Lett.* **1985**, *116*, 39.

[37] M.N. Ringnalda, M. Belhadj and R.A. Friesner, *J. Chem. Phys.* **1990**, *93*, 3397.

[38] S. Ten-No, *J. Chem. Phys.* **2004**, *121*, 117.

[39] E.G. Hohenstein, R.M. Parrish and T.J. Martínez, *J. Chem. Phys.* **2012**, *137*, 044103.

[40] R.M. Parrish, E.G. Hohenstein, T.J. Martínez and C.D. Sherrill, *J. Chem. Phys.* **2012**, *137*, 224106.

[41] F.H. Bangerter, M. Glasbrenner and C. Ochsenfeld, *J. Chem. Theory Comput.* **2021**, *17*, 211.

[42] J. Kussmann, H. Laqua and C. Ochsenfeld, *J. Chem. Theory Comput.* **2021**, *17*, 1512.

[43] H. Laqua, T.H. Thompson, J. Kussmann and C. Ochsenfeld, *J. Chem. Theory Comput.* **2020**, *16*, 1456.

[44] T.H. Thompson and C. Ochsenfeld, *J. Chem. Phys.* **2019**, *150*, 044101.

[45] F. Sacchetta, D. Graf, H. Laqua, M.A. Ambroise, J. Kussmann, A. Dreuw and C. Ochsenfeld, *J. Chem. Phys.* **2022**, *157*, 104104.

[46] J.M. Foster and S.F. Boys, *Rev. Mod. Phys.* **1960**, *32*, 300.

[47] S. Sæbø and P. Pulay, *Chem. Phys. Lett.* **1985**, *113*, 13.

[48] S. Sæbø and P. Pulay, *J. Chem. Phys.* **1987**, *86*, 914.

[49] J. Pipek and P.G. Mezey, *J. Chem. Phys.* **1989**, *90*, 4916.

[50] S. Sæbø and P. Pulay, *Annu. Rev. Phys. Chem.* **1993**, *44*, 213.

[51] S.A. Maurer, L. Clin and C. Ochsenfeld, *J. Chem. Phys.* **2014**, *140*, 224112.

[52] C. Hampel and H.J. Werner, *J. Chem. Phys.* **1996**, *104*, 6286.

[53] M. Schütz, G. Hetzer and H.J. Werner, *J. Chem. Phys.* **1999**, *111*, 5691.

[54] M.S. Lee, P.E. Maslen and M. Head-Gordon, *J. Chem. Phys.* **2000**, *112*, 3592.

[55] M. Schütz and H.J. Werner, *J. Chem. Phys.* **2001**, *114*, 661.

[56] H.J. Werner, *J. Chem. Phys.* **2008**, *129*, 101103.

[57] D.P. Tew and C. Hättig, *Int. J. Quantum Chem.* **2013**, *113*, 224.

[58] G. Schmitz, C. Hättig and D.P. Tew, *Phys. Chem. Chem. Phys.* **2014**, *16*, 22167.

[59] Q. Ma and H.J. Werner, *J. Chem. Theory Comput.* **2015**, *11*, 5291.

[60] Q. Ma and H.J. Werner, *J. Chem. Theory Comput.* **2019**, *15*, 1044.

[61] Y. Wang, Y. Guo, F. Neese, E.F. Valeev, W. Li and S. Li, *J. Chem. Theory Comput.* **2023**, *19*, 8076.

[62] H.J. Werner and A. Hansen, *J. Chem. Theory Comput.* **2023**, *19*, 7007.

[63] A. Szabo and N.S. Ostlund: *Modern quantum chemistry : introduction to advanced electronic structure theory.* Dover Publications, 1996.

[64] E. Noether, *Nachr. Ges. Wiss. Gött., Math.-Phys.* **1918**, *1918*, 235.

[65] M. Born and R. Oppenheimer, *Ann. Phys.* **1927**, *389*, 457.

[66] W. Heisenberg, *Z. Phys.* **1926**, *38*, 411.

[67] P.A.M. Dirac, *Proc. R. Soc. Lond. A* **1926**, *112*, 661.

[68] W. Pauli, *Z. Phys.* **1925**, *31*, 765.

[69] J.C. Slater, *Phys. Rev.* **1930**, *35*, 210.

[70] C.C. Roothaan, *Rev. Mod. Phys.* **1951**, *23*, 69.

[71] P.O. Löwdin, *J. Chem. Phys.* **1950**, *18*, 365.

[72] C.A. White, B.G. Johnson, P.M.W. Gill and M. Head-Gordon, *Chem. Phys. Lett.* **1994**, *230*, 8.

[73] C.A. White and M. Head-Gordon, *J. Chem. Phys.* **1996**, *104*, 2620.

[74] C. Ochsenfeld, C.A. White and M. Head-Gordon, *J. Chem. Phys.* **1998**, *109*, 1663.

[75] F. Neese, *J. Comput. Chem.* **2003**, *24*, 1740.

[76] F. Neese, F. Wennmohs, A. Hansen and U. Becker, *Chem. Phys.* **2009**, *356*, 98.

[77] F. Neese, P. Colinet, B. DeSouza, B. Helmich-Paris, F. Wennmohs and U. Becker, *J. Phys. Chem. A* **2025**, *129*, 2618.

[78] T. Helgaker, P. Jørgensen and J. Olsen: *Molecular Electronic-Structure Theory.* Wiley Blackwell, 2013.

[79] C.A. Coulson and A.H. Neilson, *Proc. Phys. Soc.* **1961**, *78*, 831.

[80] E.A. Hylleraas, *Z. Phys.* **1929**, *54*, 347.

[81] E.A. Hylleraas and B. Undheim, *Z. Phys.* **1930**, *65*, 759.

[82] P.O. Löwdin, *Phys. Rev.* **1955**, *97*, 1474.

[83] W. Ritz, *J. Reine Angew. Math.* **1909**, *135*, 1.

[84] L. Brillouin, *J. Phys. Radium* **1932**, *3*, 373.

[85] L. Brillouin, *J. Phys. Radium* **1934**, *5*, 413.

[86] O. Sinanoğlu, *J. Chem. Phys.* **1961**, *34*, 1237.

[87] G.D. Purvis and R.J. Bartlett, *J. Chem. Phys.* **1982**, *76*, 1910.

[88] T.D. Crawford and H.F. Schaefer, *Rev. Comput. Chem.* **2000**, *14*, 33.

[89] R.J. Bartlett and M. Musiał, *Rev. Mod. Phys.* **2007**, *79*, 291.

[90] T. Helgaker, W. Klopper, H. Koch and J. Noga, *J. Chem. Phys.* **1997**, *106*, 9639.

[91] A.W. Weiss, *Phys. Rev.* **1961**, *122*, 1826.

[92] C. Schwartz, *Phys. Rev.* **1962**, *126*, 1015.

[93] W. Lakin, *J. Chem. Phys.* **1965**, *43*, 2954.

[94] C.F. Bunge, *Theor. Chim. Acta* **1970**, *16*, 126.

[95] D.P. Carroll, H.J. Silverstone and R.M. Metzger, *J. Chem. Phys.* **1979**, *71*, 4142.

[96] R.N. Hill, *J. Chem. Phys.* **1985**, *83*, 1173.

[97] W. Kutzelnigg and J.D. Morgan, *J. Chem. Phys.* **1992**, *96*, 4484.

[98] R.T. Pack and W. Byers Brown, *J. Chem. Phys.* **1966**, *45*, 556.

[99] A. Halkier, T. Helgaker, P. Jørgensen, W. Klopper, H. Koch, J. Olsen and A.K. Wilson, *Chem. Phys. Lett.* **1998**, *286*, 243.

[100] W. Klopper, *Mol. Phys.* **2001**, *99*, 481.

[101] D.W. Schwenke, *J. Chem. Phys.* **2005**, *122*, 014107.

[102] T.H. Dunning, *J. Chem. Phys.* **1989**, *90*, 1007.

[103] J.C. Slater, *Phys. Rev.* **1928**, *31*, 333.

[104] J.C. Slater, *Phys. Rev.* **1928**, *32*, 349.

[105] E.A. Hylleraas, *Z. Phys.* **1928**, *48*, 469.

[106] L. Kong, F.A. Bischoff and E.F. Valeev, *Chem. Rev.* **2012**, *112*, 75.

[107] J.S. Sims and S.A. Hagstrom, *J. Phys. B At. Mol. Opt. Phys.* **2004**, *37*, 1519.

[108] J.S. Sims and S.A. Hagstrom, *J. Phys. B At. Mol. Opt. Phys.* **2007**, *40*, 1575.

[109] J.S. Sims and S.A. Hagstrom, *J. Phys. B At. Mol. Opt. Phys.* **2015**, *48*, 175003.

[110] J.S. Sims and S.A. Hagstrom, *J. Chem. Phys.* **2014**, *140*, 224312.

[111] J.S. Sims, *J. Phys. B At. Mol. Opt. Phys.* **2017**, *50*, 245003.

[112] P.M. Kozlowski and L. Adamowicz, *J. Chem. Phys.* **1991**, *95*, 6681.

[113] E. Mátyus and M. Reiher, *J. Chem. Phys.* **2012**, *137*, 024104.

[114] J. Mitroy, S. Bubin, W. Horiuchi, Y. Suzuki, L. Adamowicz, W. Cencek, K. Szalewicz, J. Komasa, D. Blume and K. Varga, *Rev. Mod. Phys.* **2013**, *85*, 693.

[115] J.O. Hirschfelder, *J. Chem. Phys.* **1963**, *39*, 3145.

[116] R. Jastrow, *Phys. Rev.* **1955**, *98*, 1479.

[117] P. López Ríos, P. Seth, N.D. Drummond and R.J. Needs, *Phys. Rev. E - Stat. Nonlinear, Soft Matter Phys.* **2012**, *86*, 036703.

[118] J.P. Haupt, S.M. Hosseini, P. López Ríos, W. Dobrautz, A. Cohen and A. Alavi, *J. Chem. Phys.* **2023**, *158*, 224105.

[119] T. Yanai and T. Shiozaki, *J. Chem. Phys.* **2012**, *136*, 084107.

[120] S.L. Ten-No, *J. Chem. Phys.* **2023**, *159*, 171103.

[121] T. Schraivogel, E.M. Christlmaier, P. López Ríos, A. Alavi and D. Kats, *J. Chem. Phys.* **2023**, *158*, 214106.

[122] A. Ammar, A. Scemama and E. Giner, *J. Chem. Phys.* **2023**, *159*, 114121.

[123] W. Klopper and C.C. Samson, *J. Chem. Phys.* **2002**, *116*, 6397.

[124] W. Klopper, *J. Chem. Phys.* **2004**, *120*, 10890.

[125] S. Ten-no, *J. Chem. Phys.* **2007**, *126*, 014108.

[126] D.P. Tew and W. Klopper, *Mol. Phys.* **2010**, *108*, 315.

[127] J. Noga, W. Kutzelnigg and W. Klopper, *Chem. Phys. Lett.* **1992**, *199*, 497.

[128] E.F. Valeev, *Phys. Chem. Chem. Phys.* **2008**, *10*, 106.

[129] T.B. Adler, G. Knizia and H.J. Werner, *J. Chem. Phys.* **2007**, *127*, 221106.

[130] J. Noga, S. Kedžuch, J. Šimunek and S. Ten-No, *J. Chem. Phys.* **2008**, *128*, 174103.

[131] M. Torheyden and E.F. Valeev, *Phys. Chem. Chem. Phys.* **2008**, *10*, 3410.

[132] T. Shiozaki, M. Kamiya, S. Hirata and E.F. Valeev, *J. Chem. Phys.* **2008**, *129*, 071101.

[133] E.F. Valeev and T. Daniel Crawford, *J. Chem. Phys.* **2008**, *128*, 244113.

[134] G. Knizia, T.B. Adler and H.J. Werner, *J. Chem. Phys.* **2009**, *130*, 054104.

[135] J. Noga and J. Šimunek, *Chem. Phys.* **2009**, *356*, 1.

[136] C. Hättig, D.P. Tew and A. Köhn, *J. Chem. Phys.* **2010**, *132*, 231102.

[137] A. Köhn, *J. Chem. Phys.* **2009**, *130*, 104104.

[138] S. Höfener, N. Schieschke, W. Klopper and A. Köhn, *J. Chem. Phys.* **2019**, *150*, 184110.

[139] C. Masteran, B. Gaudel and E.F. Valeev, *J. Chem. Theory Comput.* **2025**, *21*, 10329.

[140] C. Hättig, W. Klopper, A. Köhn and D.P. Tew, *Chem. Rev.* **2012**, *112*, 4.

[141] S. Grimme, *J. Chem. Phys.* **2003**, *118*, 9095.

[142] R.A. Distasio and M. Head-Gordon, *Mol. Phys.* **2007**, *105*, 1073.

[143] J.G. Hill and J.A. Platts, *J. Chem. Theory Comput.* **2007**, *3*, 80.

[144] R.A. King, *Mol. Phys.* **2009**, *107*, 789.

[145] R.F. Fink, *J. Chem. Phys.* **2010**, *133*, 174113.

[146] S. Grimme, *J. Comput. Chem.* **2003**, *24*, 1529.

[147] S. Grimme and E.I. Izgorodina, *Chem. Phys.* **2004**, *305*, 223.

[148] Y.M. Rhee and M. Head-Gordon, *J. Phys. Chem. A* **2007**, *111*, 5314.

[149] A. Hellweg, S.A. Grün and C. Hättig, *Phys. Chem. Chem. Phys.* **2008**, *10*, 4119.

[150] T. Takatani, E.G. Hohenstein and C.D. Sherrill, *J. Chem. Phys.* **2008**, *128*, 124111.

[151] M. Pitoňák, P. Neogrády, J. Černý, S. Grimme and P. Hobza, *ChemPhysChem* **2009**, *10*, 282.

[152] Y. Jung, R.C. Lochan, A.D. Dutoi and M. Head-Gordon, *J. Chem. Phys.* **2004**, *121*, 9793.

[153] Y. Jung and M. Head-Gordon, *Phys. Chem. Chem. Phys.* **2006**, *8*, 2831.

[154] R.C. Lochan, Y. Jung and M. Head-Gordon, *J. Phys. Chem. A* **2005**, *109*, 7598.

[155] R.C. Lochan and M. Head-Gordon, *J. Chem. Phys.* **2007**, *126*, 164101.

[156] D. Casanova, Y.M. Rhee and M. Head-Gordon, *J. Chem. Phys.* **2008**, *128*, 164106.

[157] Y.M. Rhee, D. Casanova and M. Head-Gordon, *J. Phys. Chem. A* **2009**, *113*, 10564.

[158] Y.M. Rhee, D. Casanova and M. Head-Gordon, *J. Chem. Theory Comput.* **2009**, *5*, 1224.

[159] M. Häser and J. Almlöf, *J. Chem. Phys.* **1992**, *96*, 489.

[160] S. Hofener and W. Klopper, *Mol. Phys.* **2010**, *108*, 1783.

[161] W. Gyorffy, G. Knizia and H.J. Werner, *J. Chem. Phys.* **2017**, *147*, 214101.

[162] W. Gyorffy and H.J. Werner, *J. Chem. Phys.* **2018**, *148*, 114104.

[163] E.C. Mitchell, J.M. Turney and H.F. Schaefer, *J. Chem. Theory Comput.* **2024**, *20*, 8538.

[164] S. Ten-no, *Chem. Phys. Lett.* **2007**, *447*, 175.

[165] T. Shiozaki and H.J. Werner, *J. Chem. Phys.* **2010**, *133*, 141103.

[166] T. Shiozaki, G. Knizia and H.J. Werner, *J. Chem. Phys.* **2011**, *134*, 034113.

[167] R. Haunschild, S. Mao, D. Mukherjee and W. Klopper, *Chem. Phys. Lett.* **2012**, *531*, 247.

[168] T. Shiozaki and H.J. Werner, *Mol. Phys.* **2013**, *111*, 607.

[169] G.H. Booth, D. Cleland, A. Alavi and D.P. Tew, *J. Chem. Phys.* **2012**, *137*, 164112.

[170] W. Liu, M. Hanauer and A. Köhn, *Chem. Phys. Lett.* **2013**, *565*, 122.

[171] L.B. Roskop, L. Kong, E.F. Valeev, M.S. Gordon and T.L. Windus, *J. Chem. Theory Comput.* **2014**, *10*, 90.

[172] Y. Guo, K. Sivalingam, E.F. Valeev and F. Neese, *J. Chem. Phys.* **2017**, *147*, 064110.

[173] A.S. Hehn and W. Klopper, *J. Chem. Phys.* **2013**, *138*, 181104.

[174] A.S. Hehn, D.P. Tew and W. Klopper, *J. Chem. Phys.* **2015**, *142*, 194106.

[175] A.S. Hehn, C. Holzer and W. Klopper, *Chem. Phys.* **2016**, *479*, 160.

[176] N. Mehta and J.M. Martin, *J. Phys. Chem. Lett.* **2022**, *13*, 9332.

[177] N. Mehta and J.M. Martin, *J. Chem. Theory Comput.* **2022**, *18*, 5978.

[178] N. Sylvetsky, K.A. Peterson, A. Karton and J.M. Martin, *J. Chem. Phys.* **2016**, *144*, 214101.

[179] S.D. Grande, M. Kállay and V. Barone, *J Comput Chem* **2023**, *44*, 2149.

[180] A. Yachmenev, S.N. Yurchenko, T. Ribeyre and W. Thiel, *J. Chem. Phys.* **2011**, *135*, 074302.

[181] A. Dargelos and C. Pouchan, *Chem. Phys. Lett.* **2020**, *754*, 137746.

[182] N. Inostroza-Pino, C.Z. Palmer, T.J. Lee and R.C. Fortenberry, *J. Mol. Spectrosc.* **2020**, *369*, 111273.

[183] A. Köhn, G.W. Richings and D.P. Tew, *J. Chem. Phys.* **2008**, *129*, 201103.

[184] T. Shiozaki, M. Kamiya, S. Hirata and E.F. Valeev, *J. Chem. Phys.* **2009**, *130*, 054101.

[185] H. Fliegl, W. Klopper and C. Hättig, *J. Chem. Phys.* **2005**, *122*, 084107.

[186] H. Fliegl, C. Hättig and W. Klopper, *Int. J. Quantum Chem.* **2006**, *106*, 2306.

[187] D.P. Tew, W. Klopper, C. Neiss and C. Hättig, *Phys. Chem. Chem. Phys.* **2007**, *9*, 1921.

[188] D.P. Tew, W. Klopper and C. Hättig, *Chem. Phys. Lett.* **2008**, *452*, 326.

[189] W. Klopper, B. Ruscic, D.P. Tew, F.A. Bischoff and S. Wolfsegger, *Chem. Phys.* **2009**, *356*, 14.

[190] L.R. Tucker, *Psychometrika* **1966**, *31*, 279.

[191] I. Røeggen and E. Wisløff-Nilssen, *Chem. Phys. Lett.* **1986**, *132*, 154.

[192] I. Røeggen and T. Johansen, *J. Chem. Phys.* **2008**, *128*, 194107.

[193] L. De Lathauwer, B. De Moor and J. Vandewalle, *SIAM J. Matrix Anal. Appl.* **2000**, *21*, 1253.

[194] W. Hackbusch and S. Börm, *Computing* **2002**, *69*, 1.

[195] T.G. Kolda and B.W. Bader, *SIAM Rev.* **2009**, *51*, 455.

[196] I.V. Oseledets, *SIAM J. Sci. Comput.* **2011**, *33*, 2295.

[197] J.I. Cirac, D. Pérez-García, N. Schuch and F. Verstraete, *Rev. Mod. Phys.* **2021**, *93*, 045003.

[198] J.L. Whitten, *J. Chem. Phys.* **1973**, *58*, 4496.

[199] D.S. Lambrecht and C. Ochsenfeld, *J. Chem. Phys.* **2005**, *123*, 184101.

[200] C. Ochsenfeld, J. Kussmann and D.S. Lambrecht, *Rev. Comput. Chem.* **2007**, *23*, 1.

[201] S.A. Maurer, D.S. Lambrecht, D. Flaig and C. Ochsenfeld, *J. Chem. Phys.* **2012**, *136*, 144107.

[202] S.A. Maurer, D.S. Lambrecht, J. Kussmann and C. Ochsenfeld, *J. Chem. Phys.* **2013**, *138*, 014101.

[203] B.I. Dunlap, J.W.D. Connolly and J.R. Sabin, *J. Chem. Phys.* **1979**, *71*, 3396.

[204] M. Feyereisen, G. Fitzgerald and A. Komornicki, *Chem. Phys. Lett.* **1993**, *208*, 359.

[205] K. Eichkorn, O. Treutler, H. Ohm, M. Häser and R. Ahlrichs, *Chem. Phys. Lett.* **1995**, *240*, 283.

[206] K. Eichkorn, F. Weigend, O. Treutler and R. Ahlrichs, *Theor. Chem. Acta* **1997**, *97*, 119.

[207] J.C. Womack and F.R. Manby, *J. Chem. Phys.* **2014**, *140*, 044118.

[208] R.A. Friesner, *J. Chem. Phys.* **1986**, *85*, 1462.

[209] R.A. Friesner, *J. Chem. Phys.* **1987**, *86*, 3522.

[210] B. Helmich-Paris, B. de Souza, F. Neese and R. Izsák, *J. Chem. Phys.* **2021**, *155*, 104109.

[211] A.D. Becke, *J. Chem. Phys.* **1988**, *88*, 2547.

[212] H. Laqua, J. Kussmann and C. Ochsenfeld, *J. Chem. Phys.* **2018**, *149*, 204111.

[213] D. Bokhan, S. Bernadotte and S. Ten-no, *Chem. Phys. Lett.* **2009**, *469*, 214.

[214] D. Bokhan and D.N. Trubnikov, *J. Chem. Phys.* **2012**, *136*, 204110.

[215] T.H. Thompson: *Integral Bounds and Rigorous Screening Algorithms for Reduced Scaling in Explicitly Correlated, Semi-Numerical, and Non-Hermitian Quantum Chemistry*. Dissertation, Ludwig-Maximilians-Universität München, **2020**.

[216] S. Reine, E. Tellgren, A. Krapp, T. Kjærgaard, T. Helgaker, B. Jansik, S. Høst and P. Salek, *J. Chem. Phys.* **2008**, *129*, 104101.

[217] R.M. Parrish, E.G. Hohenstein, T.J. Martínez and C.D. Sherrill, *J. Chem. Phys.* **2013**, *138*, 194107.

[218] C. Song and T.J. Martínez, *J. Chem. Phys.* **2016**, *144*, 174111.

[219] C. Song and T.J. Martínez, *J. Chem. Phys.* **2017**, *146*, 034104.

[220] F.H. Bangerter, M. Glasbrenner and C. Ochsenfeld, *J. Chem. Theory Comput.* **2022**, *18*, 5233.

[221] G. Reza Ahmadi and J. Almlöf, *Chem. Phys. Lett.* **1995**, *246*, 364.

[222] H. Laqua, J. Kussmann and C. Ochsenfeld, *J. Chem. Phys.* **2021**, *154*, 214116.

[223] A. Preiskorn and B. Żurawski, *Int. J. Quantum Chem.* **1985**, *27*, 641.

[224] A. Largo-Cabrerizo and E. Clementi, *J. Comput. Chem.* **1987**, *8*, 1191.

[225] Y. Lu and Z. Huang, *Int. J. Quantum Chem.* **1990**, *38*, 447.

[226] D. Frye, A. Preiskorn and E. Clementi, *J. Comput. Chem.* **1991**, *12*, 560.

[227] S. Ten-No, *Chem. Phys. Lett.* **2000**, *330*, 169.

[228] S. Ten-No, *Chem. Phys. Lett.* **2000**, *330*, 175.

[229] A. Komornicki and H.F. King, *J. Chem. Phys.* **2011**, *134*, 244115.

[230] S. Reine, T. Helgaker and R. Lindh, *Wiley Interdiscip. Rev. Comput. Mol. Sci.* **2012**, *2*, 290.

[231] G.M. Barca, P.F. Loos and P.M. Gill, *J. Chem. Theory Comput.* **2016**, *12*, 1735.

[232] G.M. Barca and P.F. Loos, *J. Chem. Phys.* **2017**, *147*, 024103.